Title
Meiotic regulation of kinetochore composition and function

Author
Chen, Jingxun

Publication Date
2019

Peer reviewed|Thesis/dissertation

Meiotic regulation of kinetochore composition and function

by

Jingxun Chen

A dissertation submitted in partial satisfaction of the

requirements for the degree of

Doctor of Philosophy

in

Molecular and Cell Biology

in the

Graduate Division

of the

University of California, Berkeley

Committee in charge:

Professor Elçin Ünal, Chair

Professor Rebecca Heald

Professor Michael Rape

Professor Kathleen Ryan

Summer 2019

Meiotic regulation of kinetochore composition and function

Abstract

Meiotic regulation of kinetochore composition and function

by

Jingxun Chen

Doctor of Philosophy in Molecular and Cell Biology

University of California, Berkeley

Professor Elçin Ünal, Chair

The survival and fitness of an organism rely on faithful transmission of the genome. In sexually reproducing organisms, genome transmission requires a specialized cell division named meiosis, in which the parental genome is shuffled and halved. The kinetochore, a conserved protein complex that mediates chromosome segregation, is a key player in meiosis. Here we investigated how the budding yeast kinetochore undergoes dynamic changes in this specialized cell division. The microtubule-binding part of the kinetochore (outer kinetochore) dissociates from the chromosomes in meiotic prophase and reassembles before the meiotic divisions. This dynamic behavior is crucial to establish the meiosis-specific chromosome segregation. We have discovered a multi-level network that regulates the dynamic kinetochore behavior by controlling the abundance of one single kinetochore subunit, Ndc80. Ndc80 is downregulated in meiotic prophase and later re-synthesized during the meiotic divisions. This fluctuation in the Ndc80 level requires regulation on Ndc80 synthesis and turnover. Central to the Ndc80 synthesis regulation is the toggling of two *NDC80* mRNAs: (1) a coding mRNA that is translated into Ndc80 protein, and (2) a 5'-extended mRNA termed *LUTI*. Rather than coding for Ndc80, *LUTI* expression impedes the expression of the coding mRNA via chromatin modifications, leading to Ndc80 synthesis repression. Two meiotic master transcription factors, Ime1 and Ndt80, regulate the expression of *LUTI* and the coding mRNA, respectively, and integrate Ndc80 regulation into the larger meiotic program. Besides synthesis, Ndc80 degradation is temporally controlled: Ndc80 is degraded in meiotic prophase and not in metaphase I. Ndc80 degradation requires active proteasomes, a degron sequence at Ndc80's N-terminus, and Aurora B phosphorylation on Ndc80, which is known to correct erroneous microtubule-kinetochore attachments and is rewired to degrade Ndc80 in meiotic prophase. Crucially, mis-regulation of Ndc80 abundance disrupts chromosome segregation, gamete formation, and progeny fitness, highlighting the importance of Ndc80 modulation. Altogether, this work reveals a beautiful case in evolution in which the gene expression, turnover, and activity of the kinetochore are tuned to accommodate the specialized chromosome segregation program meiosis.

for Kevin and my parents

Contents

Contents **ii**

List of Figures **v**

1 Introduction **1**
1.1 Overview of meiosis . . . 1
1.2 Kinetochore structure and function . . . 3
1.2.1 What is a kinetochore? . . . 3
1.2.2 Kinetochore composition . . . 4
1.2.3 Regulation of microtubule-kinetochore attachments . . . 7
1.3 Establishment of meiotic chromosome segregation . . . 9
1.3.1 Recombination and synapsis . . . 10
1.3.2 Centromeric cohesion protection . . . 11
1.3.3 Sister kinetochore co-orientation . . . 11
1.3.4 Delay in microtubule-kinetochore interaction . . . 12
1.4 Gene regulation in meiosis . . . 14
1.4.1 A global view of meiotic gene expression . . . 14
1.4.2 Ime1 . . . 15
1.4.3 Ndt80 . . . 16
1.4.4 Non-canonical transcription and translation in meiosis . . . 17
1.5 Protein turnover in meiosis . . . 19

2 Meiotic Regulation of Ndc80 Synthesis **21**
2.1 Introduction . . . 21
2.2 Materials and methods . . . 23
2.3 Results . . . 23
2.3.1 Ndc80 is the limiting component for kinetochore function in meiotic prophase . . . 23
2.3.2 Two distinct *NDC80* transcript isoforms exist in meiosis . . . 27
2.3.3 The long *NDC80* isoform is unable to produce Ndc80 protein due to translation of its upstream ORFs . . . 30

2.3.4 $NDC80^{LUTI}$ expression in *cis* is necessary and sufficient to downregulate $NDC80^{ORF}$ . . . 30
2.3.5 Master transcription factors Ime1 and Ndt80 regulate $NDC80^{LUTI}$ and $NDC80^{ORF}$ expression, respectively . . . 36
2.3.6 Expression of $NDC80^{LUTI}$ is required to limit kinetochore activity in meiotic prophase . . . 41
2.3.7 Re-expression of $NDC80^{ORF}$ is required to resume kinetochore activity in the meiotic divisions . . . 43
2.4 Discussion . . . 45
2.4.1 A limiting subunit controls kinetochore function in meiosis . . . 47
2.4.2 $NDC80^{LUTI}$ is an mRNA that does not produce protein . . . 49
2.4.3 The function of $NDC80^{LUTI}$ mRNA is purely regulatory . . . 49
2.4.4 Pervasiveness of *LUTI* mRNA biology in yeast meiosis and beyond . 51
2.4.5 Interpreting genome-wide data in the context of *LUTI* mRNA biology 52

3 Meiotic Regulation of Ndc80 Degradation 53
3.1 Introduction . . . 53
3.2 Materials and methods . . . 54
3.3 Results . . . 55
3.3.1 Ndc80 degradation is temporally regulated during meiosis . . . 55
3.3.2 Ndc80 degradation requires a degron sequence at its N-terminus . . . 57
3.3.3 Ndc80 degradation requires proteasome activity but is independent of recombination, paring, and DNA replication . . . 63
3.3.4 Aurora B/Ipl1 activity is necessary for Ndc80 degradation in meiotic prophase . . . 64
3.3.5 Ndc80 degradation requires Ipl1-mediated phosphorylation . . . 67
3.3.6 Defects in Ndc80 degradation predispose meiotic cells to chromosome segregation errors . . . 68
3.4 Discussion . . . 72
3.4.1 Ndc80 phosphorylation triggers its degradation in meiotic prophase . 73
3.4.2 Protein turnover as a mechanism to create meiosis-specific kinetochores 74
3.4.3 Customization of kinetochore activity by controlling kinetochore assembly or disassembly . . . 75

4 Conclusions 77
4.1 Meiotic regulation of kinetochore remodeling . . . 77
4.1.1 Regulated expression of two *NDC80* mRNAs controls Ndc80 synthesis temporally . . . 77
4.1.2 The *LUTI*-based repression mechanism . . . 78
4.1.3 Ndc80 phosphorylation triggers its degradation in meiotic prophase . 79
4.2 The biological relevance of regulating Ndc80 abundance . . . 81
4.3 A final perspective . . . 83

5 Materials and methods **84**
5.1 Yeast strains, plasmids and culture methods 84
5.1.1 Strains and plasmids 84
5.1.2 *pCUP-IME1 pCUP-IME4* synchronization system 98
5.1.3 *pGAL-NDT80 GAL4-ER* synchronization system 98
5.1.4 Alpha-factor arrest-release mitotic time course 99
5.1.5 Spot growth assay 99
5.1.6 Conservation analysis 99
5.2 Light microscopy 99
5.2.1 Fluorescence microscopy 99
5.2.2 Indirect immunofluorescence 100
5.3 RNA and Chromatin immunoprecipitation methods 100
5.3.1 Northern blotting 100
5.3.2 Chromatin immunoprecipitation (IP) 101
5.3.3 RT-qPCR 102
5.3.4 Single-molecule RNA FISH 103
5.3.5 Statistical analysis of smFISH data 108
5.3.6 Software 108
5.4 Protein methods 108
5.4.1 Denaturing IP and mass spectrometry (MS) 108
5.4.2 Native IP, Co-IP, and TMT quantitative MS 109
5.4.3 Purification of the Ndc80 complex 110
5.4.4 Kinase assay 111
5.4.5 Immunoblot 111

Bibliography **113**

List of Figures

1.1 The core kinetochore subunits in budding yeast 5

2.1 Schematics of the kinetochore structure and dynamic behavior 23
2.2 Protein abundance of the Ndc80 complex subunits in meiosis 24
2.3 Ndc80 is the limiting kinetochore subunit in meiotic prophase 25
2.4 Two distinct *NDC80* transcripts are expressed during meiosis 26
2.5 An optimized smFISH method to study *NDC80* transcripts in meiosis 28
2.6 $NDC80^{Long}$ and $NDC80^{Short}$ detected by smFISH 29
2.7 $NDC80^{Long}$ cannot synthesize Ndc80 protein due to uORF translation 31
2.8 $NDC80^{LUTI}$ is necessary to downregulate $NDC80^{ORF}$ 33
2.9 $NDC80^{LUTI}$ is necessary to downregulate $NDC80^{ORF}$ by smFISH 34
2.10 Premature termination of $NDC80^{LUTI}$ prevents $NDC80^{ORF}$ downregulation . . . 35
2.11 $NDC80^{LUTI}$ represses $NDC80^{ORF}$ in *cis* 36
2.12 $NDC80^{LUTI}$ is sufficient to downregulate $NDC80^{ORF}$ 37
2.13 $NDC80^{LUTI}$ expression requires Ime1 38
2.14 Putative Ume6 (*URS1*) and Ndt80 (*MSE*) binding sites in *NDC80* 38
2.15 Ume6 binds to the $NDC80^{LUTI}$ promoter 39
2.16 Ume6 regulates $NDC80^{LUTI}$ expression 40
2.17 Ndt80 regulates $NDC80^{ORF}$ expression 42
2.18 Sister chromatid segregation in meiosis I for the wild-type, the $\Delta NDC80^{LUTI}$ mutant, and the $\Delta 9AUG$ mutant 43
2.19 Re-expression of $NDC80^{ORF}$ is required to resume kinetochore activity in the meiotic divisions 44
2.20 Re-expression of $NDC80^{ORF}$ is required for proper meiotic progression 45
2.21 Mutation of the *NDC80 MSE* site hinders spore formation 46
2.22 *URS1* mutation causes growth defect at high temperature due to a reduced Ndc80 level 46
2.23 Induction of the uORF-free $NDC80^{LUTI}(\Delta 9AUG)$ caused no appreciable growth defect 47
2.24 Model of the *NDC80* gene regulation in budding yeast 48
2.25 Putative uORFs in budding yeast lineage 50

3.1 Regulation of Ndc80 protein synthesis in budding yeast meiosis 54
3.2 The *8lexO* system used to measure Ndc80 protein turnover 55
3.3 The *8lexO* system versus the natural promoter of *NDC80* 56
3.4 Ndc80 turnover in early or late meiotic prophase 56
3.5 Ndc80 turnover in late meiotic prophase or in metaphase I arrest 58
3.6 Ndc80 degradation is unaffected when the four D-boxes are mutated 58
3.7 Truncation analysis of Ndc80 to identify the residues necessary for Ndc80 degradation 59
3.8 Ndc80(Δ2-28) proteins localized to the kinetochore in meiotic prophase 60
3.9 Δ*2-28* does not alter the Ndc80 synthesis repression in meiotic prophase 61
3.10 Sis1 interacts with wild-type Ndc80 and not Ndc80 mutant proteins 62
3.11 Ndc80 degradation requires active proteasomes 63
3.12 Ndc80 degradation does not require recombination, synapsis, and DNA replication 64
3.13 The *ipl1-mn* mutant does not affect Ndc80 synthesis repression in meiotic prophase 65
3.14 *ipl1-mn* stabilizes Ndc80 level independent of microtubules 66
3.15 Phosphorylation sites detected on the wild-type Ndc80 and Ndc80(Δ2-28) proteins in meiotic prophase by mass spectrometry. 67
3.16 Ndc80 phosphorylation sites are required for Ndc80 degradation 68
3.17 Ndc80-7A proteins localized to the partially clustered kinetochores in meiotic prophase 69
3.18 *In vitro* kinase assay for wild-type Ndc80 or Ndc80(Δ2-28) 70
3.19 Growth phenotype associated with the Ndc80 N-terminal tail truncations 71
3.20 Homozygous *CENV-GFP* dots segregation in wild-type and the Δ*2-28* mutant . 71
3.21 Spore formation for the wild-type and the Δ*2-28* mutant 72
3.22 Spore viability for the wild-type and the Δ*2-28* mutant 72
3.23 Sister chromatid segregration in meiosis I for the wild-type versus the Δ*2-28* mutant 73

Acknowledgments

I would like to thank all the past and current members of the Brar and Ünal laboratories for creating a nurturing environment, and for all the stimulating scientific discussions, technical advice, and friendship. I would like to thank the following people who contributed to the execution of this work, its development, or its presentation: Amy Tresenrider, Minghao Chia, David McSwiggen, Hanna Liao, Andrew Liao, Emily Powers, Victoria Jorgensen, Rachel Cohen-Kupiec, Ryan Holly, Folkert van Werven, Gloria Brar, Rebecca Heald, Michael Rape, Kathleen Ryan, Xavier Daczacq, Jeremy Thorner, Jasper Rine, David Drubin, Doug Koshland, Abby Dernburg, Barbara Meyer, Christiane Brune, Leon Chan, Eric Saywer, Jay Goodman, Grant King, and Tina Sing. In addition, Rena Evans provided experimental support for purifying the Ndc80 complex. Lori Kohlstaedt and the Vincent J. Coates Proteomics/Mass Spectrometry Laboratory provided technical assistance for mass spectrometry analysis. Marko Jovanovic from Columbia University performed the TMT quantitative mass spectrometry analysis.

Most of all, I would like to thank Elçin Ünal for her unconditional support of my growth as a scientist and a teacher. This work would not have been possible without Elçin's mentorship and enthusiasm for biology.

I also thank the following funding sources for their support of this and other work in the Ünal lab: the Pew Charitable Trusts (00027344), Damon Runyon Cancer Research Foundation (35-15), National Institutes of Health (DP2 AG055946-01), and Glenn Foundation for Medical Research. My graduate training was further supported by a National Science Foundation Graduate Research Fellowship (DGE-1106400) and National Institutes of Health Traineeship (T32 GM007127). Mass spectrometry was performed by the University of California, Berkeley, Coates Proteomics Lab, which is supported by the National Institutes of Health S10 Instrumentation Grant S10RR025622.

Chapter 1

Introduction

Reproduction is a fundamental property of life. All organisms face the same challenge in reproduction to pass on their genes to the next generation faithfully. Organisms that reproduce asexually utilize mitosis to duplicate and distribute chromosomes to two identical descendants. Conversely, organisms that reproduce sexually utilize an alternative mode of genetic inheritance. An offspring results from the fusion of two sex cells (or gametes). Each gamete has distinct and only half the amount of genetic content as the parents' somatic cells. A specialized cell division named meiosis is essential to generate the haploid gametes. The success of meiosis requires temporal coordination of gene expression, protein turnover, and the modification of the molecular machines that segregate the chromosomes. One such machine is the kinetochore, which bridges between the centromere and the dynamic microtubules to mediate chromosome segregation. The kinetochore undergoes meiosis-specific remodeling, which is necessary to ensure the proper genome reduction and ultimately the progeny's fitness. This chapter will provide an overview of what meiosis is and why it is important, how the kinetochore restructures to accommodate the meiosis-specific chromosome segregation pattern, and how the gene expression and protein turnover programs regulate meiotic genome partitioning.

1.1 Overview of meiosis

The overall goal of meiosis is to reduce the genome content by half. A diploid individual has pairs of chromosomes that consist of the same genes and are derived from each of its two biological parents. These chromosome pairs are known as homologous chromosomes or homologs. After entry into meiosis, a single round of DNA replication occurs, and the duplicated DNA copies, or sister chromatids, become tethered by a ring-like protein complex called cohesin. Meanwhile, developmentally induced double-stranded breaks trigger the homologous chromosomes to undergo recombination and, in some organisms, pairing. The paired homologs are further bound by the synaptonemal complex. After the double-stranded breaks are repaired, two consecutive rounds of chromosome segregation follow: In meiosis

I, the homologs are separated, and in meiosis II, sister chromatids are split. Since there is no intervening round of DNA replication between meiosis I and II, four haploid gametes are generated at the end of meiosis. In the meiosis of budding yeast and male animals, all four meiotic products later develop into mature gametes. However, in the meiosis of female animals, only one haploid gamete develops into an egg and participates in fertilization, while the other three gametes are discarded as polar bodies.

In many organisms, meiosis is part of a larger developmental program called gametogenesis. This program consists of not only genome segregation (meiosis) but also the development of the specialized gamete morphologies. These post-meiotic events are crucial for the gametes' functions. For example, in humans, the male gamete known as sperm matures into a tadpole-like structure with a long tail and a head packed with DNA. Development of the tail is essential for sperm motility and successful fertilization. In contrast, the female gamete known as egg remains as a large, round cell. While the thesis does not focus on these topics specifically, the development of the diverse gamete morphologies is absolutely fascinating and highly relevant to sexual reproduction.

Successful meiosis is essential for the survival and fitness of a species. Deleterious consequences will result if gametes inherit either broken or an incorrect number of chromosomes. Gaining or losing a chromosome is often lethal but, for a subset of chromosomes, an altered copy number can sustain viability but lead to severe defects (reviewed in Zhu *et al.* 2018). For example, aneuploidy (an abnormal number of chromosome) casts growth defects and various cellular stresses in budding yeast (Torres *et al.* 2007; Pavelka *et al.* 2010; Sheltzer *et al.* 2011; Oromendia *et al.* 2012; Zhu *et al.* 2012; Thorburn *et al.* 2013; Dephoure *et al.* 2014; Hwang *et al.* 2017), mouse embryonic fibroblasts (Williams *et al.* 2008), plants (Sheltzer *et al.* 2012) and human cells (Stingele *et al.* 2012; Donnelly *et al.* 2014; Ohashi *et al.* 2015; Aivazidis *et al.* 2017; Meena *et al.* 2015; Passerini *et al.* 2016; Lamm *et al.* 2016). Downs Syndrome in humans, caused by an extra copy of chromosome 21, results in altered facial features, weakened cognitive abilities, and shorten life expectancy (Carfi *et al.* 2014; Roper & Reeves 2006). The Turner syndrome, caused by the loss of an X chromosome in women, results in short height, heart defects, and infertility (Shankar & Backeljauw 2018). Meiotic errors are the leading causes of genetic disorders, congenital disabilities, and miscarriages in humans (Hassold *et al.* 2007). Therefore, accurate chromosome segregation in meiosis is of great importance.

Meiosis is not only a crucial means for gene transmission but an essential platform for evolution. During meiosis, homologous chromosomes undergo recombination, which generates new combinations of alleles for natural selection to act upon. In addition, since only one of the four possible haploid genomes would become an egg in female meiosis, this unequal chance of inheritance drives competition among the genomes to gain preferential segregation into the egg, resulting in a phenomenon known as the "meiotic drive" (reviewed in Malik & Henikoff 2009; Lampson & Black 2017). Understanding meiosis is critical not only for human health but also for grasping the fundamental principles of evolution.

As revealed by studies over the past several decades, the molecular execution of meiosis is highly complex, requiring coordinated regulation on gene expression, cell cycle progres-

sion, and meiosis-specific modifications of the chromosomes. Much of our understanding of meiosis comes from simple model systems, such as *Saccharomyces cerevisiae*, also known as the budding yeast or Baker's yeast. In budding yeast, gametogenesis is called sporulation. This naming is used because the final meiotic products are four spores encapsulated in a structure called a tetrad. Spores contain a thick cell wall (known as the spore wall) to help them resist harsh environments. Although spores look different from the gametes of other organisms, budding yeast shares many essential features of meiosis with more complex eukaryotes. Furthermore, unlike many other organisms, budding yeast is highly genetically tractable. There are also genetic tools to induce a population of yeast cells to undergo meiosis synchronously. Therefore, this organism has been an excellent model system to understand meiotic regulations.

This thesis work uses budding yeast as the experimental system, and thus, most discussions will focus on budding yeast. However, differences between this system and other organisms will be noted when applicable. In the following sections, I will first introduce an essential cellular machine that segregates the chromosomes known as the kinetochore. Next, I will discuss how the kinetochore is modified to establish the meiosis-specific chromosome segregation pattern. Lastly, I will describe the regulatory networks in meiosis and how they control meiotic chromosome segregation.

1.2 Kinetochore structure and function

1.2.1 What is a kinetochore?

The kinetochore is a large, conserved protein complex that mediates chromosome segregation by interacting with dynamic microtubules. This protein complex is comprised of 80-100 polypeptides (depending on the species). It assembles on a specific region of the chromosome named centromere. Organisms (including fission yeast, flies, mice, and human) have "regional centromeres," which are defined by epigenetic marks rather than specific DNA sequences. Budding yeast has a simple centromere known as "point centromere," which is defined solely by DNA sequence. The budding yeast centromere is 125 base pairs (bp) long, subdivided into *CDEI*, *CDEII*, and *CDEIII* regions (reviewed in Biggins 2013). Due to this sequence specificity, the first centromere was cloned in budding yeast (Clarke & Carbon 1980), which significantly aided the studies of kinetochores. During cell divisions, the centromere-localized kinetochore interacts with the microtubules designated to segregate chromosomes. Electron microscopy has shown that each kinetochore binds to a single microtubule in budding yeast mitosis and meiosis (Winey *et al.* 1995; Winey *et al.* 2005), whereas multiple microtubules are attached in metazoans (McDonald *et al.* 1992). Regardless of the number of microtubules interacting with each kinetochore, sufficient force is generated to facilitate the movement of chromosomes in response to microtubule dynamics in all species.

It is important to note that the kinetochore is not a passive bridge between the centromere and the spindle microtubules. Instead, it is an active signaling platform for monitoring

whether chromosomes are attached to the microtubules correctly. In mitosis, to segregate sister chromatids into two daughter cells, the spindle microtubules emanating from opposite spindle poles need to attach to the two sister chromatids. This process is referred to as "bi-orientation". The bi-orientation of sister chromatids allows each daughter cell to inherit precisely one copy of the genome. Since chromosome mis-segregation can be detrimental, cells have evolved a checkpoint known as the spindle assembly checkpoint to ensure that the sister chromatids of each chromosome bi-orient before segregation occurs. The kinetochore serves as the site where many of these checkpoint proteins localize (reviewed in Corbett 2017). Ultimately, the checkpoint induces changes on the microtubule-binding subunits of the kinetochore (often by post-translational modifications) to correct the wrong attachments. In all aspects, the kinetochore is a central hub for chromosome segregation.

1.2.2 Kinetochore composition

Kinetochores are composed of a defined set of subcomplexes that can be biochemically purified or reconstituted from recombinant proteins (Biggins 2013). In a simplified view, these subcomplexes can organize and assemble into two broad categories known as the inner and outer kinetochore (Figure 1.1). The inner kinetochore localizes close to the chromatin, and the outer kinetochore mediates microtubule interactions (Biggins 2013). The subcomplexes in both inner and outer kinetochores are highly conserved from budding yeast to humans. However, the exact organization of these subcomplexes and their dependency on one another to localize to the centromere can vary among organisms. To this end, about 45 core kinetochore subunits have been identified in budding yeast, and about 120 auxiliary components have been identified if both structural and transiently associating proteins are included (De Wulf *et al.* 2003; Westermann *et al.* 2003; Fischbock-Halwachs *et al.* 2019).

1.2.2.1 Inner kinetochore

The kinetochore generally assembles inside out (De Wulf *et al.* 2003). The components that directly bind to the centromere first localize to a newly replicated centromere. Shortly afterward, the other sub-complexes in the inner kinetochore localize to the centromere-binding subunits, and then the outer kinetochore subunits are recruited through interacting with the inner kinetochore components. Therefore, the localization of the inner kinetochore proteins is a key step to initiate the *holo* kinetochore assembly at the specific sites of the chromosome.

In budding yeast, the inner kinetochore consists of the centromeric histone variant Cse4/CENP-A, the CBF3 complex (Ctf13, Skp1, Cep3, and Ndc10), Cbf1, Mif2/CENP-C, Mhf1/CENP-S and Mhf2/CENP-X, and the Ctf19 complex. Cse4 is a histone H3 variant that forms a specialized nucleosome together with H2A, H2B, and H4. The Cse4-containing nucleosome is deposited at the *CDEII* motif of the yeast centromere by the histone chaperone Scm3/HJURP (Furuyama & Biggins 2007; Mizuguchi *et al.* 2007; Cho & Harrison 2011; Stoler *et al.* 2007; Camahort *et al.* 2007; Zhou *et al.* 2011; Cole *et al.* 2011; Krassovsky

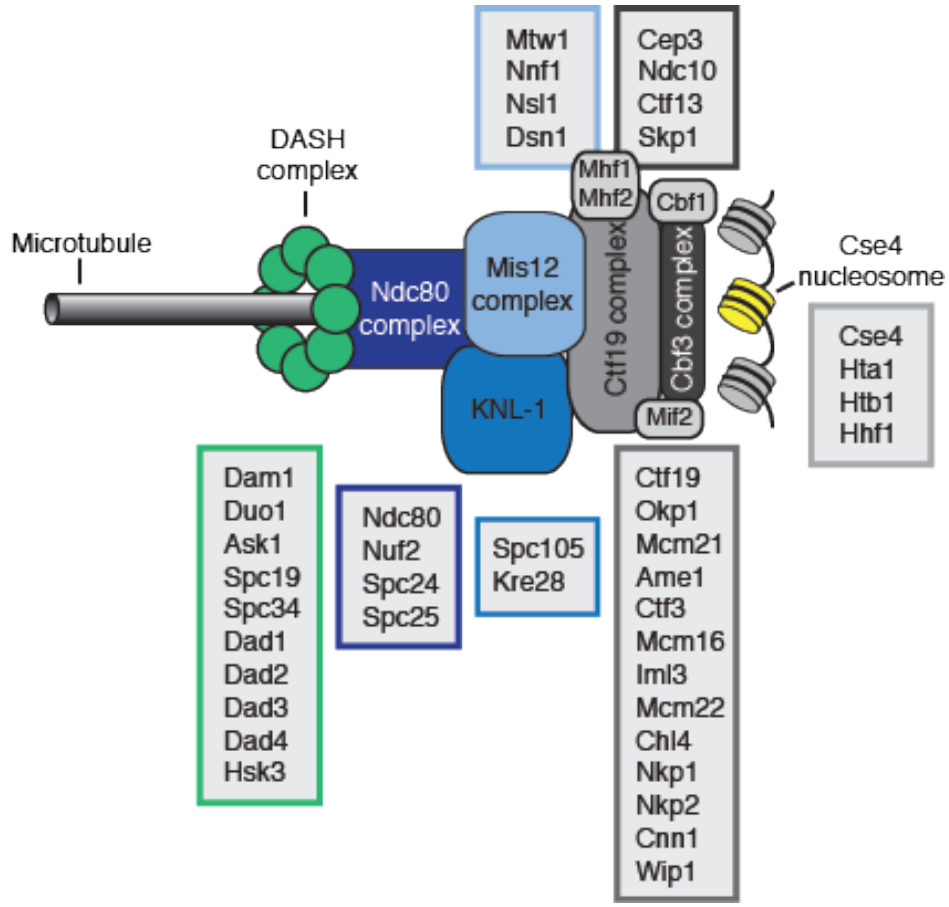

Figure 1.1: The core kinetochore subunits in budding yeast. This figure is derived from Miller *et al.* 2012.

et al. 2012). In addition to Cse4, also binding to the yeast centromere (at the *CDEIII* motif) is the CBF3 complex (Jehn *et al.* 1991; Lechner & Carbon 1991). The assembly of the CBF3 complex requires Sgt1 and Hsp90 through an elaborate pathway that involves phosphorylation, chaperone-mediated protein folding, and ubiquitination (Kaplan *et al.* 1997; Kitagawa *et al.* 1999; Stemmann *et al.* 2002; Bansal *et al.* 2004; Lingelbach & Kaplan 2004; Gillis *et al.* 2005; Catlett & Kaplan 2006). The Ndc10 subunit of the CBF3 complex recruits Cbf1 to bind to the *CDEI* centromeric motif (Cho & Harrison 2012). One report has proposed that Ndc10 loops the centromeric DNA to bring *CDEI* and *CDEIII* in proximity (Cho & Harrison 2012),), generating a centromere-specific structure.

While little is known about the recruitment and function of Mhf1/Mhf2, recent work has provided new insights into the Ctf19 complex. The yeast Ctf19 complex corresponds to the constitutive centromere associated network (CCAN) in higher eukaryotes (Biggins 2013). This complex consists of (1) the COMA complex (Ctf19/CENP-P, Okp1, Mcm21/CENP-O, Ame1), (2) the Ctf3 complex (Ctf3/CENP-I, Mcm16/CENP-H, Mcm22), (3) Cnn1/CENP-

T and Wip1/CENP-W, (4) Chl4/CENP-H and Iml3/CENP-M, and (5) the budding yeast specific Nkp1/Nkp2 heterodimer (Cheeseman *et al.* 2002; Westermann *et al.* 2003; Biggins 2013; Musacchio & Desai 2017; Pekgoz Altunkaya *et al.* 2016). The Ctf19 complex localizes to the kinetochore through interactions with Cse4, the CBF3 complex, and Mif2 (Hinshaw *et al.* 2019). Interestingly, the Ctf19 complex is not only a bridge between the inner and outer kinetochores but also serves to regulate cohesin loading. As cells enter S phase, DDK phosphorylates Ctf19 to generate a binding site for the cohesin loading complex (Hinshaw *et al.* 2017). Therefore, the Ctf19 complex is both important for kinetochore assembly and cohesion.

1.2.2.2 Outer kinetochore

The outer kinetochore of budding yeast consists of the Spc105 complex, the MIND/Mis12 complex, the Ndc80 complex, and the budding yeast specific Dam1 complex. In higher eukaryotes, the Spc105 complex (KNL-1), the MIND/Mis12 complex, the Ndc80 complex form a more extensive, highly conserved network named the KNL-1/Mis12/Ndc80 complex, or KMN (reviewed in Musacchio & Desai 2017). In budding yeast, the Ndc80 and Dam1 complexes are the major microtubule-binding sites of the kinetochore. The heterodimeric Spc105 complex (Spc105/SPC105/Knl-1 and Kre28/Zwint-1) has weak microtubule-binding activity *in vitro*, while its ortholog KNL1 in *C. elegans* binds to microtubules (Cheeseman *et al.* 2006). Although the yeast Spc105 does not directly interact with microtubules, it is a central platform for the spindle assembly checkpoint (see the next section for details).

The tetrameric MIND complex (Mtw1/MIS12, Nnf1/PMF1, Nsl1/Nsl1R, and Dsn1/Dsn1R) is a central bridge that links the inner kinetochore components Mif2 and COMA to the Ndc80 complex, an outer kinetochore component (Maskell *et al.* 2010; Hornung *et al.* 2011; Dimitrova *et al.* 2016). The Dsn1 subunit has an N-terminal extension that causes the autoinhibition of the MIND complex and prevents MIND from binding to Mif2 and COMA. This autoinhibition is removed when Ipl1/Aurora B phosphorylates Dsn1 as MIND localizes to the kinetochore (Dimitrova *et al.* 2016).

The conserved Ndc80 complex has four subunits formed at a stoichiometric ratio of 1:1:1:1 (Ndc80/Hec1, Nuf2/hNuf2, Spc24/hSpc24, Spc25/hSpc25) (Wei *et al.* 2005). The complex has two globular heads and a central coiled-coil rod. One of the globular heads contains the calponin-homology domains (CH) of Nuf2 and Ndc80. The CH domains are highly positively charged, so they readily bind to the negatively charged tubulins, the building blocks of microtubules (reviewed in Biggins 2013). Ndc80 has an unstructured N-terminal tail that also binds to microtubules. This tail is not essential in yeast due to redundant functions with Dam1. However, it contains Ipl1/Aurora B kinase phosphorylation sites and plays a role in correcting attachment errors (Akiyoshi *et al.* 2009). Also, Ndc80 contains a loop in the middle of the coiled-coil rod that is important for Dam1 interaction (Maure *et al.* 2011; Lampert *et al.* 2013).

The Ndc80 complex localizes to the kinetochore in two ways: First, the C-terminal extension of Dsn1 recruits the Ndc80 complex by interacting with Spc24/Spc25 heterodimer

(Maskell *et al.* 2010; Malvezzi *et al.* 2013). Second, Cnn1 (Ctf19 subunit) competes with Dsn1 to bind to the same sites on Spc24/Spc25 (Malvezzi *et al.* 2013). Once the Ndc80 complex localizes to the kinetochore, it undergoes a conformational change (Scarborough *et al.* 2019). A recent study showed that in solution, the Ndc80 complex adopts a tight bending conformation, leading to the auto-inhibition of microtubule binding. This bending conformation can be relieved when the Ndc80 complex binds to the MIND complex (Scarborough *et al.* 2019). This mechanism may prevent the Ndc80 complex from prematurely interacting with microtubules until it assembles onto the kinetochore. Alternatively, this pathway may ensure that the kinetochore assembles hierarchically (Scarborough *et al.* 2019), from inner kinetochore toward outer kinetochore (De Wulf *et al.* 2003; Biggins 2013).

When budding yeast kinetochores begin to interact with a microtubule, they first attach to the lateral surface of the microtubule. Next, such attachments are converted into stable end-on attachments (Tanaka *et al.* 2007; Tanaka 2010). The Dam1 complex is necessary for end-on attachments to occur (Tanaka *et al.* 2007). This complex is composed of 10 essential subunits: Ask1, Dad1, Dad2, Dad3, Dad4, Dam1, Duo1, Hsk3, Spc19, and Spc34 (Hofmann *et al.* 1998; Jones *et al.* 1999; Cheeseman *et al.* 2001a; Cheeseman *et al.* 2001b; Enquist-Newman *et al.* 2001; Janke *et al.* 2002; Li *et al.* 2002; De Wulf *et al.* 2003; Li *et al.* 2005; Miranda *et al.* 2005; Westermann *et al.* 2005). These subunits form a ring-like structure encircling the microtubule both *in vitro* and *in vivo* (Miranda *et al.* 2005; Westermann *et al.* 2005; Wang *et al.* 2007; Ramey *et al.* 2011b; Ramey *et al.* 2011a; Kim *et al.* 2017; Jenni & Harrison 2018). Aside from the ring structure, the Dam1 complex also has flexible extensions that link it to partner protein complexes, including the Ndc80 complex and the microtubule (Jenni & Harrison 2018), even though these partners are in different orientations, with unmatched stoichiometry and symmetry. Both microtubules and KMN control the localization of the Dam1 complex to kinetochore (Ramey *et al.* 2011b; Ramey *et al.* 2011a; Janke *et al.* 2002; Li *et al.* 2002; Tanaka *et al.* 2007; Miranda *et al.* 2005). Lastly, oligomerization of the Dam1 complex is also critical to support stable attachments (Umbreit *et al.* 2014), and is disrupted when Aurora B/Ipl1 phosphorylates Dam1 (Zelter *et al.* 2015). Although the Dam1 complex is not found in vertebrates, a functional homolog has been discovered, known as the Ska complex (Hanisch *et al.* 2006; Daum *et al.* 2009; Gaitanos *et al.* 2009; Raaijmakers *et al.* 2009; Theis *et al.* 2009; Welburn *et al.* 2009).

1.2.3 Regulation of microtubule-kinetochore attachments

Over the past 20 years, the cell cycle field has gained a tremendous amount of molecular insight into how microtubule-kinetochore attachments are regulated. We now know most of the molecular players, which are described extensively in recent reviews (Biggins 2013; Corbett 2017). Here, I will summarize the main points and highlight the role of the kinetochore in correcting wrong microtubule attachments in a process known as error correction.

Mitotic cells use the spindle assembly checkpoint to monitor whether kinetochores and microtubules are correctly attached. Central to this checkpoint is the idea of "tension-sensing," or the ability of the cell to detect counteracting forces generated from sister chromatid co-

hesion and microtubule instability. During DNA replication, cohesion between the sister chromatids is established. In prometaphase, which occurs after DNA replication, microtubules are rapidly growing and shrinking (microtubule instability). This dynamic behavior of microtubules can generate force toward specific directions. When the two sister kinetochores are attached to microtubules emanating from the opposite spindle poles (bi-oriented), spindle forces pull the sister kinetochores toward the poles, while the cohesion between the sister chromatids resists this pulling. Therefore, tension across the sister kinetochores forms. The presence of tension signifies correct microtubule-kinetochore attachment and leads to the silencing of the spindle assembly checkpoint and the metaphase-to-anaphase transition.

Kinetochore-microtubules attachments are unstable in the absence of tension. In *vivo* experiments in both budding yeast and grasshopper spermatocytes show that once the kinetochore experiences tension, it maintains stable attachment to microtubules (Nicklas & Koch 1969; Nicklas 1997; Dewar *et al.* 2004). Two mechanisms have been proposed to explain how the microtubule-kinetochore attachments lacking tension become destabilized. First, tension directly modulates microtubule dynamics (Franck *et al.* 2007; Akiyoshi *et al.* 2010). In *vitro* experiments showed that when tension increased, the rate of microtubule catastrophes (rapid microtubule shrinkage) decreased, and microtubule rescue occurred more frequently. When microtubules were assembling, kinetochores stayed bound to microtubules longer (Akiyoshi *et al.* 2010). Therefore, tension results in a microtubule state that favors kinetochore binding.

In the second mechanism, the Aurora B/Ipl1 kinase phosphorylates kinetochore subunits, such as Dam1 and Ndc80 (Cheeseman *et al.* 2002; Akiyoshi *et al.* 2009). Such phosphorylation weakens the interaction between kinetochores and microtubules. Since the microtubule surface is mostly negatively charged, phosphorylation on kinetochores can lead to charge repulsion (Biggins 2013). Besides weakening attachments, Dam1 phosphorylation also reduces its ability to oligomerize and assembles into rings (Wang *et al.* 2007), decreasing its interaction with the Ndc80 complex (Lampert *et al.* 2010; Tien *et al.* 2010), and promoting microtubule catastrophe (Akiyoshi *et al.* 2010; Sarangapani *et al.* 2013). Thus, Aurora B/Ipl1 alters the kinetochore in multiple ways to weaken the wrong attachments.

When kinetochores become unattached, the kinase Mps1 binds to Ndc80. How Mps1 recruitment occurs is debatable. In one model, Mps1 and microtubules compete for Ndc80 binding. In support of this idea, microtubules suppress Mps1-Ndc80 binding *in vitro* (Hiruma *et al.* 2015; Ji *et al.* 2015). In another model, Mps1 binds Ndc80 constitutively but fails to phosphorylate Spc105 once microtubule attachment occurs (Aravamudhan *et al.* 2015). Regardless of how Mps1 is recruited, it is clear that Mps1 phosphorylates the MELT repeats on Spc105. Such phosphorylation recruits Bub1/Bub3 to Spc105. Once Bub1 is at the kinetochore, Mps1 phosphorylates it, which then recruits Mad1:Mad2 (London & Biggins 2014; Ji *et al.* 2017). Lastly, Mps1 phosphorylates Mad1 to promote Mad1-Cdc20 interaction (Hardwick *et al.* 1996; Faesen *et al.* 2017; Ji *et al.* 2017). Through structural changes that are still not understood, the mitotic checkpoint complex (MCC) is then assembled.

The MCC consists of Cdc20, Mad2, and BubR1 (Mad3 in yeast). Cdc20 is the adaptor of the ubiquitin ligase Anaphase Promoting Complex (APC) and confers APC's substrate specificity. When Cdc20 and APC interact, APC becomes active to trigger the metaphase-

to-anaphase transition (See details below). Mad2 has two conformations—"open" (O-Mad2) and "closed" (C-Mad2). O-Mad2 is recruited to unattached kinetochore and converted into C-Mad2 by Mad1:C-Mad2 at the kinetochore. C-Mad2 then binds to Cdc20, and BubR1/Mad3 stabilizes this interaction (Sczaniecka *et al.* 2008; Tipton *et al.* 2011; Chao *et al.* 2012; Faesen *et al.* 2017). As a result, Cdc20 is sequestered away from APC, leaving APC inactive.

Once all the kinetochores correctly attach to spindles, the spindle assemble checkpoint is silenced. Ndc80 binding to microtubules suppresses Mps1 activity. Aurora B/Ipl1 activity at the outer kinetochore is reduced (Lampson & Cheeseman 2011; van der Horst & Lens 2014; Krenn & Musacchio 2015). Since both kinases become less active on the kinetochore, phosphatases PP2A and PP1 will dephosphorylate Spc105 (Liu *et al.* 2010; Rosenberg *et al.* 2011; Meadows *et al.* 2011; London *et al.* 2012), leading to dissociation of the spindle assembly checkpoint components. The existing MCC are removed by ubiquitinylation and degradation of $Cdc20^{MCC}$ (Pan & Chen 2004; King *et al.* 2007; Reddy *et al.* 2007; Ge *et al.* 2009; Foe *et al.* 2011), as well as by extraction of Mad2 by p31comet and the AAA+ ATPase TRIP13 in animal cells (Teichner *et al.* 2011; Tipton *et al.* 2012; Eytan *et al.* 2014; Wang *et al.* 2014; Miniowitz-Shemtov *et al.* 2015; Ma & Poon 2016).

Anaphase begins when the activated APC^{Cdc20} ubiquitinates a group of mitotic regulators, leading to their proteasomal degradation. Among these regulators is the securin Pds1, an inhibitor of the separase Esp1. Pds1 degradation leads to activation of Esp1, which cleaves the Scc1/Mcd1 subunit of the cohesin complex. Once the cohesin is destroyed, the sister chromatids become liberated to move toward the spindle poles. Separation of the duplicated DNA copies is then completed.

1.3 Establishment of meiotic chromosome segregation

Although meiosis and mitosis use many of the same cell cycle regulators, unique modifications to the chromosome segregation machinery are required to achieve meiosis. Chromosomes segregate in two steps during meiosis, rather than one step during mitosis: In meiosis I, the homologous chromosomes separate. Next, the sister chromatids segregate in meiosis II. There are a few challenges to establish this segregation pattern. First, homologous chromosomes, instead of sister chromatids, need to bi-orient in meiosis I. Also, tension needs to present across the homologous chromosomes to satisfy the spindle assembly checkpoint, which is active in metaphase I (Shonn *et al.* 2000; Shonn *et al.* 2003; Tsuchiya *et al.* 2011). In mitosis, tension is present because the sister chromatids are physically connected to one another through cohesion, which resists the pulling force of the microtubules. How do the homologous chromosomes connect to one another in meiosis? Furthermore, how does meiosis promote homologous chromosomes to attach to the spindle microtubules emanating from opposite spindle poles, while inhibiting sister chromatids from doing so?

By the same logic, the sister chromatids need to bi-orient, and tension needs to be established between them for them to segregate in meiosis II. However, since cohesins would have been cleaved in meiosis I, the sister chromatids would have no physical linkage by

meiosis II. There is also no DNA replication between meiosis I and meiosis II, so cohesion could not be re-generated between the sister chromatids. How is the physical connection between the sister chromatids maintained until meiosis II?

Studies over the past three decades have revealed four key events that altogether solve these problems. Two of these events are meiosis-specific chromosome transactions: (1) recombination and synapsis and (2) protection of the centromeric cohesion in meiosis I. The other two events require modulation of the kinetochore: (1) sister kinetochore co-orientation during meiosis I and (2) restriction of microtubule-kinetochore interactions in meiotic prophase.

1.3.1 Recombination and synapsis

Recombination and synapsis establish a physical linkage between the homologous chromosomes. These two topics have been reviewed extensively (Hunter 2015) and will be mentioned only briefly to highlight their connection to meiotic chromosome segregation. In budding yeast, these two events start during DNA replication and finish in meiotic prophase. To initiate recombination, the meiosis-specific endonuclease Spo11 induces double-stranded breaks throughout the genome (reviewed in Keeney 2001; Keeney 2008). The repair of the double-stranded breaks results in exchanges on the homologous chromosomes. Since cohesins tether the sister chromatids, the recombined sections of the homologous chromosomes become interwound. Recombination also allows the homologs to find one another and pair. In budding yeast and mice, following pairing, the homologous chromosomes become synapsed by a large protein complex called the synaptonemal complex (reviewed in Zickler & Kleckner 1999; Zickler & Kleckner 2015). In other organisms, such in *C. elegans*, synapsis occurs independent of homologous recombination but requires chromosomal regions called the pairing centers (MacQueen *et al.* 2005; Albertson *et al.* 1997, reviewed in Rog & Dernburg 2013). As a result of recombination and synapsis, homologous chromosomes become physically connected. The sister-chromatid cohesion distal to the chiasmata (sites of reciprocal recombination/crossover) resists the pulling force exerted by the spindle microtubules in prometaphase I. As a result, the tension required to silence the spindle assembly checkpoint can be generated.

Since double-stranded breaks are generated during recombination, these breaks need to be repaired entirely before the chromosomes segregate. Otherwise, chromosome breakage can happen, which could lead to cell death. A checkpoint called the recombination checkpoint monitors the completion of DNA repair. This checkpoint uses the canonical DNA damage checkpoint machinery to control the activity of cyclin-dependent kinase (CDK) and a key transcription factor Ndt80 (reviewed in Winter 2012). Ndt80 is required to express the genes needed for the meiotic divisions (Xu *et al.* 1995; Benjamin *et al.* 2003; Chu *et al.* 1998; Chu & Herskowitz 1998; Hepworth *et al.* 1998; Brar *et al.* 2012; Cheng *et al.* 2018). When the checkpoint is active (i.e., DNA is not entirely repaired), Swe1 inactivates CDK by phosphorylating the tyrosin-19 of Cdc28 (Leu & Roeder 1999). At the same time, a high level of a repressor of *NDT80* called Sum1 is maintained, leading to delayed transcription of *NDT80* (reviewed in Winter 2012). Also, the checkpoint protein Mek1 phosphorylates

the small pool of Ndt80 that is present in meiotic prophase. As a result, Ndt80's nuclear localization is restricted (Chen *et al.* 2018a; Wang *et al.* 2011). Only until the checkpoint is turned off can Ime2 phosphorylate Ndt80 to fully activate Ndt80, which then induces expression of its target genes (Tung *et al.* 2000; Chen *et al.* 2018a). All these mechanisms ensure that meiotic cells complete DNA repair before chromosome segregation.

1.3.2 Centromeric cohesion protection

To segregate in meiosis II, sister chromatids need to maintain their physical connection until metaphase II. Otherwise, sister chromatids would segregate randomly, leading to inviable gametes containing abnormal numbers of chromosomes. To sustain cohesion between sister chromatids past meiosis I, meiotic cells have evolved a mechanism to remove cohesins in two steps. Cohesins at chromosome arms are cleaved in meiosis I while the centromeric cohesins are protected from cleavage until meiosis II. Two molecular players are central to this protection mechanism: (1) a meiosis-specific cohesin subunit Rec8 and (2) Sgo1-PP2A.

Cohesin consists of four core subunits: Smc1, Smc3, Scc3, and Scc1/Mcd1. In meiosis, Rec8 replaces Scc1/Mcd1. Phosphorylation of Scc1/Mcd1 and Rec8 sensitizes them for cleavage by separase Esp1, which is activated at the metaphase-to-anaphase transition. The polo-like kinase Cdc5 phosphorylates Scc1/Mcd1 in mitosis, whereas Cdc5, the Dbf4-dependent kinase Cdc7, and Hrr25 most likely phosphorylate Rec8 in meiosis (Alexandru *et al.* 2001; Katis *et al.* 2010; Brar *et al.* 2006). However, unlike Scc1/Mcd1, Rec8 can be dephosphorylated by the phosphatase $PP2A^{Rts1}$. A highly conserved protein named shugoshin 1 (guardian spirit in Japanese), or Sgo1, localizes to kinetochore in prometaphase I and recruits $PP2A^{Rts1}$ to dephosphorylate the Rec8 proteins at the centromeric region (Riedel *et al.* 2006; Kitajima *et al.* 2006; Marston *et al.* 2004). As a result, Rec8 cleavage does not occur at the centromere in meiosis I. This residual cohesion is sufficient to generate tension across the sister chromatids, allowing them to bi-orient in meiosis II. Since Sgo1 no longer localizes to the kinetochore in meiosis II, the centromeric Rec8 proteins can be phosphorylated sufficiently and cleaved. The shugoshin protein family protects centromeric cohesion in budding yeast, fission yeast, flies, plants, and mice (Kitajima *et al.* 2006; Marston *et al.* 2004; Rabitsch *et al.* 2004; Katis *et al.* 2004; Tang *et al.* 1998; Hamant *et al.* 2005; Lee *et al.* 2008), suggesting that this strategy to ensure the success of meiosis II is conserved.

1.3.3 Sister kinetochore co-orientation

In meiosis I, the homologous chromosomes, instead of the sister chromatids, need to bi-orient in order to segregate. How does a meiotic cell suppress sister bi-orientation while promoting homolog bi-orientation? Budding yeast employs two strategies. The first one is to use a specialized protein complex called monopolin. This complex consists of four subunits: Lrs4, Csm1, Hrr25, and Mam1. Lrs4 and Csm1 localize to the nucleolus during the mitotic cell cycle and function to silence the rDNA locus as a means to prevent unequal sister chromatid exchange between the rDNA repeats (Huang *et al.* 2006; Waples *et al.* 2009).

After exiting from meiotic prophase, the transcription factor Ndt80 induces the expression of Mam1. Concomitantly, the polo-like kinase Cdc5 triggers the release of Csm1 and Lrs4 from the nucleolus. After release, Lrs4 is hyper-phosphorylated by Dbf4-dependent kinase Cdc7 and Cdc5 (Spo13 acts with Cdc5). Such hyper-phosphorylation is thought to help the monopolin complex to localize to the kinetochore (Lee & Amon 2003; Clyne *et al.* 2003; Matos *et al.* 2008). The monopolin complex resembles a "V" shape, with two Csm1 proteins whose head domains are separated by about 10 nm (Corbett *et al.* 2010). It has been proposed that the two Csm1 heads respectively bind to the Dsn1 protein on either of the two sister kinetochores, thereby crosslinking the sister kinetochores (Corbett *et al.* 2010; Plowman *et al.* 2019). Consistent with this idea, when recombinant monopolin complex is added to mitotic kinetochores, these kinetochores bind to microtubule as strongly as meiosis I kinetochores (Sarangapani *et al.* 2014). After the monopolin complex localizes to the kinetochore, the kinase activity of Hrr25 establishes monopolar attachment *in vivo* by an unknown mechanism (Petronczki *et al.* 2006). The fusion of the sister kinetochores facilitates the sister chromatids to co-orient in meiosis I and allow the homologous chromosomes to bi-orient at this time. Recent studies have also identified the functional homologs of the monopolin complex in fission yeast (Moa1) (Yokobayashi & Watanabe 2005) and mice (MEIKIN) (Kim *et al.* 2015). These findings suggest that regulating sister kinetochore mono-orientation is a conserved feature of meiosis I.

1.3.4 Delay in microtubule-kinetochore interaction

The second strategy to promote homolog bi-orientation is to delay microtubule-kinetochore interactions until prometaphase I. Two mechanisms achieve this delay: (1) altering kinetochore composition and (2) modulating spindle formation. During the mitotic cell cycle of budding and fission yeast, the *holo* kinetochore assembles on the centromere and is connected to a microtubule throughout the cell cycle. During DNA replication, the whole kinetochore transiently dissociates from the centromere, and then rapidly re-assembles and reattaches to microtubules once the centromere is replicated (Kitamura *et al.* 2007). In contrast, in the pre-meiotic S phase and meiotic prophase, the Ndc80 complex and the Dam1 complex do not enrich on the kinetochore (Asakawa *et al.* 2005; Miller *et al.* 2012; Meyer *et al.* 2013; Kim *et al.* 2013; Meyer *et al.* 2015). Ndc80 turnover triggers the disassembly of the Ndc80 complex (Asakawa *et al.* 2005; Miller *et al.* 2012; Meyer *et al.* 2015). Since the Ndc80 complex constitutes one of the major microtubule-binding sites, its disassembly renders meiotic prophase kinetochores inactive. Meanwhile, the kinetochores become dispersed from the spindle pole bodies (SPB) (Meyer *et al.* 2013; Kim *et al.* 2013; Meyer *et al.* 2015), presumably due to the lack of microtubule-kinetochore interaction and telomere movement. Both the outer kinetochore disassembly and the kinetochore dispersion require the Aurora B/Ipl1 kinase activity (Meyer *et al.* 2013; Kim *et al.* 2013).

Aside from altering kinetochore composition, meiotic cells also modify the timing of spindle formation in meiosis in order to delay microtubule-kinetochore interactions. During the mitotic cell cycle, the SPBs separate within minutes after duplication. In contrast, they

remain linked by the half-bridge for hours in meiotic prophase (Li *et al.* 2015; Li *et al.* 2017). Cohesin may also contribute to SPB linkage indirectly in budding yeast meiosis (Shirk *et al.* 2011; Jin *et al.* 2012). The prolonged tethering of SPBs requires high Ipl1/Aurora B activity and low Clb1- and Clb4-CDK activity. In meiotic prophase, Ipl1 localizes to the SPBs to inhibit SPB separation (Kim *et al.* 2013; Shirk *et al.* 2011). How Ipl1 achieves such inhibition remains unknown.

After cells exit meiotic prophase, the SPBs quickly separate. The rise of Clb1- and Clb4-CDK activities, facilitated by Ndt80 activation, is thought to induce SPB splitting by phosphorylating Ipl1 and delocalizing it from SPBs. Consistent with this idea, overexpression of these cyclins in meiotic prophase leads to de-localization of Ipl1 from nuclear microtubules and untimely SPB separation (Kim *et al.* 2013). Before the SPBs separate, the half-bridge component Mps3 is phosphorylated and cleaved at its N-terminus (Li *et al.* 2017). The N-terminus of Msp3 binds to the meiosis-specific protein Ndj1, which is degraded after meiotic prophase (Li *et al.* 2015). It has been proposed that Mps3 cleavage and Ndj1 degradation lead to disassembly of Mps3 oligomers and SPB separation (Li *et al.* 2017). Interestingly, phosphorylation at the cytoplasmic side of the half-bridge also regulates SPB separation (Elserafy *et al.* 2014; Avena *et al.* 2014). Therefore, meiotic cells use both post-translational modification and irreversible proteolysis to ensure the timely separation of the SPBs and spindle formation.

These meiosis-specific alterations on both kinetochore and the SPB function to restrict microtubule-kinetochore interaction in meiotic prophase. Why is such restriction critical to meiotic success? One can answer this question by analyzing the mutant condition where kinetochore interact with spindles prematurely. This condition can result from overexpressing Ndc80 together with cyclin Clb1 or Clb3 in meiotic prophase (Miller *et al.* 2012). The effect of this premature kinetochore-microtubule interaction is drastic: sister chromatids, instead of homologous chromosomes, segregate in meiosis I (Carlile & Amon 2008; Miller *et al.* 2012). Essentially, meiosis I is turned into mitosis or meiosis II. Recombination is not affected by this mutant condition, but the monopolin complex fails to localize to the kinetochore in prometaphase I. Also, centromeric cohesins are not protected in meiosis I even though Sgo1-PP2A localization is not affected (Miller *et al.* 2012). Expressing the monopolin complex in mitosis can co-orient sister chromatids (Monje-Casas *et al.* 2007). However, this co-orientation cannot occur if kinetochore-microtubule interaction precedes monopolin expression (Miller *et al.* 2012). This observation suggests that monopolin localization requires microtubule-free kinetochores. It is worth to note that premature microtubule-kinetochore interaction also disrupts chromosome segregation in mice oocytes (Davydenko *et al.* 2013). Therefore, this strategy of delaying kinetochore-microtubule interaction until after sister co-orientation is evolutionarily conserved.

In summary, all four of these events are required to establish the meiotic chromosome segregation pattern. Mutants that disrupt any of these events lead to meiotic defect, highlighting their significance. It is important to note that these events need to occur at the right stage of meiosis. For example, the centromeric Rec8 proteins need to be protected and the monopolin complex needs to localize to the kinetochore in meiosis I, rather than meiosis II.

If these two events were to occur in meiosis II, meiotic failure would result. Therefore, there must exist temporal regulation to ensure these meiotic events happening at the right place and right time. In the following two sections, I will describe two of such crucial regulation, namely controlling gene expression and protein turnover.

1.4 Gene regulation in meiosis

As with most developmental processes, meiosis is driven by waves of stage-specific gene expression. This temporal regulation restricts the molecules that perform specific functions to particular meiotic stages and ensures meiotic events occur in a defined, unidirectional fashion. An ordered series of transcription factors, known as transcription cascades, help establish the temporal order of gene expression. In budding yeast, two master transcription factors, Ime1 and Ndt80, control the expression of early and middle meiotic genes, respectively. Expression of Ndt80, the later transcription factor, depends on Ime1 activity and the completion of cellular events induced by Ime1 (Chu & Herskowitz 1998; Xu *et al.* 1995). Decades of research have focused on the transcription relay between Ime1 and Ndt80 and demonstrated that the timely expression of Ime1 and Ndt80 is crucial to meiotic success.

Recently, RNA-seq and ribosome profiling analyses have provided higher temporal resolution of the yeast meiotic gene expression program. Such global information reveals which cellular events occur at the same time, how they are coordinated, and what other transcription factors may regulate these events. Furthermore, non-canonical transcription and translation strategies have been observed in meiosis, leaving the question of how these features alter and regulate gene expression. The following section will describe our current knowledge about the gene expression program of budding yeast meiosis, as well as the regulation of Ime1 and Ndt80.

1.4.1 A global view of meiotic gene expression

With the advancement of genome-wide sequencing techniques, we can now obtain global transcription and translation measurements over time. Two methods are widely used. One is mRNA-seq, which quantifies the mRNA level expressed by each gene. Another is ribosome profiling, which maps the genomic regions of active translation based on the sequences protected by ribosomes ("footprints") and the footprint signatures (Ingolia *et al.* 2009). These two techniques have greatly facilitated the identification of novel gene regulators, as well as the spatio-temporal regulation of cellular processes.

In 2012, Brar *et al.* provided the first comprehensive characterization of the yeast meiotic gene expression program using matched mRNA-seq and ribosome profiling datasets. This groundbreaking study revealed an impressive extent and magnitude of gene regulation in meiosis (Brar *et al.* 2012). Almost the entire yeast genome (6134 out of 6708 genes) is translated at some point in meiosis, and most of the genes are temporally regulated. More than 2/3 of the genes vary in their expression by at least 10-fold.

Based on when a gene is expressed over the course of meiosis, genes can be organized into hierarchical clusters based on similarity. The genes in each cluster share a similar temporal expression pattern, and often participate in the same cellular function. For example, *SPO11* and *DMC1* reside in the same cluster and become highly expressed during recombination, a process that requires both Spo11 and Dmc1. Specifically, Spo11 includes double-stranded breaks, and Dmc1 facilitates strand invasion together with Rad51 (reviewed in Hunter 2015). Broadly, four groups of genes are apparent based on expression timing (Brar *et al.* 2012). The first group expresses before meiosis I and becomes repressed in later meiotic stages. The second group expresses during the meiotic divisions and spore development, but not earlier. The third group is on throughout meiosis. The last group is off mostly in meiosis, except in a narrow window. Many genes in the first group are controlled by Ime1, while Ndt80 regulates many in the second group. Given the importance of Ime1 and Ndt80, the following subsections will describe the regulation of these two transcription factors.

1.4.2 Ime1

IME1 (or "Inducer of MEiosis I") encodes the master transcription factor that controls entry into meiosis (Kassir *et al.* 1988). The decision to enter meiosis is complicated. A budding yeast cell integrates information about its sex type (mating type in yeast), respiratory state, and nutritional cues from its surroundings. Meiosis initiation requires a yeast cell to be a *MAT***a**/*MAT*α diploid (see details below), respiratory competent and subjected to nitrogen depletion and a non-fermentable carbon source. Together, these signals converge on the *IME1* promoter to control *IME1* expression (reviewed in van Werven & Amon 2011, Smith *et al.* 1990). Overexpression of Ime1 can bypass the nutritional and mating-type controls and causes untimely initiation of meiosis (Smith & Mitchell 1989; Mitchell & Bowdish 1992), highlighting Ime1's essential role in entry to meiosis. Therefore, understanding the regulation of *IME1* is central to understand meiotic entry.

The *IME1* promoter is over two kilobases (reviewed in van Werven & Amon 2011), which is exceptionally long in budding yeast. Residing in this promoter is a long non-coding RNA (lncRNA) transcript called *IRT1*, which is transcribed in the same direction as *IME1* (van Werven *et al.* 2012). The expression of *IRT1* requires a transcription factor called Rme1 ("Repressor of MEiosis 1") (Covitz *et al.* 1991; Mitchell & Herskowitz 1986). *IRT1* transcription recruits the histone methyltransferases Set2 and the Set3 histone deacetylase complex to establish repressive chromatin marks at the promoter of *IME1*, leading to *IME1* transcription repression (van Werven *et al.* 2012). Curiously, another gene that facilitates meiotic entry, *IME4*, is also subjected to lncRNA-mediated repression, although this lncRNA is expressed in the opposite direction of *IME4* (antisense). Therefore, two lncRNAs play a central role in regulating meiotic entry in budding yeast.

How do mating type and nutritional signals control *IME1* expression? The mating type of a yeast cell is defined by a single genetic locus called *MAT* (reviewed in Haber 2012). Two versions of the *MAT* locus exist, namely *MAT***a** and *MAT*α. Haploid yeast cells can have either the *MAT***a** or the *MAT*α version, whereas diploid cells have both (heterozygous

at the *MAT* locus). The different transcription factors encoded by *MAT***a** and *MAT*α regulate the expression of distinct genes based on a cell's mating type. For example, diploid cells express the transcription factors a1 and α2, which form a heterodimeric repressor that inhibits transcription of haploid-specific genes. Since Rme1 is a target of a1/α2, *IRT1* is not expressed in diploids, leading to *IME1* expression. In haploid cells, a1/α2 is absent, so Rme1 is constitutively active, and *IME1* becomes repressed.

IME1 expression requires the depletion of fermentable carbon sources, such as glucose and nitrogen. In the presence of glucose, budding yeast ferments and activates the Ras/protein kinase A (PKA) signaling pathway. High PKA levels inactivate two stress-related transcription factors Msn2 and Msn4 via phosphorylation (Smith *et al.* 1998). Msn2 and Msn4 induce expression of genes that have a stress-response element (Görner *et al.* 1998; Martínez-Pastor *et al.* 1996), which is also present in the *IME1* promoter (Sagee *et al.* 1998). Thus, high PKA levels repress *IME1* expression. Also, PKA activates a repressor of *IME1* called Sok2 by phosphorylation, as well as the kinase Rim15, which regulates *IME1* expression by an unknown mechanism. Asides from PKA, the AMP kinase of budding yeast Snf1 also responds to glucose level and activates *IME1* expression by inhibiting Tup1-Ssn6, a repressor of *IME1* (Mizuno *et al.* 1998). How nitrogen starvation alters *IME1* expression mechanistically is not well understood.

Once a sufficient level of Ime1 is present, expression of the "early meiotic genes" are activated, including *IME2*, a meiosis-specific CDK-like kinase, and genes for pre-meiotic DNA replication, recombination, homolog pairing, and synapsis. A DNA-binding protein called Ume6 represses many of these genes during the mitotic cell cycle (Buckingham *et al.* 1990; Strich *et al.* 1994). Ume6 binds to a sequence motif called upstream regulatory sequence 1 (*URS1*) and recruits Sin3 and Rpd3, which are subunits of a histone deacetylase complex, to establish repressive chromatin at the target genes. As a result, the transcription of these target genes becomes repressed (Anderson *et al.* 1995; Kadosh & Struhl 1997; Kadosh & Struhl 1998b; Kadosh & Struhl 1998a; Rundlett *et al.* 1998). When yeast cells enter meiosis, Rim11 and Mck1 phosphorylate Ume6. Phosphorylated Ume6 interacts with Ime1 to form a transcription coactivator. This coactivator induces the expression of the early meiotic genes (Bowdish *et al.* 1995; Rubin-Bejerano *et al.* 1996; Washburn & Esposito 2001; Malathi *et al.* 1997; Xiao & Mitchell 2000), which sets meiosis in motion.

1.4.3 Ndt80

After DNA repair finishes in meiotic prophase, meiotic yeast cells activate the transcription factor Ndt80, which autoregulates itself while inducing expression of a large group of genes referred to as "middle meiosis genes." These genes include the M-phase cyclins Clb1, Clb4 and Clb3; the polo-like kinase (PLK) Cdc5; the monopolin complex subunit Mam1; the components and regulators of spore development; and many others (Benjamin *et al.* 2003; Chu *et al.* 1998; Chu & Herskowitz 1998; Hepworth *et al.* 1998; Sourirajan & Lichten 2008; Brar *et al.* 2012; Berchowitz *et al.* 2013; Cheng *et al.* 2018). These genes are critical for

the meiotic divisions (See previous sections for details), organelle remodeling (Sawyer *et al.* 2019), and spore development (reviewed in Neiman 2005).

Since a previous section ("Recombination and synapsis") has described how Ndt80 activity is regulated post-translationally, this section will focus on how Ndt80 regulates its target genes and a meiotic process known as "meiotic commitment." Almost all the Ndt80 target genes have a consensus sequence motif in their promoters called the middle sporulation element (*MSE*) (Ozsarac *et al.* 1997; Hepworth *et al.* 1998). Some of the Ndt80 target genes are also regulated by the repressor Sum1, which inhibits the expression of these genes during the mitotic cell cycle, most likely by competing for the core *MSE* site with Ndt80 (Pierce *et al.* 2003). Interestingly, Sum1 binds to the promoter of *NDT80* in meiotic prophase (Wang *et al.* 2005) and contributes to Ndt80 repression in meiotic prophase when the recombination checkpoint is active. At meiotic prophase exit, Ndt80 proteins quickly accumulate due to both the removal of Sum1, a negative regulator, and establishment of a positive-feedback loop made from Ndt80 autoregulation and Ndt80 activation by Cdc5, an Ndt80 target.

The accumulation of Ndt80 is crucial for meiotic commitment, which refers to the point in meiosis, once past it, sporulation will go to completion despite nutritional changes. Poor nutrients induce sporulation; however, budding yeast can exit meiosis and resume growth when nutrients are added to its surroundings, even after undergoing pre-meiotic replication, recombination, pairing, and synapsis. This phenomenon known as "return to growth" readily occurs in *ndt80*Δ cells but does not happen once the yeast cell reaches prometaphase I (reviewed in Winter 2012). While the molecular details of meiotic commitment remain elusive, some targets of Ndt80, and perhaps Ndt80 itself, are almost certainly involved.

1.4.4 Non-canonical transcription and translation in meiosis

While Ime1 and Ndt80 control the expression of many genes in budding yeast meiosis, the full complement of gene regulatory networks in meiosis are highly complex. For example, meiosis-specific transcripts are often produced from transcription start sites located either upstream or internal to canonical ORFs (Brar *et al.* 2012; Kim Guisbert *et al.* 2012; Lardenois *et al.* 2011). Up to about 30% of the ribosome footprints map outside of the annotated ORFs in meiosis, in contrast with about 5% in the mitotic cell cycle (Brar *et al.* 2012). Such discrepancy likely comes from the expression of meiosis-specific mRNAs, as well as the usage of upstream ORFs (uORFs) and near-cognate start codons. In addition, over 10,000 meiotic uORFs are annotated, belonging to 3026 genes in total. Many of these uORFs are initiated at AUG, while some at the near-cognate codons UUG and CUG. All of these non-canonical, multi-level alterations on gene expression highlight the complexity of this developmental program.

What are the biological functions of these non-canonical transcription and translation events? One idea is that they can produce new proteins or RNAs to perform meiosis-specific functions. In plants and insects, there are a few reports of biologically functional short peptides made from non-coding RNAs and intergenic regions (Wang *et al.* 2014; Rohrig *et al.* 2002; Casson *et al.* 2002; Narita *et al.* 2004; Qurashi *et al.* 2007; Garelli *et al.* 2012;

Magny *et al.* 2013). For example, in flies, a lncRNA called tarsal-less (tal) expresses four short ORFs with nearly an identical sequence. These short peptides result in post-translational modification of the transcription factor Ovo, leading to Ovo activation during embryonic development. Inactivation of tal is embryonic lethal (Magny *et al.* 2013; Galindo *et al.* 2007; Kondo *et al.* 2007; Kondo *et al.* 2010). Given these examples, it is possible that the novel transcripts present in yeast meiosis can also encode small, biologically active peptides to perform unique functions.

Another possibility is that the non-canonical regulatory mechanisms in meiosis serve to modulate the expression of the genes that have biological functions. There is some evidence for this idea. First, antisense transcripts and lncRNAs are known to regulate gene expression of their associated ORFs (reviewed in Rinn & Chang 2012). In yeast meiosis, at least two cases, *IME1* and *IME4*, have been shown to use such regulation (see the "Ime1" section for details). Transcription of antisense transcripts and lncRNAs can recruit histone-modifying enzymes, such as methyltransferases and histone deacetylases, to alter the chromatin landscapes and the transcription level of neighboring genes (reviewed in Rinn and Chang, 2012). Also, when two proximal genes undergo transcription at the same time, the act of transcription could interfere with one another. This phenomenon is known as "transcription interference" (reviewed in Abeliovich & Klionsky 2001). All these mechanisms are not mutually exclusive and can all occur in yeast meiosis.

Second, almost all known uORFs regulate translation of their downstream ORF (reviewed in Andrews & Rothnagel 2014). Two regulatory mechanisms have been identified so far. In one of them—the more common one—uORFs can reduce translation of their downstream ORF by capturing scanning ribosomes before the ribosomes are able to reach the coding sequence. The sequence and/or the mRNA secondary structure around the uORFs can prevent ribosomes from re-initiating at the start site of the downstream ORF, leading to translation repression of the downstream ORF. Some uORFs have been shown to positively correlate with the translation of the downstream ORF (Brar *et al.* 2012), but the mechanism behind such regulation is currently unknown.

In another mechanism, uORFs can produce small peptides that stall ribosomes. For example, the yeast *CPA1* mRNA has a uORF that encodes a 25-residue short peptide. When arginine interacts with this peptide while this peptide is still attached to the ribosome, the ribosome will fail to translocate, and nonsense-mediated decay of the transcript will begin. Therefore, at high arginine levels, translation of the coding sequence of *CPA1* is repressed (Gaba *et al.* 2005). Plants and mammals also have examples that use the interaction between uORFs and small molecules to stall ribosomes (Rahmani *et al.* 2009; Hanfrey *et al.* 2005; Alatorre-Cobos *et al.* 2012; Law *et al.* 2001), highlighting that this mode of uORF function is also widespread.

In the next several years, the challenge will be to discover what regulates these novel gene expression patterns, how they link to the cellular events in meiosis, and what consequences will take place when they are misregulated. Excitingly, my thesis work has revealed that a meiosis-specific mRNA regulates the expression of the kinetochore subunit Ndc80 in meiosis, ultimately altering kinetochore composition and activity. Chapter 2 will describe these

results in detail.

1.5 Protein turnover in meiosis

Besides transcriptional and translational regulation, protein degradation also plays a critical role in controlling meiosis. Protein degradation machineries are essential for meiotic entry, progression, and spore formation. Furthermore, a recent study showed that meiotic cells often synthesize the subunits of a protein complex in imprecise stoichiometric levels and, through proteolysis, adjusts the protein levels of each subunit to the proper stoichiometry (Eisenberg *et al.* 2018). Therefore, it is of great importance to understand the regulation of protein degradation in meiosis.

Two major protein degradation systems are present in eukaryotes: the ubiquitin-proteasome system (UPS) and the autophagy-lysosome system. To initiate protein degradation in UPS, specific ubiquitin ligase(s) add one or more ubiquitin on the substrate protein. The ubiquitin moiety or chain is recognized by the 26S proteasome, a multi-subunit proteolytic machine that degrades the protein (reviewed in Finley *et al.* 2012). In comparison, autophagy uses the lysosome as its proteolytic center. In macroautophagy, the major type of autophagy, membrane-bound compartments called autophagosomes engulf specific cytoplasmic proteins and organelles. Next, autophagosomes fuse with lysosomes, in which the engulfed material is degraded (reviewed in Abeliovich & Klionsky 2001). The common substrates of UPS include short-lived or misfolded proteins, whereas autophagy degrades and recycles long-lived proteins and organelles. Compared to UPS, autophagy has less substrate constraint and can degrade many types of macromolecules at the same time. It is worth to note that degradation substrates often receive other post-translational modifications, such as phosphorylation, before being recognized by either of the degradation systems (reviewed in Finley *et al.* 2012). Thus, the degradation systems integrate cellular signals to decide whether a protein should be degraded.

Both UPS and autophagy are important for budding yeast sporulation. Autophagy is upregulated in early meiosis, and sporulation requires autophagy genes, such as *ATG1* (Tsukada & Ohsumi 1993). Meiotic regulation of yeast macroautophagy and selective autophagy of organelles are currently under active investigation. In comparison, the UPS is not required for meiosis initiation (Wen *et al.* 2016) but known to regulate many meiotic events. For example, proteasomes and a family of ubiquitin ligases are essential for efficient double-strand break formation, crossovers, and inter-homology synapsis in yeast meiosis (Ahuja *et al.* 2017). UPS also regulates crossovers in the meiosis of male mouse (Rao *et al.* 2017), highlighting a conserved role of the proteasomes in recombination. Also, the major ubiquitin ligase APC is crucial for meiotic divisions. As described in earlier sections, APC^{Cdc20} regulates metaphase-to-anaphase transition. Depletion of Cdc20 arrests meiotic cells in meiosis I (Salah & Nasmyth 2000). The meiosis-specific APC adaptor Ama1 is required for degradation of mitotic regulators in early meiosis (Ndd1, M-phase cyclins, and Cdc5) (Okaz *et al.* 2012). *AMA1* deletion causes defects in interhomolog crossover, synapsis, recombination

checkpoint maintenance, and homolog segregation in meiosis I (Cooper *et al.* 2000; Okaz *et al.* 2012). Ama1 is also required for degradation of various proteins at the end of meiosis (e.g. Ndt80), and for spore development (Diamond *et al.* 2009; McDonald *et al.* 2005; Eisenberg *et al.* 2018).

Although these examples highlight the importance of UPS and autophagy, relatively little is known about them in meiosis. For example, for most ubiquitin ligases, their meiotic substrates have not been identified. The biological functions and regulation of these ligases are also unclear. Interestingly, many yeast ubiquitin ligases are expressed in meiosis; many become upregulated at the end of meiosis (Brar *et al.* 2012). Their gene expression pattern suggests that there exist temporal regulation on UPS. A major challenge in the future will be to characterize what substrate(s) the ubiquitin ligases target, how they do so, what controls their expression in meiosis, and what meiotic events they regulate. This thesis work reveals that the kinetochore subunit Ndc80 is a target of UPS in meiotic prophase. Furthermore, Ndc80 degradation is a critical means to regulate meiotic kinetochore composition and activity. Thus, this thesis provides an exciting example of how UPS controls kinetochore function. Chapter 3 will describe these results in detail.

Chapter 2

Meiotic Regulation of Ndc80 Synthesis

2.1 Introduction

Cellular differentiation is temporally controlled by waves of gene activation and inactivation. These waves drive the morphogenetic events that ultimately transform one cell type into another. As elucidated by differentiation models ranging from *Bacillus subtilis* sporulation to mouse embryogenesis, the expression of gene clusters are activated temporally by transcription factor relays (Errington 2003; Zernicka-Goetz *et al.* 2009). In comparison, it is less well understood how gene repression is mechanistically achieved during development, as well as how gene inactivation is coordinated with the waves of gene activation.

An example that relies on inactivation is the loss of kinetochore function during meiotic prophase. The kinetochore is a protein complex that binds to centromeric DNA and serves as the attachment site for spindle microtubules to mediate chromosome segregation (Musacchio & Desai 2017) (Figure 2.1, Panel A). In multiple systems, it has been shown that kinetochores do not bind to microtubules in meiotic prophase (Asakawa *et al.* 2005; Kim *et al.* 2013; Meyer *et al.* 2015; Miller *et al.* 2012; Sun *et al.* 2011). Furthermore, this temporal inactivation is achieved through removal of the outer kinetochore, the site where microtubule attachments occur (Asakawa *et al.* 2005; Kim *et al.* 2013; Meyer *et al.* 2015; Miller *et al.* 2012; Sun *et al.* 2011) (Figure 2.1, Panel B). In the presence of a spindle, cells that fail to disassemble the outer kinetochore undergo catastrophic missegregation of meiotic chromosomes. Therefore, kinetochore downregulation during meiotic prophase is crucial to meiotic success (Miller *et al.* 2012). Importantly, the kinetochore is reactivated when the outer kinetochore reassembles upon transition from prophase to the meiotic divisions. How the initial removal and subsequent reassembly of the outer kinetochore is coordinated with

the meiotic gene expression program is unknown.

Budding yeast provides a powerful model to address how the dynamic regulation of kinetochore function is integrated into the meiotic gene expression program. Entry into meiosis marks a clear cell-fate transition defined by the induction of Ime1, a master transcription factor. Ime1 activates the expression of the genes involved in DNA replication and meiotic recombination (Kassir *et al.* 1988; van Werven & Amon 2011). Successful completion of recombination, in turn, induces a second transcription factor Ndt80, which activates the expression of the genes involved in the meiotic divisions and gamete development (Chu & Herskowitz 1998; Xu *et al.* 1995). Thus, the landmark morphogenetic events in budding yeast meiosis are coordinated by the relay between these two transcription factors. Furthermore, a high-resolution map of the gene expression waves that drive meiosis has been generated for budding yeast (Brar *et al.* 2012). Importantly, analysis of this dataset revealed that, of the 38 genes that encode kinetochore subunits, *NDC80* displays the most regulated expression pattern between meiotic prophase and the subsequent division phases (RN212).

Ndc80 is the namesake member of an evolutionarily conserved complex that forms the microtubule-binding interface of the outer kinetochore (Tooley & Stukenberg 2011) (Figure 2.1). Numerous lines of evidence indicate that the tight regulation of *NDC80* is essential for the timely function of kinetochores during meiosis. First, the decline of Ndc80 protein in meiotic prophase correlates with the dissociation of the outer kinetochore from the chromosomes (Kim *et al.* 2013; Meyer *et al.* 2015; Miller *et al.* 2012). Second, even though the other outer kinetochore subunits are expressed in meiotic prophase, they do not localize to the kinetochores (Meyer *et al.* 2015). Third, the subsequent increase in the Ndc80 protein level coincides with outer kinetochore reassembly (Meyer *et al.* 2015; Miller *et al.* 2012). Finally, in the presence of a spindle, prophase misexpression of *NDC80* disrupts proper meiotic chromosome segregation (Miller *et al.* 2012). Together, these results indicate that *NDC80* regulation is necessary for the proper timing of kinetochore function in meiosis and highlight the importance of controlling Ndc80 protein levels during meiotic differentiation.

Here we uncovered how the timely function of kinetochores is achieved through the regulation of Ndc80 protein synthesis during budding yeast meiosis. This mechanism is based on the use of two *NDC80* mRNA isoforms, which have opposite functions and display distinct patterns of expression. In addition to the canonical protein-translating *NDC80* mRNA, we found that meiotic cells also expressed a 5'-extended *NDC80* isoform. Despite carrying the entire *NDC80* open reading frame (ORF), this alternate isoform cannot produce Ndc80 protein due to the presence of regulatory upstream ORFs (uORFs) in its extended 5' leader. Rather, its transcription plays a repressive role in inhibiting transcription of the canonical *NDC80* mRNA and thereby resctricting Ndc80 protein synthesis. Furthermore, we found that the expression of the 5'-extended isoform was activated by the meiotic initiation transcription factor Ime1. Upon exiting meiotic prophase, the mid-meiotic transcription factor Ndt80 activated the expression of the canonical *NDC80* mRNA isoform. Taken together, this study uncovers how *NDC80* gene repression is achieved and how inactivation and subsequent reactivation of the kinetochore is coordinated with the transcription factor-driven waves of meiotic gene expression.

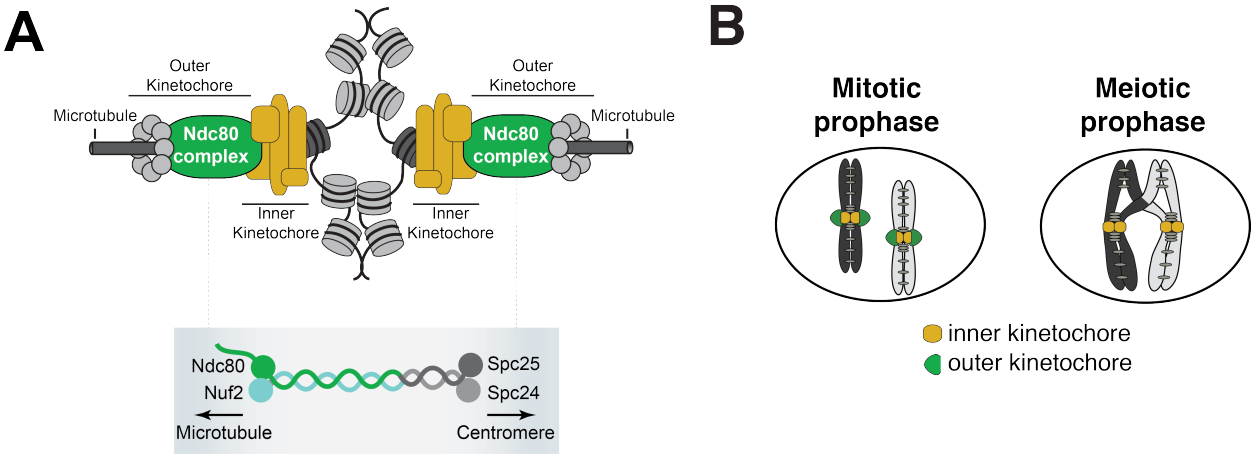

Figure 2.1: Schematics of the kinetochore structure and dynamic behavior. (A) kinetochores assembled on the centromere and attached to microtubules. Bottom: the Ndc80 complex. (B) During mitosis, the outer kinetochores are fully assembled, while in meiotic prophase, the outer kinetochores disassemble.

2.2 Materials and methods

The strain information and experimental methods are described in Chapter 5.

2.3 Results

2.3.1 Ndc80 is the limiting component for kinetochore function in meiotic prophase

The Ndc80 complex consists of four subunits, namely Ndc80, Nuf2, Spc24, and Spc25 (Figure 2.1). All the subunits other than Ndc80 persist in meiotic prophase (Meyer *et al.* 2015). Consistent with this report, we found that even in an extended meiotic prophase arrest, Ndc80 was the only subunit of its complex whose abundance decreased at this meiotic stage (Figure 2.2). Nuf2, Spc24, and Spc25 were all expressed, though it has been reported that these proteins fail to localize to the kinetochores during meiotic prophase (Meyer *et al.* 2015).

Based on these observations, we posited that Ndc80 could be the limiting kinetochore subunit in meiosis. If correct, then the elevation of Ndc80 protein levels, but not the other subunits, should reactivate kinetochore function in meiotic prophase. To test this prediction, we overexpressed each of the Ndc80 complex subunits (Figure 2.3), in conjunction with the B-type cyclin Clb3, under an inducible *CUP1* promoter (*pCUP*). *CLB3* misexpression causes bipolar spindle assembly in meiotic prophase (Miller *et al.* 2012). In *pCUP-CLB3* cells, if kinetochores are functional in meiotic prophase, they attach to the spindle microtubules prematurely. These premature attachments, in turn, cause sister chromatid segregation in

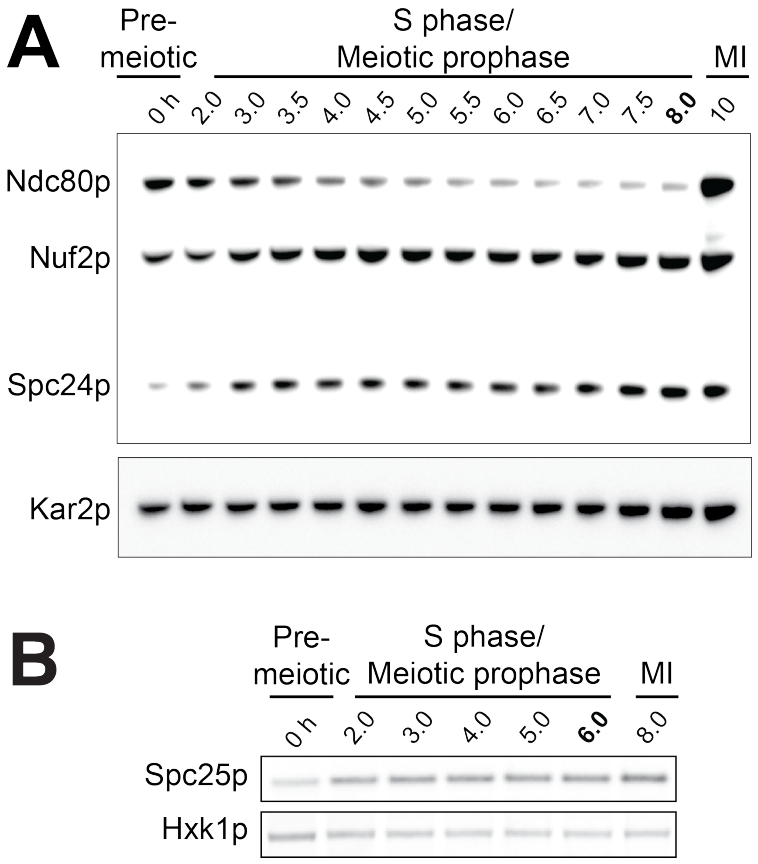

Figure 2.2: Protein abundance of the Ndc80 complex subunits in meiosis. (A) Ndc80, Nuf2, and Spc24 were tagged with a 3V5 epitope in a single strain (UB4361). Using the *pGAL-NDT80 GAL4-ER* synchronization method (Carlile & Amon 2008), cells were arrested in pachytene and then released into the meiotic divisions after an 8-hour incubation in the sporulation medium (SPO). Each subunit was detected by anti-V5 immunoblot. Hxk1, loading control. (B) Spc25 abundance in meiosis. Cells (UB1051) were transferred to SPO at 0 hr, arrested in pachytene as in (A), and released after 6 hrs in SPO.

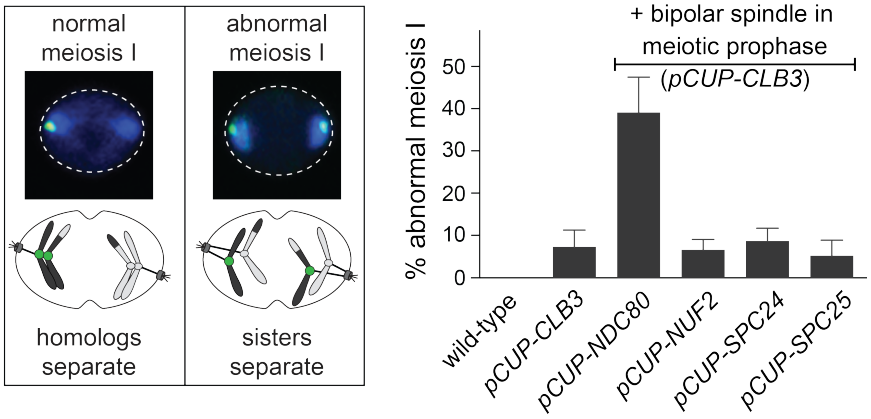

Figure 2.3: Ndc80 is the limiting kinetochore subunit in meiotic prophase. Sister chromatid segregation in the wild-type (UB4432), *pCUP-CLB3* (UB4434), *pCUP-CLB3 pCUP-NDC80* (UB880), *pCUP-CLB3 pCUP-NUF2* (UB4436), *pCUP-CLB3 pCUP-SPC24* (UB980), and *pCUP-CLB3 pCUP-SPC25* (UB885). A pair of sister chromatids of chromosome V was labeled with the centromeric TetO/TetR-GFP system (*CENV-GFP*). Left: A schematic depicting CENV-GFP dot localization in normal and abnormal meiosis I. In normal meiosis I, when homologous chromosomes segregate, a single GFP dot is present in one of the two nuclear masses of a binucleated cell. In abnormal meiosis I, when sister chromatids segregate, both nuclear masses of a binucleated cell contain a GFP dot. Right: The average fraction of binucleates that displayed sister chromatid segregation in meiosis I. Expression of Clb3 and each Ndc80 complex subunit (both regulated by the *pCUP* promoter) were co-induced by addition of $CuSO_4$ 6 hrs after the cells were transferred to SPO. Concomitantly, cells were released from pachytene arrest by addition of β-estradiol. Cells were fixed 1 hr and 45 min after the release. The error bars represent the standard error of the mean from three independent experiments. 100 cells were counted per strain, per experiment.

meiosis I, essentially disrupting proper meiotic chromosome segregation (Miller *et al.* 2012). When *NDC80* was overexpressed in *pCUP-CLB3* cells during meiotic prophase, over 30% of the cells displayed an abnormal segregation pattern in meiosis I. In contrast, misexpression of *CLB3* alone resulted in only a 7% segregation defect. Importantly, this defect was not further enhanced by the overexpression of *NUF2*, *SPC24* or *SPC25* (Figure 2.3). Based on this observation, we conclude that kinetochore function is repressed in meiotic prophase due to the limiting levels of Ndc80. Following prophase, Ndc80 becomes highly abundant during the meiotic divisions (Miller *et al.* 2012) (Figure 2.2, 10 h time point), consistent with its role in facilitating chromosome segregation (Wigge & Kilmartin 2001). Together, these results demonstrate that Ndc80 is the sole subunit of its complex that is tightly regulated during meiotic differentiation and strongly support the notion that *NDC80* downregulation and re-synthesis govern kinetochore functionality in meiosis.

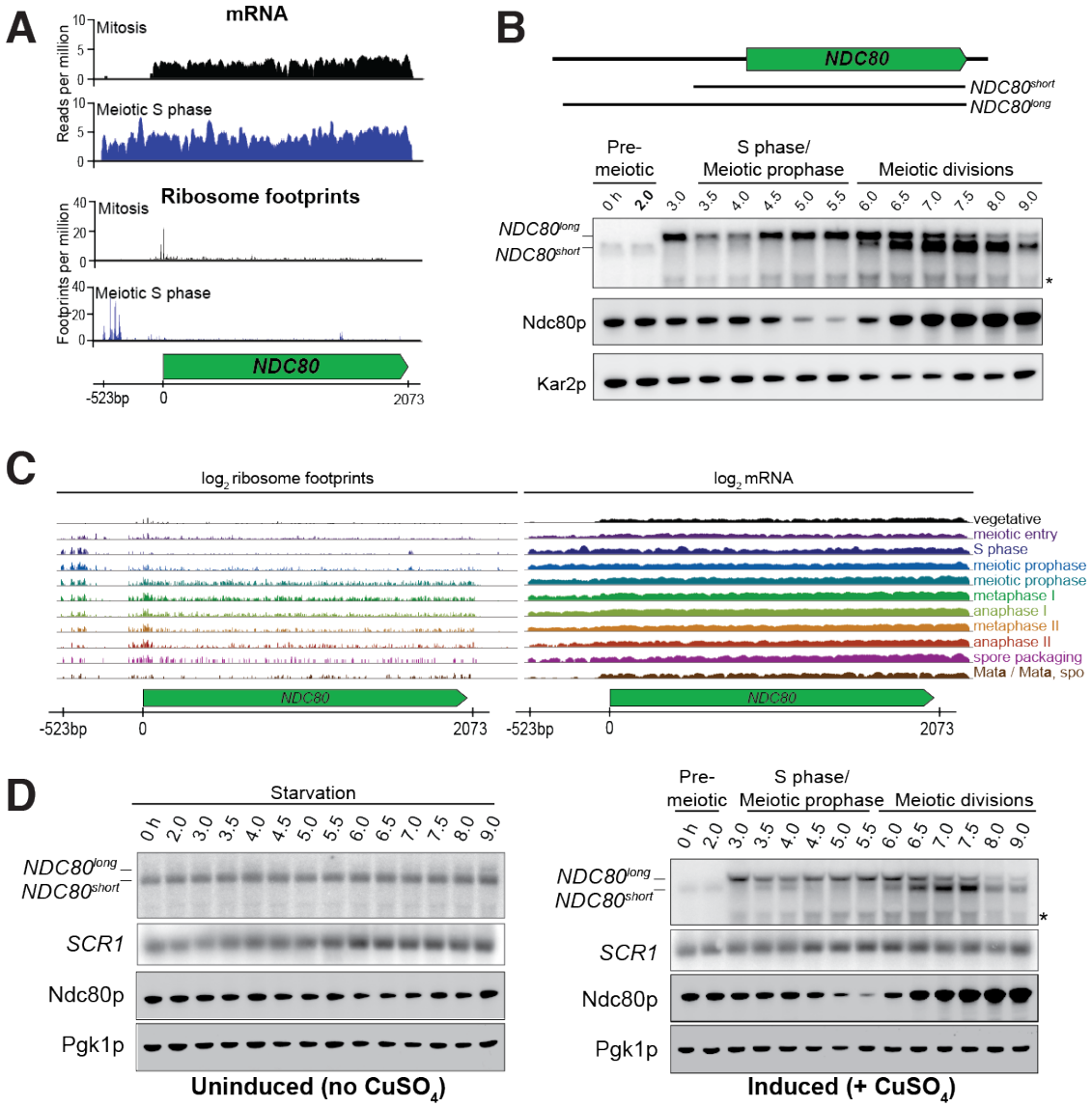

Figure 2.4: Two distinct *NDC80* transcripts are expressed during meiosis. (A, C) Ribosome profiling and mRNA-seq reads over the *NDC80* locus during vegetative growth, throughout meiosis, or in starvation (*MAT***a**/*MAT***a**). Data are derived from (Brar *et al.* 2012). (B) *NDC80* mRNA isoforms and Ndc80 levels in meiosis. $NDC80^{Long}$ and $NDC80^{Short}$ levels were determined by northern blot, and Ndc80 level was determined by anti-V5 immunoblot. To induce meiotic entry, *IME1* and *IME4* expression was induced by addition of $CuSO_4$ 2 hrs after the strain (UB1337) was transferred to SPO. *SCR1*, loading control for northern blot. Kar2, loading control for immunoblot. * indicates a smaller RNA product, which likely represents a truncated form of $NDC80^{Long}$. (D) The abundance of *NDC80* mRNA isoforms and Ndc80 protein level in starvation versus in meiosis. Pgk1, loading control for immunoblot. Uninduced, *IME1* and *IME4* expression was never induced, and thus cells stayed in starvation. Induced, *IME1* and *IME4* expression was induced by addition of $CuSO_4$. Note: the blots for the induced conditions were the reruns of (B).

2.3.2 Two distinct *NDC80* transcript isoforms exist in meiosis

As shown by previous reports, the protein level of Ndc80 declines in meiotic prophase and increases during the meiotic divisions (Asakawa *et al.* 2005; Miller *et al.* 2012). To dissect the molecular mechanism for the strict temporal regulation of the *NDC80* gene in meiosis, we first took advantage of the high-resolution RNA-seq and ribosome profiling dataset generated for budding yeast meiosis (Brar *et al.* 2012). Analysis of this dataset revealed the presence of meiosis-specific RNA-seq reads that extend to about 500 base pairs (bp) upstream of the *NDC80* ORF (Figure 2.4, panel A). These reads appeared after meiotic entry and persisted until the end of meiosis, but were absent during vegetative growth (Figure 2.4, panel C, vegetative) or starvation (Figure 2.4, panel C, $MAT\mathbf{a}/MAT\mathbf{a}$).

To monitor the different RNA molecules generated from the *NDC80* locus, we performed northern blotting. In the absence of meiotic progression, when cells were subject to nutrient poor conditions, we detected only a single *NDC80* transcript throughout the starvation regime (no $CuSO_4$, Figure 2.4, panel D). However, in cells undergoing synchronous meiosis, two distinct *NDC80* transcript isoforms became evident: a longer, meiosis-specific isoform, and a shorter isoform that was also present under non-meiotic conditions (Figure 2.4, panel B and D). The longer isoform appeared after meiotic entry, persisted throughout meiotic prophase and gradually disappeared during the meiotic divisions. The shorter isoform was present in vegetative cells prior to meiotic entry, but was weakly expressed during S phase and meiotic prophase. Its abundance dramatically increased during the meiotic divisions (Figure 2.4, panel B and D). Interestingly, the Ndc80 protein levels were noticeably higher during the meiotic stages when the shorter transcript was the predominant isoform, but lower when the longer transcript was predominant (Figure 2.4, panel B and D).

In addition to northern blotting, we used single molecule RNA fluorescence *in situ* hybridization (smFISH) to assess the cell-to-cell variability in transcript expression and subcellular localization of these two *NDC80* transcript isoforms. With two sets of probes that bind to the same region of *NDC80* ORF (odd/even probes), we verified that our smFISH could uniquely pair the FISH spots with an accuracy of 88% (Figure 2.5, Panel A), a value similar to what was reported previously (Raj *et al.* 2008). Furthermore, we confirmed that the number of cells analyzed per sample per experimental repeat (>95 cells) exceeded the minimal number of cells required to achieve a stable sampling average (Figure 2.5, Panel B), and thus our sample size is large enough to reflect the population mean.

To differentiate between the two *NDC80* isoforms, we used another two sets of probes: one set (Q 670), conjugated to Quasar 670, is complementary to the sequences common between the short and the long isoforms. The other set (CF 590), conjugated to CAL Fluor Red 590, is unique to the long isoform. The long isoforms were identified as the spots where the signal from both probe sets colocalized, whereas the short isoforms were identified as the spots with signal only from Q 670 (Figure 2.6, Panel A).

The smFISH analysis revealed that the expression of the two *NDC80* isoforms was temporally regulated. Vegetative cells expressed only the short *NDC80* isoform; fewer than 2% of these cells expressed the long isoform (Figure 2.6, Panel B). In meiotic prophase, a

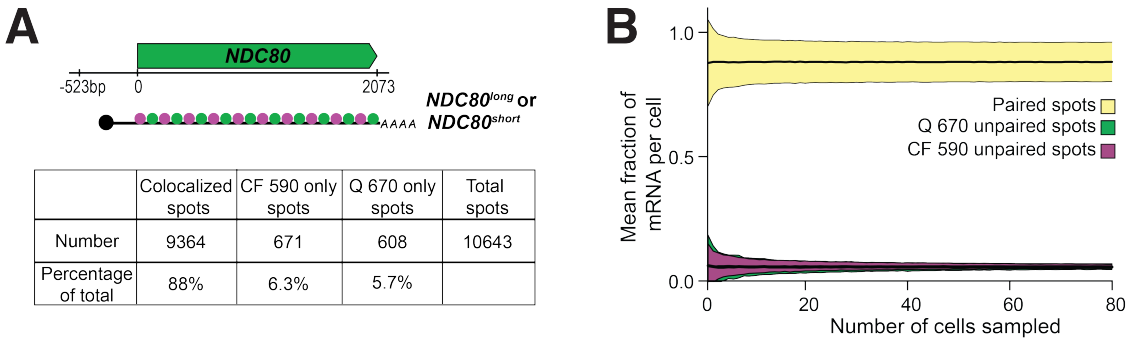

	Colocalized spots	CF 590 only spots	Q 670 only spots	Total spots
Number	9364	671	608	10643
Percentage of total	88%	6.3%	5.7%	

Figure 2.5: An optimized smFISH method to study *NDC80* transcripts in meiosis. (A) Percentage of the colocalized or non-colocalized smFISH spots, using the odd and even smFISH probe sets. Fifty-four oligonucleotide probes tiling the common region of $NDC80^{Long}$ and $NDC80^{ORF}$ were used. All the odd number probes were labeled with one fluorophore (CAL Fluor Red 590, magenta), and the even number probes, with another fluorophore (Quasar 670, green). Samples (UB8144) were fixed after 6 hrs in SPO. A total of 428 cells were analyzed, pooling from two independent experiments. (B) Bootstrapping analysis for the data in (A). All quantified cells were pooled, and then a given number (n) of cells were randomly sampled 500 times. The mean and 95% credible interval were calculated for the fraction of paired and unpaired mRNA per cell. These data were plotted for each choice of the number n.

stage defined by the presence of the synaptonemal complex component Zip1, 100% of cells expressed the long isoform, and over 50% of them had more than 20 transcripts per cell. During the same stage, the level of the short isoform significantly decreased in comparison to its levels in vegetative growth (Figure (2.6, Panel B) ($p=0.0260$, two-tailed Wilcoxon Rank Sum test)and pre-meiotic starvation (Figure 2.6, Panel C) ($p=0.0090$). As cells entered meiosis I, the level of the short isoform dramatically increased while that of the long isoform declined, in comparison to the levels of these isoforms during meiotic prophase ($p<0.0001$ for both $NDC80^{Short}$ and $NDC80^{Long}$ mRNAs) (Figure 2.6, Panel B). Thus, the two *NDC80* isoforms have expression signatures specific to different cellular states.

In addition, the two *NDC80* isoforms localized to both the nucleus and cytoplasm (Figure (2.6, Panel A). We saw no evidence that the $NDC80^{Long}$ isoform was solely retained in the nucleus; all of the Zip1-positive cells had at least one $NDC80^{Long}$ mRNA localized outside of the DAPI-stained region. This localization pattern was consistent with the possibility that both transcripts were translated, as shown by ribosome profiling (Figure 2.4, panel A) (Brar *et al.* 2012).

Altogether, the combined analyses of northern and western blotting, as well as smFISH, reveal two interesting trends: (1) In meiosis, the expression of the long and short *NDC80* isoforms are anticorrelated. (2) Ndc80 protein levels positively correlate with the presence of the short isoform and negatively correlate with the long isoform (Figure 2.4, Panel B).

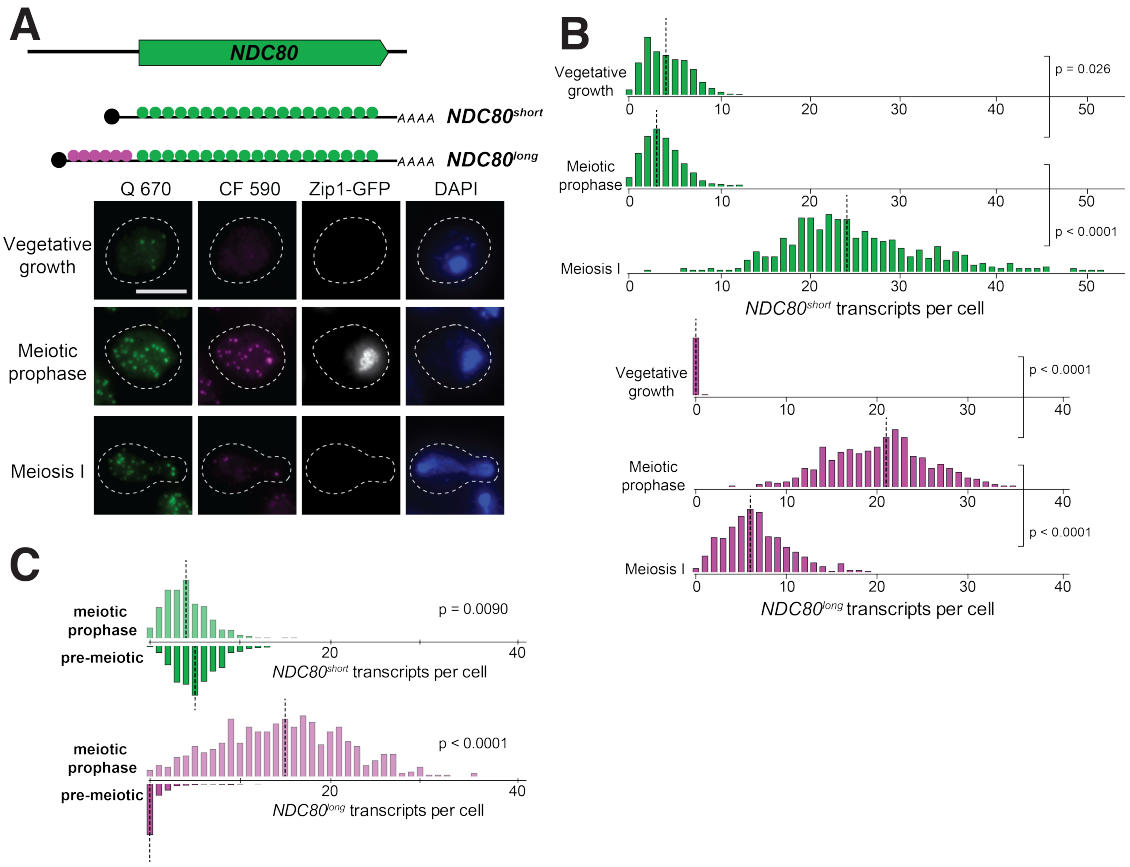

Figure 2.6: *NDC80*^{Long} and *NDC80*^{Short} detected by smFISH. (A) Representative smFISH images for *NDC80*^{Long} and *NDC80*^{Short} in vegetative growth and meiosis. Vegetative samples were taken when cells (UB8144) were growing exponentially in nutrient rich medium. Meiotic prophase samples were taken after the strain was incubated in SPO for 6 hrs, a time when these cells were arrested in pachytene. Meiosis I samples were taken 1.5 hr after cells were released from pachytene. The Q 670 probes (green) hybridize to the common region shared between *NDC80*^{Long} and *NDC80*^{Short}, whereas the CF 590 probes (shown in magenta) hybridize to the unique 5' region of *NDC80*^{Long}. DNA was stained with DAPI (blue). Each cell was staged by its Zip1-GFP signal. Vegetative growth: Zip1-GFP negative. Meiotic prophase: Zip1-GFP positive. Meiosis I: Zip1-GFP negative and post *NDT80* induction. Images here and throughout are shown as the maximum-intensity projections of z-stacks. Scale bar: 5 μm. (B) Quantification of the smFISH data shown in (A), graphed as the relative frequency histograms of cells with a given number of *NDC80*^{Long} and *NDC80*^{Short} transcripts per cell, pooling the data from three independent experiments. The dashed line indicates the median number of *NDC80*^{Long} and *NDC80*^{Short} transcripts per cell. Each histogram here and throughout was normalized so that the maximum bin height is the same across all histograms. Two-tailed Wilcoxon Rank Sum test was performed between each pair of conditions as indicated by the bracket.

2.3.3 The long *NDC80* isoform is unable to produce Ndc80 protein due to translation of its upstream ORFs

The negative correlation between the longer *NDC80* isoform and Ndc80 protein levels suggested that this longer isoform was unable to support the synthesis of Ndc80 protein. In addition to the *NDC80* ORF, the longer isoform contains nine uORFs, each with an AUG start codon. The first six of these uORFs, those closest to the 5' end of the mRNA, have ribosome profiling signatures consistent with them being translated in meiosis (Figure 2.7, Panel A). Upstream start codons in transcript leaders can capture scanning ribosomes to alternate reading frames, thereby restricting ribosome access to the main ORF (Arribere & Gilbert 2013; Calvo *et al.* 2009; Johnstone *et al.* 2016).

We mutated the start codon of the first six uORFs ($\Delta 6AUG$) to test whether these uORFs repress the translation of actual ORF within this $NDC80^{Long}$ mRNA. In the $\Delta 6AUG$ strain, the negative correlation between the long isoform and Ndc80 protein level persisted (Figure 2.7, Panel B), potentially because the remaining three uORFs could still repress translation of the ORF. Indeed, when all nine AUGs were mutated, Ndc80 protein became highly abundant during meiotic prophase, even though the long isoform remained the predominant *NDC80* transcript in these cells (Figure 2.7, Panel B). These results demonstrate that although the longer isoform of *NDC80* contains the entire ORF, the presence of the uORFs in its 5' leader prevents Ndc80 translation from this mRNA.

Next, we tested whether the repressive role of the uORFs resulted from the act of translation or the peptides encoded by these uORFs. We modified the long isoform, such that it still contained all the upstream AUG start codons, but each start codon was followed by a single amino acid and then immediately by a stop codon (*mini uORF*). Thus, this construct retained the translation ability of the uORFs but rendered them incapable of producing a peptide chain. We found that Ndc80 levels were still reduced during meiotic prophase in the *mini uORF* strain (Figure 2.7, Panel B). Therefore, the uORFs translation represses the translation of the *NDC80* ORF from the long *NDC80* isoform, rendering this isoform unable to synthesize Ndc80 protein.

Our analyses so far demonstrate that the two *NDC80* mRNA isoforms differ with regards to their size and the ORF coding capacity. The shorter isoform is capable of translating the *NDC80* ORF. In contrast, although the longer isoform contains the entire ORF, it does not support Ndc80 synthesis. The coding information is not decoded from this isoform because the uORF translation prevents ribosomes from accessing the actual ORF. To signify the unique features of each *NDC80* transcript isoform, we named the short mRNA $NDC80^{ORF}$, and the longer mRNA $NDC80^{LUTI}$ for long un-decoded transcript isoform.

2.3.4 $NDC80^{LUTI}$ expression in *cis* is necessary and sufficient to downregulate $NDC80^{ORF}$

Given that $NDC80^{LUTI}$ does not appear to produce Ndc80 protein, we set out to understand why meiotic cells express this mRNA isoform. Based on the observation that

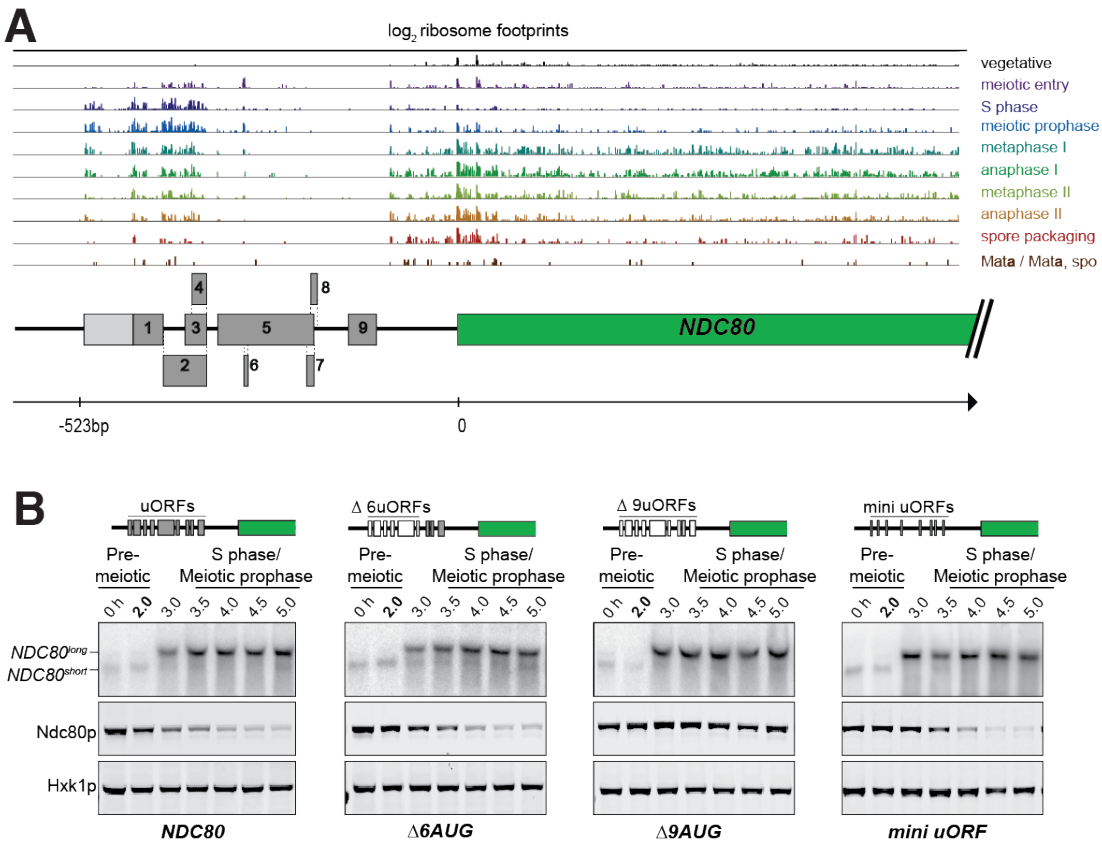

Figure 2.7: $NDC80^{Long}$ cannot synthesize Ndc80 protein due to uORF translation. (A) The first 6 AUG uORFs in the $NDC80^{Long}$ mRNA have ribosome footprint signatures consistent with them being translated. Ribosome profiling reads over the *NDC80* locus throughout meiosis (Brar *et al.* 2012). Dark grey boxes, the locations of the nine AUG uORFs. Lighter grey box, the location of a uORF with a near cognate start site (AUU) and ribosome footprints characteristic of translated regions. The uORF positions are drawn proportional to the axis, with the start of *NDC80* ORF marked as 0, and the approximate 5' end of $NDC80^{Long}$ mRNA marked as -523 bp. (B) $NDC80^{Short}$, $NDC80^{Long}$, and Ndc80 abundance during synchronous meiosis (as described in Figure 2.4) in the wild-type (UB6190), $\Delta 6AUG$ (UB6181), $\Delta 9AUG$ (UB6183), and *mini uORF* (UB9243) strains. In the $\Delta 6AUG$ and $\Delta 9AUG$ strains, the first 6 or 9 uORF AUGs in the 5' leader of $NDC80^{Long}$ were converted to AUCs, respectively. The *mini uORF* construct contained all 9 uORF start sites in the $NDC80^{Long}$ leader; however, the third codon of each of the 9 uORFs was mutated to a stop codon.

the expression levels of these two isoforms are anti-correlated, we posited that the transcription of $NDC80^{LUTI}$ represses $NDC80^{ORF}$. To test this hypothesis, we first eliminated $NDC80^{LUTI}$ production by deleting its promoter along with different portions of the $NDC80^{LUTI}$ transcript ($\Delta NDC80^{LUTI}$). As shown by northern blotting, $NDC80^{ORF}$ was detected during meiotic prophase in two different $\Delta NDC80^{LUTI}$ mutant strains (Figure 2.8). Analysis of smFISH also confirmed that the level of $NDC80^{ORF}$ in $\Delta NDC80^{LUTI}$ cells significantly increased during meiotic prophase (Figure 2.9, Panel B) (p=0.0004), with a median exceeding that of pre-meiotic cells (Figure 2.6, Panel C). Accordingly, Ndc80 protein levels increased throughout meiotic prophase (Figure 2.8).

Additionally, we inserted a termination sequence about 220 bp downstream of the $NDC80^{LUTI}$ transcription start site ($NDC80^{LUTI}$-*Ter*). We observed that, upon early termination of $NDC80^{LUTI}$, $NDC80^{ORF}$ mRNA and Ndc80 protein persisted in meiotic prophase (Figure 2.10). This observation suggests that continuous transcription through the $NDC80^{ORF}$ promoter is necessary for $NDC80^{ORF}$ repression. It also indicates that the repression of $NDC80^{ORF}$ is not due to competition between the $NDC80^{ORF}$ promoter and the $NDC80^{LUTI}$ promoter for RNA polymerase and the general transcription machinery. Altogether, we conclude that expression of the $NDC80^{LUTI}$ mRNA is required to repress the $NDC80^{ORF}$ transcript and reduce Ndc80 protein levels during meiotic prophase.

By what mechanism does $NDC80^{LUTI}$ reduce the steady-state level of $NDC80^{ORF}$? We posited that$NDC80^{LUTI}$ acts in *cis* based on other instances of overlapping transcription in budding yeast (Bird *et al.* 2006; Martens *et al.* 2004; van Werven & Amon 2011). To test this, we engineered strains to have one wild-type $NDC80^{LUTI}$ allele and another allele in which the promoter of $NDC80^{LUTI}$ has been deleted ($\Delta NDC80^{LUTI}$). To monitor Ndc80 protein levels, we inserted a 3V5 epitope as a C-terminal fusion to *NDC80* in either the wild-type or the $\Delta NDC80^{LUTI}$ allele. If $NDC80^{LUTI}$ functions in *trans*, then Ndc80-3V5 should be downregulated to the same extent in both strains. Instead, we found that Ndc80-3V5 was downregulated only when $NDC80^{LUTI}$ was generated on the same chromosome, directly upstream of *NDC80-3V5* (Figure 2.11, middle panel). This result demonstrates that $NDC80^{LUTI}$-mediated repression occurs in *cis*, since $NDC80^{LUTI}$ cannot reduce Ndc80 protein expression from a copy of *NDC80* on another chromosome (Figure 2.11, right panel). Chia *et al.* revealed that this cis-acting mechanism results from the chromatin alterations across the $NDC80^{ORF}$ promoter induced by the $NDC80^{LUTI}$ transcription (Chia *et al.* 2017).

Since $NDC80^{LUTI}$ is necessary to repress $NDC80^{ORF}$ during meiosis, we next investigated whether the $NDC80^{LUTI}$ leader is sufficient to regulate other genes in meiosis. We replaced the promoter and 5' leader of *NUF2*, the gene encoding the binding partner of Ndc80, with the promoter and 5' leader region of $NDC80^{LUTI}$ ($NDC80^{LUTI}$-*NUF2*). In the wild-type cells, a single *NUF2* mRNA species was expressed in meiotic prophase, a stage when *NUF2* mRNA levels and Nuf2 protein levels were stable (Figure 2.12, Panel A and B). In contrast, $NDC80^{LUTI}$-*NUF2* cells expressed a longer mRNA ($NUF2^{LUTI}$) in meiotic prophase (Figure $NDC80^{LUTI}$-*NUF2*, Panel A), and the abundance of $NUF2^{ORF}$ transcripts was reduced by 60% compared to that in the pre-meiotic stage, a reduction level similar to that of the Nuf2 protein (Figure 2.12, Panel B). This result demonstrates that the promoter and 5' leader

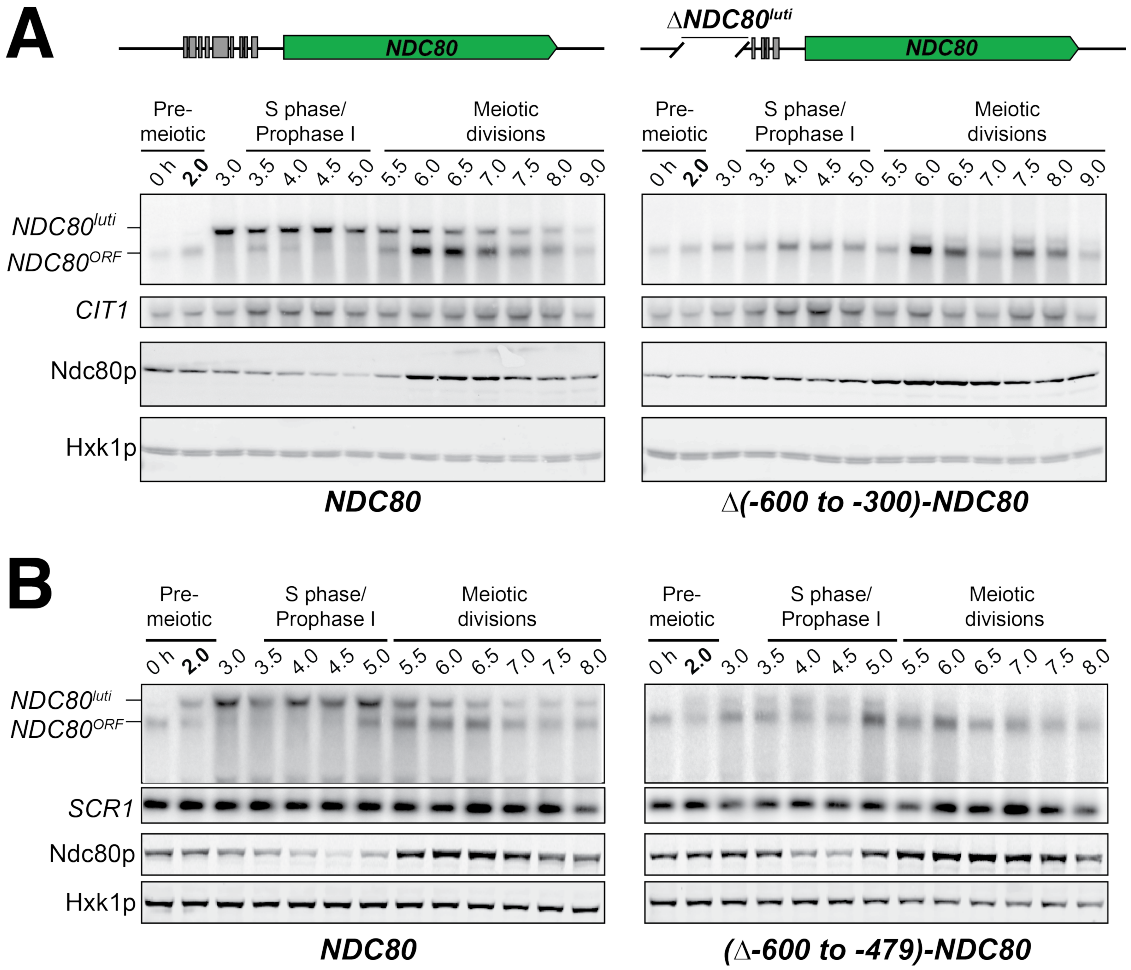

Figure 2.8: *NDC80^{LUTI}* is necessary to downregulate *NDC80^{ORF}*. *NDC80^{ORF}*, *NDC80^{LUTI}*, and Ndc80 abundance during synchronous meiosis (as described in Figure 2.4) in the wild-type cells (FW1902 in (A) and UB6190 in (B)), in *(Δ-600 to -300)-NDC80* cells (FW1871), in which 300–600 bp upstream of the Ndc80 translation start site were deleted, as well as in *(Δ-600 to -479)-NDC80* cells (UB6079), in which the 479-600 bps upstream of the Ndc80 translation start site were deleted. Ndc80 level was determined by anti-V5 immunoblot. *CIT1*, loading control for northern blot. Hxk1, the loading control for immunoblot.

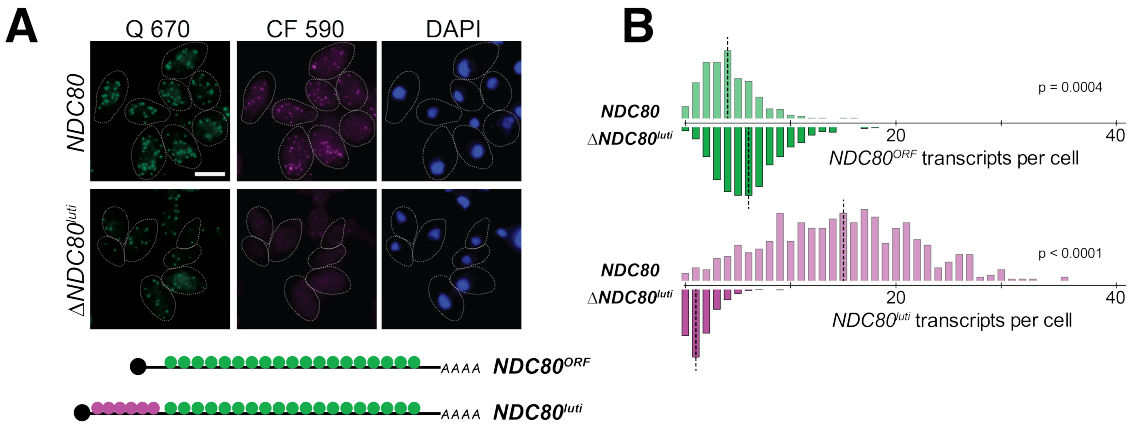

Figure 2.9: $NDC80^{LUTI}$ is necessary to downregulate $NDC80^{ORF}$ by smFISH. (A) Representative smFISH images for $NDC80^{LUTI}$ and $NDC80^{ORF}$ during meiotic prophase in the wild-type cells (UB6190) and in $\Delta NDC80^{LUTI}$ cells (UB6079), in which 479-600 bps upstream of the Ndc80 translation start site were deleted. This deletion construct was used, as opposed to the (-600 to -300) deletion, because this construct retains all the binding sites for the CF 590 probes (bind to the unique region of $NDC80^{LUTI}$). Samples were taken 2 hr after *IME1* and *IME4* induction in a synchronous meiosis and hybridized with the Q 670 probes (bind to the common region of $NDC80^{LUTI}$ and $NDC80^{ORF}$, shown in green) and the CF 590 probes (shown in magenta). DNA was stained with DAPI (blue). Scale bar: 5 μm. (B) Quantification of the smFISH data in (A), graphed as the relative frequency histograms of cells with a given number of $NDC80^{LUTI}$ and $NDC80^{ORF}$ transcripts per cell, pooling the data from three independent experiments. The dashed line indicates the median number of $NDC80^{LUTI}$ and $NDC80^{ORF}$ transcripts per cell. Two-tailed Wilcoxon Rank Sum test was performed for $NDC80^{ORF}$ and $NDC80^{LUTI}$, respectively, comparing wild-type with $\Delta NDC80^{LUTI}$ during meiotic prophase.

sequence of $NDC80^{LUTI}$ is sufficient to downregulate another protein in meiotic prophase.

As $NDC80^{LUTI}$ expression is naturally restricted to meiosis, we tested whether the expression of $NDC80^{LUTI}$ was sufficient to downregulate $NDC80^{ORF}$ outside of meiosis. We artificially expressed $NDC80^{LUTI}$ during mitosis, a time when $NDC80^{LUTI}$ is naturally absent. We replaced the endogenous promoter of $NDC80^{LUTI}$ with the inducible *GAL1-10* promoter ($pGAL\text{-}NDC80^{LUTI}$) and made this construct the sole copy of the *NDC80* gene. This alteration had minimal effect on cell growth (Figure 2.23), suggesting that the expression of $NDC80^{ORF}$ transcript and Ndc80 protein is largely unaffected in the absence of $pGAL$ induction. In the wild-type cells synchronously progressing through the mitotic cell cycle, a single mRNA isoform, $NDC80^{ORF}$, was present at all stages (Figure 2.12, Panel C, left). In contrast, the $NDC80^{ORF}$ transcript became undetectable in $pGAL\text{-}NDC80^{LUTI}$ cells one hour after $NDC80^{LUTI}$ induction (Figure 2.12, Panel C, right). Four hours post induction, Ndc80 protein levels were reduced to 20% of the initial level but in the wild-type cells, increased to 116% (Figure 2.12, Panel D). Based on these data, we conclude that $NDC80^{LUTI}$ expression is sufficient to repress $NDC80^{ORF}$ outside of meiosis. The reduction in $NDC80^{ORF}$ expression

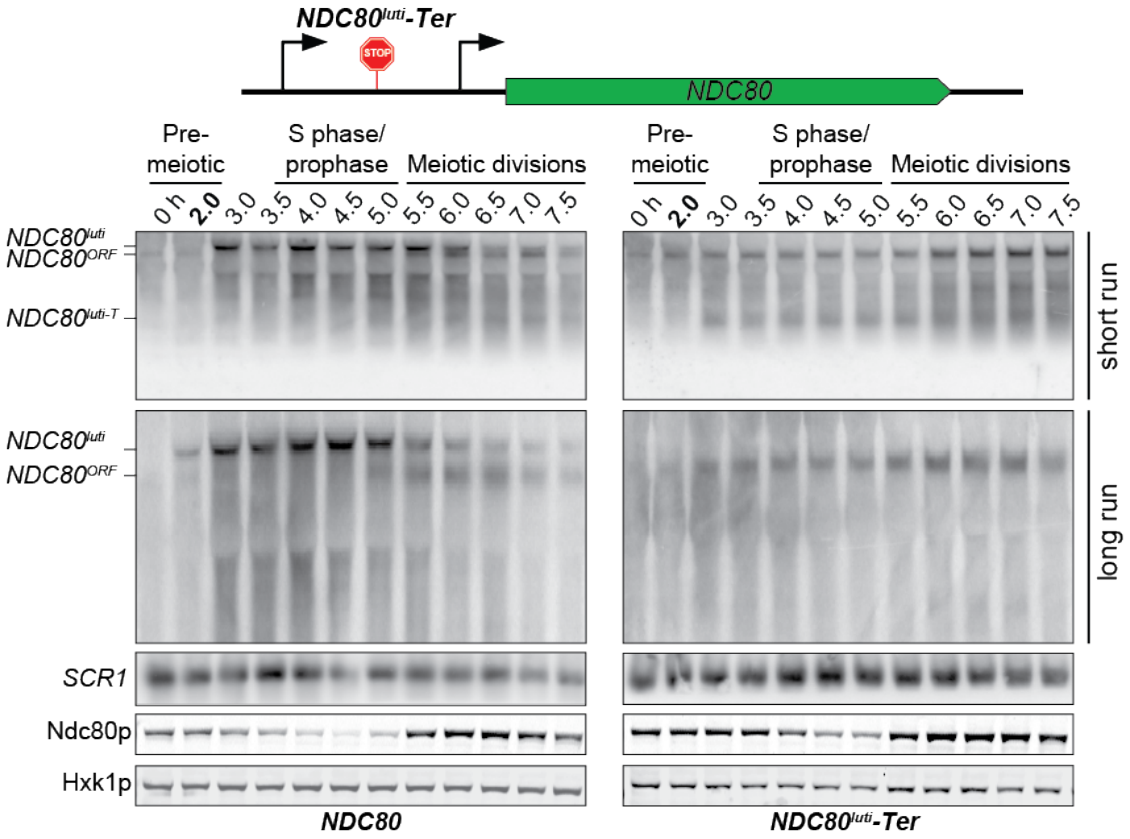

Figure 2.10: Premature termination of $NDC80^{LUTI}$ prevents $NDC80^{ORF}$ downregulation. $NDC80^{ORF}$, $NDC80^{LUTI}$, and Ndc80 abundance during synchronous meiosis in the wild-type cells (UB6190) and in $NDC80^{LUTI}$-*Ter* cells (UB6077), which harbor a terminator sequence inserted after the second uORF of $NDC80^{LUTI}$. Ndc80 protein level was determined by anti-V5 immunoblot. *SCR1*, loading control for northern blot. Hxk1, loading control for immunoblot. Top (short run): the gel was run for 1.5 hr. Middle: (long run) the gel was run for 3 hr. Note that the $NDC80^{LUTI}$ and $NDC80^{ORF}$ isoforms could be sufficiently resolved only in the long run conditions, while the truncated $NDC80^{LUTI}$ transcript due to early termination ($NDC80^{LUTI}$-*Ter*) could only be detected in the short run conditions.

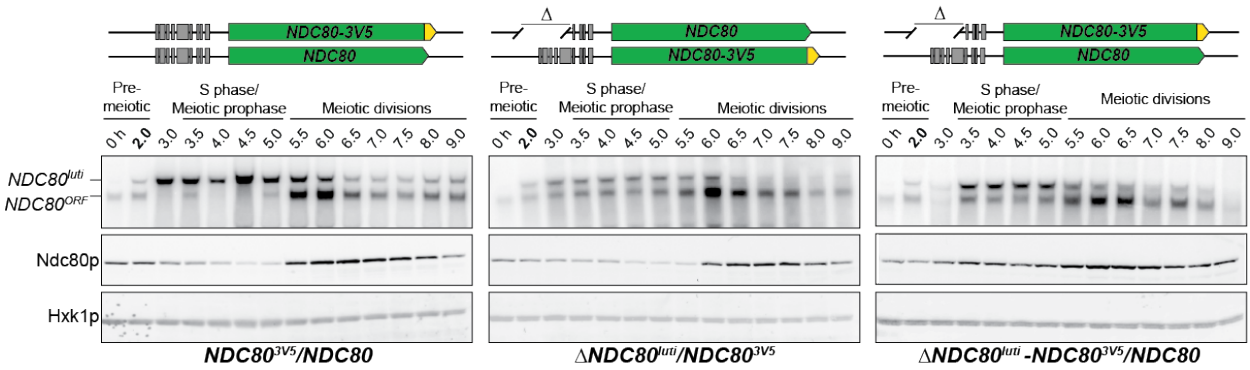

Figure 2.11: *NDC80*^{LUTI} represses *NDC80*^{ORF} in *cis*. Meiosis was induced and samples were collected and processed as Figure 2.8. Ndc80 level was determined by anti-V5 immunoblot. Hxk1, loading control. Three yeast strains were used in this experiment: 1) a strain (FW1900) with one *NDC80-3V5* allele and one wild-type *NDC80* allele (left), 2) a strain (FW1899) with one *NDC80-3V5* allele and one Δ*NDC80*^{LUTI} allele, in which 300–600 bp upstream of the Ndc80 translation start site were deleted (middle), and 3) a strain (FW1923) with one Δ*NDC80*^{LUTI}*-NDC80-3V5* allele, which has the aforementioned 300–600 bps deletion, and one wild-type *NDC80* allele (right).

subsequently reduces Ndc80 protein synthesis, essentially turning off the *NDC80* gene.

2.3.5 Master transcription factors Ime1 and Ndt80 regulate *NDC80*^{LUTI} and *NDC80*^{ORF} expression, respectively

Since the timely expression of *NDC80*^{LUTI} and *NDC80*^{ORF} is crucial to establish the temporal pattern of Ndc80 protein levels in meiosis, we next investigated which transcription factors directly control *NDC80*^{LUTI} and *NDC80*^{ORF} expression. In *S. cerevisiae*, meiotic gene expression is orchestrated by two master transcription factors: Ime1 and Ndt80 (Chu & Herskowitz 1998; Kassir *et al.* 1988; Xu *et al.* 1995). Diploid *MAT***a**/*MAT***a** cells initiate meiosis by expressing *IME1* in response to nutrient deprivation (van Werven & Amon 2011). Interestingly, *IME1* expression correlated with the time of *NDC80*^{LUTI} expression, suggesting that Ime1 might regulate *NDC80*^{LUTI} transcription. Indeed, deletion of *IME1* abolished *NDC80*^{LUTI} production and resulted in persistent levels of *NDC80*^{ORF} transcript and Ndc80 protein (Figure 2.13).

Ime1 does not directly bind to DNA but functions as a co-activator for Ume6 (Washburn & Esposito 2001). In the absence of Ime1, Ume6 represses early meiotic genes in mitosis by binding to a consensus site called the upstream repressive sequence (*URS1*) in the promoters of these genes. Upon meiotic entry and subsequent interaction with Ime1, the Ume6-Ime1 complex activates the transcription of these early meiotic genes (Bowdish *et al.* 1995; Park *et al.* 1992). Given the close relationship between Ime1 and Ume6, we inspected the 5' intergenic region of *NDC80* and identified a consensus site for Ume6 583 bps upstream of the Ndc80 translation start site (Figure 2.14), within the *NDC80*^{LUTI} promoter. ChIP

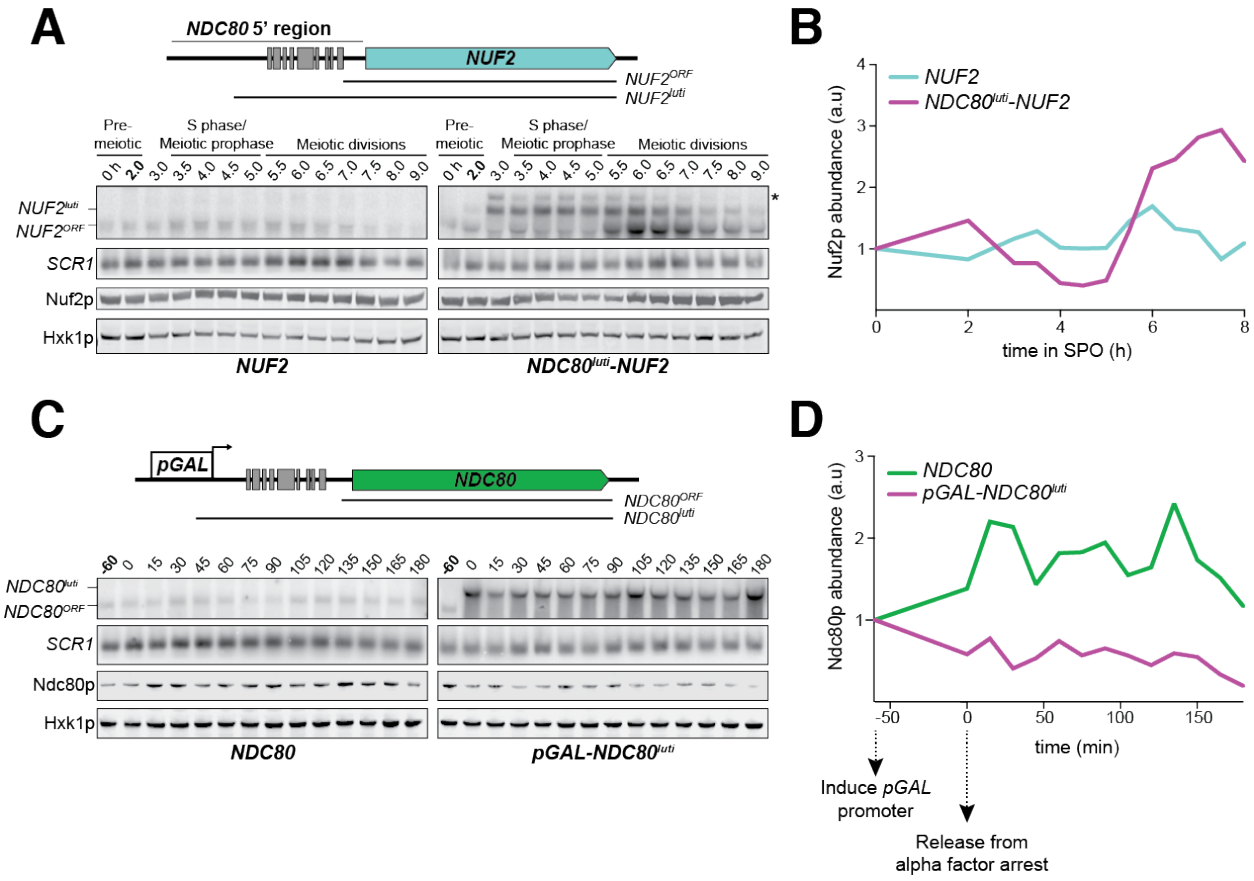

Figure 2.12: $NDC80^{LUTI}$ is sufficient to downregulate $NDC80^{ORF}$.(A) A *LUTI mRNA* is produced by the $NDC80^{LUTI}$-*NUF2* fusion construct ($NUF2^{LUTI}$) in meiosis. To generate the $NDC80^{LUTI}$-*NUF2* construct, the promoter and leader sequence of $NDC80^{LUTI}$(1000 bps directly upstream of the *NDC80* ORF start site) was placed immediately upstream of the *NUF2* coding region. $NUF2^{LUTI}$ and $NUF2^{ORF}$ expression was detected by northern blot, and Nuf2 was detected by anti-V5 immunoblot. *SCR1*, loading control for northern blot. Hxk1, loading control for immunoblot. Samples were taken when the wild-type (UB5103) and $NDC80^{LUTI}$-*NUF2* (UB5101) cells were undergoing synchronous meiosis. * indicates a band of unknown origin. (B) Quantification of the Nuf2 protein abundance from the experiment shown in (A). For each time point, Nuf2 signal was first normalized to Hxk1. This normalized value was set to 1 for the 0 hr time point (t_0), and all the subsequent time points were calibrated to t_0. (C) $NDC80^{ORF}$, $NDC80^{LUTI}$, and Ndc80 levels when $NDC80^{LUTI}$ is expressed in synchronous mitosis. *MAT***a** wild-type control (UB2389) and *pGAL-*$NDC80^{LUTI}$ (UB2388) cells, both harboring the Gal4-ER fusion protein, were arrested in G_1 with α-factor. *pGAL* expression was induced 2 hrs later by addition of β-estradiol (-60 min). One hour after the β-estradiol addition (0 min), cells were released from G_1 arrest. (D) Quantification of the Ndc80 abundance from the experiment shown in (C). For each time point, Ndc80 signal was first normalized to Hxk1. This normalized value was set to one for the first time point at -60 min (t_{-60}), the time of β-estradiol addition. All the subsequent time points were then calibrated to t_{-60}.

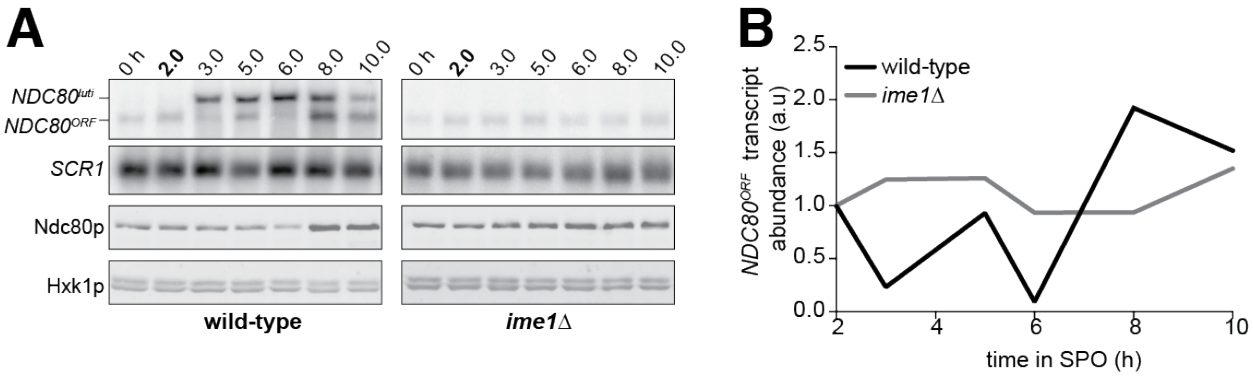

Figure 2.13: *NDC80*^{LUTI} expression requires Ime1. (A) *NDC80*^{ORF}, *NDC80*^{LUTI}, and Ndc80 abundance during meiosis in *pCUP-IME1 pCUP-IME4* (FW1902) and *pCUP-IME4 ime1*Δ (FW3058) cells. Expression from the *pCUP* promoter was induced after the cells were incubated in SPO for 2 hrs. (B) Quantification of the *NDC80*^{ORF} transcript abundance shown in (A), a time course comparing the *pCUP-IME1 pCUP-IME4* strain (FW1902) during meiosis with the *pCUP-IME4 ime1*Δ strain (FW3058). *NDC80*^{ORF} signal was first normalized to *SCR1*. The normalized value for the 2 hr time point (immediately prior to *IME1* and *IME4* induction) was set to 1, and all the subsequent time points were calibrated to this time point.

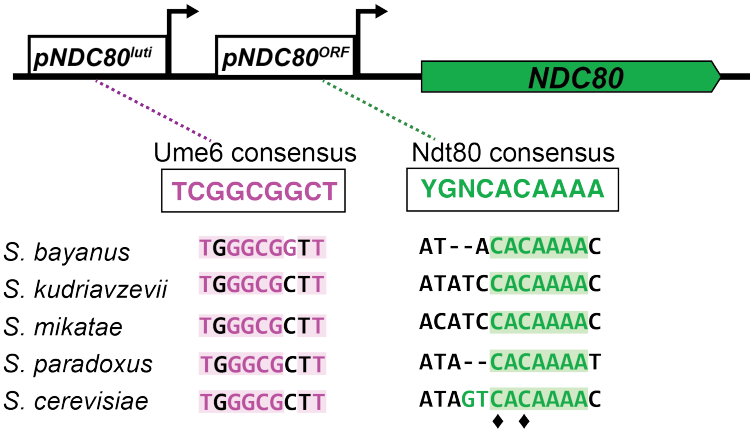

Figure 2.14: Putative Ume6 (*URS1*) and Ndt80 (*MSE*) binding sites are present in the intergenic region upstream of *NDC80*. Colored bases match the consensus binding sequences. Highlighted areas indicate the conserved regions across all five *Saccharomyces* species by Clustal analysis. The black diamonds indicate the two sites mutated from C to A in the *ndc80-mse* strain.

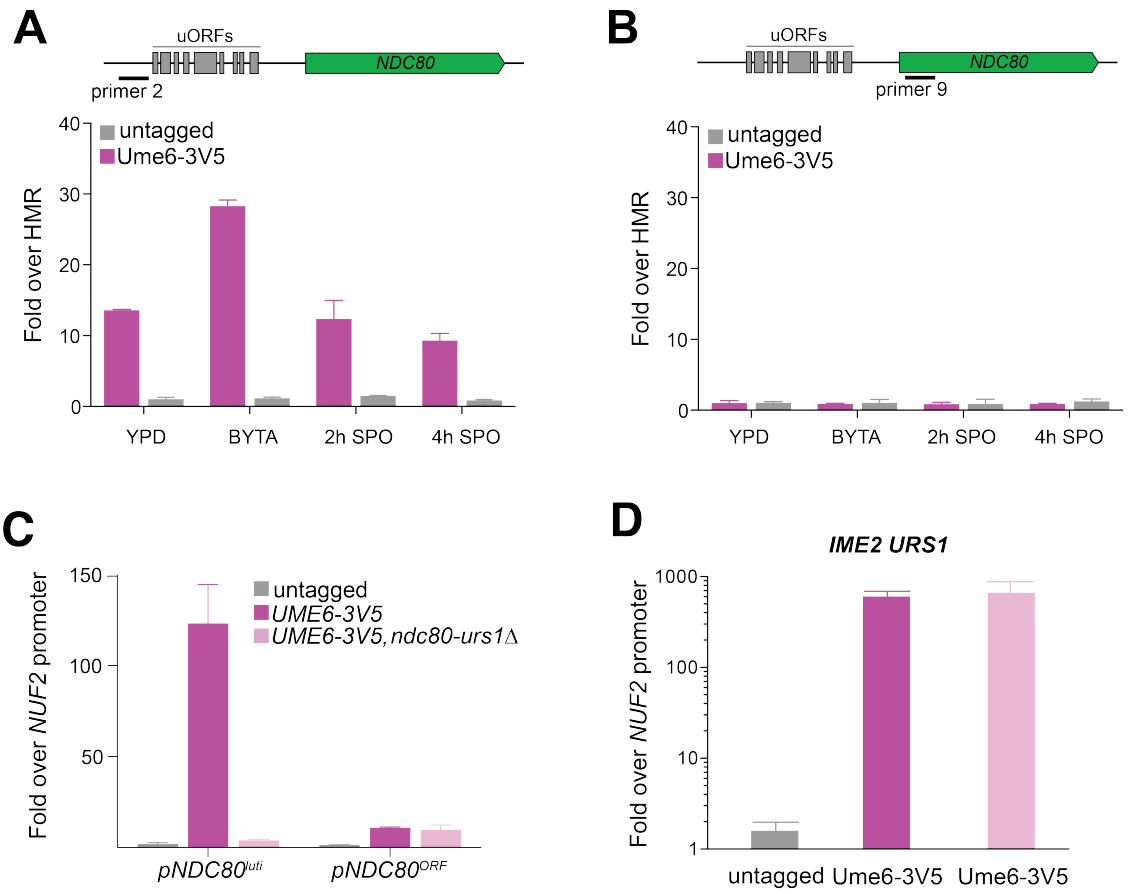

Figure 2.15: Ume6 binds to the $NDC80^{LUTI}$ promoter. (A-B) Ume6 is enriched at the $NDC80^{LUTI}$ promoter and not the *NDC80* coding region before and during early meiosis. Ume6-3V5 chromatin immunoprecipitation (ChIP) was performed for the untagged (FW1511) and Ume6-3V5 (FW1208) strains exponentially grown in nutrient rich medium, during stationary phase in BYTA, and after transfer to SPO. The recovered DNA fragments from the Ume6-3V5 ChIP were quantified by qPCR using the primer sets specific for the $NDC80^{LUTI}$ promoter (primer 2, shown in A) and the *NDC80* coding region (primer 9, shown in B). Enrichment at these loci was normalized to the signal from *HMR*, to which Ume6 does not bind. (C) Ume6-3V5 ChIP for the untagged (UB2531), *UME6-3V5* (UB3301), and *UME6-3V5 ndc80-urs1*Δ (UB6760) strains. For (C) and (D), cells were harvested after overnight growth in BYTA. The DNA fragments recovered from the Ume6-3V5 ChIP were quantified by qPCR using the following primer pairs specific for: (1) the $NDC80^{LUTI}$ promoter, (2) the $NDC80^{ORF}$ promoter, and (3) the *IME2 URS1* site. Enrichment at these loci was normalized to the signal from the *NUF2* promoter, to which Ume6 does not bind. (A-D) graph the mean fold enrichment from 3 independent experiments, as well as the standard error of the mean.

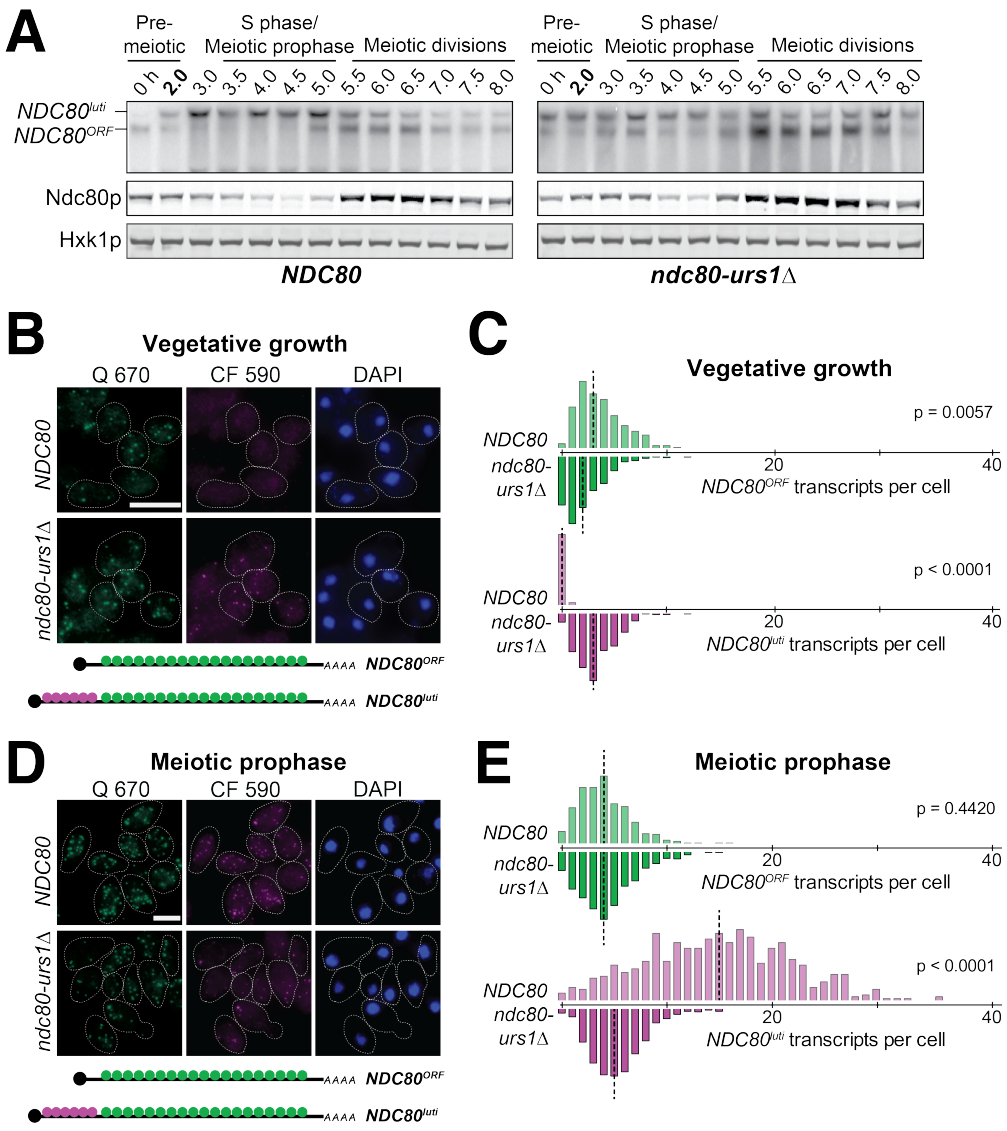

Figure 2.16: Ume6 regulates $NDC80^{LUTI}$ expression. (A) $NDC80^{ORF}$, $NDC80^{LUTI}$, and Ndc80 levels during synchronous meiosis (as described in Figure 2.4) in the wild-type cells (UB6190) and *ndc80-urs1*Δ cells (UB6075). (B, D) Representative smFISH images for $NDC80^{LUTI}$ and $NDC80^{ORF}$ during vegetative growth (B) in the wild-type (UB5875) and *ndc80-urs1*Δ (UB5473) strains, or during meiotic prophase (D) in the wild-type (UB6190) and *ndc80-urs1*Δ (UB6075) strains. For vegetative growth samples, cells were grown to exponential phase in nutrient rich medium. For meiotic samples, cells were fixed at 2 hr after *IME1* and *IME4* induction. DNA was stained with DAPI (blue). Scale bar: 5 μm. (C, E) Quantification of (B) and (D), respectively, and graphed as the relative frequency histograms of cells with a given number of $NDC80^{LUTI}$ and $NDC80^{ORF}$ transcripts per cell. Data were pooled from 3 independent experiments. Dashed line, the median number of $NDC80^{LUTI}$ and $NDC80^{ORF}$ transcripts per cell. Two-tailed Wilcoxon Rank Sum test was performed for $NDC80^{ORF}$ and $NDC80^{LUTI}$, respectively, comparing wild-type with the *ndc80-urs1*Δ mutant.

analysis revealed that Ume6 binding was enriched over the predicted *URS1* site in mitosis and early meiosis, whereas Ume6 binding was undetectable within the $NDC80^{ORF}$ promoter (Figure 2.15, Panel A-C). Deletion of the *URS1* site (*ndc80-urs1*Δ) completely abolished Ume6 binding to the $NDC80^{LUTI}$ promoter (Figure 2.15, Panel C) but did not affect another Ime1-Ume6 target gene *IME2* (Figure 2.15, Panel D). Consistent with the role of Ume6 as a transcriptional repressor in mitosis, deletion of the *URS1* site resulted in leaky expression of $NDC80^{LUTI}$ during vegetative growth (Figure 2.16, Panel B and C) ($p<0.0001$) and reduced expression of $NDC80^{ORF}$ (Figure 2.16, Panel B and C) ($p=0.0057$). Abolishing Ume6 binding eliminated the strong induction of $NDC80^{LUTI}$ in meiosis (Figure 2.16, Panel D and E) ($p<0.0001$), causing moderately increased levels of $NDC80^{ORF}$ transcript by northern blot and Ndc80 protein in meiotic prophase (Figure 2.16, Panel A). We did not detect significant increase in $NDC80^{ORF}$ in the *urs1*Δ cells by smFISH (Figure 2.16, Panel F), likely due to technical reasons. We conclude that similar to early meiotic genes, Ime1 and Ume6 directly regulate the transcription of $NDC80^{LUTI}$.

The second key meiotic transcription factor, Ndt80, is required for meiotic chromosome segregation and spore formation (Chu & Herskowitz 1998; Xu *et al.* 1995). Expression of *NDT80* occurs shortly before the reappearance of $NDC80^{ORF}$ transcript. Within the budding yeast lineage, an Ndt80 consensus site, called the mid-sporulation element (*MSE*), was identified 184 bp upstream of the Ndc80 translation start site (Figure 2.14), within the $NDC80^{ORF}$ promoter. One hour after Ndt80 expression was induced in the *pGAL-NDT80 GAL4-ER* system, Ndt80 binding was enriched over the predicted *MSE* by ChIP analysis; moreover, mutations in the *MSE* (*ndc80-mse*) led to a complete loss of Ndt80 enrichment (Figure 2.17, Panel A) but did not affect another Ndt80 target gene *MAM1* (Figure 2.17, Panel B). Furthermore, when Ndt80 failed to bind to the $NDC80^{ORF}$ promoter, both the $NDC80^{ORF}$ transcript and Ndc80 protein levels reduced during the meiotic divisions (Figure 2.17, Panel C). These results demonstrate that Ndt80 directly induces $NDC80^{ORF}$ expression after meiotic prophase, and this timely induction of $NDC80^{ORF}$ elevates the levels of Ndc80 protein prior to the meiotic divisions.

2.3.6 Expression of $NDC80^{LUTI}$ is required to limit kinetochore activity in meiotic prophase

Since Ndc80 appears to be the limiting subunit of the kinetochore, we posited that the regulated expression of $NDC80^{LUTI}$ and $NDC80^{ORF}$ serves to inactivate and reactivate kinetochores, respectively, through modulating Ndc80 protein levels. In budding yeast, kinetochores are inactive in meiotic prophase, but they can be activated upon Ndc80 overexpression (Miller *et al.* 2012, and Figure 2.3). We asked whether functional kinetochores could also be generated in meiotic prophase if cells failed to express $NDC80^{LUTI}$ ($\Delta NDC80^{LUTI}$) or expressed a version of $NDC80^{LUTI}$ that could translate Ndc80 protein ($\Delta 9AUG$). Both conditions caused an increase in Ndc80 levels in meiotic prophase (Figures 2.8 and Figure 2.7). Using the same assay described in Figure 2.3, we observed that over 50% of the $\Delta NDC80^{LUTI}$

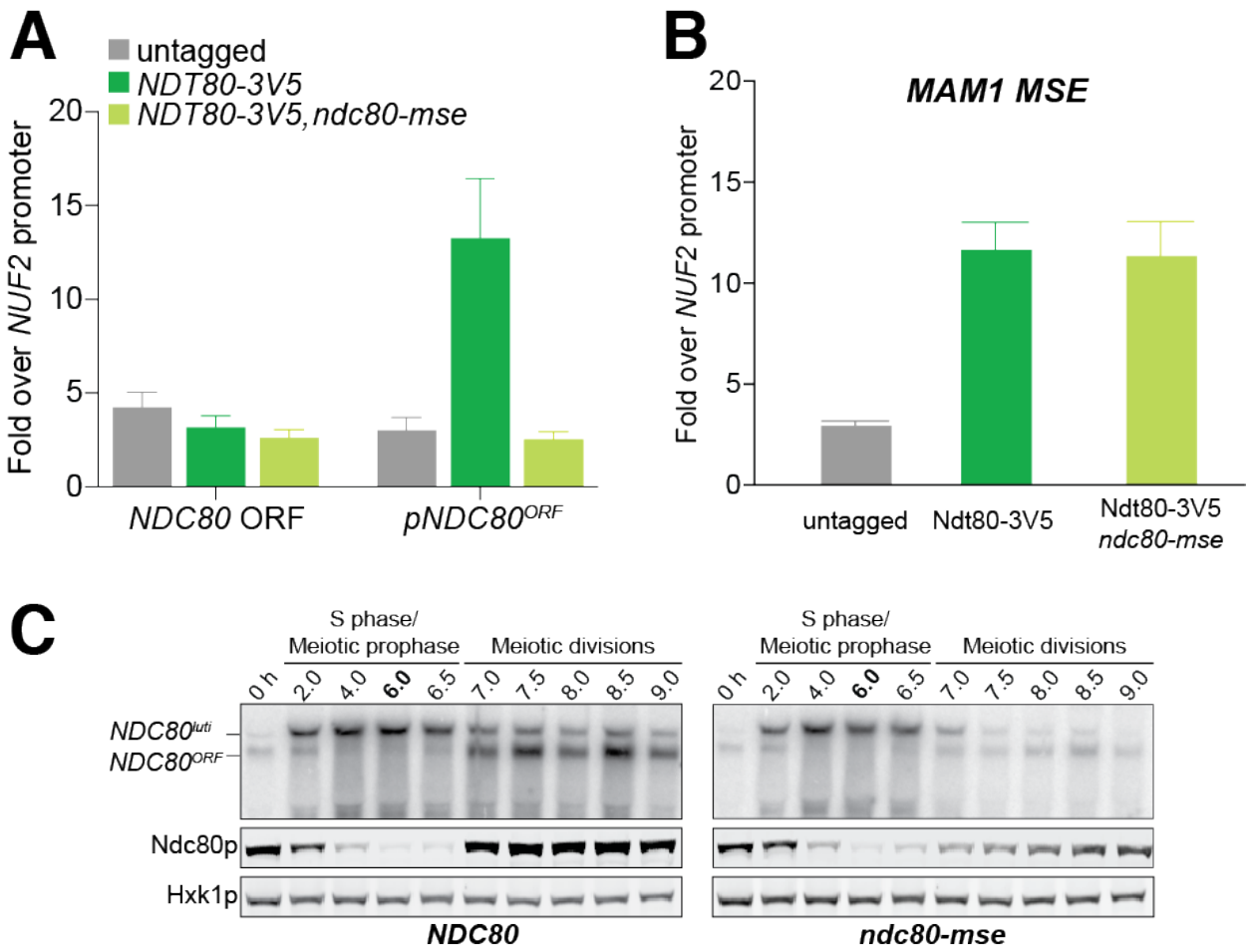

Figure 2.17: Ndt80 regulates $NDC80^{ORF}$ expression. (A-B) Ndt80-3V5 ChIP for the untagged (UB7997), *NDT80-3V5* (UB7999), and *NDT80-3V5 ndc80-mse* strains (UB7496). After 5 hrs in SPO, *NDT80* expression was induced with β-estradiol. Cells were harvested 1 hr after Ndt80 induction. The recovered DNA fragments were quantified by qPCR using the following primer pairs specific for: (1) the $NDC80^{ORF}$ promoter ($pNDC80^{ORF}$), (2) the *NDC80* coding region (*NDC80* ORF), and (3) the *MAM1 MSE* site. Enrichment at these loci was normalized to the signal from the *NUF2* promoter, to which Ndt80 does not bind. The mean fold enrichment over the *NUF2* promoter from 3 independent experiments, as well as the standard error of the mean, is displayed. (C) $NDC80^{ORF}$, $NDC80^{LUTI}$, and Ndc80 level during meiosis in the wild-type (UB4074) and *ndc80-mse* (UB3392) strains. Both strains harbor the *pGAL-NDT80 GAL4-ER* system. Cells were transferred to SPO at 0 hr and released from pachytene arrest at 6 hr by addition of β-estradiol.

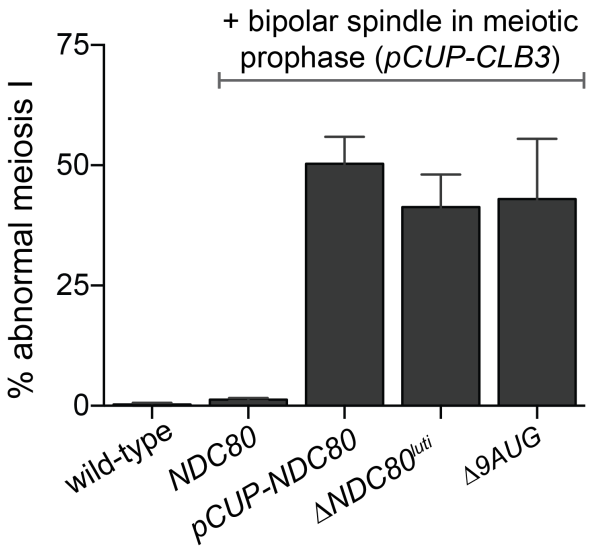

Figure 2.18: Sister chromatid segregation in the the wild-type (UB2942), *pCUP-CLB3* (UB877), *pCUP-CLB3 pCUP-NDC80* (UB880), *pCUP-CLB3* $\Delta NDC80^{LUTI}$ (UB2940), and *pCUP-CLB3* $\Delta 9AUG$ (UB2936) cells. Cells were induced to sporulate by transferring to SPO, and 6 hrs later, the expression of the cyclin Clb3 was induced by addition of $CuSO_4$. Immediately after induction, cells were released from pachytene by addition of β-estradiol. Samples were taken 1 hr 45 min after the release. Premature segregation of sister chromatids in meiosis I (abnormal meiosis I) was detected as two separated GFP dots in binucleates, one in each nucleus. The average fraction of binucleates that displayed sister segregation in meiosis I from three independent experiments, as well as the standard error of the mean, was graphed. 100 cells were counted per strain, per experiment.

or $\Delta 9AUG$ cells displayed abnormal chromosome segregation in meiosis I (Figure 2.18), suggesting premature kinetochore activity in meiotic prophase. The extent of this phenotype was indistinguishable from that when Ndc80 was overexpressed in meiotic prophase (*pCUP-NDC80*) (Figure 2.18). Therefore, the $NDC80^{ORF}$ repression by $NDC80^{LUTI}$ transcription is crucial to inhibit untimely kinetochore function during meiotic prophase.

2.3.7 Re-expression of $NDC80^{ORF}$ is required to resume kinetochore activity in the meiotic divisions

Functional kinetochores must be present after meiotic prophase to faithfully execute chromosome segregation during the two meiotic divisions. Since Ndc80 protein levels become nearly undetectable during prophase (Figure 2.2), Ndc80 must be resynthesized to restore the ability of kinetochores to interact with microtubules upon exit from prophase. This resynthesis relies on the transcription factor Ndt80 to induce transcription of $NDC80^{ORF}$ (Figure 2.17). To test the significance of Ndt80-dependent induction of $NDC80^{ORF}$ in meiosis, we monitored the segregation pattern of chromosome V in the cells with a mutated Ndt80 binding site in the $NDC80^{ORF}$ promoter (*ndc80-mse*). Only 1% of the wild-type cells mis-

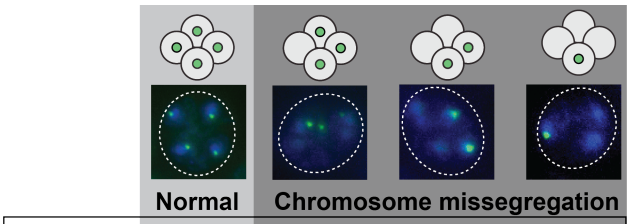

	Normal	Chromosome missegregation
NDC80	98.5%	1.5%
ndc80-mse	2%	98%

Figure 2.19: Re-expression of $NDC80^{ORF}$ is required to resume kinetochore activity in the meiotic divisions. How accurately chromosomes segregated in the wild-type (UB5876) and *ndc80-mse* (UB5437) strains was determined by counting the homozygous *CENV-GFP* dots in tetranucleates. Samples were taken 7.5 hrs after the cells were incubated in SPO, a time when most cells had completed meiosis in an asynchronous system. The fraction of tetranucleates that displayed normal segregation (one GFP dot in each nucleus), or missegregation (multiple or zero GFP dots in any of the four nuclei) was quantified. The average fraction of normal segregation or missegregation from two independent experiments is shown. Over 100 cells were counted per strain, per experiment.

segregated chromosome V, whereas 98% of the *ndc80-mse* cells failed to properly segregate this chromosome (Figure 2.19), suggesting that kinetochores are not functional in *ndc80-mse* cells. In support of this conclusion, in *ndc80-mse* cells, elongated bipolar spindles (over 2 μm) appeared earlier and persisted longer than in the wild-type cells (Figure 2.20), a phenomenon consistent with defective microtubule-kinetochore attachments (Wigge *et al.* 1998; Wigge & Kilmartin 2001). Additionally, the abundance of short meiosis II spindles (less than 2 μm) was reduced in the *ndc80-mse* cells (Figure 2.20). At the end of meiosis, more than four nuclei were often observed (representative images shown in Figure 2.19). The *ndc80-mse* mutation also severely affected the sporulation efficiency (Figure 2.21). All of these results demonstrate that Ndt80-dependent induction of $NDC80^{ORF}$ is essential for re-establishing kinetochore function to mediate meiotic chromosome segregation.

Unlike $NDC80^{ORF}$ transcript, $NDC80^{LUTI}$ is absent in vegetative growth due to repression by Ume6 (Figure 2.16). We hypothesized that $NDC80^{LUTI}$ is repressed during the mitotic cell cycle because its expression could inactivate kinetochore function (Figure 2.12). Indeed, when the Ume6 repressor-binding site within the $NDC80^{LUTI}$ promoter was deleted ($urs1\Delta$), these cells grew similar to the wild-type cells at 30 °C, but they had a severe growth defect at 37 °C because the Ndc80 level was reduced (Figure 2.22). Thus, the repression of $NDC80^{LUTI}$ by Ume6 is critical for the fitness of mitotically dividing cells.

When $NDC80^{LUTI}$ was strongly induced in vegetative growth using the inducible *GAL1-10* promoter, these cells had a severe growth defect (Figure 2.23). This defect was rescued by a second copy of *NDC80* at an ectopic locus, consistent with the model that $NDC80^{LUTI}$-mediated repression of $NDC80^{ORF}$ occurs in *cis* (Figure 2.23 and Figure 2.11). Induction of the uORF-free $NDC80^{LUTI}(\Delta 9AUG)$ caused no appreciable growth defect (Figure 2.23), consistent with the observation that the $\Delta 9AUG$ cells could express Ndc80 protein (Figure

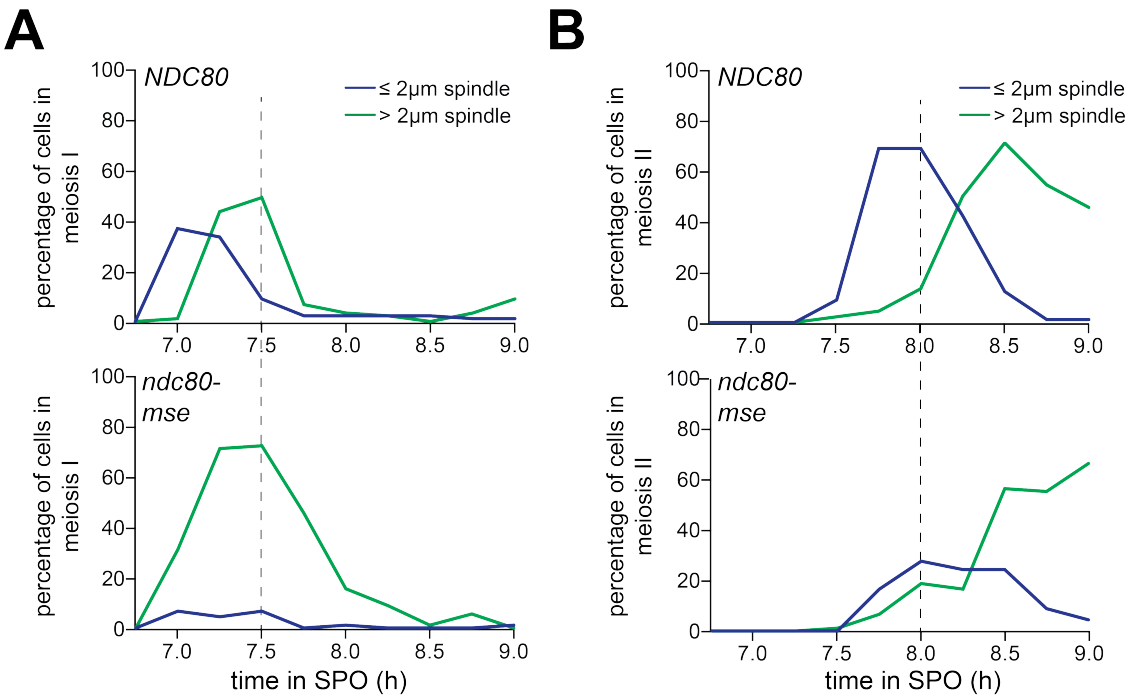

Figure 2.20: Re-expression of $NDC80^{ORF}$ is required for proper meiotic progression. (A-B) Percentage of the wild-type (UB4074) and *ndc80-mse* (UB3392) cells with meiosis I spindles (shown in A) or meiosis II spindles (shown in B) that were longer than 2 μm, as well as the percentage of cells with spindles that were shorter than 2 μm. Both strains harbor the *pGAL-NDT80 GAL4-ER* system. After 6 hrs in SPO, the cells were released from pachytene by addition of β-estradiol, and samples were taken every 15 min after the release. Over 100 cells per time point were quantified, and the results of one representative repeat from two independent experiments are shown.

2.7).

2.4 Discussion

In this study, we have identified an integrated regulatory circuit that controls the inactivation and subsequent reactivation of the meiotic kinetochore (Figure 2.24). This circuit controls the synthesis of a limiting kinetochore subunit, Ndc80, and relies on the regulated expression of two distinct *NDC80* mRNAs. A meiosis-specific switch in promoter usage induces the expression of a 5' extended transcript isoform, $NDC80^{LUTI}$, which itself cannot produce Ndc80 protein. Rather, its function is purely regulatory. Transcription of this alternate isoform leads to repression of the protein-translating $NDC80^{ORF}$ isoform in *cis*. This results in inhibition of Ndc80 protein synthesis and ultimately the inactivation of kinetochore function in meiotic prophase. Reactivation of the kinetochore is achieved by the transcription of $NDC80^{ORF}$ upon exiting meiotic prophase. Temporally coordinated by two

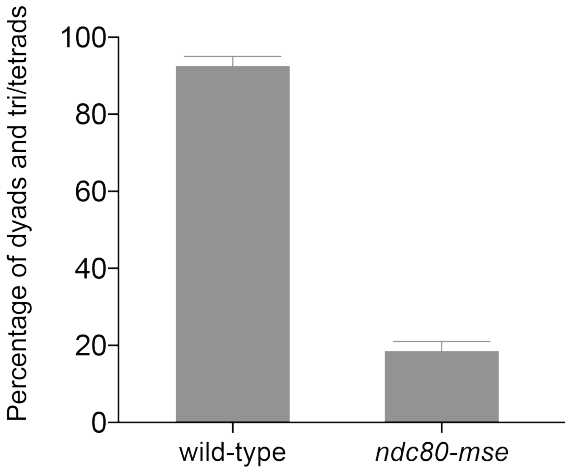

Figure 2.21: Mutation of the *NDC80 MSE* site hinders spore formation. Spore formation (dyad, triads, and tetrads) in the wild-type (UB5876) and *ndc80-mse* (UB5437) strains after meiosis. The average fraction of spore formation in two independent experiments, as well as the range of the two repeats, is displayed.

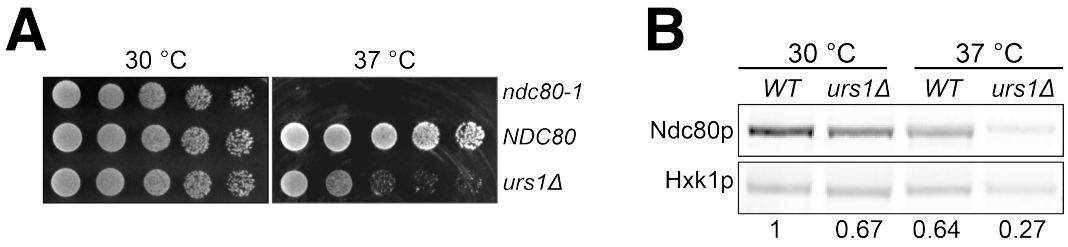

Figure 2.22: *URS1* mutation causes growth defect at high temperature due to a reduced Ndc80 level. (A) Growth phenotype of the *ndc80-urs1*Δ cells at 30 °C and 37 °C. The temperature-sensitive *ndc80-1* (UB494), wild-type (UB3262), and *urs1*Δ (UB4212) cells were serially diluted and grown on nutrient rich medium (YPD) plates at 30 °C or 37 °C for 2 days. (B) Ndc80 level in the wild-type (UB3262) and *urs1*Δ (UB4212) cells grown at 30 °C or 37 °C. For each condition, equal OD_{600} of cells were taken, and Ndc80 was visualized by anti-V5 immunoblot. Hxk1, loading control. WT, wild-type. The number under each lane is the ratio of the relative Ndc80 levels (normalized to Hxk1 levels) compared with that of the wild-type at 30 °C.

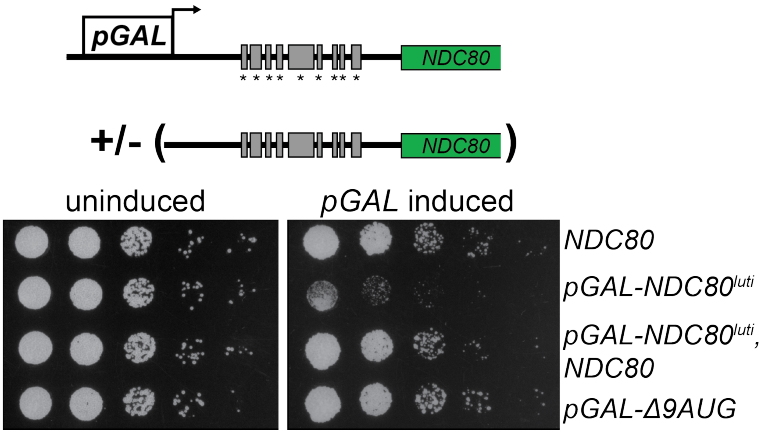

Figure 2.23: Induction of the uORF-free $NDC80^{LUTI}(\Delta 9AUG)$ caused no appreciable growth defect. Growth phenotype of the haploid control (UB1240), $pGAL\text{-}NDC80^{LUTI}$ (UB1217), $pGAL\text{-}NDC80^{LUTI}$ with a second copy of *NDC80* at the *LEU2* locus (UB8001), and $pGAL\text{-}\Delta 9AUG$ (UB1323). Cells were serially diluted and grown on YEP-raffinose/galactose (YEP-RG) plates (uninduced) or YEP-RG plates supplemented with β-estradiol (*pGAL* induced) at 30 °C for 2 days.

master transcription factors, the timely expression of these two mRNA isoforms is essential for kinetochore function, accurate chromosome segregation, and gamete viability.

2.4.1 A limiting subunit controls kinetochore function in meiosis

In meiosis, kinetochore function is transiently inactivated to facilitate accurate chromosome segregation (Miller *et al.* 2013). This transient inactivation is achieved by the removal of the outer kinetochore from chromosomes and has been described in organisms ranging from yeast to mice (Asakawa *et al.* 2005; Kim *et al.* 2013; Meyer *et al.* 2015; Miller *et al.* 2012; Sun *et al.* 2011). In budding yeast, we found that the outer kinetochore removal is mediated by limiting the abundance of a single subunit, Ndc80. Ndc80 is the only member of its complex whose protein abundance is essentially absent in meiotic prophase (Meyer *et al.* 2015 and Figure 2.2). Furthermore, prophase overexpression of *NDC80*, but none of the other Ndc80 complex subunits, promotes premature spindle attachments and causes meiotic chromosome segregation errors (Figure 2.3). Thus, in the case of the meiotic kinetochore, the cell regulates the activity of a multi-protein complex by limiting the availability of a single subunit.

Controlling the activity of the whole protein complex by limiting a key subunit is a more general principle. As revealed by a genome-wide study that analyzed the composition of protein complexes during the cell cycle, most protein complexes in budding yeast have both constitutively and periodically expressed subunits (de Lichtenberg *et al.* 2005). It is proposed that due to the periodically expressed subunits, these protein complexes assemble "just-in-time" to restrict their function to specific cell cycle stages (de Lichtenberg *et al.* 2005). The regulatory circuit controlled by the LUTI mRNAs may more broadly address

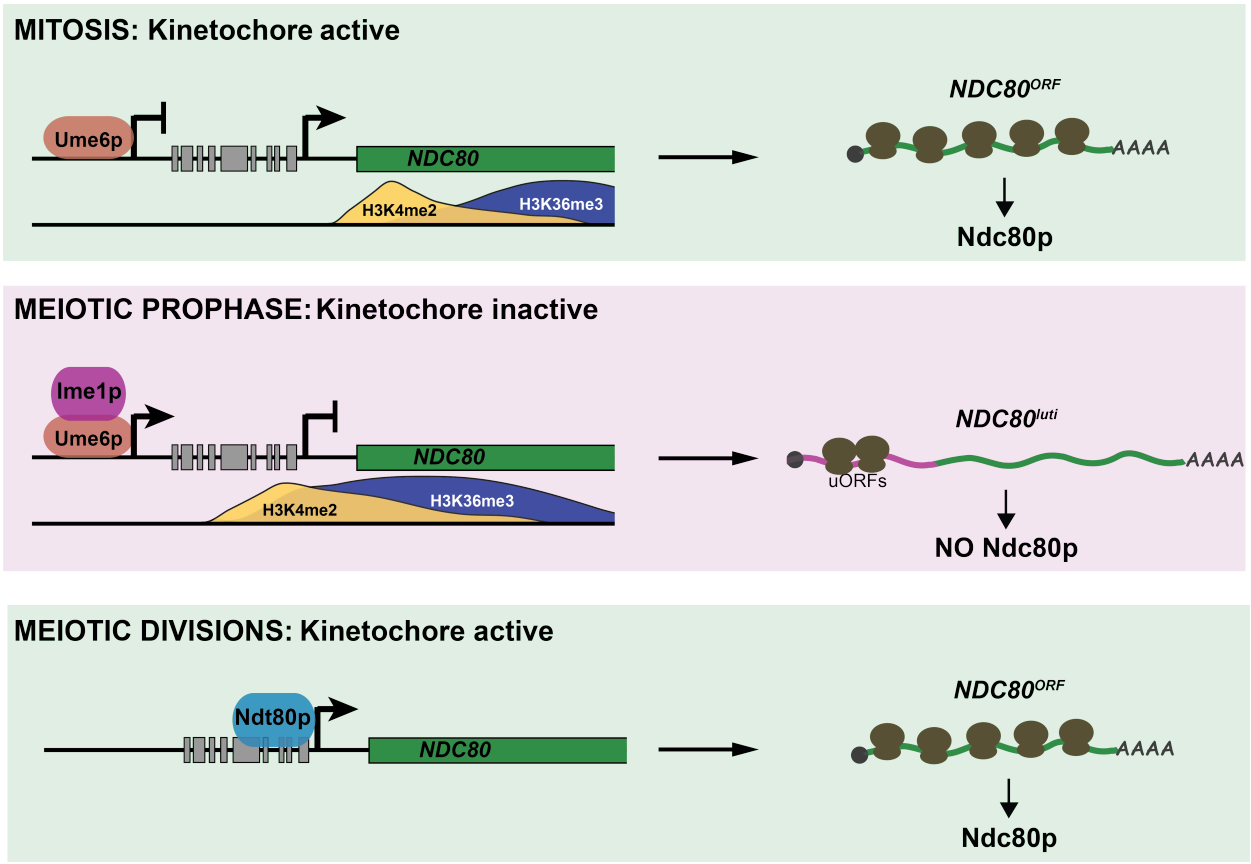

Figure 2.24: Model of the *NDC80* gene regulation in budding yeast. During vegetative growth, a stage in which kinetochores are active, a short *NDC80* mRNA isoform $NDC80^{ORF}$ is expressed, and the 5' extended isoform $NDC80^{LUTI}$ is repressed by Ume6. Translation of $NDC80^{ORF}$ results in Ndc80 protein synthesis (top panel). At meiotic entry, the master transcription factor Ime1 induces expression of $NDC80^{LUTI}$. Transcription from this distal $NDC80^{LUTI}$ promoter silences the proximal $NDC80^{ORF}$ promoter through a mechanism that increases H3K4me2 and H3K36me3 marks over the $NDC80^{ORF}$ promoter (Chia *et al.* 2017). $NDC80^{LUTI}$ does not support Ndc80 synthesis due to translation of the uORFs. The overall synthesis of Ndc80 is repressed in meiotic prophase, and the kinetochores are inactive (middle panel). As cells enter the meiotic divisions, the transcription factor Ndt80 induces $NDC80^{ORF}$ re-expression, allowing for Ndc80 re-synthesis and formation of active kinetochores (bottom panel).

how regulated subunits are provided "just-in-time" and, importantly, at no other time.

2.4.2 *NDC80^{LUTI}* is an mRNA that does not produce protein

A surprising finding of our work is that an mRNA can serve a purely regulatory function. Indeed, *NDC80^{LUTI}* is a *bona fide* mRNA. It is poly-adenylated, is engaged by the ribosome and, most importantly, when the uORF start codons are ablated, Ndc80 protein is translated from this extended mRNA isoform (Brar *et al.* 2012 and Figure 2.7). Moreover, *NDC80^{LUTI}* is likely a RNA Polymerase II transcript because its promoter is occupied by the pre-initiation complex member Sua7 (TFIIB) and because Pol II-associated chromatin marks are detected downstream of the *NDC80^{LUTI}* promoter when this transcript is made (Chia *et al.* 2017). *NDC80^{LUTI}* cannot be decoded by the ribosome due to the presence of the AUG-uORFs contained in its extended 5' leader. By competitively engaging the ribosome, these uORFs prevent the translation of Ndc80 protein. The polypeptides that the uORFs encode are unlikely to play a role in repressing kinetochore function since these uORFs can be minimized to 2-codon units while maintaining the *NDC80^{LUTI}*-based repression (Figure 2.7). Interestingly, upstream AUG codons are also present in the putative *NDC80^{LUTI}* mRNAs predicted from the other fungal species. Three regions were enriched for the presence of such AUGs, but the sequences and the length of these putative uORFs did not seem conserved (Figure 2.25). This observation is consistent with the idea that the act of uORF translation, rather than the identity of the uORF peptides, serves as a conserved feature in evolution.

The repressive nature of the uORFs contained in *NDC80^{LUTI}* mirrors those found in the uORF-containing prototype transcript, *GCN4* (Mueller & Hinnebusch 1986). However, in the case of *GCN4*, changes in nutrient availability can relieve the uORF-mediated translational repression, whereas for *NDC80^{LUTI}*, the uORF-mediated repression appears to be constitutive. In both cases, *GCN4* and *NDC80* can exist in on and off states. For *GCN4*, this switch is manifested in the two translational states of the same mRNA molecule. For *NDC80*, the switch is manifested instead by two distinct transcripts, one that results in protein synthesis and one that represses protein synthesis. It is important to note that for other potential *LUTI* mRNAs, the precise mechanism of the translational repression may not be conserved and could instead involve other means such as RNA hairpins or binding sites for translational repressors.

2.4.3 The function of *NDC80^{LUTI}* mRNA is purely regulatory

Why do meiotic cells express an mRNA that does not encode any functional polypeptides? We propose that the biological purpose of *NDC80^{LUTI}* is to shut down Ndc80 protein synthesis by repressing *NDC80^{ORF}* in *cis*, thereby inactivating kinetochore function during meiotic prophase. Multiple lines of evidence support this model. First, disruption of *NDC80^{LUTI}* expression in meiosis results in elevated levels of *NDC80^{ORF}* and Ndc80 protein in meiotic prophase, leading to premature kinetochore activation (this study and Chia *et al.* 2017). Second, induction of *NDC80^{LUTI}* transcription in *cis* is sufficient to repress

Predicted peptide sequences for the putative AUG uORFs.

Species	Number of uORFs	Predicted uORF peptide sequence
S. bayanus	10	MARRTEQDNKKKVTRQTNAG* MRADLMPFDSLW* MVMVFKYRKEHQRCKYVSRFVGTRWLRPVLT* MVFKYRKEHQRCKYVSRFVGTRWLRPVLT* MCLDLSVHGG* MI* MSDHGGNKHTARSGWLCSAVKGLSMALAT* MVVINIQLDRVGSARRLRGFQWHLLPNLLPSAAKLRYPASN TQKDAFLRTK* MIIHKTKISKINKRHQKWQKTKEIDSIEEVGIYHWLFRDRTVK K* MAKNKRNR*
S. kudriavzevii	8	MRLVLE* MRTKRLRVLNQFRFIGAKIEQRLCCSAC* MLEPIAIVL* MS* MALSDS* MGYPSQEIQFNASPRTK* MIYPQNENTQNKQTTPKMVKQKR* MVKQKR*
S. mikatae	5	MIQVLLVYYHQIVVRE* MLRKAKKTGGPKSIGVRIGEELYYTTGHI* MTTSRWDPCLVTLNI* MFSKVNKEHQK* MEIDNLGGG*
S. paradoxus	6	MS* MHIGWEPC* MLTMVRM* MDHNV* MIYTKLNSPKINKQHQKWQELLE* MARIIGIDCVGEVQSVPSFCQKLKQSKKNN*
S. cerevisiae	9	MQRKDGWRSEKHY* MLGLKRNSPYYVPDGYN* MCQMVITEH* MVITEH* MGWLRAPLSIVKDVSSLLRLAVKIPFQGLPILKVPKEKKITYG MI* M* ME* MI* MVEIIGIHSQER*

Figure 2.25: Putative uORFs found in the upstream intergenic region of *NDC80* in five budding yeast species. Only the uORFs that fall between the putative binding sites of Ume6 and Ndt80 are counted.

NDC80^{ORF} and inactivate kinetochore function in mitotic cells (this study). Third, transcription of *NDC80*^{LUTI} introduces repressive chromatin marks at the *NDC80*^{ORF} promoter that are necessary for the downregulation of *NDC80*^{ORF} and Ndc80 protein (Chia *et al.* 2017). Altogether, these findings strongly suggest that the primary function of the *NDC80*^{LUTI} mRNA is to turn off the *NDC80* gene.

2.4.4 Pervasiveness of *LUTI* mRNA biology in yeast meiosis and beyond

The defining sequence features of the *NDC80 LUTI* mRNA are a 5' extended mRNA leader coupled with repressive uORFs contained in this extended leader. Analysis of the mRNA-seq, ribosome profiling, and quantitative mass spectrometry datasets revealed at least 380 transcripts with potential *LUTI*-like signatures in meiosis (Cheng *et al.* 2018). Two other genes, *ORC1* and *BOI1*, have also been shown to express meiosis-specific transcript isoforms with uORF-containing leader extensions (Xie *et al.* 2016; Liu *et al.* 2015). Rather than dissecting each candidate *LUTI* mRNA on a case by case basis, future studies that integrate additional genome-wide datasets to measure stage-specific transcription factor binding sites, transcription-coupled chromatin modification states, mRNA translation status with isoform specificity and protein abundance would result in a high-confidence map of *LUTI* mRNA and aid in the dissection of their cellular functions.

Beyond budding yeast meiosis, we argue that the regulatory circuit described in our study would be present in other developmental programs and organisms. This is because various organisms also possess the three principles of this module, namely, (1) alternative promoter usage, (2) transcription-coupled repression, and (3) uORF-mediated translational repression. Alternative promoter usage is widespread in development and among different cell types. For example, in the fruit fly, more than 40% of developmentally expressed genes have at least two promoters with distinct regulatory programs (Batut *et al.* 2013). Half of human genes have more than one promoter, resulting in the expression of mRNA isoforms with 5' heterogeneity (Kimura *et al.* 2006). Furthermore, transcription-based interference mechanisms, as well as transcription-coupled histone modifications, have been described in a variety of organisms (Corbin & Maniatis 1989; Eissenberg & Shilatifard 2010; Shearwin *et al.* 2005; Wagner & Carpenter 2012). Finally, recent studies have shown that uORF translation is much more widespread than traditionally believed and acts in a regulatory manner (Calvo *et al.* 2009; Chew *et al.* 2016; Johnstone *et al.* 2016). Therefore, we envision that the regulatory circuit described here can be used as a roadmap in future studies to uncover transcription-coupled gene repression during cell fate transitions across multiple species.

2.4.5 Interpreting genome-wide data in the context of *LUTI* mRNA biology

A key implication of this model of gene regulation is a blurring of the line between "coding" and "non-coding" RNAs. Seminal work has uncovered multiple classes of non-coding RNAs that play regulatory functions in the cell, such as long non-coding RNAs, microRNAs, small interfering RNAs, and piwiRNAs (Ambros 2001; Batista & Chang 2013; Cech & Steitz 2014; Guttman *et al.* 2009). Our study demonstrates that mRNAs, which are deemed protein coding units, can themselves be direct regulators of gene expression by at least two simultaneous means: (1) they can induce transcription-coupled silencing of a downstream promoter. (2) Features in their 5' leaders, such as the presence of uORFs or secondary structures, could directly impact translation efficiency in a positive or negative manner (Arribere & Gilbert 2013; Brar *et al.* 2012; Rojas-Duran & Gilbert 2012). Notably, multiple studies have reported poor correlation between mRNA and protein abundance (Maier *et al.* 2009). For those mRNAs that anti-correlate with their protein levels, this apparent contradiction might be due to a *LUTI* mRNA being misattributed as a canonical protein-coding transcript. Our study could transform how we understand the function of alternate mRNA isoforms and aid in the proper biological interpretation of genome-wide transcription studies.

Chapter 3

Meiotic Regulation of Ndc80 Degradation

3.1 Introduction

Reproduction is a fundamental feature of life. Eukaryotic cells pass on their genetic information by using a conserved protein complex known as the kinetochore, which mediates chromosome segregation. Research over the past three decades has identified at least 40 different proteins that constitute the core of this essential machinery (De Wulf *et al.* 2003; Westermann *et al.* 2003; Fischbock-Halwachs *et al.* 2019). While the function of different kinetochore components is well studied, much less is understood about how the level of specific subunits is regulated under varying cellular states and developmental contexts and how these changes affect kinetochore composition and function.

Changes in the abundance of a single subunit can have a profound impact on kinetochore activity and genome inheritance. For instance, overexpression of CENP-A in yeast, flies, and human cells causes chromosome missegregation and genome instability (Heun *et al.* 2006; Au *et al.* 2008; Shrestha *et al.* 2017). In addition, overexpression of Hec1/Ndc80 and SKA1 has been observed in many types of cancers (Hayama *et al.* 2006; Chen *et al.* 1997; Li *et al.* 2014; Shen *et al.* 2016; Chen *et al.* 2018b). Aside from these pathological states, physiological changes also occur in kinetochore composition. In budding yeast, the Ndc80 level conspicuously fluctuates during meiosis such that the protein is barely detectable in meiotic prophase but is highly expressed during the meiotic divisions. Consequently, the Ndc80 complex disassembles from the kinetochore in early meiosis, leading to a transient shutdown of kinetochore activity (Asakawa *et al.* 2005; Miller *et al.* 2012; Meyer *et al.* 2015; Chen *et al.* 2017). Failure to regulate the Ndc80 level leads to meiotic chromosome segregation defects and gamete inviability (Miller *et al.* 2012; Chen *et al.* 2017), highlighting the importance of its timely regulation.

Both the synthesis and degradation of Ndc80 is regulated in meiosis. Ndc80 is synthesized only during the meiotic divisions and not prior (Figure 3.1) (Chen *et al.* 2017; Chia *et al.*

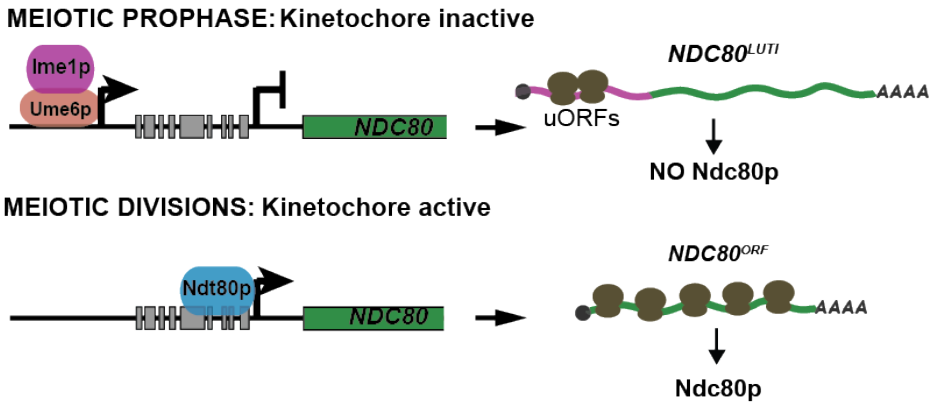

Figure 3.1: Regulation of Ndc80 protein synthesis in budding yeast meiosis.

2017). The ON/OFF switch in Ndc80 synthesis is mediated by the expression of two distinct *NDC80* mRNAs, which are transcriptionally induced by two key meiotic transcription factors. One of the transcripts, $NDC80^{ORF}$, can be translated into Ndc80 protein. The other mRNA isoform, $NDC80^{LUTI}$, cannot be translated into Ndc80 protein due to the presence of upstream open reading frames in its 5' leader, which compete with the translation machinery. Furthermore, $NDC80^{LUTI}$ expression represses transcription initiation from the proximal $NDC80^{ORF}$ promoter. As a result, Ndc80 protein synthesis is turned off in meiotic prophase, a stage when $NDC80^{LUTI}$ is highly expressed. After cells exit from meiotic prophase, the expression of $NDC80^{ORF}$ is induced, leading to Ndc80 protein synthesis and kinetochore activation (Chen *et al.* 2017). While the mechanism controlling Ndc80 synthesis has been revealed, how the meiotic regulation of Ndc80 degradation occurs is not understood. The human homolog of Ndc80, Hec1, undergoes degradation in a cell-cycle-dependent manner, but the turnover mechanism remains elusive (Ferretti *et al.* 2010). In fact, little is known about the factors that mediate kinetochore subunit degradation in a developmental context.

Here, we describe the mechanism by which Ndc80 degradation is controlled in budding yeast meiosis. We found that Ndc80 degradation specifically occurs in meiotic prophase and not in metaphase I. Proteasome activity and a 27-residue degron sequence at the N-terminus of Ndc80 are necessary for Ndc80 proteolysis. In addition, Ndc80 degradation is triggered by Aurora B kinase-dependent phosphorylation, which has been previously linked to correcting erroneous microtubule-kinetochore attachments. Failure to degrade Ndc80 causes premature assembly of the outer kinetochore in meiotic prophase and predisposes meiotic cells to chromosome segregation defects. These results highlight the importance of timely degradation of Ndc80.

3.2 Materials and methods

The strain information and experimental methods are described in Chapter 5.

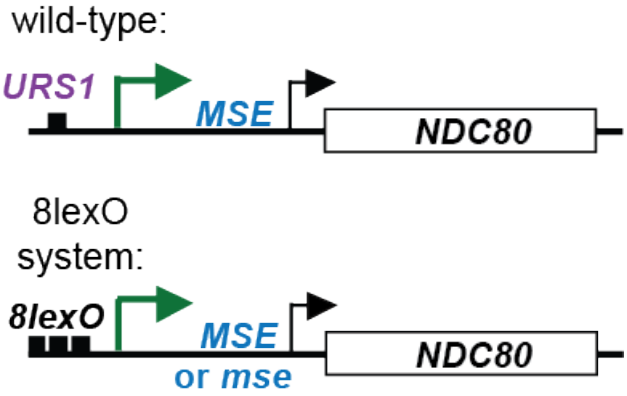

Figure 3.2: The *8lexO* system used to measure Ndc80 protein turnover. Top: Regulatory elements of the *NDC80* gene. *URS1*, binding site for Ume6. *MSE*, binding site for Ndt80; *mse*, a mutant *MSE* site defective of Ndt80 binding. Bottom: The *8lexO* system. Eight tandem *lex* operators (*8lexO*), along with a basal *pCYC1* promoter, are inserted at 536 bps upstream of $NDC80^{LUTI}$ transcription start site. In the presence of the inducer LexA.ER, this system allows the expression of $NDC80^{LUTI}$ mRNA to be induced by β-estradiol, and thus conditionally inhibits the expression of $NDC80^{ORF}$ mRNA and Ndc80 protein synthesis. Throughout this study, a final concentration of 40 nM β-estradiol was used to induce the *8lexO* system.

3.3 Results

3.3.1 Ndc80 degradation is temporally regulated during meiosis

In meiotic prophase, the residual Ndc80 protein from the pre-meiotic cell cycle is turned over by an unknown mechanism (Chen *et al.* 2017). To study Ndc80 degradation without a confounding effect from its synthesis regulation, we took advantage of a previously established method (Chia *et al.* 2017), which allowed us to turn off Ndc80 synthesis in a conditional manner. With this system, we were able to address when and how Ndc80 degradation occurred in meiosis. In this system, an array of 8 *lex* operators (*8lexO*) replaces the endogenous $NDC80^{LUTI}$ promoter. The same strain carries a chimeric lexA-B112 transcription factor fused to an estradiol-binding domain (lexA-B112-ER), which allows inducible transcription from the *8lexO* promoter in the presence of β-estradiol (Ottoz *et al.* 2014). In the absence of β-estradiol (uninduced), $NDC80^{ORF}$ continues to be expressed, and Ndc80 synthesis occurs. Upon β-estradiol addition, $NDC80^{LUTI}$ is expressed, leading to repression of Ndc80 synthesis (Figure 3.2). In comparison to the wild-type cells, this induction system led to similar kinetics of Ndc80 degradation after meiotic entry (Figure 3.3).

Using this system, we measured the Ndc80 turnover rate at different stages of meiosis. Ndc80 synthesis is normally turned off shortly after meiotic entry, and Ndc80 degradation begins soon after (Chen *et al.* 2017). We asked whether Ndc80 degradation is temporally restricted to early meiosis. To address this question, we treated cells with β-estradiol either close to meiotic entry (1.5 hrs after meiosis induction) or in late prophase I (4 hrs after meio-

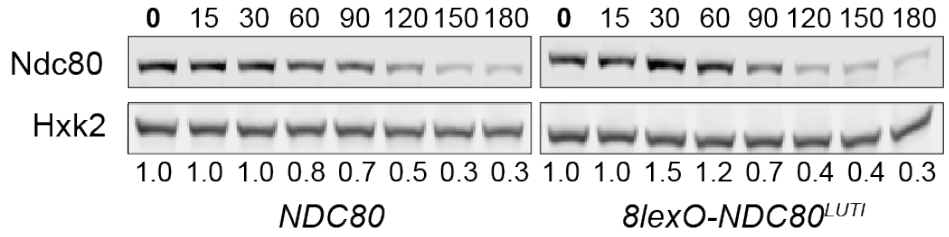

Figure 3.3: Ndc80 level in meiotic prophase when the $NDC80^{LUTI}$ expression was controlled by its natural promoter (UB13530) or the *8lexO* system (UB13532). Both strains harbor the *pCUP-IME1 pCUP-IME4* synchronization system. Meiosis was induced by $CuSO_4$ addition after 2 hrs in SPO, and β-estradiol was added simultaneously. Ndc80 level was determined by anti-V5 immunoblot. Hxk2, loading control. Here and throughout, the numbers below the immunoblots are calculated by first normalizing the Ndc80 level to the Hxk2 level in each lane, and then dividing the normalized value to that of the 0 hr time point.

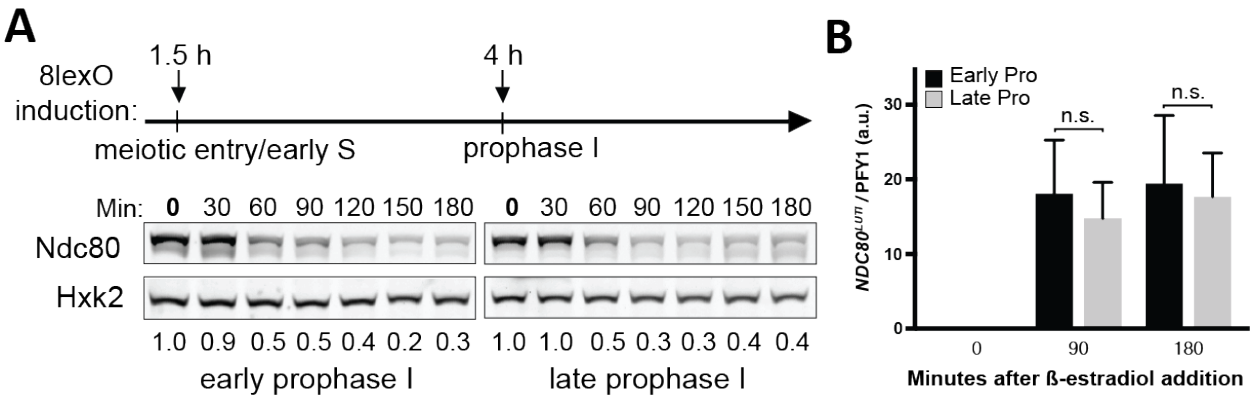

Figure 3.4: Ndc80 turnover in early or late meiotic prophase. (A) To measure Ndc80 turnover in early or late prophase, the strain that carries the *8lexO* system (UB14883) was induced to enter meiosis at 0 hr. β-estradiol was added to culture 1.5 hrs or 4 hrs after meiosis induction, respectively. In either case, the strain was halted in meiotic prophase using an *ndt80*Δ block. Ndc80 level was determined by anti-V5 immunoblot. Hxk2, loading control. (B) Induction level of the $NDC80^{LUTI}$ mRNA for the experiment in (A), measured by quantitative reverse transcription PCR (RT-qPCR). For all RT-qPCR experiments, the $NDC80^{LUTI}$ signals were normalized to that of *PFY1*. a.u., arbitrary unit; n.s., not significant. The mean from 3 independent experiments, along with the standard error of the mean, is displayed.

sis induction) while the cells were arrested in meiotic prophase due to deletion of *NDT80*, a transcription factor required for meiotic prophase exit. We found that Ndc80 was degraded at similar kinetics (Figure 3.4, Panel A). Ndc80 synthesis was successfully repressed in either condition since the levels of $NDC80^{LUTI}$ induction were similar by quantitative RT-PCR (qRT-PCR) (Figure 3.4, Panel B). This result suggests that Ndc80 turnover can occur throughout meiotic prophase.

Could Ndc80 be degraded outside of meiotic prophase? To test this, we monitored Ndc80 levels during a metaphase I arrest, induced by Cdc20 depletion (*cdc20-mn*). Cdc20 is an activator of the anaphase-promoting complex, APC, which is an E3 ligase necessary for metaphase-to-anaphase transition (Visintin *et al.* 1997; Hwang *et al.* 1998, reviewed in Yu 2007). For this experiment, we mutated the mid-sporulation element (*MSE*) at the $NDC80^{ORF}$ promoter to prevent Ndt80-dependent expression of $NDC80^{ORF}$ (Chen *et al.* 2017). While Ndc80 was degraded in S-phase/prophase I, it remained remarkably stable during the metaphase I arrest (Figure 3.5, Panel A). We ruled out the possibility that Cdc20 was directly involved in Ndc80 degradation based on two observations. First, Cdc20 was dispensable for Ndc80 degradation in prophase I (*ndt80*Δ, *cdc20-mn*) (Figure 3.5, Panel A). Second, mutating the four D-boxes on Ndc80, the putative substrate recognition sites for APC^{Cdc20}, had no effect on Ndc80 degradation (Figure 3.6). The level of $NDC80^{LUTI}$ was not significantly different at 90 minutes after β-estradiol treatment, although it eventually declined after 180 minutes in *cdc20-mn* cells (Figure 3.5, Panel B). In principle, this reduction of $NDC80^{LUTI}$ could lead to an increase in Ndc80 synthesis. To exclude the possibility that increased synthesis, rather than decreased degradation, was contributing to the elevated Ndc80 levels in *cdc20-mn* cells, we used cycloheximide to globally inhibit protein synthesis. Ndc80 was still stable during metaphase I arrest but not in late prophase I under these conditions (Figure 3.5, Panel C). Altogether, these results suggest that Ndc80 degradation is temporally regulated.

3.3.2 Ndc80 degradation requires a degron sequence at its N-terminus

To identify the residues necessary for Ndc80 proteolysis, we systematically created truncations within Ndc80. We found the first 28 residues to be required for Ndc80 degradation (Figure 3.7, Panel A). Within this segment, the residues 11-19 were the most critical (Figure 3.7, Panel A). It is worth noting that Ndc80 turnover was not altered when the 11 serines and threonines in this 2-28 region (underlined in Figure 3.7, Panel B) were mutated to alanines (*NDC80-11A*) (Figure 3.7, Panel C), or when the 4 histidines in this region (green letters in Figure 3.7, Panel B) were mutated to alanines (*NDC80(4H to A)*) or leucines (*NDC80(4H to L)*)(Figure 3.7, Panel C).

Next, we examined the localization of the Ndc80(Δ2-28) by fusing it to enhanced green fluorescent protein (eGFP). We found that Ndc80(Δ2-28) localized to the dispersed kinetochores in almost all meiotic prophase cells (99%), whereas fewer than 5% of meiotic prophase cells had wild-type Ndc80 at the kinetochores (Figure 3.8). This localization analysis demonstrates that the deletion of the 2-28 residues does not disrupt Ndc80 from assembling into the kinetochore. Furthermore, kinetochore dispersion does not appear to require Ndc80 turnover.

How do the 2-28 residues regulate Ndc80 abundance? We first asked whether Ndc80 synthesis repression was affected in the Δ*2-28* mutant by examining the $NDC80^{LUTI}$ expression.

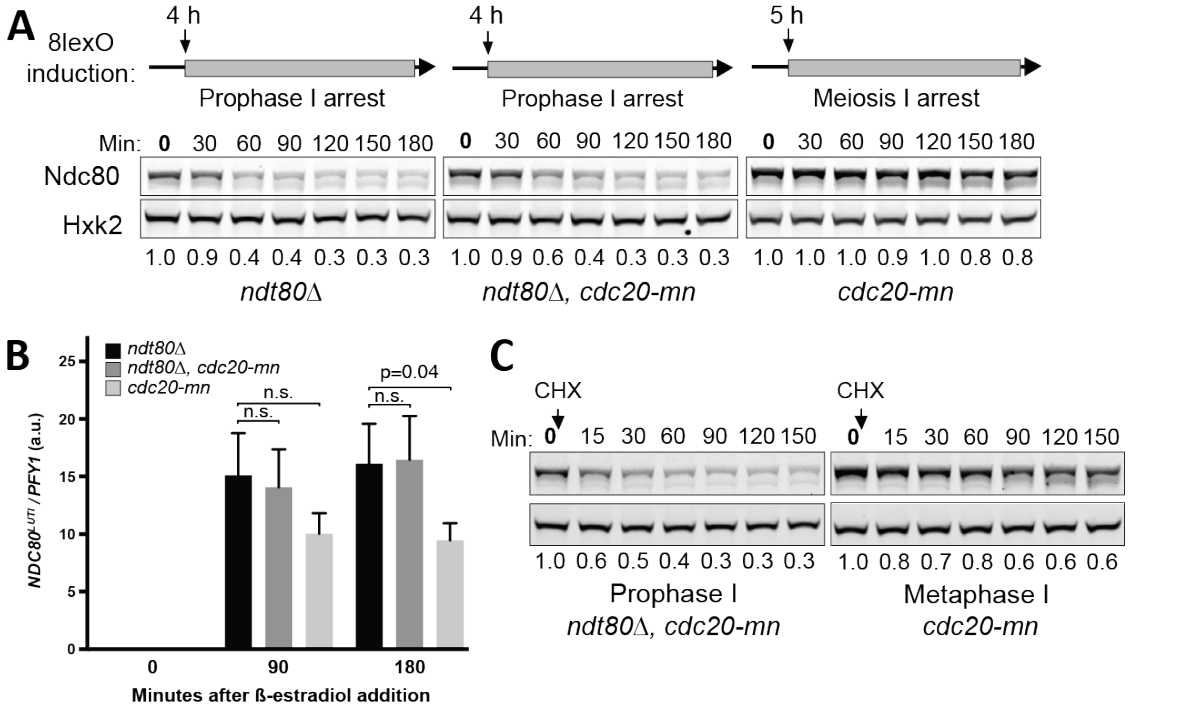

Figure 3.5: Ndc80 turnover in late meiotic prophase or in metaphase I arrest. MI, metaphase I. (A) To measure Ndc80 turnover in late prophase, two strains UB19616 (*ndt80*Δ) and UB19618 (*ndt80*Δ *cdc20-mn*) were cultured in sporulation medium (SPO) for 4 hrs before β-estradiol was added. To measure Ndc80 turnover in metaphase I, the Cdc20-meiotic null mutant (UB19678, *cdc20-mn*) was cultured in SPO for 5 hrs, and then β-estradiol was added. By this time, 50% cells had metaphase I spindles. Cells were subsequently halted in metaphase I for 3 hrs. (B) Induction level of the $NDC80^{LUTI}$ mRNA for the experiment in (A), measured by RT-qPCR and graphed as Figure 3.4, Panel B. (C) Ndc80 turnover in late meiotic prophase or in metaphase I arrest, measured by cyclohexamide (CHX) chase experiments. Strains UB19618 (*ndt80*Δ *cdc20-mn*) and UB1967 (*cdc20-mn*) were cultured in SPO for 5 hrs before a final concentration of 0.2 mg/ml cyclohexamide was added. During the entire CHX experiment, the *ndt80*Δ *cdc20-mn* strain was halted in meiotic prophase and the *cdc20-mn* strain, in metaphase I.

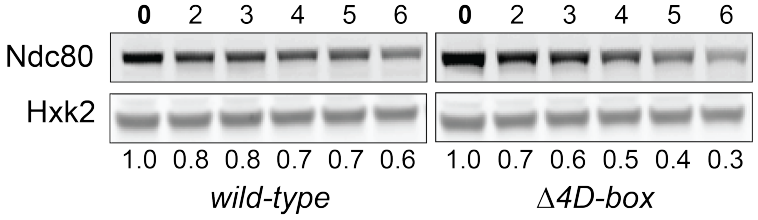

Figure 3.6: Wild-type cells (UB3380) or the strain harboring the four D-box mutations (Δ*4D-box*, UB3699) were sporulated and halted in meiotic prophase using the *pGAL-NDT80 GAL4.ER* system for 6 hrs in SPO.

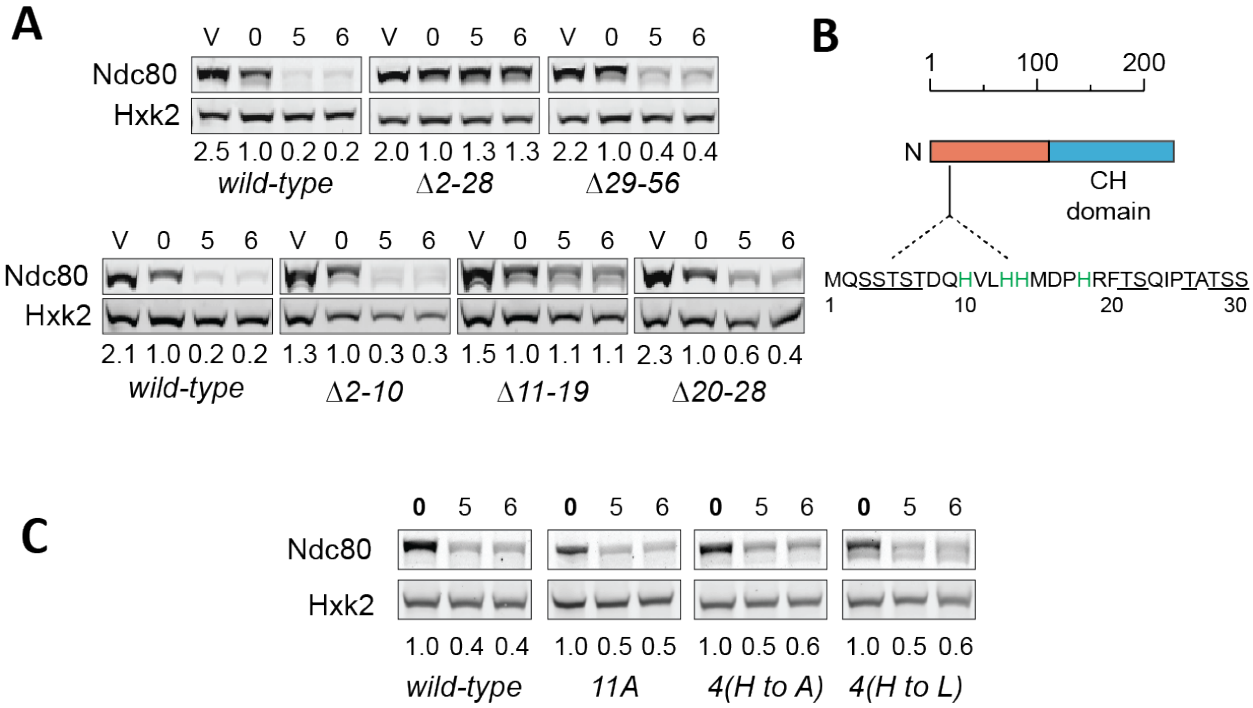

Figure 3.7: Truncation analysis of Ndc80 to identify the residues necessary for Ndc80 degradation. (A) Strains harboring deletions of the 2-28 residues (Δ*2-28*, UB5662), the 29-56 residues (Δ*29-56*, UB15922), the 2-10 residues (Δ*2-10*, UB7039), the 11-19 residues (Δ*11-19*, UB7029), and the 20-28 residues (Δ*20-28*, UB7031) were sporulated along with the wild-type cells (UB4074). All the strains were halted in meiotic prophase using the *pGAL-NDT80 GAL4.ER* system for 6 hrs in SPO. The vegetative samples (V) were taken while each strain was growing exponentially in rich medium. Note: Hxk2 level declined slightly as meiotic prophase progressed. Thus, the normalized level of Ndc80 became over 1.0 in the later stages of meiotic prophase. (B) An abridged schematic of Ndc80. The sequence of the first 30 residues is displayed. The underlined residues are the 11 serines and threonines mutated in *NDC80-11A*. The residues in green are the 4 histidines mutated in Panel C. (C) *NDC80-11A* (UB5475), *NDC80(4H to A)* (UB12297) and *NDC80(4h to L)* (UB12299), along with the wild-type cells (UB4074), were sporulated as in (A).

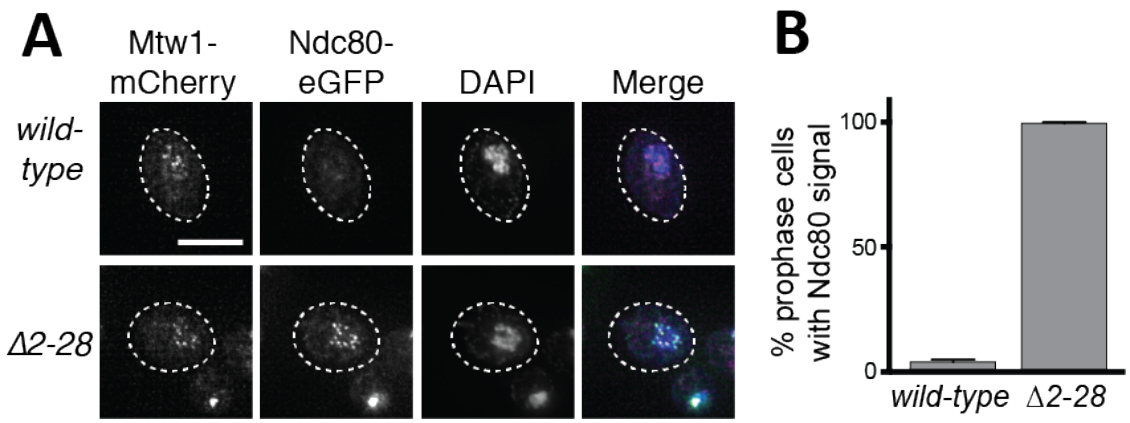

Figure 3.8: Ndc80(Δ2-28) proteins localized to the kinetochore in meiotic prophase. (A) The wild-type (UB1083) and Δ*2-28* (UB15619) cells were fixed after 6 hrs in SPO. Mtw1 was tagged with mCherry and Ndc80, with eGFP. DNA was stained with DAPI. Scale bar: 5 μm. (B) Quantification of (A). Over 70 meiotic prophase cells were counted. The average percentages of meiotic prophase cells with colocalized Ndc80-eGFP and Mtw1-mCherry signals, as well as the range, of 2 independent experiments are displayed.

We found that the wild-type, Δ*2-28* and Δ*11-19* cells had a similar level of $NDC80^{LUTI}$ expression (Figure 3.9, Panel A). Moreover, Ndc80 protein levels were additively increased when the Δ*11-19* mutant was combined with a mutant that fails to inhibit Ndc80 synthesis ($\Delta NDC80^{LUTI}$) (Figure 3.9, Panel B). Despite such difference in protein level, the expression of the translationally competent $NDC80^{ORF}$ mRNA did not differ statistically between the double mutant and the single mutant $\Delta NDC80^{LUTI}$ (Figure 3.9, Panel C and D) ($p = 0.07$, Wilcoxon Rank Sum test), further demonstrating that the N-terminal region does not regulate Ndc80 synthesis. Rather, we consider the 2-28 residues of Ndc80 to be a degron sequence that regulates Ndc80 protein turnover.

We attempted to identify the Ndc80's interactors that depend on the 2-28 residues by immunoprecipating Ndc80 during meiotic prophase followed by quantitative mass spectrometry. We found that Sis1, a J-domain protein that regulates heat shock protein activity (Kampinga & Craig 2010), was associated with the wild-type but not the N-terminally deleted Ndc80 protein in meiosis (Figure 3.10, Panel A). However, Sis1 association did not correlate with Ndc80 degradation, since mutations that did not affect Ndc80 degradation (e.g., Δ*29-56*) still perturbed Sis1-Ndc80 association (Figure 3.10, Panel B). We posit that Sis1 association with Ndc80 serves a different biological purpose such as protein quality control. Since we were unable to find other candidates for Ndc80 degradation using the Δ*2-28* mutant, we next surveyed the involvement of the key proteolytic and meiotic events as a way to identify the regulators of this process.

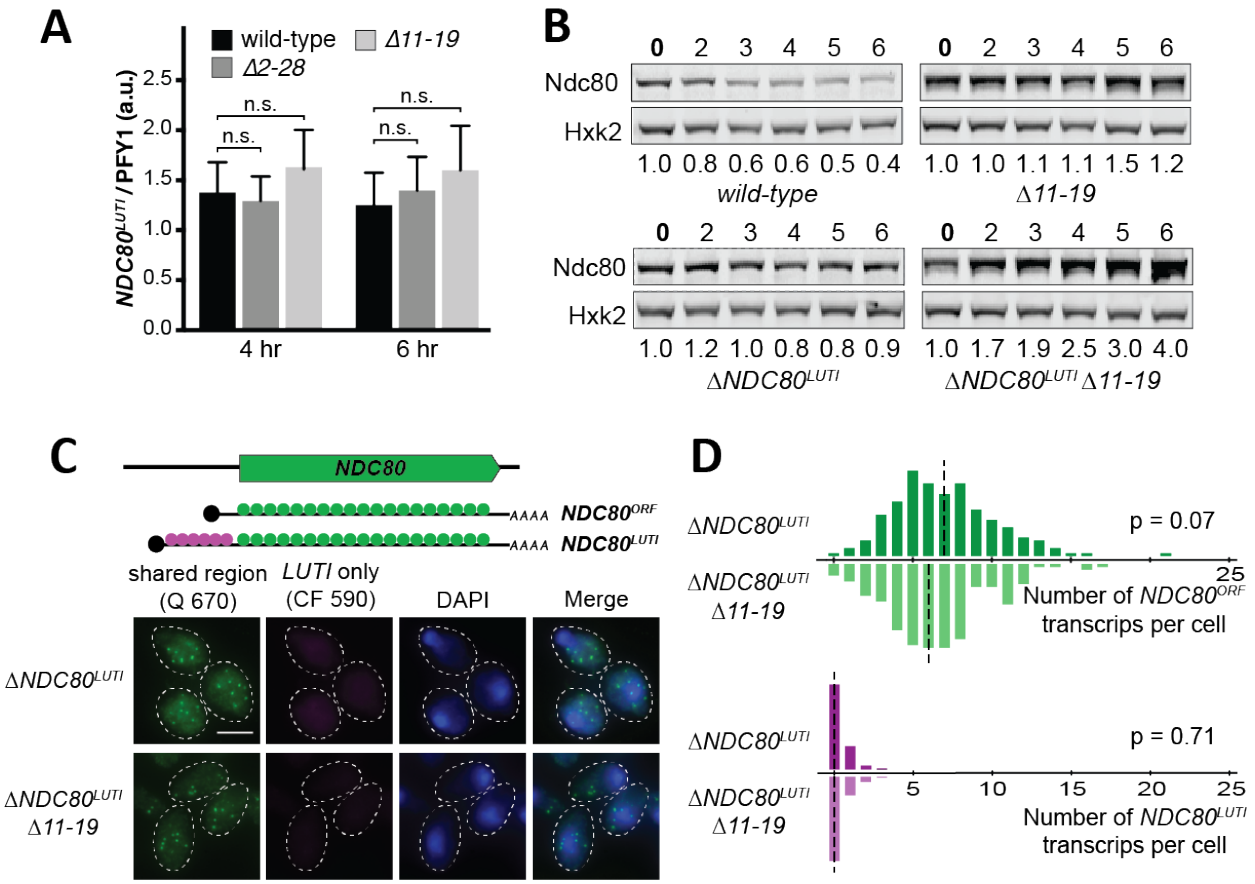

Figure 3.9: Δ*2-28* does not alter the Ndc80 synthesis repression in meiotic prophase. (A) The expression level of $NDC80^{LUTI}$ in the wild-type (UB4074) and Δ*2-28* (UB5662) cells in meiotic prophase (4 hr and 6 hr after the cells were transferred to SPO), measured by RT-qPCR. (B) Ndc80 level could be increased additively by the Δ*11-19* mutant and a mutant that fails to repress Ndc80 synthesis ($\Delta NDC80^{LUTI}$). The wild-type (UB4074), Δ*11-19* (UB7029), $\Delta NDC80^{LUTI}$ (UB11797), and $\Delta NDC80^{LUTI}$ Δ*11-19* (UB11799) cells were sporulated as described in Figure 3.7, Panel A. (C) Representative smFISH images comparing the $\Delta NDC80^{LUTI}$ strain (UB11797) and the $\Delta NDC80^{LUTI}$ Δ*11-19* double mutant (UB11799). Samples were taken after the cells were incubated in SPO for 6 hrs. Top: a schematic for the smFISH probes. The Q 670 probes (green) hybridize to the common region shared between $NDC80^{LUTI}$ and $NDC80^{ORF}$, whereas the CF 590 probes (magenta) hybridize to the unique 5' region of $NDC80^{LUTI}$. DNA was stained with DAPI (blue). The smFISH images are shown as the maximum-intensity projections of z-stacks. Scale bar: 5 μm. (D) smFISH quantification of the $NDC80^{ORF}$ and $NDC80^{LUTI}$ levels in Panel C. Data were graphed as the relative frequency histograms of cells with a given number of $NDC80^{LUTI}$ and $NDC80^{ORF}$ transcripts per cell, pooling the data from 2 independent experiments. Dashed line, the median number of transcripts per cell. Two-tailed Wilcoxon Rank Sum test was performed.

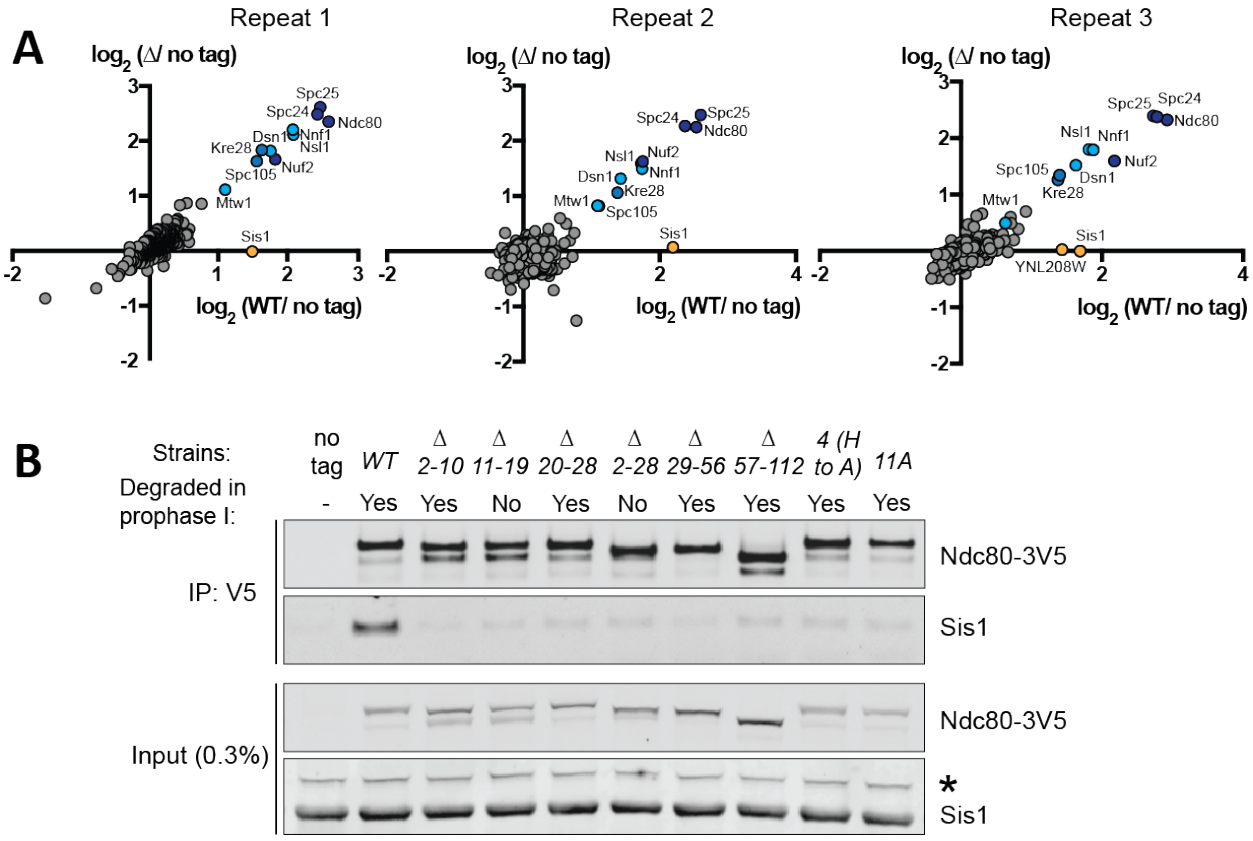

Figure 3.10: (A) The proteins that co-immunoprecipitated with the wild-type Ndc80 protein (UB2932) or the Ndc80(Δ2-28) protein (UB5662) in meiotic prophase, identified by TMT quantitative mass spectrometry. For each detected protein, the log2 ratio between either strain and an untagged control (no tag, UB95) was calculated, and the ratios for the wild-type Ndc80 (WT/no tag) and the Ndc80(Δ2-28) (Δ/no tag) were plotted as a scatterplot. The Ndc80 complex (Ndc80, Nuf2, Spc24, Spc25) is marked dark blue; Spc105 and Kre28, cerulean; the MIND complex (Mtw1, Nnf1, Nsl1, Dsn1), light blue; non-kinetochore protein, golden yellow; and the proteins with less than 2-fold enrichment, gray. (D) Co-immunoprecipitation of Sis1 by different Ndc80 protein variants, including an untagged control (UB95), the wild-type Ndc80 (UB2932), the mutation of four histidines to alanines (4(H to A), UB21255) and 11 serines and threonines to alanines (11A, UB21363), as well as the following deletion mutations: 2-10 residues (Δ2-10, UB21253), 11-19 residues (Δ11-19, UB7029), 20-28 residues (Δ20-28, UB21259), 2-28 residues (Δ2-28, UB5662), 29-56 residues (Δ29-56, UB21251), and 57-112 residues (Δ57-112, UB21361). For the Ndc80 variants degraded in meiotic prophase, the 400-600 bp upstream of the *NDC80* promoter was disrupted to allow Ndc80 protein synthesis in meiotic prophase so that their interaction with Sis1 could be assessed. * indicates a background band.

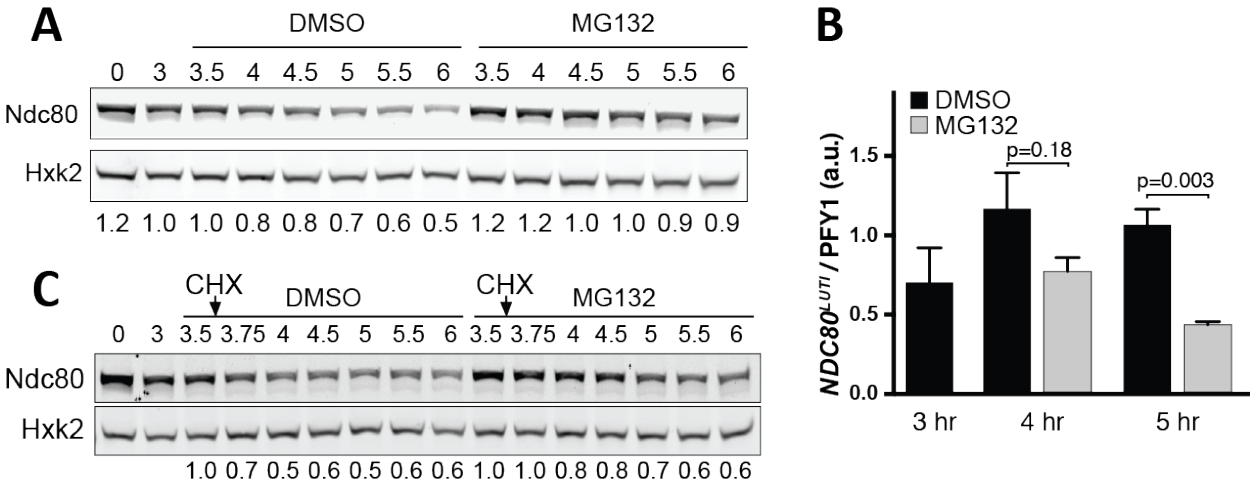

Figure 3.11: Ndc80 degradation in meiotic prophase requires active proteasomes. (A-B) Both Ndc80 degradation and the expression of $NDC80^{LUTI}$ are affected by MG132 treatment. Cells (*pdr5*Δ, UB2405) were induced to sporulate at 0 hr. After 3 hrs in SPO, the cells were split and treated with either DMSO or the proteasome inhibitor MG132 (100 μM). For either condition (DMSO or MG132), all the time points were normalized to the time point immediately before the cells were split (3 hr). (B) The expression level of $NDC80^{LUTI}$ for the experiment in (A), measured by RT-qPCR. (C) The *pdr5*Δ cells were induced to sporulate at 0 hr. After 3 hrs in SPO, cells were split and treated with either DMSO or the proteasome inhibitor MG132. 30 min later, cycloheximide (CHX) was added (0.2 mg/ml). For either condition (DMSO or MG132), all the time points were normalized to the time point immediately before the cycloheximide addition (3.5 hr).

3.3.3 Ndc80 degradation requires proteasome activity but is independent of recombination, paring, and DNA replication

The ubiquitin-proteasome system is a major pathway by which proteins are degraded in the cell (Finley *et al.* 2012). In meiotic prophase, proteasomes are found on chromosomes and are required for synapsis (Ahuja *et al.* 2017). Ndc80 also localizes to the chromosomes; and thus, proteasomes are expected to be in close proximity to Ndc80 and may mediate its degradation.

To test if the proteasome activity is required for Ndc80 degradation, we treated meiotic cells with the proteasome inhibitor MG132. Comparing to the vehicle control, Ndc80 level was stabilized in the MG132 treatment (Figure 3.11, Panel A). However, $NDC80^{LUTI}$ expression decreased by about 50% in the second hour of drug treatment (Figure 3.11, Panel B), suggesting that Ndc80 synthesis repression may be affected by MG132. To eliminate the confounding effect from Ndc80 synthesis, we treated meiotic cells with cycloheximide, along with MG132, to inhibit global translation. We found that Ndc80 level was stabilized in the presence of MG132, suggesting that the proteasome activity is necessary for Ndc80 degradation (Figure 3.11, Panel C).

Despite a requirement for the proteasome activity, Ndc80 degradation is independent of

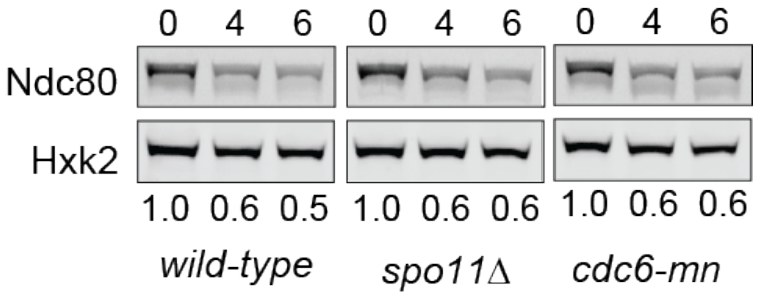

Figure 3.12: Ndc80 degradation does not depend on recombination, synapsis, and DNA replication. Wild-type (UB1338), *spo11*Δ (UB11795), and Cdc6-meiotic null (*cdc6-mn*, UB13656) cells were induced to sporulate as in Figure 3.7.

recombination, synapsis, and DNA replication. Ndc80 degradation was normal in the *spo11*Δ cells despite the lack of recombination and synapsis (Cao *et al.* 1990; Keeney *et al.* 1997; Giroux *et al.* 1989; Loidl *et al.* 1994) (Figure 3.12). Ndc80 degradation also occurred normally in cells depleted of the DNA replication factor Cdc6 (*cdc6-mn*) (Hochwagen *et al.* 2005; Brar *et al.* 2009; Blitzblau *et al.* 2012), consistent with a previous report (RN215)(Figure 3.12). These results suggest that Ndc80 degradation, and kinetochore remodeling by inference, is independent of the major meiosis-specific changes to chromosomes.

3.3.4 Aurora B/Ipl1 activity is necessary for Ndc80 degradation in meiotic prophase

Besides recombination, synapsis, and replication, microtubule dynamics are also altered in meiotic prophase. Nuclear microtubules are shortened during meiotic prophase in an Aurora B/Ipl1 kinase-dependent manner (Kim *et al.* 2013; Shirk *et al.* 2011). Previously, it has been shown that Aurora B/Ipl1 is required for the decline of Ndc80 protein level in meiotic prophase (Meyer *et al.* 2015). However, it has remained unknown how Ipl1 regulates Ndc80 level. We posited that at least three models are possible: First, Ipl1 could regulate Ndc80 protein synthesis. Second, Ipl1 could affect Ndc80 levels indirectly by altering microtubule-kinetochore attachments. Third, Ipl1 could promote Ndc80 turnover by phosphorylating Ndc80 and/or other factors involved in Ndc80 degradation.

We ruled out the possibility that Ipl1 is involved in regulating Ndc80 synthesis based on three independent observations. First, $NDC80^{LUTI}$ levels were not altered in the *ipl1-mn* mutants (Figure 3.13, Panel A). Second, the *ipl1-mn* mutation increased Ndc80 level additively with a mutant that fails to repress Ndc80 synthesis ($\Delta NDC80^{LUTI}$) (Figure 3.13, Panel B). Finally, the expression of the translationally competent $NDC80^{ORF}$ isoform did not significantly change in the double mutant ($\Delta NDC80^{LUTI}$ *ipl1-mn*) compared to the single mutant $\Delta NDC80^{LUTI}$ (Figure 3.13, Panel C and D)($p = 0.18$, Wilcoxon Rank Sum test). Altogether, we conclude that Ipl1 is likely to regulate Ndc80 turnover rather than synthesis.

In the second model, Ipl1 inactivation may affect Ndc80 stability indirectly by modu-

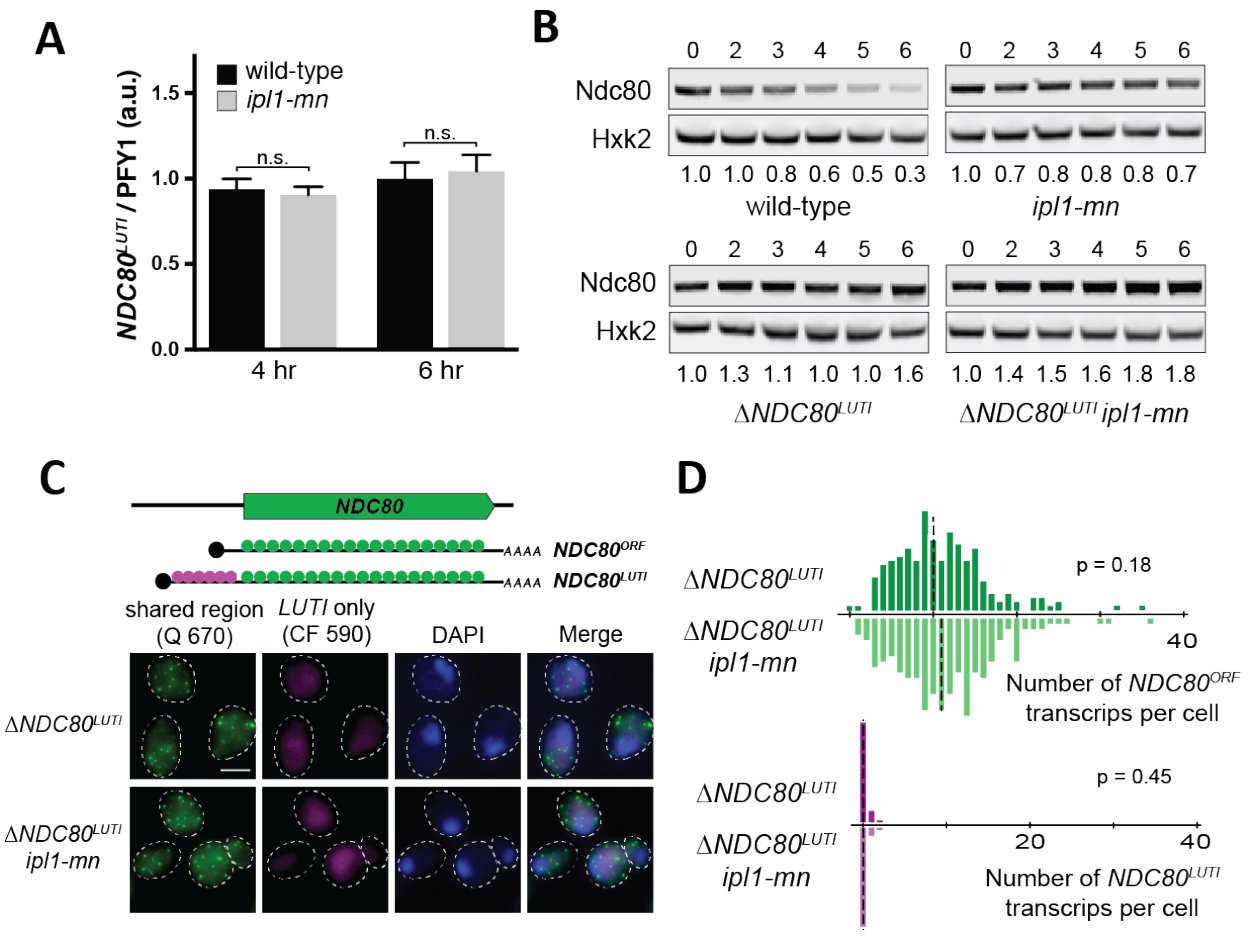

Figure 3.13: The *ipl1-mn* mutant does not affect Ndc80 synthesis repression in meiotic prophase. (A) The expression level of $NDC80^{LUTI}$ in the wild-type (UB4074) and *ipl1-mn* (UB15064) cells in meiotic prophase (4 hr and 6 hr in SPO), measured by RT-qPCR. (B) Ndc80 level could be increased additively by the meiotic depletion of *IPL1* (*ipl1-mn*) and a mutant that fails to repress Ndc80 synthesis ($\Delta NDC80^{LUTI}$). The wild-type (UB1338), *ipl1-mn* (UB1013), $\Delta NDC80^{LUTI}$(UB2932), and $\Delta NDC80^{LUTI}$ *ipl1-mn* (UB3948) cells were sporulated as described in Figure 3.7. (C) Representative smFISH images for the $\Delta NDC80^{LUTI}$ strain (UB2932) and the $\Delta NDC80^{LUTI}$ *ipl1-mn* double mutant (UB3948). Samples were taken after 6 hrs in SPO. Top: a schematic for the smFISH probes. The Q 670 probes (green) hybridize to the common region shared between $NDC80^{LUTI}$ and $NDC80^{ORF}$, whereas the CF 590 probes (magenta) hybridize to the unique 5' region of $NDC80^{LUTI}$. DNA was stained with DAPI (blue). The smFISH images are shown as the maximum-intensity projections of z-stacks. Scale bar: 5 μm. (D) smFISH quantification of $NDC80^{ORF}$ and $NDC80^{LUTI}$ levels in $\Delta NDC80^{LUTI}$ cells (UB2932) and $\Delta NDC80^{LUTI}$ *ipl1-mn* (UB3948) cells in meiotic prophase. Data were graphed as the relative frequency histograms of cells with a given number of $NDC80^{LUTI}$ and $NDC80^{ORF}$ transcripts per cell, pooling the data from 2 independent experiments. Dashed line, the median number of transcripts per cell. Two-tailed Wilcoxon Rank Sum test was performed.

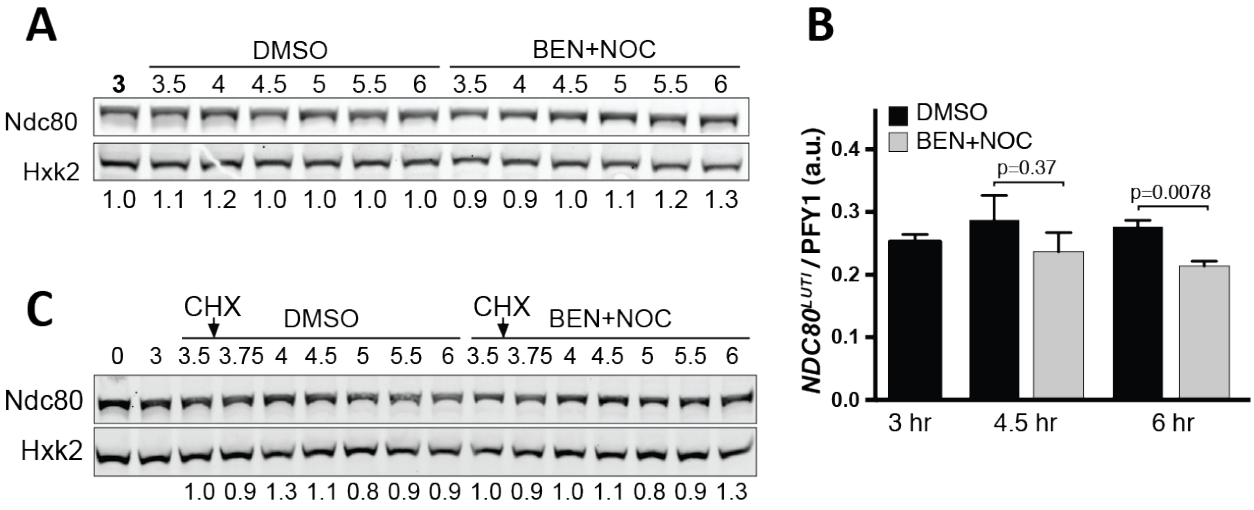

Figure 3.14: *ipl1-mn* stabilizes Ndc80 level in a microtubule-independent manner. (A-B) The *ipl1-mn* cells (UB15064) were induced to sporulate at 0 hr. After 3 hrs in SPO, cells were split and treated with either DMSO or a microtubule depolymerizing cocktail (BEN+NOC: 30 μg/ml benomyl and 150 μg/ml nocodazole). For either condition, all the time points were normalized to the time point immediately before the cells were split (3 hr). (D) The expression level of $NDC80^{LUTI}$ for the experiment in (A), measured by RT-qPCR. (C) The *ipl1-mn* strain (UB15064) was induced to enter meiosis at 0 hr. After 3 hrs in SPO, the cells were split and treated with DMSO or the microtubule depolymerizing cocktail. 30 min later, cycloheximide (CHX) was added (0.2 mg/ml). For either condition (DMSO or BEN+NOC), all the time points were normalized to the time point immediately before the cycloheximide addition (3.5 hr).

lating microtubule-kinetochore engagement in meiotic prophase. In contrast to wild-type cells, in which short microtubule arrays are present in meiotic prophase, the *ipl1-mn* cells prematurely separate the duplicated spindle pole bodies and form long microtubules (Kim *et al.* 2013; Shirk *et al.* 2011). These microtubules interact with the kinetochores, leading to kinetochore re-clustering and potentially stabilization of Ndc80 protein. In this model, the effect of *ipl1-mn* depends on the presence of microtubule polymers. To test this model, we depolymerized microtubules in the *ipl1-mn* cells using a microtubule poison cocktail (benomyl and nocodazole), and found that Ndc80 remained stable in the treatment (Figure 3.14, Panel A). Since this cocktail treatment slightly reduced $NDC80^{LUTI}$ expression in the *ipl1-mn* cells (Figure 3.14, Panel B), we used cycloheximide to inhibit global protein synthesis while treating the *ipl1-mn* cells with the poison cocktail. We also observed no rescue of Ndc80 degradation in meiotic prophase (Figure 3.14, Panel C). Thus, it is unlikely that Ipl1 regulates Ndc80 degradation through affecting microtubule dynamics.

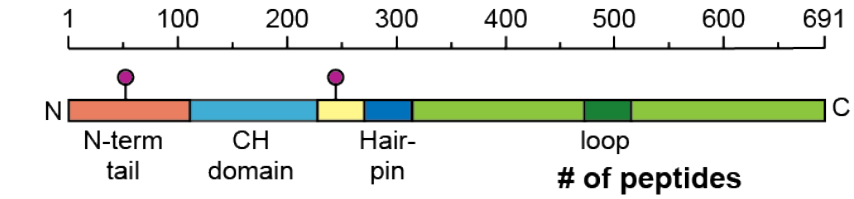

Phospho site	Peptide sequences	# of peptides (pS or pT/Total) *wild-type*	# of peptides (pS or pT/Total) *Δ2-28*
T54	N(pT)ISGTGIPTGGINK	1/8, 2/13	5/21, 3/7
T248	SLINQN(pT)QEITILSQPLK	0/6, 3/17	3/39, 0/7
	% Ndc80 coverage	55%, 57%	71%, 59%

Figure 3.15: Phosphorylation sites detected on the wild-type Ndc80 and Ndc80(Δ2-28) proteins in meiotic prophase by mass spectrometry (MS). The wild-type (*pdr5*Δ, UB2405) cells were induced to sporulated and treated with MG132 as in Figure 3.11. Samples were collected 1 hr after MG132 treatment. Samples were collected from the Δ*2-28* cells after 5 hrs in SPO. Top: a schematic of Ndc80 and the *in vivo* phosphorylation sites detected by MS (pink circles). N-term, N terminal. CH, calponin homology domain. Bottom: Detected Ndc80 phosphopeptides. The detected number of phosphopeptides and the total peptides (phosphorylated and unmodified combined), as well as the overall sequence coverage of Ndc80, are reported for two biological replicates.

3.3.5 Ndc80 degradation requires Ipl1-mediated phosphorylation

In a third model, Ipl1 may promote Ndc80 turnover by phosphorylating factors that turn over Ndc80, or by phosphorylating Ndc80 itself, which is a known target of Ipl1 (Cheeseman *et al.* 2002; Akiyoshi *et al.* 2009). To investigate the latter possibility, we immunoprecipitated Ndc80 from cells in meiotic prophase after 1 hour of MG132 treatment, and analyzed the post-translational modifications of Ndc80 by mass spectrometry. We found two high confident phosphorylation sites T54 and T248 (Figure 3.15). The first site has been previously characterized and belongs to the Ipl1 consensus sequence (Cheeseman *et al.* 2002; Akiyoshi *et al.* 2009), whereas the second site lacks the Ipl1 consensus sequence.

Next, we mutated the seven known Ipl1 consensus sites on Ndc80 (*NDC80-7A*), which has been shown to reduce Ndc80 phosphorylation by Ipl1 *in vitro* (Akiyoshi *et al.* 2009). We found that Ndc80-7A was stable in meiotic prophase (Figure 3.16, Panel A), and the mutation did not affect $NDC80^{LUTI}$ expression (Figure 3.16, Panel B). Mutating additional serines and threonines around T54 and T248 (*NDC80-14A*) did not enhance Ndc80 stabilization (Figure 3.16, Panel A). We conclude that the seven Ipl1 consensus sites at the N-terminal region of Ndc80 are required for its turnover in meiotic prophase.

Next, we examined where the excess Ndc80-7A protein localized in meiotic prophase. We found that 60% of the *NDC80-7A* cells have Ndc80-7A-eGFP signal (Figure 3.17, Panel A and B), and almost all of these cells had clustered or partially clustered kinetochores. Interestingly, 34% of the *NDC80-7A* cells had partially clustered kinetochores, whereas fewer than 10% of the wild-type cells had them at this time (Figure 3.17, Panel C, "partial"). The

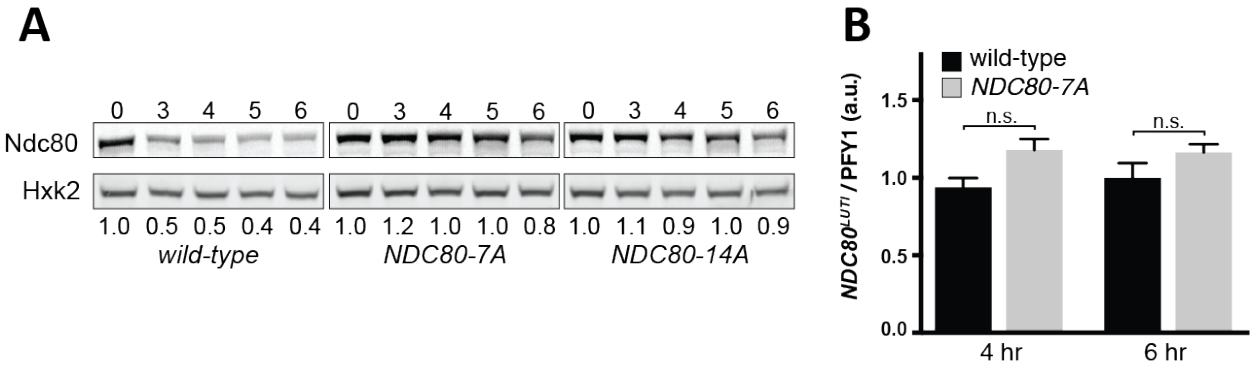

Figure 3.16: Ndc80 phosphorylation sites are required for Ndc80 degradation. Ndc80 level in meiotic prophase for the wild-type (UB4074), *NDC80-7A* (UB13658), *NDC80-14A* (UB17707) cells. Samples were taken and processed as in Figure 3.7. (B) The expression level of $NDC80^{LUTI}$ in the wild-type (UB4074) and *NDC80-7A* (UB) cells in meiotic prophase (4 hr and 6 hr in SPO), measured by RT-qPCR.

presence of the partially clustered kinetochores suggests that the Ipl1 phosphorylation of Ndc80 may facilitate the kinetochore detachment from microtubules in meiotic prophase, similar to what occurs during error correction in prometaphase (reviewed in Biggins 2013).

To test if Ndc80 phosphorylation is dependent on its 2-28 residues, we immunoprecipitated Ndc80(Δ2-28) proteins from meiotic prophase cells, and subjected the precipitated proteins for mass spectrometry. We detected the two phosphorylation sites observed in the wild-type Ndc80 protein (Figure 3.15), suggesting that Ndc80 phosphorylation is not affected by the deletion of the 2-28 residues. In addition, we performed an *in vitro* kinase assay using a recombinant Ipl1 variant (AurB*) (de Regt *et al.* 2018). No detectable difference in the degree of Ndc80 phosphorylation was observed between wild-type and Ndc80(Δ2-28) (Figure 3.18). Both results demonstrate that the Ipl1-depedent Ndc80 phosphorylation occurs normally in the *Δ2-28* mutant. Therefore, the 2-28 residues are required for Ndc80 degradation at a step downstream or in parallel to Ipl1-dependent phosphorylation.

3.3.6 Defects in Ndc80 degradation predispose meiotic cells to chromosome segregation errors

How is Ndc80 degradation related to kinetochore activity and function? The degron mutant (*Δ2-28*) provides a suitable way to address this question without (1) altering global Ipl1 activity, which can have pleiotropic effects, or (2) mutating the Ipl1-dependent phosphorylation sites (Ndc80-7A), which causes defects in correcting spindle attachment errors in prometaphase (Akiyoshi *et al.* 2009).

We first examined the growth phenotypes of the *Δ2-28* mutant (1) at higher temperature (37 °C) during vegetative growth and (2) on the plates that contain the microtubule depolymerizing drug benomyl. Mutants with defective kinetochores often exhibit growth defects

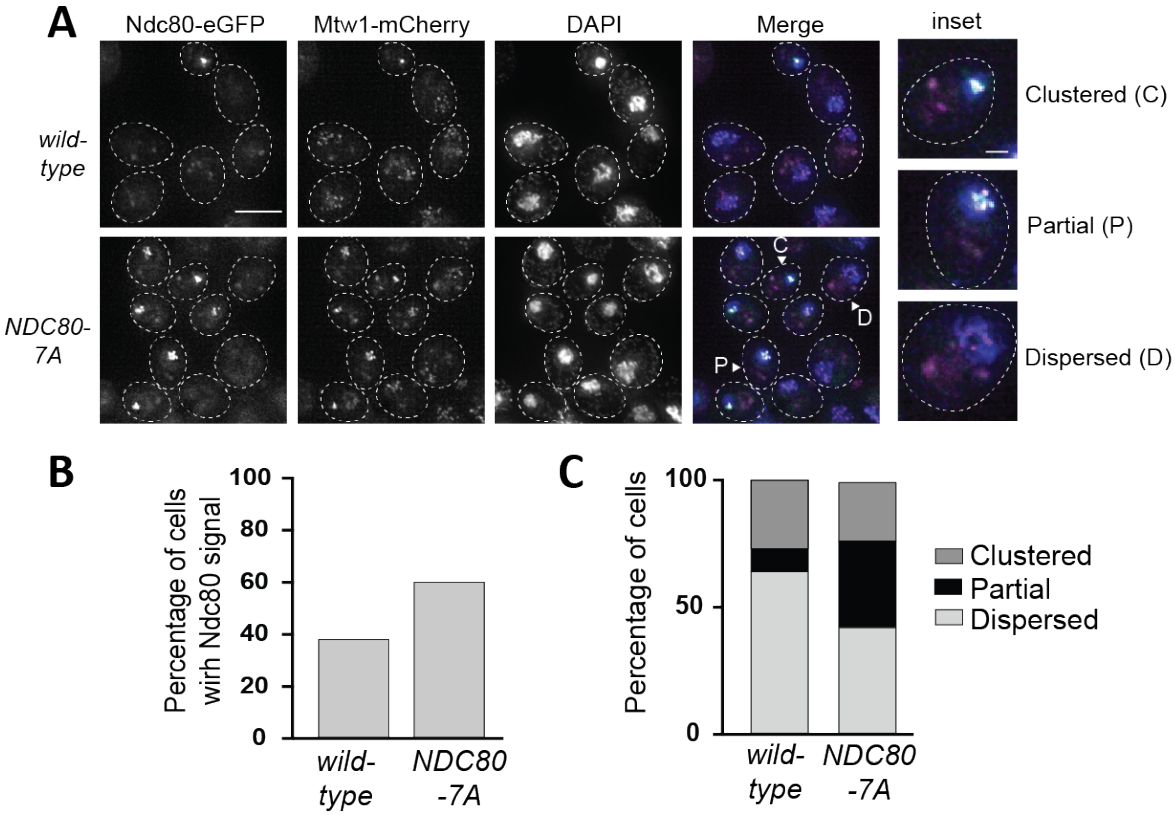

Figure 3.17: Ndc80-7A proteins localized to the kinetochores in meiotic prophase. The wild-type (UB1083) and *NDC80-7A* (UB15701) cells were fixed after 5 hrs in SPO. Mtw1 was tagged with mCherry and Ndc80, with eGFP. DNA was stained with DAPI. Scale bar: 5 μm. Inset scale bar: 1 μm. (B-C) Quantification of (A). Over 100 cells were counted. (B) The percentage of cells with colocalized Ndc80-eGFP and Mtw1-mCherry signals. (C) The percentage of cells with clustered, partially clustered, or dispersed kinetochores.

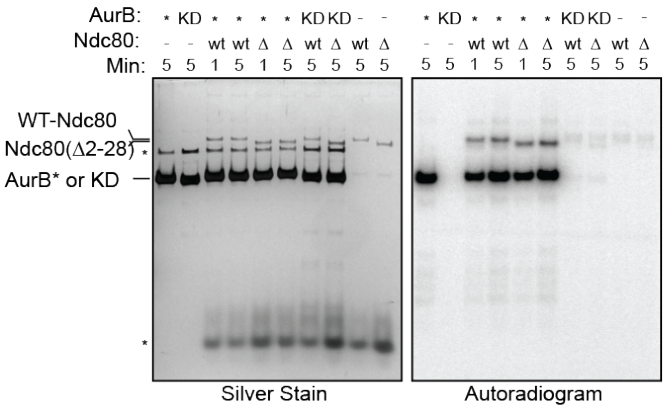

Figure 3.18: The wild-type Ndc80 and Ndc80(Δ2-28) proteins purified from UB16284 and UB19957, respectively, were phosphorylated *in vitro* by either 1 μM recombinant AurB* (fusion of the C-terminal activation box of INCEP/sli15 to Aurora B/Ipl1) or 1 μM kinase-dead AurB* (KD) and γ-32P-ATP. All the reactions were performed at room temperature for either 1 min or 5 min, analyzed by SDS-PAGE, and then visualized by silver stain and autoradiography. WT, wild-type Ndc80. Δ, Ndc80(Δ2-28). *, background bands.

in these conditions. We found the Δ*2-28* mutant grew similarly as the wild-type cells in both conditions (Figure 3.19), suggesting that this Ndc80 mutant does not drastically alter kinetochore functions in mitotic cells.

To probe how Ndc80 degradation affects kinetochore function in meiosis, we asked whether the Δ*2-28* mutant had chromosome segregation defects in meiosis. We tracked the segregation of the homozygous *CENV-GFP*. Both the wild-type and Δ2-28 strains had >99% tetrads with one GFP dot in each spore, the correct segregation pattern (Figure 3.20). This result suggested that altering Ndc80 degradation alone does not affect meiotic chromosome segregation, at least in the laboratory conditions. Both the wild-type and Δ*2-28* strains had >95% sporulation efficiency (Figure 3.21), although the Δ*2-28* mutant had a subtle decline in spore viability. This mutant had 96% spore viability in comparison to the 99% of the wild-type strain (Figure 3.22), suggesting a potential minor defect in kinetochore function, spore wall development, or germination.

When we combined the Δ*2-28* and Δ*11-19* mutants with a mutant that prematurely produces spindle microtubules in meiotic prophase (*pCUP-CLB3*), we observed chromosome segregation defects such that sister chromatids, instead of homologous chromosomes, segregated in meiosis I (Figure 3.23). This phenotype was reported previously when Ndc80 was overexpressed in meiotic prophase (Miller *et al.* 2012). Therefore, we concluded that

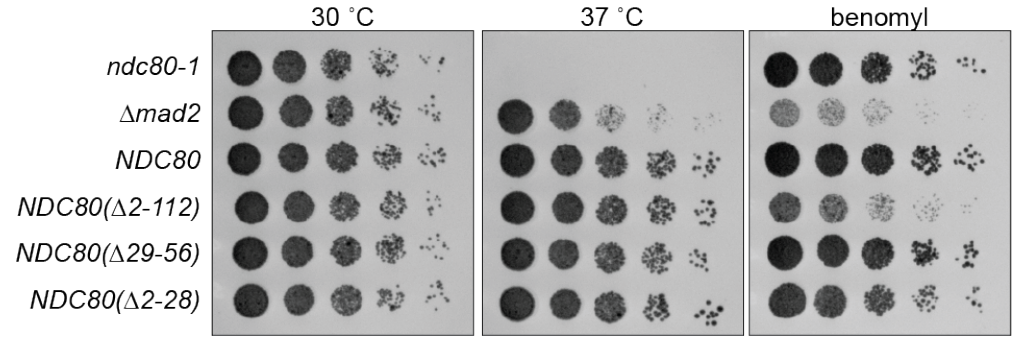

Figure 3.19: Growth phenotype associated with the various truncations of the Ndc80 N-terminal tail. Tested strains included the temperature-sensitive *ndc80-1* (UB494), the spindle assembly checkpoint mutant Δ*mad2* (UB700), wild-type *NDC80* (UB3262), as well as the *NDC80* mutants that carry the following deletion: residues 2-112 (*NDC80(Δ2-112)*, UB3275), residues 29-56 (*NDC80(Δ29-56)*, UB4695), and residues 2-28 (*NDC80(Δ2-28)*, UB5105). Cells were serially diluted and grown on the nutrient rich medium (YPD) plates at 30 °C or 37 °C for 1 day, as well as on a benomyl plate (15 μg/ml) at 23 °C for 2 days.

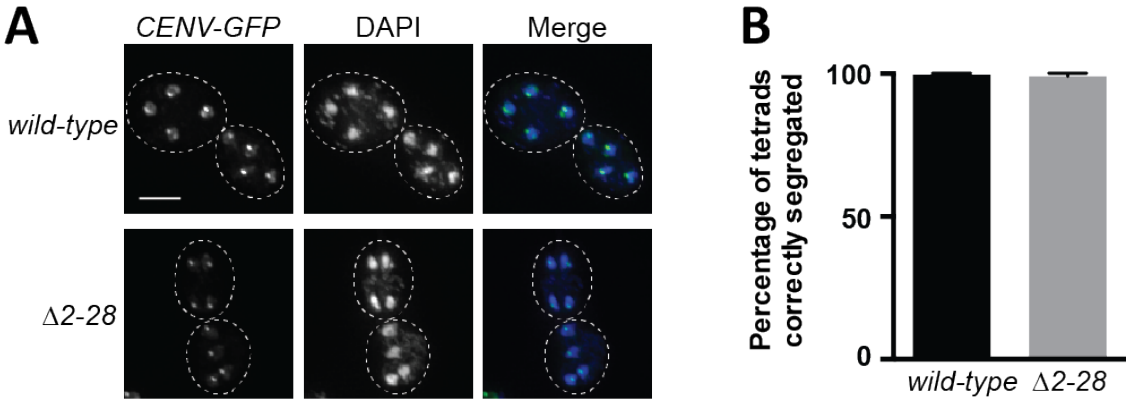

Figure 3.20: Homozygous *CENV-GFP* dots segregation in the wild-type (UB21757) and the Δ*2-28* mutant (UB21758). These strains carry a TetR-GFP fusion protein, and both homologs of chromosome V are marked by the centromeric TetO repeats (*CENV-GFP*). Strains were sporulated for 7 hrs before formaldehyde fixation. The images are shown as the maximum-intensity projections of z-stacks. Scale bar: 2 μm. (B) Quantification of Panel A. Over 90 cells were counted for each strain. The mean and the range of two independent experiments are graphed.

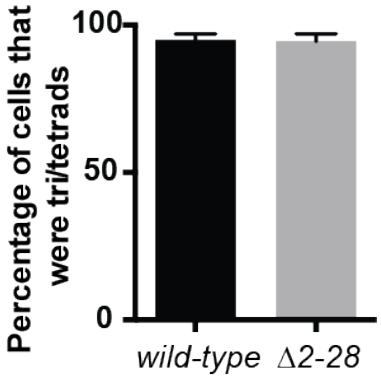

Figure 3.21: Spore formation for the wild-type (UB21756) and the Δ*2-28* mutant (UB21758). The mean and the range of two independent experiments are graphed.

A

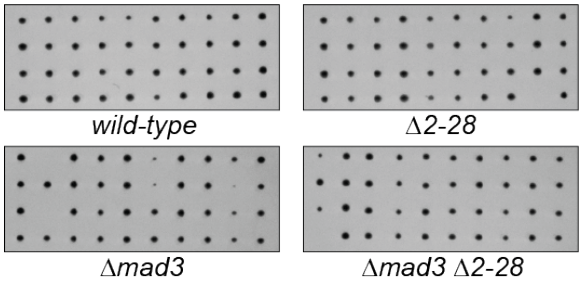

B

	Repeat 1	Repeat 2
wild-type	159/160 (99.4%)	188/192 (97.9%)
Δ2-28	154/160 (96.3%)	186/192 (96.9%)
Δmad3	147/160 (91.9%)	187/192 (97.4%)
Δmad3 Δ2-28	153/160 (95.6%)	188/192 (97.9%)

Figure 3.22: Spore viability for the wild-type (UB5875), the Δ*2-28* mutant (UB6010), the spindle assembly checkpoint mutant Δ*mad3* (UB15689), and the double mutant Δ*2-28* Δ*mad3* (UB15687). (A) Representative images of the germinated spores for each strain. (B) The number and percentage (in parentheses) of the surviving spores for each strain.

while Ndc80 degradation does not drastically affect kinetochore function, the lack of Ndc80 degradation predisposes cells to meiotic chromosome segregation errors.

3.4 Discussion

In this study, we have shown that Ndc80 degradation in meiosis is a temporally regulated process. Ndc80 is degraded in meiotic prophase and not in metaphase I. Ndc80 degradation requires a 27-residue degron sequence at its N-terminus and proteasome activity. Furthermore, Ndc80 degradation is coupled to Aurora B/Ipl1-mediated phosphorylation on Ndc80, a post-translational modification known for correcting the errors in kinetochore-microtubule attachments. The failure to degrade Ndc80 in meiotic prophase causes premature activation of kinetochores and predisposes meiotic cells to chromosome segregation errors. These results highlight the importance of regulating Ndc80 turnover in meiosis.

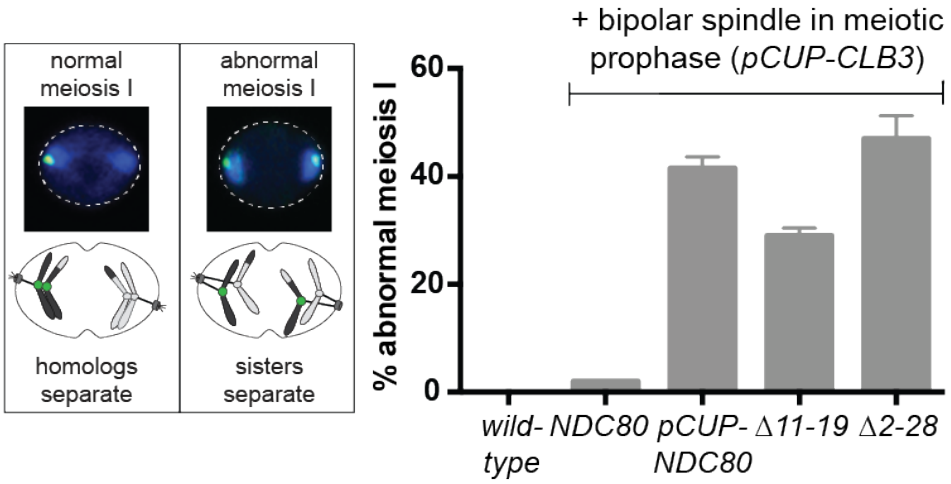

Figure 3.23: Sister chromatid segregation in the wild-type (UB2942), *pCUP-CLB3 NDC80* (UB877), *pCUP-CLB3 pCUP-NDC80* (UB880), *pCUP-CLB3 NDC80(Δ11-19)* (UB16561), and *pCUP-CLB3 NDC80(Δ2-28)* (UB16565) cells. Each strain carries the TetR-GFP fusion proteins, and a pair of the sister chromatids of chromosome V are marked by the centromeric *tetO* repeats (*CENV-GFP*). Cells were sporulated for 5 hrs before adding $CuSO_4$ to induce cyclin Clb3 expression. Immediately after induction, cells were released from meiotic prophase using β-estradiol. Samples were taken 1 hr 45 min after the release. Left: a schematic for normal and abnormal meiosis I. In an abnormal meiosis I, two separated GFP dots were observed in binucleates, one in each nucleus. The average fraction of binucleates that displayed sister segregation in meiosis I, as well as the range of two independent experiments, was graphed for each strain. 100 cells were counted per strain, per experiment.

3.4.1 Ndc80 phosphorylation triggers its degradation in meiotic prophase

Three lines of evidence support a model in which Aurora B/Ipl1–dependent phosphorylation of Ndc80 triggers its degradation in meiotic prophase. First, the kinase activity of Ipl1 is required for Ndc80 degradation, but Ipl1 acts through a mechanism independent of microtubules. Second, at least one Ipl1 consensus site on Ndc80 (T54) is phosphorylated during meiotic prophase, the time when Ndc80 degradation occurs. Lastly, mutating the seven Ipl1 consensus sites leads to Ndc80 stabilization in meiotic prophase, suggesting that these sites are necessary for Ndc80 degradation. Altogether, these results are consistent with a phosphorylation-dependent degradation mechanism.

Interestingly, it is well established that Ndc80 phosphorylation by Aurora B/Ipl1 helps correct microtubule-kinetochore mis-attachments (Biggins 2013). Ndc80 phosphorylation is thought to weaken microtubule binding, resulting in microtubule detachment and thus providing the opportunity for the kinetochore to re-attach in the correct orientation. How is the error correction process interrelated with Ndc80 degradation given that both processes require Ndc80 phosphorylation by Aurora B/Ipl1? We found that disrupting Ndc80 degradation (*Δ2-28*) does not appear to affect meiotic chromosome segregation (Figure 3.19

and Figure 3.22). This observation is consistent with that error correction is functional in the Ndc80 degradation mutants. It is unlikely that Ndc80 degradation is required for error correction.

Instead, we propose that the completion of error correction may repress Ndc80 degradation in metaphase I, during which Ndc80 level is stable (Figure 3.5). Once the chromosomes attach to spindles properly, Ndc80 phosphorylation is removed by phosphatases to stabilize the microtubule attachments (Biggins 2013). Thus, it is possible that Ndc80 level becomes stable after the removal of Ndc80 phosphorylation, the degradation signal, in metaphase I.

This model, however, leads to a puzzle. As the major microtubule-binding site, Ndc80 is required to build new attachments during error correction. And yet, in this model, Ndc80 phosphorylation would cause its degradation at a time when the presence of Ndc80 is essential. We posit that one explanation may be kinetics: Ndc80 degradation is relatively slow (a few hours) compared to the time required for error correction. Live-cell imaging experiments reveal that meiotic cells typically spend less than an hour from spindle formation (initiated by the splitting of spindle pole bodies) to homolog separation in meiosis I (See Shirk *et al.* 2011 for the time-lapse data). This difference in kinetics may explain why the effect of Ndc80 turnover on error correction is minimal. Furthermore, Ndc80 protein is upregulated at meiotic prophase exit (Chen *et al.* 2017), which may provide extra proteins to compensate for the loss due to degradation. Alternatively, there exist other mechanisms to suppress Ndc80 degradation after meiotic prophase, even before error correction is completed.

3.4.2 Protein turnover as a mechanism to create meiosis-specific kinetochores

In vegetative growth, the yeast kinetochores transiently disassemble during DNA replication when the centromeric DNA replicates, but they attach to microtubules for the rest of the cell cycle. It has been shown that the subunit stoichiometry of the kinetochore is regulated during the cell cycle (Dhatchinamoorthy *et al.* 2017; Dhatchinamoorthy *et al.* 2019). However, it is unclear whether the protein levels of the kinetochore subunits are regulated in vegetative growth. Degradation of a few kinetochore proteins has been reported in yeast. These include Dsn1 (Akiyoshi *et al.* 2013), Cbf13 (Kaplan *et al.* 1997), Spc-7 in fission yeast (Kriegenburg *et al.* 2014), and the centromeric histone Cse4 (Ranjitkar *et al.* 2010; Hewawasam *et al.* 2010; Cheng *et al.* 2017; Cheng *et al.* 2016; Ohkuni *et al.* 2016). The degradation pathways of these subunits have been proposed to be quality controls that remove nonfunctional or excess proteins, rather than direct means to alter kinetochore function.

In contrast, regulating protein abundance is the key mechanism to control kinetochore activity in meiosis. The outer kinetochore component, the Ndc80 complex, disassembles in meiotic prophase and reassembles in prometaphase I. This disassembly is triggered by a declining level of the subunit Ndc80, as a result of the synthesis repression and degradation of Ndc80. In meiosis, Ndc80 degradation is not a passive consequence of DNA replication

but a targeted process. It is coupled to spindle suppression in meiotic prophase by a common regulator, the Aurora B/Ipl1 kinase (Shirk *et al.* 2011; Kim *et al.* 2013). We propose that Ipl1 prevents premature microtubule-kinetochore interaction in meiotic prophase through two independent ways—one by altering microtubule behaviors, and the other by triggering Ndc80 degradation. This dual mechanism ensures that the kinetochore interacts with spindles only after meiotic prophase. This delay in microtubule-kinetochore interaction is required for proper chromosome segregation in meiosis I (Miller *et al.* 2012).

It remains unclear what acts downstream of Ndc80 phosphorylation to mediate Ndc80 degradation. We have shown that active proteasomes are required (Figure 3.11). Thus, we propose that Ndc80 is degraded through the ubiquitin-proteasome system. In this system, degradation substrates are ubiquitinated by E3 ligase(s) before they are targeted by the proteasomes. We posit that one or multiple unknown E3 ligases mediate Ndc80 degradation, perhaps by interacting with the 2-28 residues. So far, we have ruled out the role of APC^{Cdc20} (Figure 3.5) and 38 non-essential ubiquitin ligases (unpublished results) in Ndc80 degradation. Future work to identify this ligase will be important to fully grasp the meiotic regulation of Ndc80 turnover.

3.4.3 Customization of kinetochore activity by controlling kinetochore assembly or disassembly

Besides budding yeast meiosis, examples in other organisms also indicate that regulating kinetochore assembly or disassembly is a common way to customize kinetochore activity based on the specific cell cycle stage or cell type. During the mitosis of human cells, the KMN network dissociates from the inner kinetochore in every cell cycle. A failure to do so causes chromosome mis-segregation in the next cell cycle (Gascoigne & Cheeseman 2013). During the female meiosis of *C. elegans*, the worm kinetochores facilitate homolog bi-orientation and error sensing in meiosis I, but they do not segregate the chromosomes. Instead, the ring-complex and microtubule motors, such as dynein, segregate the chromosomes, while the kinetochore proteins disappear from the chromosomes in anaphase I (Dumont *et al.* 2010; Muscat *et al.* 2015; Laband *et al.* 2017; Davis-Roca *et al.* 2017). Lastly, in *C. elegans*, *Drosophila*, and iPS-derived human motor neurons, some or all of the core kinetochore proteins localize to the regions of synaptic neuropil and axons that are devoid of nuclei. There, they control axon outgrowth and dendritic extension in the developing sensory nervous system (Cheerambathur *et al.* 2019; Zhao *et al.* 2019). All these examples highlight that when and where the kinetochore is assembled are tuned to the cell cycle and cell types.

Based on our finding that the Aurora B kinase regulates the turnover of kinetochore subunit, it will be interesting to test if other kinetochore restructuring events also depend on Aurora B. For example, the protein level of Ndc80/Hec1 declines at the mitotic exit in human cells (Ferretti *et al.* 2010), but the mechanism is unknown. We posit that Aurora B and/or Aurora A may trigger Ndc80/Hec1 degradation at the mitotic exit in human cells, contributing to the KMN dissociation. In addition, the worm Aurora B kinase, AIR-2, lo-

calizes with microtubules during anaphase I (Schumacher *et al.* 1998; Speliotes *et al.* 2000; Romano *et al.* 2003). Thus, it is possible that AIR-2 phosphorylation causes the dissociation or degradation of kinetochore subunit(s), leading to kinetochore disassembly at that time. Our discovery that Aurora B phosphorylation can cause the turnover of kinetochore proteins adds one more mechanism by which Aurora B can influence kinetochore composition and activity: Aurora B not only regulates the construction but also the destruction of the kinetochore.

Chapter 4

Conclusions

4.1 Meiotic regulation of kinetochore remodeling

This thesis describes the discovery of a multi-level network that regulates the dynamic kinetochore behavior in budding yeast meiosis. The main logic of this network is to control the protein abundance of a linchpin kinetochore subunit, Ndc80. In meiotic prophase, the steady-state level of Ndc80 is low, leading to the dissociation of the microtubule-binding part of the kinetochore. After meiotic prophase, Ndc80 is re-synthesized, leading to the timely assembly of the *holo* kinetochore prior to the meiotic divisions. The fluctuation in Ndc80 levels requires regulation of both Ndc80 synthesis and turnover. This regulation is essential for accurate chromosome segregation, spore formation, and gamete fitness. Altogether, this work illustrates how the kinetochore activity is modulated by coordinating the synthesis and turnover of a single subunit, thereby establishing the specialized cell division of meiosis.

4.1.1 Regulated expression of two *NDC80* mRNAs controls Ndc80 synthesis temporally

The core of the *NDC80* synthesis regulation is the toggling between two *NDC80* mRNA isoforms: a canonical mRNA capable of Ndc80 protein production ($NDC80^{ORF}$) and a 5'-extended mRNA termed $NDC80^{LUTI}$. Although $NDC80^{LUTI}$ contains the entire open reading frame of *NDC80*, this ORF cannot be translated into Ndc80 protein. Rather, the meiotic cells use $NDC80^{LUTI}$ transcription to impede the expression of the protein-producing $NDC80^{ORF}$ mRNA. We term this repression system the "*LUTI*-based repression mechanism," which will be summarized further in the next subsection. When coupled with Ndc80 turnover, $NDC80^{LUTI}$ expression causes a reduction in Ndc80 protein levels.

How do meiotic cells coordinate Ndc80 synthesis with the meiotic progression? Two key meiotic transcription factors temporally control the expression of $NDC80^{ORF}$ and $NDC80^{LUTI}$ (Figure 2.13-2.17). Before meiosis, when yeast cells are undergoing the mitotic cell cycle (vegetative growth), the repressor Ume6 inhibits $NDC80^{LUTI}$ expression by

binding to the *URS1* site at the $NDC80^{LUTI}$ promoter. This mode of Ume6-dependent repression in vegetative cells occurs ubiquitously for the early meiotic genes. Mutating the *URS1* site causes a leaky expression of $NDC80^{LUTI}$ in vegetative growth (Figure 2.16), which is sufficient to reduce the $NDC80^{ORF}$ mRNA and Ndc80 protein levels (Figure 2.22).

As diploid yeast cells enter meiosis, the binding of Ime1 to Ume6 converts Ume6 into a co-activator of early meiotic genes and $NDC80^{LUTI}$ (Figure 2.13, 2.16). The expression of $NDC80^{LUTI}$ suppresses $NDC80^{ORF}$ transcription through the $LUTI$-based repression mechanism (Figure 2.8-2.11). As a result, Ndc80 protein synthesis is turned off. Ndc80 turnover is also upregulated in meiotic prophase. Due to the dual regulation of its synthesis and degradation, the protein level of Ndc80 drops at this time. Consequently, Ndc80 becomes a limiting kinetochore subunit, triggering the disassembly of the Ndc80 complex and inactivating the kinetochore.

After exiting from meiotic prophase, Ndt80 re-induces the expression of $NDC80^{ORF}$ (Figure 2.17). Ndt80 seems capable of bypassing the $LUTI$-based repression since $NDC80^{ORF}$ can be expressed when both Ndt80 and $NDC80^{LUTI}$ are co-expressed under the same promoter (the *GAL* promoter) in vegetative growth (Chia *et al.* 2017). Furthermore, after exiting meiotic prophase, the increased Ime2 activity enhances Ime1 degradation (Guttmann-Raviv *et al.* 2002). Thus, the induction strength of $NDC80^{LUTI}$ likely declines after meiotic prophase, weakening the $LUTI$-based repression. Since $NDC80^{ORF}$ can produce Ndc80 protein, Ndc80 reaccumulates to allow the Ndc80 complex to assemble on the kinetochore. As a result, the kinetochore is reactivated to interact with microtubules and segregate the chromosomes during the two meiotic divisions.

4.1.2 The *LUTI*-based repression mechanism

The $LUTI$-based repression mechanism belongs to a larger class of RNA-mediated gene regulation models. The main features of the $LUTI$ mechanism are present in other RNA-mediated regulatory systems, such as those for long non-coding RNAs or antisense RNAs. How does the $LUTI$ mechanism work? This mechanism acts in *cis* (Figure 2.11) through chromatin modifications. $NDC80^{LUTI}$ transcription induces two main changes in the $NDC80^{ORF}$ promoter (Chia *et al.* 2017). First, the histone modifications H3K4me2 and H3K36me3 are co-transcriptionally deposited to the $NDC80^{ORF}$ promoter. The loss of these marks (by mutating the Set2 methyltransferase and the Set3 deacetylase) relieves $NDC80^{ORF}$ repression despite the expression of $NDC80^{LUTI}$ (Chia *et al.* 2017). Second, the nucleosomes are repositioned in the $NDC80^{ORF}$ promoter. Currently, it is unclear how nucleosome remodeling contributes to the $LUTI$ mechanism. The two histone marks, H3K4me2 and H3K36me3, are also used by *IRT1* to repress *IME1* expression (van Werven & Amon 2011). Set2 and Set3 have been reported to repress the promoters with overlapping lncRNA transcription from an upstream promoter or downstream antisense promoter (Kim Guisbert *et al.* 2012; Kim *et al.* 2016). Therefore, the $LUTI$ mechanism seems to recycle a common transcription repression strategy to perform its function.

However, the *LUTI* mechanism faces a unique challenge; that is, the *NDC80*^{LUTI} mRNA contains the entire ORF of the gene that it aims to repress. The shutdown of Ndc80 synthesis requires the *NDC80*^{LUTI} mRNA to repress the translation of the ORF that it carries. *NDC80*^{LUTI} solves this problem with the upstream ORFs (uORFs) in its 5' extended leader, which compete for ribosome translation and thus prevent translation of the main ORF. Two observations support this conclusion. First, when the start codons of the nine uORFs become nonfunctional, this uORF-less *NDC80*^{LUTI} (Δ*9AUG*) produces high levels of Ndc80 protein in meiotic prophase (Figure 2.7). Thus, the uORFs are necessary to repress the translation of the main ORF on the *NDC80*^{LUTI} mRNA. Second, when the nine uORFs are shortened to two-codon units, this *NDC80*^{LUTI} mutant (*mini-uORF*) cannot produce Ndc80. Thus, the act of uORF translation, rather than the uORF peptides, represses the translation of the *NDC80* ORF. Altogether, the *NDC80*^{LUTI}-based repression relies on both transcription and translation features to reach its ultimate goal of inhibiting Ndc80 protein synthesis.

It is remarkable that meiotic yeast cells widely use RNA-mediated mechanisms to regulate gene expression. As described in Chapter 1, the expression of *IME1* and *IME4* is regulated by a lncRNA and an antisense RNA, respectively. Matched mRNA-seq, ribosome profiling, and quantitative mass spectrometry datasets have shown that over 380 genes display anti-correlation between their protein and transcript levels in meiosis, pointing to the possibility that these genes are regulated by the *LUTI* mechanism (Cheng *et al.* 2018). Transcript leader-sequencing and nanopore sequencing also have revealed that 74 early-meiosis genes express *LUTI* mRNAs, with 46 containing the Ume6 binding site (*URS1*) and bound to Ume6 (Trensenrider *et al.* in preparation). All these observations suggest that *LUTI*s are common in yeast meiosis.

It is important to note that the *LUTI* mechanism is present beyond yeast meiosis. Examples of *LUTI*s have been found in the unfolded protein response (Van Dalfsen *et al.* 2018) and the zinc depletion response (Taggart *et al.* 2017) of budding yeast, and the human *MDM2* gene (Hollerer *et al.* 2019). Furthermore, the core of the *LUTI* mechanism—alternative start site usage, uORF translation, and transcription-coupled chromatin modifications—are common in many organisms (reviewed in Tresenrider & Unal 2018). Therefore, we envision that the *LUTI*-based mechanism also exists in other organisms, and future studies will continue to uncover new examples of *LUTI*s.

4.1.3 Ndc80 phosphorylation triggers its degradation in meiotic prophase

Besides Ndc80 synthesis, meiotic cells temporally regulate Ndc80 degradation. Specifically, Ndc80 is degraded in meiotic prophase and not in metaphase I (Figure 3.5). Ndc80 degradation requires active proteasome and a 27-residue degron sequence at the N-terminus of Ndc80 but not other chromosomal transactions in meiotic prophase, including replication, recombination, and synapsis (Figure 3.7, Figure 3.11, Figure 3.12). Interestingly, inhibiting the Aurora B/Ipl1 kinase leads to a high steady-state level of Ndc80 in meiotic prophase

(Figure 3.13). Ipl1 depletion does not affect the repression of Ndc80 synthesis (Figure 3.13), nor stabilizes Ndc80 indirectly by altering microtubule behaviors (Figure 3.14). Therefore, Ipl1 most likely regulates Ndc80 degradation. In support of this model, we detected in meiotic prophase a phosphorylated residue of Ndc80 known to be targeted by Ipl1. The timing of phosphorylation coincides with when Ndc80 is degraded (Figure 3.15). Furthermore, mutating the seven Ipl1 consensus sites on the Ndc80 N-terminal tail stabilizes Ndc80 (Figure 3.16). Therefore, we propose that Ndc80 degradation occurs through a phosphorylation-mediated, proteasome-dependent mechanism.

Several outstanding questions remain. First, what acts downstream of Ndc80 phosphorylation to target Ndc80 for degradation? Our study suggests that Ndc80 degradation requires the proteasome activity. Therefore, it is likely that a specific ubiquitin ligase, or multiple ones, target Ndc80 for degradation. We attempted to identify such ligase through a small-scale screen in which 38 non-essential ligases and four ubiquitin-conjugating enzymes (E2) were deleted individually. These deletions did not significantly alter Ndc80 degradation in meiotic prophase (unpublished results). While this screen is not exhaustive, we posit that multiple ubiquitin ligases might act redundantly to target Ndc80 for degradation. For example, multiple ligases are found to target the centromeric histone Cse4 (Hewawasam *et al.* 2010; Cheng *et al.* 2017; Cheng *et al.* 2016; Ohkuni *et al.* 2016). Therefore, it is possible that Ndc80 is also a substrate for multiple ligases, and in that case, alternative strategies would be needed to identify the ubiquitin ligase(s) of Ndc80.

Regardless of how Aurora B/Ipl1 phosphorylation leads to Ndc80 degradation, the rewiring of this phosphorylation for a new function is quite clever. Meiotic yeast cells use a common regulator, Aurora B/Ipl1, to trigger both microtubule suppression and kinetochore inactivation in meiotic prophase. This strategy ensures that microtubule-kinetochore interactions are fully disrupted in meiotic prophase, as Aurora B/Ipl1 coordinates both events to occur simultaneously. Additionally, the Aurora B/Ipl1-mediated Ndc80 phosphorylation is used to correct attachment errors in essentially all dividing cells. Thus, this system is already present for most cells. It is quite economical to simply modify the core of this system slightly and obtain a new function. Conceptually, this idea is similar to using the G-protein coupled receptors to control multiple signaling processes. While each signaling event adds some process-specific features (e.g., different ligand binding sites), the core of the signaling cascade remains the same. It will be interesting to see whether other cellular processes also rewire this conserved kinase-substrate relationship for new functions.

Second, how does Ndc80 become stable in metaphase I? Interestingly, Aurora B/Ipl1 phosphorylation on Ndc80 is known to correct erroneous microtubule-kinetochore attachment in prometaphase. Perhaps Ndc80 only becomes stable after the error correction process finishes. Alternatively, additional factors required for Ndc80 degradation become limiting or inactivated in metaphase I. One possible factor could be the ubiquitin ligase of Ndc80. After exiting meiotic prophase, drastic proteomic and post-translational changes occur due to Ndt80 transcription and the rise of several kinase activities, including the polo-like kinase Cdc5, the Clb1- and Clb4-CDK, and Ime2. Thus, it is possible that these changes repress the degradation factors for Ndc80, leading to Ndc80 stabilization.

Third, is Ndc80 degradation restricted to meiotic prophase? My preliminary data showed that Ndc80 is unstable during an α-factor G_1 arrest, in which a *MAT***a** haploid cell arrests in the G_1 stage in response to the mating pheromone α-factor (unpublished results). This observation suggests that Ndc80 degradation can occur outside of meiosis. Does the degron sequence that we identified regulate Ndc80 degradation in G_1? Does Ipl1 phosphorylation also contribute to Ndc80's instability at that time? What is the function of degrading Ndc80 in G_1? Future work will shed light on these questions.

4.2 The biological relevance of regulating Ndc80 abundance

As mentioned in Chapter 1, to segregate the homologous chromosomes in meiosis I, meiotic cells need to restrict microtubule-kinetochore interactions until prometaphase I. If microtubules and the kinetochores prematurely interact in meiotic prophase, then drastic changes on the meiotic chromosome segregation pattern occur (Miller *et al.* 2012). The monopolin complex fails to localize to the kinetochores. Also, the centromeric cohesin fails to be protected in meiosis I. As a result, the sister chromatids (instead of the homologous chromosomes) segregate in meiosis I, essentially converting meiosis I into a mitosis-like division. Therefore, it is important to prevent premature microtubule-kinetochore interactions in meiosis.

Meiotic yeast cells use two strategies to prevent premature microtubule-kinetochore interactions. First, meiotic cells suppress the formation of bipolar spindles until the meiotic prophase exit. Second, the outer kinetochore disassembles in meiotic prophase, thus eliminating the kinetochore's microtubule-binding ability. In this work, we showed that the kinetochore is inactivated due to a limiting level of Ndc80 protein in meiotic prophase. The overexpression of Ndc80, and not any other subunit in its complex, can reactivate the kinetochore in meiotic prophase (Figure 2.3). This result suggest that Ndc80 is the limiting component in meiotic prophase that restricts kinetochore activity.

It is perhaps no surprise that Ndc80 is selected for extensive meiotic regulation. It is the only subunit used for both microtubule binding and the spindle assembly checkpoint signaling. Irreversibly eliminating Ndc80 in meiotic prophase ensures that all the kinetochore-associated activities are turned off. Also, since all the other kinetochore subunits are constantly present (Figure 2.2), meiotic cells only need to regulate Ndc80 abundance to control the kinetochore activity directly. This elegant strategy ensures that the kinetochore assembles and disassembles in a rapid and timely manner.

To demonstrate the importance of regulating Ndc80 abundance, we examined the phenotypes associated with the mutants that affect Ndc80 synthesis and degradation. In this work, we have identified three types of mutants that result in a high level of Ndc80 in meiotic prophase: (1) disrupting the expression of $NDC80^{LUTI}$($\Delta NDC80^{LUTI}$), (2) expressing an uORF-less $NDC80^{LUTI}$($\Delta 9AUG$), and (3) inhibiting Ndc80 degradation (Δ*11-19* and Δ*2-*

28). In the sensitized background that produces spindle microtubules in meiotic prophase (*pCUP-CLB3*), each of these mutant causes the sister chromatids to segregate in meiosis I, and the extent of the meiotic errors is similar to that of Ndc80 overexpression (Figure 2.18 and Figure 3.23). These observations indicate that both synthesis repression and degradation are necessary to reduce the Ndc80 level sufficiently to prevent premature kinetochore activity.

While Ndc80 is downregulated in meiotic prophase, such downregulation should not occur all the time. For budding yeast, the kinetochores are attached to microtubules almost throughout the mitotic cell cycle, and during both meiosis I and meiosis II. Therefore, an untimely elimination of Ndc80 at these stages would inactivate the kinetochore inappropriately, leading to deleterious consequences. Two mutants exemplify this point. First is the *ndc80-urs1*Δ mutant. The *URS1* deletion abolishes Ume6 binding, leading to a leaky expression of $NDC80^{LUTI}$ in vegetative growth and a weak induction of $NDC80^{LUTI}$ in meiotic prophase (Figure 2.22). Although the leaky expression of $NDC80^{LUTI}$ does not reach the high level of $NDC80^{LUTI}$ in meiotic prophase, it is sufficient to repress the $NDC80^{ORF}$ mRNA and Ndc80 protein to a detectable level (Figure 2.16 and Figure 2.22). At an elevated temperature (37 °C), the *ndc80-urs1*Δ mutant has growth defects (Figure 2.22), highlighting the importance of restricting Ndc80 downregulation to meiosis.

The second mutant is *ndc80-mse*. This mutant fails to re-express the $NDC80^{ORF}$ mRNA after meiotic prophase because the binding site of the Ndt80 transcription factor (*MSE*) is disrupted. Thus, Ndc80 does not reaccumulate for the meiotic divisions (Figure 2.17). In this mutant, over 98% of the cells have chromosome mis-segregation, whereas only 2% of wild-type cells do so (Figure 2.19). Only 20% of the mutant cells form spores, in contrast to >90% in wild-type cells (Figure 2.21). These drastic differences underscore the significance of re-expressing Ndc80 after meiotic prophase.

It is somewhat surprising that the *ndc80-mse* mutant is defective in spore formation. In contrast to the *ndc80-mse* mutant, the *spo11*Δ mutant undergoes random chromosome segregation in meiosis I because the homologs fail to recombine. And yet, the *spo11*Δ mutant readily forms spores (Esposito *et al.* 1972). Therefore, chromosome mis-segregation per se does not prevent spore formation. Consistent with this idea, disrupting Mad3, a spindle assembly checkpoint protein, cannot rescue the spore formation defect in the *ndc80-mse* mutant (unpublished results). Thus, it is likely that the spore formation defect is not a result of checkpoint activation. Future work will monitor each step of the spore development in the *ndc80-mse* mutant and examine where the defect arises. Also, it will be interesting to analyze whether other kinetochore mutants also affect spore formation. This experiment will reveal if Ndc80 has a moonlighting role in spore development, beyond its canonical role in chromosome segregation.

4.3 A final perspective

Altogether, this work reveals a beautiful case in evolution in which the gene expression, protein turnover, and activity of the kinetochore are tuned to establish a specialized chromosome segregation program, namely meiosis. We have demonstrated that the success of meiosis relies on the regulatory systems that we characterized in this work. Through analyzing how meiosis works in budding yeast, we hope to contribute to understanding the fundamental principles of meiosis and providing new insights into the reproductive health of humans.

Beyond kinetochore regulation, our findings also elicit broader implications on gene regulation. We have revealed that bona fide mRNAs, exemplified by *LUTI*s, can serve a purely regulatory function. These mRNAs defy the canonical protein-coding role imposed by the Central Dogma and join other non-coding RNAs to regulate gene expression. This blurring line between "coding" and "non-coding" RNAs forces us to reconsider how the genome functions. Perhaps, the genome is less functionally partitioned and constrained than we have previously thought. Perhaps to the genome, there need not be a strict division of labors, provided that the right circumstances appear.

Chapter 5

Materials and methods

5.1 Yeast strains, plasmids and culture methods

5.1.1 Strains and plasmids

All the strains used in this thesis are derivatives of SK1 unless noted. The strain genotypes are listed at the end of this subsection. The centromeric TetR/TetO GFP dot assay was first described in Michaelis *et al.* 1997, the *ndc80-1* temperature-sensitive mutant in Wigge *et al.* 1998, *pCUP-NDC80 pCUP-CLB3* in Miller *et al.* 2012, the meiotic-depletion alleles *pCLB2-3HA-CDC20* in Lee & Amon 2003, and *pSCC1-3HA-CDC6* in Hochwagen *et al.* 2005, *SPC24-6His-3Flag* in Miller *et al.* 2016,and the Zip1::GFP(700) in Salah & Nasmyth 2000. The following alleles were generated at the endogenous gene loci using PCR-based methods (Longtine *et al.* 1998): *NDC80-3V5*, *NUF2-3V5*, *SPC24-3V5*, *SPC25-3V5*, *NDT80-3V5*, *UME6-3V5*, *pCUP-NUF2*, *pCUP-SPC24*, *pCUP-SPC25*, *pSCC1-3HA-IPL1*, *spo11*Δ, Δ*pdr5*, Δ*mad2*, Δ*mad3*, *amn1*Δ, *ndc80*Δ, *nuf2*Δ, *NDC80-eGFP*, *MTW1-mCherry pGAL-NDC80*^{LUTI}, *pGAL-*Δ*9AUG*, *(*Δ*600 to 300)-NDC80*, and *(*Δ*600 to 400)-NDC80*. The V5 plasmid is a kind gift from Vincent Guacci.

Single integration plasmids carrying either *NDC80* or *NUF2* were constructed by Gibson Assembly (Gibson *et al.* 2009), and were digested with PmeI to integrate at the *LEU2* locus. For *NDC80*, the *LEU2* integration plasmid included the SK1 genomic sequence spanning from 1000 bp upstream to 357 bp downstream of the *NDC80* coding region; and for *NUF2*, spanning from 1000 bp upstream to 473 bp downstream of the *NUF2* coding region. Both constructs included a C-terminal fusion of the 3V5 epitope to *NDC80* and *NUF2*, and both completely rescued the full deletion of *NDC80* or *NUF2*, respectively. Deletions (*ndc80-urs1*Δ, Δ*600 to 400)-NDC80*, and Δ*600 to 479)-NDC80*) and point mutations (*ndc80-mse*) were generated from the *NDC80 LEU2* single integration plasmid using the site-directed mutagenesis kit (Q5 Site-Directed Mutagenesis Kit, NEB, Ipswich, MA). The entire *URS1* site and the "A" right upstream of the site were deleted in the *ndc80-urs1*Δ strain. The *ndc80-mse* construct has two C to A mutations marked using black diamonds in Figure 2.14. The Δ*6AUG*, Δ*9AUG*, *mini uORF*, *NDC80*^{LUTI}*-Ter*, and *NDC80*^{LUTI}*-NUF2* constructs were

generated by Gibson assembly (Gibson *et al.* 2009) using the *NDC80* and *NUF2 LEU2* integration plasmids, as well as gBlocks gene fragments (IDT, Redwood City, CA) for the *Δ9AUG* and *mini uORF* constructs.

Generated by Gibson assembly (Longtine *et al.* 1998), the *8lexO-luti-mse-NDC80-3V5* construct has two features: (1) Eight *lex* operators (*lexO*) and the promoter from *CYC1* were inserted at 536 bp upstream of the translation start site of *NDC80 ORF*. This insertion allows LexA to control the expression of $NDC80^{LUTI}$ mRNA in a dose-dependent manner (Chia *et al.* 2017). (2) The Ndt80 binding site was mutated (*mse*) as described above, which greatly reduced the Ndt80-dependent expression of $NDC80^{ORF}$ mRNA (Chen *et al.* 2017). The *8lexO-luti-NDC80-3V5* construct has wild-type *MSE*. The *NDC80-7A*, *NDC80-14A*, *NDC80(4H to A)*, *NDC80(4H to L)*, *NDC80-11A*, and *NDC80-Δ4D-box* constructs were also generated by Gibson assembly (Longtine *et al.* 1998), using gBlocks gene fragments (IDT, Redwood City, CA). Systematic deletions of the N-terminal residues of Ndc80 (*Δ2-28, Δ29-56, Δ2-10, Δ11-19, Δ20-28, Δ57-112, Δ2-112*) were made in the *NDC80 LEU2* plasmid using the Q5 Site-Directed Mutagenesis Kit (NEB, Ipswitch, MA).

To generate the *Δ2-28*, *Δ11-19*, and *NDC80-7A* alleles at the endogenous locus of *NDC80*, the CRISPR/Cas9 method was used (Anand *et al.* 2017). The oligonucleotides encoding the guide RNA (5'-TACATCACATGGACCCTCATCGG-3') was cloned into a centromeric plasmid carrying a *URA3* maker and *pPGK1-Cas9* (a gift from G Schlissel, University of California, Berkeley, Berkeley, CA). This plasmid was co-transformed into yeast along with the following repair templates. For *Δ2-28* and *Δ11-19*, the repair templates were amplified from the respective *LEU2* single integration plasmids by PCR. For *NDC80-7A*, the following primers (5'-ACATGTGCTACATCACATGGACCCTCATCGGTTTGCTTCaCAAATACCAACTGCA ACATC-3' and 5'-CTCTTGAATAGCGCTTTGGAAGTTTTTGTCTCTTAGTGGtCTT GGATCTCTATTGCTCAG-3') were used to amplify the repair template from the *NDC80-7A LEU2* single integration plasmid. The lowercase letters correspond to the synonymous mutations that abolish the PAM site: a C-to-A mutation at the 66th nucleotide of the translation start site of Ndc80, as well as a G-to-A at the 351st nucleotide.

Table 5.1: Strains

Strain	***Genotype***
FW1208	*MAT**a** /MATα UME6-3V5::His3MX/UME6-3V5::His3MX*
FW1511	*MAT**a** /MATα*
FW1871	*MAT**a** /MATα* *ime1::pCUP-IME1::NatMX/ime1::pCUP-IME1::NatMX* *ime4::pCUP-IME4::NatMX/ime4::pCUP-3HA-IME4::NatMX* *NDC80-3V5::KanMX/NDC80-3V5::KanMX (Δ-600 to* *-300)-NDC80::His3MX/(Δ-600 to -300)-NDC80::His3MX*

Table 5.1: continued

FW1899	*MAT**a** /MATα ime1::pCUP-IME1::NatMX/ime1::pCUP-IME1::NatMX ime4::pCUP-IME4::NatMX/ime4::pCUP-IME4::NatMX NDC80-3V5:KanMX/(Δ-600 to -300)-NDC80::His3MX*
FW1900	*MAT**a** /MATα ime1::pCUP-IME1::NatMX/ime1::pCUP-IME1::NatMX ime4::pCUP-IME4::NatMX/ime4::pCUP-IME4::NatMX NDC80-3V5:KanMX*
FW1902	*MAT**a** /MATα ime1::pCUP-IME1::HphMX/ime1::pCUP-IME1:: HphMX ime4::pCUP-IME4::NatMX/ime4::pCUP-IME4:: NatMX NDC80-3V5::KanMX/ NDC80-3V5::KanMX*
FW1923	*MAT**a** /MATα ime1::pCUP-IME1::NatMX/ime1::pCUP-IME1::NatMX ime4::pCUP-IME4::NatMX/ime4::pCUP-IME4::NatMX HisMX::(Δ-600 to -300)-NDC80-3V5:KanMX/NDC80*
FW3058	*MAT**a** /MATα ime1::His3MX/ime1::His3MX ime4::pCUP-IME4::NatMX/ime4::pCUP-IME4::NatMX NDC80-3V5::KanMX/NDC80-3V5::KanMX*
UB13	*ho::LYS2 lys2 ura3 leu2::hisG his3::hisG trp1::hisG (SK1 wild-type)*
UB95	*MAT**a** /MATα GAL-NDT80::TRP1/GAL-NDT80::TRP1 ura3::pGPD1-GAL4(848).ER::URA3/ura3::pGPD1-GAL4(848).ER::URA3*
UB494	*MAT**a** ndc80-1*
UB700	*MAT**a** ho::LYS2 lys2 ura3 leu2::hisG his3::hisG trp1::hisG mad2Δ:CNAT*
UB877	*MAT**a** /MATα ura3::pGPD1-GAL4(848).ER::URA3/ura3::pGPD1-GAL4(848).ER::URA3 GAL-NDT80::TRP1/GAL-NDT80::TRP1 leu2::pURA3-TetR-GFP::LEU2 CENV::TetOx224::HIS3 Ndc80-3V5:KanMX pCUP-CLB3::KANMX*
UB880	*MAT**a** /MATα ura3::pGPD1-GAL4(848).ER::URA3/ura3::pGPD1-GAL4(848).ER::URA3 GAL-NDT80::TRP1/GAL-NDT80::TRP1 leu2::pURA3-TetR-GFP::LEU2 CENV::TetOx224::HIS3 KanMX:pCUP-Ndc80-3V5:CNAT pCUP-CLB3::KANMX*
UB885	*MAT**a** /MATα ura3::pGPD1-GAL4(848).ER::URA3/ura3::pGPD1-GAL4(848).ER::URA3 GAL-NDT80::TRP1/GAL-NDT80::TRP1 leu2::pURA3-TetR-GFP::LEU2 CENV::TetOx224::HIS3 Ndc80-3V5:KanMX pCUP-CLB3::KANMX HISMX:pCUP-Spc25*

Table 5.1: continued

UB980	*MAT**a** /MATα GAL-NDT80::TRP1/GAL-NDT80::TRP1 ura3::pGPD1-GAL4(848).ER::URA3/ura3::pGPD1-GAL4(848).ER::URA3 leu2::pURA3-TetR-GFP::LEU2 CENV::TetOx224::HIS3 Ndc80-3V5:KanMX pCUP-CLB3::KANMX pCUP-SPC24::KANMX*
UB1013	*MAT**a** /MATα GAL-NDT80::TRP1/GAL-NDT80::TRP1 ura3::pGPD1-GAL4(848).ER::URA3/ura3::pGPD1-GAL4(848).ER::URA3 NDC80-3V5:CNAT/ NDC80-3V5:CNAT KanMX6:pSCC1-3HA-IPL1/KanMX6:pSCC1-3HA-IPL1*
UB1051	*MAT**a** /MATα GAL-NDT80::TRP1/GAL-NDT80::TRP1 ura3::pGPD1-GAL4(848).ER::URA3/ura3::pGPD1-GAL4(848).ER::URA3 Spc25-3V5:HisMX/Spc25-3V5:HisMX*
UB1083	*MAT**a** /MATα GAL-NDT80::TRP1/GAL-NDT80::TRP1 ura3::pGPD1-GAL4(848).ER::URA3/ura3::pGPD1-GAL4(848).ER::URA3 Ndc80-eGFP:KanMX/Ndc80-eGFP:KanMX MTW1-mCherry::HphMX4/MTW1-mCherry::HphMX4*
UB1217	*MAT**a** HISMX:pGAL-Ndc80-3V5:KanMX ura3::pGPD1-GAL4(848).ER::URA3 (pGAL integrated 536 bp upstream of NDC80 AUG)*
UB1240	*MAT**a** Ndc80-3V5:KanMX ura3::pGPD1-GAL4(848).ER::URA3*
UB1323	*MAT**a** KanMX:pGAL-Δ9AUG-5'UTR-Ndc80-3V5:CNAT ura3::pGPD1-GAL4(848).ER::URA3 (pGAL integrated 536 bp upstream of NDC80 AUG. ATG-ATC mutation in 9 of the 9 potential upstream start codons within NDC80-5'UTR. The leader sequence contains 2 SNPs from S288C introduced by a gene block and a third mutation (TtoC) 8 bp after the 6th ATG)*
UB1337	*MAT**a** /MATα pCUP-IME1::NAT/pCUP-IME1::NAT pCUP-IME4::NAT/pCUP-IME4::NAT Ndc80-3V5:KanMX/Ndc80-3V5:KanMX*
UB1338	*MAT**a** /MATα GAL-NDT80::TRP1/GAL-NDT80::TRP1 ura3::pGPD1-GAL4(848).ER::URA3/ura3::pGPD1-GAL4(848).ER::URA3 Ndc80-3V5:KanMX/Ndc80-3V5:KanMX*
UB2388	*MAT**a** amn1::KanMX6 ura3::pGPD1-GAL4(848).ER::URA3 HISMX:pGAL-Ndc80-3V5:KanMX (pGAL integrated 536 bp upstream of NDC80 AUG)*
UB2389	*MAT**a** amn1::KanMX6 Ndc80-3V5:KanMX ura3::pGPD1-GAL4(848).ER::URA3*

Table 5.1: continued

UB2405	*MAT**a** /MATα GAL-NDT80::TRP1/GAL-NDT80::TRP1 ura3::pGPD1-GAL4(848).ER::URA3/ura3::pGPD1-GAL4(848).ER::URA3 Ndc80-3V5:CNAT/Ndc80-3V5:CNAT pdr5::KanMX6/pdr5::KanMX6*
UB2531	*MAT**a** /MATα irt1:cup1::Hphmx/irt1:cup1::Hphmx ime4::cup1::NAT/ime4::cup1::NAT*
UB2932	*MAT**a** /MATα GAL-NDT80::TRP1/GAL-NDT80::TRP1 ura3::pGPD1-GAL4(848).ER::URA3/ura3::pGPD1-GAL4(848).ER::URA3 HIS3MX:pNDC80(600-400)-Ndc80-3V5:KanMX/HIS3MX:pNDC80(600-400)-Ndc80-3V5:KanMX*
UB2936	*MAT**a** /MATα ura3::pGPD1-GAL4(848).ER::URA3/ura3::pGPD1-GAL4(848).ER::URA3 GAL-NDT80::TRP1/GAL-NDT80::TRP1 leu2::pURA3-TetR-GFP::LEU2 CENV::TetOx224::HIS3 HisMX:Δ9AUG-5'UTR-Ndc80-3V5:CNAT/HisMX:Δ9AUG-5'UTR-Ndc80-3V5:CNAT pCUP-CLB3::KANMX (ATG-ATC mutation in 9 of the 9 potential upstream start codons within NDC80-5'UTR. The leader sequence contains 2 other point mutations, in addition to the ATCs)*
UB2940	*MAT**a** /MATα ura3::pGPD1-GAL4(848).ER::URA3/ura3::pGPD1-GAL4(848).ER::URA3 GAL-NDT80::TRP1/GAL-NDT80::TRP1 leu2::pURA3-TetR-GFP::LEU2 CENV::TetOx224::HIS3 pCUP-CLB3::KANMX HIS3MX::(Δ-600 to -400)-NDC80-3V5::KanMX/HIS3MX::(Δ-600 to -400 bp)-NDC80-3V5::KanMX*
UB2942	*MAT**a** /MATα ura3::pGPD1-GAL4(848).ER::URA3/ura3::pGPD1-GAL4(848).ER::URA3 GAL-NDT80::TRP1/GAL-NDT80::TRP1 leu2::pURA3-TetR-GFP::LEU2 CENV::TetOx224::HIS3 Ndc80-3V5:KanMX/Ndc80-3V5:KanMX*
UB3262	*MAT**a** ndc80Δ:KanMX4 leu2::NDC80-3V5:LEU2*
UB3275	*MAT**a** ndc80Δ:KanMX4 leu2::NDC80(Δaa2-112)-3V5:LEU2*
UB3301	*MAT**a** /MATα UME6-3V5::His3MX/UME6-3V5::His3MX irt1:cup1::Hphmx/irt1:cup1::Hphmx ime4::cup1::NAT/ime4::cup1::NAT*
UB3380	*MAT**a** /MATα GAL-NDT80::TRP1/GAL-NDT80::TRP1 ura3::pGPD1-GAL4(848).ER::URA3/ura3::pGPD1-GAL4(848).ER::URA3 ndc80Δ:KanMX4/ndc80Δ:KanMX4 leu2::NDC80-3V5:LEU2/leu2::NDC80-3V5:LEU2*

Table 5.1: continued

UB3392	*MAT**a** /MATα GAL-NDT80::TRP1/GAL-NDT80::TRP1 ura3::pGPD1-GAL4(848).ER::URA3/ura3::pGPD1-GAL4(848).ER::URA3 ndc80Δ(-1000 and ORF):KanMX4/ndc80Δ(-1000 and ORF):KanMX4 leu2::mse-NDC80-3V5:LEU2/leu2::mse-NDC80-3V5:LEU2*
UB3699	*MAT**a** /MATα GAL-NDT80::TRP1/GAL-NDT80::TRP1 ura3::pGPD1-GAL4(848).ER::URA3/ura3::pGPD1-GAL4(848).ER::URA3 ndc80Δ:KanMX4/ndc80Δ:KanMX4 leu2::NDC80(R270A, L273A, R423A, L426A, R476A, L479A, R639A, L642A) -3V5:LEU2/leu2::NDC80(R270A, L273A, R423A, L426A, R476A, L479A, R639A, L642A) -3V5:LEU2 (4D-box)*
UB3948	*MAT**a** /MATα GAL-NDT80::TRP1/GAL-NDT80::TRP1 ura3::pGPD1-GAL4(848).ER::URA3/ura3::pGPD1-GAL4(848).ER::URA3 HIS3MX:pNDC80(600-400)-Ndc80-3V5:KanMX/HIS3MX:pNDC80(600-400)-Ndc80-3V5:KanMX KanMX6:pSCC1-3HA-IPL1/KanMX6:pSCC1-3HA-IPL1*
UB4074	*MAT**a** /MATα GAL-NDT80::TRP1/GAL-NDT80::TRP1 ura3::pGPD1-GAL4(848).ER::URA3/ura3::pGPD1-GAL4(848).ER::URA3 ndc80Δ(-1000 and ORF):KanMX4/ndc80Δ(-1000 and ORF):KanMX4 leu2::NDC80-3V5:LEU2/leu2::NDC80-3V5:LEU2*
UB4212	*MAT**a** leu2::urs1Δ-NDC80-3V5:LEU2 ndc80Δ::KanMX*
UB4361	*MAT**a** /MATα GAL-NDT80::TRP1/GAL-NDT80::TRP1 ura3::pGPD1-GAL4(848).ER::URA3/ura3::pGPD1-GAL4(848).ER::URA3 SPC24-3V5:KanMX/SPC24-3V5:KanMX NUF2-3V5:HisMX/NUF2-3V5:HisMX NDC80-3V5:CNAT/NDC80-3V5:CNAT*
UB4432	*MAT**a** /MATα ura3::pGPD1-GAL4(848).ER::URA3/ura3::pGPD1-GAL4(848).ER::URA3 GAL-NDT80::TRP1/GAL-NDT80::TRP1 CENV::TetOx224::HIS3 leu2::pURA3-TetR-GFP::LEU2 NDC80-3V5:KanMX*
UB4434	*MAT**a** /MATα ura3::pGPD1-GAL4(848).ER::URA3/ura3::pGPD1-GAL4(848).ER::URA3 GAL-NDT80::TRP1/GAL-NDT80::TRP1 CENV::TetOx224::HIS3 leu2::pURA3-TetR-GFP::LEU2 NDC80-3V5:KanMX pCUP-CLB3::KANMX*
UB4436	*MAT**a** /MATα ura3::pGPD1-GAL4(848).ER::URA3/ura3::pGPD1-GAL4(848).ER::URA3 GAL-NDT80::TRP1/GAL-NDT80::TRP1 CENV::TetOx224::HIS3 leu2::pURA3-TetR-GFP::LEU2 Ndc80-3V5:KanMX pCUP-Nuf2::KANMX pCUP-CLB3::KANMX*

Table 5.1: continued

UB4695	*MAT**a** ndc80Δ:KanMX4 leu2::NDC80(Δaa29-56)-3V5:LEU2*
UB5015	*MAT**a** ndc80Δ:KanMX4 leu2::NDC80(Δaa2-28)-3V5:LEU2*
UB5101	*MAT**a** /MATα pCUP-IME1::NAT/pCUP-IME1::NAT pCUP-IME4::NAT/pCUP-IME4::NAT nuf2::KanMX/nuf2::KanMX leu2::NDC80(-1000 to -1)-NUF2-3V5:LEU2/leu2::NDC80(-1000 to -1)-NUF2-3V5:LEU2*
UB5103	*MAT**a** /MATα pCUP-IME1::NAT/pCUP-IME1::NAT pCUP-IME4::NAT/pCUP-IME4::NAT nuf2::KanMX/nuf2::KanMX leu2::NUF2-3V5:LEU2/leu2::NUF2-3V5:LEU2*
UB5437	*MAT**a** /MATα ndc80Δ(-1000 and ORF):KanMX4/ndc80Δ(-1000 and ORF):KanMX4 leu2::mse-NDC80-3V5:LEU2/leu2::mse-NDC80-3V5:LEU2 CENV::tetOx224::HIS3/CENV::tetOx224::HIS3 his3::pURA3-TetR-GFP::HIS3/his3::pURA3-TetR-GFP::HIS3*
UB5473	*MAT**a** /MATα leu2::urs1Δ-NDC80-3V5:LEU2/leu2::urs1Δ-NDC80-3V5:LEU2 ndc80Δ(-1000 and ORF):KanMX4/ndc80Δ(-1000 and ORF):KanMX4*
UB5475	*MAT**a** /MATα GAL-NDT80::TRP1/GAL-NDT80::TRP1 ura3::pGPD1-GAL4(848).ER::URA3/ura3::pGPD1-GAL4(848).ER::URA3 leu2::NDC80 (11A)-3V5:LEU2/leu2::NDC80(11A)-3V5:LEU2 ndc80Δ(-1000 and ORF):KanMX4/ndc80Δ(-1000 and ORF):KanMX4 (11A = S3A, S4A, T5A, S6A, T7A, T21A, S22A, T26A, T28A, S29A, S30A)*
UB5662	*MAT**a** /MATα GAL-NDT80::TRP1/GAL-NDT80::TRP1 ura3::pGPD1-GAL4(848).ER::URA3/ura3::pGPD1-GAL4(848).ER::URA3 leu2::(Δaa2-28)NDC80-3V5:LEU2/leu2::(Δaa2-28)NDC80-3V5:LEU2 ndc80Δ(-1000 and ORF):KanMX4/ndc80Δ(-1000 and ORF):KanMX4*
UB5875	*MAT**a** /MATα leu2::NDC80-3V5:LEU2/leu2::NDC80-3V5:LEU2 ndc80Δ(-1000 and ORF):KanMX4/ndc80Δ(-1000 and ORF):KanMX4*
UB5876	*MAT**a** /MATα ndc80Δ(-1000 and ORF):KanMX4/ndc80Δ(-1000 and ORF):KanMX4 leu2::NDC80-3V5:LEU2/leu2::NDC80-3V5:LEU2 CENV::tetOx224::HIS3/CENV::tetOx224::HIS3 his3::pURA3-TetR-GFP::HIS3/his3::pURA3-TetR-GFP::HIS3*

Table 5.1: continued

UB6010	*MAT**a** /MATα leu2::NDC80(Δaa2-28)-3V5:LEU2/leu2::NDC80(Δaa2-28)-3V5:LEU2 ndc80Δ(-1000 and ORF):KanMX4/ndc80Δ(-1000 and ORF):KanMX4*
UB6075	*MAT**a** /Matα irt1:cup1::Hphmx/irt1:cup1::Hphmx ime4::cup1::NAT/ime4::cup1::NAT leu2::urs1Δ-NDC80-3V5:LEU2/leu2::urs1Δ-NDC80-3V5:LEU2 ndc80Δ(-1000 and ORF):KanMX4/ndc80Δ(-1000 and ORF):KanMX4*
UB6077	*MAT**a** /Matα irt1:cup1::Hphmx/irt1:cup1::Hphmx ime4::cup1::NAT/ime4::cup1::NAT leu2::(-295::ADH1)-NDC80-3V5:LEU2/leu2::(-295::ADH1)-NDC80-3V5:LEU2 ndc80Δ(-1000 and ORF):KanMX4/ndc80Δ(-1000 and ORF):KanMX4 ($NDC80^{LUTI}$-Ter)*
UB6079	*MAT**a** /Matα irt1:cup1::Hphmx/irt1:cup1::Hphmx ime4::cup1::NAT/ime4::cup1::NAT leu2::(Δ-600 to -479)-NDC80-3V5:LEU2/leu2::(Δ-600 to -479)-NDC80-3V5:LEU2 ndc80Δ(-1000 and ORF):KanMX4 /ndc80Δ(-1000 and ORF):KanMX4*
UB6181	*MAT**a** /Matα irt1:cup1::Hphmx/irt1:cup1::Hphmx ime4::cup1::NAT/ime4::cup1::NAT leu2::Δ6AUG-NDC80-3V5:LEU2/leu2::Δ6AUG-NDC80-3V5:LEU2 ndc80Δ(-1000 and ORF):KanMX4/ndc80Δ(-1000 and ORF):KanMX4 (ATG-ATC mutation in 6 of the 9 potential upstream start codons within NDC80-5'UTR)*
UB6183	*MAT**a** /MATα irt1:cup1::Hphmx/irt1:cup1::Hphmx ime4::cup1::NAT/ime4::cup1::NAT leu2::Δ9AUG-NDC80-3V5:LEU2/leu2::Δ9AUG-NDC80-3V5:LEU2 ndc80Δ(-1000 and ORF):KanMX4 /ndc80Δ(-1000 and ORF):KanMX4 (ATG-ATC mutation in 9 of the 9 potential upstream start codons within NDC80-5'UTR)*
UB6190	*MAT**a** /MATα irt1:cup1::Hphmx/irt1:cup1::Hphmx ime4::cup1::NAT/ime4::cup1::NAT ndc80Δ(-1000 and ORF):KanMX4 /ndc80Δ(-1000 and ORF):KanMX4 leu2::NDC80-3V5:LEU2/leu2::NDC80-3V5:LEU2*
UB6760	*MAT**a** /MATα Ume6-3V5::His3MX/Ume6-3V5::His3MX irt1:cup1::Hphmx/irt1:cup1::Hphmx ime4::cup1::NAT/ime4::cup1::NAT leu2::urs1Δ-NDC80:LEU2/leu2::urs1Δ-NDC80:LEU2 ndc80Δ(-1000 and ORF):KanMX4/ndc80Δ(-1000 and ORF):KanMX4*

Table 5.1: continued

UB7029	*MAT**a** /MATα GAL-NDT80::TRP1/GAL-NDT80::TRP1 ura3::pGPD1-GAL4(848).ER::URA3/ura3::pGPD1-GAL4(848).ER::URA3 leu2::(Δaa11-19)NDC80-3V5:LEU2/leu2::(Δaa11-19)NDC80-3V5:LEU2 ndc80Δ(-1000 and ORF):KanMX4/ndc80Δ(-1000 and ORF):KanMX4*
UB7031	*MAT**a** /MATα GAL-NDT80::TRP1/GAL-NDT80::TRP1 ura3::pGPD1-GAL4(848).ER::URA3/ura3::pGPD1-GAL4(848).ER::URA3 leu2::(Δaa20-28)NDC80-3V5:LEU2/leu2::(Δaa20-28)NDC80-3V5:LEU2 ndc80Δ(-1000 and ORF):KanMX4/ndc80Δ(-1000 and ORF):KanMX4*
UB7039	*MAT**a** /MATα GAL-NDT80::TRP1/GAL-NDT80::TRP1 ura3::pGPD1-GAL4(848).ER::URA3/ura3::pGPD1-GAL4(848).ER::URA3 leu2::(Δaa2-10)NDC80-3V5:LEU2/leu2::(Δaa2-10)NDC80-3V5:LEU2 ndc80Δ(-1000 and ORF):KanMX4/ndc80Δ(-1000 and ORF):KanMX4*
UB7496	*MAT**a** /MATα TRP1::GAL-NDT80-3V5::KanMX/TRP1::GAL-NDT80-3V5::KanMX ura3::pGPD1-GAL4(848).ER::URA3/ura3::pGPD1-GAL4(848).ER::URA3 ndc80Δ(-1000 and ORF):KanMX4/ndc80Δ(-1000 and ORF):KanMX4 leu2::mse-NDC80:LEU2/leu2::mse-NDC80:LEU2*
UB7997	*MAT**a** /MATα GAL-NDT80::TRP1/GAL-NDT80::TRP1 ura3::pGPD1-GAL4(848).ER::URA3/ura3::pGPD1-GAL4(848).ER::URA3 leu2::NDC80:LEU2/leu2::NDC80:LEU2 ndc80Δ(-1000 and ORF):KanMX4/ndc80Δ(-1000 and ORF):KanMX4*
UB7999	*MAT**a** /MATα TRP1::GAL-NDT80-3V5::KanMX/TRP1::GAL-NDT80-3V5::KanMX ura3::pGPD1-GAL4(848).ER::URA3/ura3::pGPD1-GAL4(848).ER::URA3 leu2::NDC80:LEU2/leu2::NDC80:LEU2 ndc80Δ(-1000 and ORF):KanMX4/ndc80Δ(-1000 and ORF):KanMX4*
UB8001	*MAT**a** HISMX:pGAL-Ndc80-3V5:KanMX ura3::pGPD1-GAL4(848).ER::URA3 leu2::NDC80-3V5:LEU2 (pGAL integrated 536 bp upstream of Ndc80 AUG)*

Table 5.1: continued

UB8144	*MAT**a** /MATα GAL-NDT80::TRP1/GAL-NDT80::TRP1 ura3::pGPD1-GAL4(848).ER::URA3/ura3::pGPD1-GAL4(848).ER::URA3 ZIP1::GFP(700)/ZIP1::GFP(700) (GFP is inserted internally of the coding region of ZIP1)*
UB9243	*MAT**a** /MATα irt1:cup1::Hphmx/irt1:cup1::Hphmx ime4::cup1::NAT/ime4::cup1::NAT leu2::uORF(mini)-NDC80-3V5::LEU2/leu2::uORF(mini)-NDC80-3V5::LEU2 ndc80Δ(-1000 and ORF):KanMX4/ndc80Δ(-1000 and ORF):KanMX4*
UB11793	*MAT**a** /MATα GAL-NDT80::TRP1/GAL-NDT80::TRP1 ura3::pGPD1-GAL4(848).ER::URA3/ura3::pGPD1-GAL4(848).ER::URA3 Ndc80-3V5:KanMX/Ndc80-3V5:KanMX spo11Δ:URA3/spo11Δ:URA3*
UB11797	*MAT**a** /MATα GAL-NDT80::TRP1/GAL-NDT80::TRP1 ura3::pGPD1-GAL4(848).ER::URA3/ura3::pGPD1-GAL4(848).ER::URA3 ndc80Δ(-1000 and ORF):KanMX4/ndc80Δ(-1000 and ORF):KanMX4 leu2::(Δ-400:600)-NDC80-3V5:LEU2/leu2::(Δ-400:600)-NDC80-3V5:LEU2*
UB11799	*MAT**a** /MATα GAL-NDT80::TRP1/GAL-NDT80::TRP1 ura3::pGPD1-GAL4(848).ER::URA3/ura3::pGPD1-GAL4(848).ER::URA3 ndc80Δ(-1000 and ORF):KanMX4/ndc80Δ(-1000 and ORF):KanMX4 leu2::(Δ-400:600)-NDC80(Δaa11-19)-3V5:LEU2/leu2::(Δ-400:600)-NDC80(Δaa11-19)-3V5:LEU2*
UB12297	*MAT**a** /MATα GAL-NDT80::TRP1/GAL-NDT80::TRP1 ura3::pGPD1-GAL4(848).ER::URA3/ura3::pGPD1-GAL4(848).ER::URA3 leu2::NDC80(H10A, H13A, H14A, H18A)-3V5:LEU2/leu2::NDC80(H10A, H13A, H14A, H18A)-3V5:LEU2 ndc80Δ(-1000 and ORF):KanMX4/ndc80Δ(-1000 and ORF):KanMX4 (4H to A)*
UB12299	*MAT**a** /MATα GAL-NDT80::TRP1/GAL-NDT80::TRP1 ura3::pGPD1-GAL4(848).ER::URA3/ura3::pGPD1-GAL4(848).ER::URA3 leu2::NDC80(H10L, H13L, H14L, H18L)-3V5:LEU2/leu2::NDC80(H10L, H13L, H14L, H18L)-3V5:LEU2 ndc80Δ(-1000 and ORF):KanMX4/ndc80Δ(-1000 and ORF):KanMX4 (4H to L)*
UB13530	*MAT**a** /MATα irt1:cup1::Hphmx/irt1:cup1::Hphmx ime4::cup1::NAT/ime4::cup1::NAT trp1::pGPD1-LexA-ER-HA-B112::TRP1/trp1::pGPD1-LexA-ER-HA-B112::TRP1 Ndc80-3V5:KanMX/Ndc80-3V5:KanMX*

Table 5.1: continued

UB13532	*MAT**a** /MATα irt1:cup1::Hphmx/irt1:cup1::Hphmx ime4::cup1::NAT/ime4::cup1::NAT trp1::pGPD1-LexA-ER-HA-B112::TRP1/trp1::pGPD1-LexA-ER-HA-B112::TRP1 KanMX:8LexO-luti-NDC80-3V5:CNAT/KanMX:8LexO-luti-NDC80-3V5:CNAT (8X-LexO-pCyc1 integrated 536 bp upstream of Ndc80 AUG, thus replacing the LUTI promoter)*
UB13656	*MAT**a** /MATα GAL-NDT80::TRP1/GAL-NDT80::TRP1 ura3::pGPD1-GAL4(848).ER::URA3/ura3::pGPD1-GAL4(848).ER::URA3 Ndc80-3V5:KanMX/Ndc80-3V5:KanMX KanMX6:pSCC1-3HA-CDC6/KanMX6:pSCC1-3HA-CDC6*
UB13658	*MAT**a** /MATα GAL-NDT80::TRP1/GAL-NDT80::TRP1 ura3::pGPD1-GAL4(848).ER::URA3/ura3::pGPD1-GAL4(848).ER::URA3 leu2::NDC80(7A)-3V5:LEU2/leu2::NDC80(7A)-3V5:LEU2 ndc80Δ(-1000 and ORF):KanMX4/ndc80Δ(-1000 and ORF):KanMX4 (7A = T21A, S37A, T54A, T71A, T74A,S95A, S100A)*
UB14883	*MAT**a** /MATα KanMX:8LexO-luti-NDC80-3V5:CNAT/KanMX:8LexO-luti-NDC80-3V5:CNAT trp1::pGPD1-LexA-ER-HA-B112::TRP1/trp1::pGPD1-LexA-ER-HA-B112::TRP1 ndt80::LEU2/ndt80::LEU2 (8X-LexO-pCyc1 integrated 536 bp upstream of Ndc80 AUG, thus replacing the LUTI promoter)*
UB15064	*MAT**a** /MATα GAL-NDT80::TRP1/GAL-NDT80::TRP1 ura3::pGPD1-GAL4(848).ER::URA3/ura3::pGPD1-GAL4(848).ER::URA3 leu2::NDC80-3V5:LEU2/leu2::NDC80-3V5:LEU2 ndc80Δ(-1000 and ORF):KanMX4/ndc80Δ(-1000 and ORF):KanMX4 KanMX6:pSCC1-3HA-IPL1/KanMX6:pSCC1-3HA-IPL1*
UB15619	*MAT**a** /MATα GAL-NDT80::TRP1/GAL-NDT80::TRP1 ura3::pGPD1-GAL4(848).ER::URA3/ura3::pGPD1-GAL4(848).ER::URA3 MTW1-mCherry::HphMX4/MTW1-mCherry::HphMX4 Ndc80(Δaa2-28)-eGFP:KanMX/Ndc80(Δaa2-28)-eGFP:KanMX*
UB15687	*MAT**a** /MATα leu2::NDC80(Δaa2-28)-3V5:LEU2/leu2::NDC80(Δaa2-28)-3V5:LEU2 ndc80Δ(-1000 and ORF):KanMX4/ndc80Δ(-1000 and ORF):KanMX4 mad3Δ:CNAT/mad3Δ:CNAT*
UB15689	*MAT**a** /MATα mad3Δ:CNAT/mad3Δ:CNAT*

Table 5.1: continued

UB15701	*MAT**a** /MATα GAL-NDT80::TRP1/GAL-NDT80::TRP1 ura3::pGPD1-GAL4(848).ER::URA3/ura3::pGPD1-GAL4(848).ER::URA3 MTW1-mCherry::HphMX4/MTW1-mCherry::HphMX4 Ndc80(7A)-eGFP:KanMX/Ndc80(7A)-eGFP:KanMX (7A = T21A, S37A, T54A, T71A, T74A,S95A, S100A)*
UB15972	*MAT**a** /MATα GAL-NDT80::TRP1/GAL-NDT80::TRP1 ura3::pGPD1-GAL4(848).ER::URA3/ura3::pGPD1-GAL4(848).ER::URA3 leu2::(Δaa29-56)NDC80-3V5:LEU2/leu2::(Δaa29-56)NDC80-3V5:LEU2 ndc80Δ(-1000 and ORF):KanMX4/ndc80Δ(-1000 and ORF):KanMX4*
UB16284	*MAT**a** ADE2 leu2-3 ura3 trp1-1 his3-11,15? can1-100 GAL phi+? bar1-1? NDC80-3V5:HisMX SPC24-6HIS-3FLAG:URA3 (Strain background is W303)*
UB16561	*MAT**a** /MATα GAL-NDT80::TRP1/GAL-NDT80::TRP1 ura3::pGPD1-GAL4(848).ER::URA3/ura3::pGPD1-GAL4(848).ER::URA3 Ndc80(Δaa11-19)-3V5:CNAT/Ndc80(Δaa11-19)-3V5:CNAT leu2::pURA3-TetR-GFP::LEU2 CENV::TetOx224::HIS3 pCup1-CLB3::KANMX*
UB16565	*MAT**a** /MATα GAL-NDT80::TRP1/GAL-NDT80::TRP1 ura3::pGPD1-GAL4(848).ER::URA3 Ndc80(Δaa2-28)-3V5:CNAT/Ndc80(Δaa2-28)-3V5:CNAT leu2::pURA3-TetR-GFP::LEU2/leu2::pURA3-TetR-GFP::LEU2 CENV::TetOx224::HIS3 pCup1-CLB3::KANMX*
UB17707	*MAT**a** /MATα GAL-NDT80::TRP1/GAL-NDT80::TRP1 ura3::pGPD1-GAL4(848).ER::URA3/ura3::pGPD1-GAL4(848).ER::URA3 leu2::NDC80(14A)-3V5:LEU2/leu2::NDC80(14A)-3V5:LEU2 ndc80Δ(-1000 and ORF):KanMX4/ndc80Δ(-1000 and ORF):KanMX4 (7A = T21A, T28A, S29A, S37A, S38A, T54A, T71A, T74A, T79A, S95A, S100A, S242A, T248A, S255A)*

Table 5.1: continued

UB19616	*MAT**a** /MATα HIS3/HIS3 trp1::pGPD1-LexA-ER-HA-B112::TRP1/trp1::pGPD1-LexA-ER-HA-B112::TRP1 leu2::KanMX:8LexO-luti-mse-NDC80-3V5:LEU2/leu2::KanMX:8LexO-luti-mse-NDC80-3V5:LEU2 ndc80Δ(-1000 and ORF):KanMX4/ ndc80Δ(-1000 and ORF):KanMX4 ndt80::LEU2/ndt80::LEU2 (8X-LexO-pCyc1 integrated 536 bp upstream of Ndc80 AUG, thus replacing the LUTI promoter)*
UB19618	*MAT**a** /MATα HIS3/HIS3 trp1::pGPD1-LexA-ER-HA-B112::TRP1/trp1::pGPD1-LexA-ER-HA-B112::TRP1 leu2::KanMX:8LexO-luti-mse-NDC80-3V5:LEU2/leu2::KanMX:8LexO-luti-mse-NDC80-3V5:LEU2 ndc80Δ(-1000 and ORF):KanMX4/ ndc80Δ(-1000 and ORF):KanMX4 ndt80::LEU2/ndt80::LEU2 cdc20::pCLB2-3HA-CDC20::KanMX6/cdc20::pCLB2-3HA-CDC20::KanMX6 (8X-LexO-pCyc1 integrated 536 bp upstream of Ndc80 AUG, thus replacing the LUTI promoter)*
UB19678	*MAT**a** /MATα HIS3/HIS3 trp1::pGPD1-LexA-ER-HA-B112::TRP1/trp1::pGPD1-LexA-ER-HA-B112::TRP1 leu2::KanMX:8LexO-luti-mse-NDC80-3V5:LEU2/leu2::KanMX:8LexO-luti-mse-NDC80-3V5:LEU2 ndc80Δ(-1000 and ORF):KanMX4/ ndc80Δ(-1000 and ORF):KanMX4 cdc20::pCLB2-3HA-CDC20::KanMX6/cdc20::pCLB2-3HA-CDC20::KanMX6 (8X-LexO-pCyc1 integrated 536 bp upstream of Ndc80 AUG, thus replacing the LUTI promoter)*
UB19957	*MAT**a** ADE2 leu2-3 ura3 trp1-1 his3-11,15? can1-100 GAL phi+? bar1-1? NDC80(Δaa2-28)-3V5:HisMX SPC24-6HIS-3FLAG:URA3 (Strain background is W303)*
UB21251	*MAT**a** /MATα GAL-NDT80::TRP1/GAL-NDT80::TRP1 ura3::pGPD1-GAL4(848).ER::URA3/ura3::pGPD1-GAL4(848).ER::URA3 leu2::HIS3MX:pNDC80(600-400)-NDC80(Δaa29-56)-3V5:LEU2/leu2::HIS3MX:pNDC80(600-400)-NDC80(Δaa29-56)-3V5:LEU2 ndc80Δ(-1000 and ORF):KanMX4/ndc80Δ(-1000 and ORF):KanMX4 (Δaa29-56) with LUTI promoter deleted*

Table 5.1: continued

UB21253	*MAT**a** /MATα GAL-NDT80::TRP1/GAL-NDT80::TRP1 ura3::pGPD1-GAL4(848).ER::URA3/ura3::pGPD1-GAL4(848).ER::URA3 leu2::HIS3MX:pNDC80(600-400)-NDC80(Δaa2-10)-3V5:LEU2/leu2::HIS3MX:pNDC80(600-400)-NDC80(Δaa2-10)-3V5:LEU2 ndc80Δ(-1000 and ORF):KanMX4/ndc80Δ(-1000 and ORF):KanMX4 (Δaa2-10) with LUTI promoter deleted*
UB21255	*MAT**a** /MATα GAL-NDT80::TRP1/GAL-NDT80::TRP1 ura3::pGPD1-GAL4(848).ER::URA3/ura3::pGPD1-GAL4(848).ER::URA3 leu2::HIS3MX:pNDC80(600-400)-NDC80(H10A, H13A, H14A, H18A)-3V5:LEU2/leu2::HIS3MX:pNDC80(600-400)-NDC80(H10A, H13A, H14A, H18A)-3V5:LEU2 ndc80Δ(-1000 and ORF):KanMX4/ndc80Δ(-1000 and ORF):KanMX4 (4H to A) with LUTI promoter deleted*
UB21259	*MAT**a** /MATα GAL-NDT80::TRP1/GAL-NDT80::TRP1 ura3::pGPD1-GAL4(848).ER::URA3/ura3::pGPD1-GAL4(848).ER::URA3 leu2::HIS3MX:pNDC80(600-400)-NDC80(Δaa20-28)-3V5:LEU2/leu2::HIS3MX:pNDC80(600-400)-NDC80(Δaa20-28)-3V5:LEU2 ndc80Δ(-1000 and ORF):KanMX4/ndc80Δ(-1000 and ORF):KanMX4 (Δaa20-28) with LUTI promoter deleted*
UB21361	*MAT**a** /MATα GAL-NDT80::TRP1/GAL-NDT80::TRP1 ura3::pGPD1-GAL4(848).ER::URA3/ura3::pGPD1-GAL4(848).ER::URA3 leu2::HIS3MX:pNDC80(600-400)-NDC80(Δaa57-112)-3V5:LEU2/leu2::HIS3MX:pNDC80(600-400)-NDC80(Δaa57-112)-3V5:LEU2 ndc80Δ(-1000 and ORF):KanMX4/ndc80Δ(-1000 and ORF):KanMX4 (Δaa57-112) with LUTI promoter deleted*
UB21363	*MAT**a** /MATα GAL-NDT80::TRP1/GAL-NDT80::TRP1 ura3::pGPD1-GAL4(848).ER::URA3/ura3::pGPD1-GAL4(848).ER::URA3 leu2::HIS3MX:pNDC80(600-400)-NDC80(11A)-3V5:LEU2/leu2::HIS3MX:pNDC80(600-400)-NDC80(11A)-3V5:LEU2 ndc80Δ(-1000 and ORF):KanMX4/ndc80Δ(-1000 and ORF):KanMX4 (11A) with LUTI promoter deleted*
UB21756	*MAT**a** /MATα leu2::pURA3-TetR-GFP::LEU2/leu2::pURA3-TetR-GFP::LEU2 CENV::TetOx224::HIS3/CENV::TetOx224::HIS3 Ndc80-3V5:CNAT/Ndc80-3V5:CNAT*

Table 5.1: continued

UB21757	*MAT**a** /MATα* *leu2::pURA3-TetR-GFP::LEU2/leu2::pURA3-TetR-GFP::LEU2* *CENV::TetOx224::HIS3/CENV::TetOx224::HIS3* *Ndc80-3V5:CNAT/Ndc80-3V5:CNAT*
UB21758	*MAT**a** /MAT$α* *leu2::pURA3-TetR-GFP::LEU2/leu2::pURA3-TetR-GFP::LEU2* *CENV::TetOx224::HIS3/CENV::TetOx224::HIS3* *Ndc80(Δaa2-28)-3V5:CNAT/Ndc80(Δaa2-28)-3V5:CNAT*

5.1.2 *pCUP-IME1 pCUP-IME4* synchronization system

Synchronously sporulating cultures were prepared as in Benjamin *et al.* 2003; Berchowitz *et al.* 2013. In short, the endogenous promoters of *IME1* and *IME4* were replaced with the inducible *CUP1* promoter. Diploid cells were grown in YPD (1% yeast extract, 2% peptone, 2% glucose, and supplemented with 22.4 mg/l uracil and 80 mg/l tryptophan) for 20-24 hr at room temperature or at 30 °C. For optimal aeration, the total volume of the flask exceeded the volume of the medium by 10 fold. Subsequently, cells were transferred to BYTA (1% yeast extract, 2% bacto tryptone, 1% potassium acetate, 50 mM potassium phthalate) and grown for another 16-18 hr at 30 °C. The cells were then pelleted, washed with sterile milliQ water, and resuspended at an OD_{600} of 1.85 in sporulation (SPO) media (0.5% (w/v) potassium acetate [pH 7], 0.02% (w/v) raffinose) at 30 °C. To initiate synchronous sporulation, expression of *IME1* and *IME4* was induced 2 hr after cells were transferred to SPO by adding copper (II) sulphate to a final concentration of 50 μM.

5.1.3 *pGAL-NDT80 GAL4-ER* synchronization system

The *pGAL-NDT80 GAL4-ER* system was used to generate populations of cells synchronously undergoing the meiotic divisions (Carlile & Amon 2008). Cells were prepared for meiosis as in the *pCUP-IME1 pCUP-IME4* protocol, and resuspended at an OD_{600} of 1.85 in SPO. The flasks were placed at 30 °C for 5–8 hr to block cells in meiotic prophase (See figure legend for the specific arrest duration for each experiment). To release cells from pachytene, *NDT80* expression was induced with 1 μM β-estradiol. Subsequently, cells progressed through meiosis synchronously.

For figure 3.20, the cells were sporulated in 2% SPO (2% (w/v) potassium acetate [pH 7], 0.02% (w/v) raffinose, supplemented with 40 mg/l uracil, 20 mg/l histidine, 20 mg/l leucine, 20 mg/l tryptophan). Increasing the concentration of acetate and supplementing amino acids improved sporulation efficiency.

5.1.4 Alpha-factor arrest-release mitotic time course

*MAT***a** cells were first grown to an OD_{600} of 1–2 at 30 °C in YPD, diluted back to an OD_{600} of 0.005 in YEP-RG (2% raffinose (w/v) and 2% galactose (w/v) in YEP supplemented with 22.4 mg/l uracil and 80 mg/l tryptophan), and then grown at room temperature for 15–17 hr. Exponentially growing cells were diluted again to an $OD_{600}$of 0.19 in YEP-RG, and arrested in G_1 with 4.15 μg/ml alpha-factor. 1.5 hr later, an additional 2.05 μg/ml of alpha-factor was added to the cells. After 2 hr in alpha-factor, 1 μM β-estradiol was added to cultures to induce pGAL expression. One hour after the β-estradiol addition, cells were filtered, rinsed with YEP (10 times volume of the culture volume) to remove the alpha-factor, and placed into a receiving flask containing YEP-RG with 1 μM β-estradiol. Time points were taken before β-estradiol induction, before release, and every 15 min after release, for 3 hr.

5.1.5 Spot growth assay

Cells were grown on YPG (2% glycerol + YEP) plates overnight, resuspended in milliQ H_2O, and then diluted to an OD_{600} of 0.1 or 0.2. 5-fold serial dilutions were performed. For figure 2.23, cells were spotted onto YEP-RG plates with or without supplement of 1 μM β-estradiol and incubated at 30 °C for 1-2 days. For figure 2.22 and 3.19, cells were spotted onto YPD plates and for figure 3.19, also onto the YPD plates supplemented with 15 μg/ml benomyl (benomyl plates). The cells on the YPD plates were incubated at 30 °C for 1-2 days, and those on benomyl plates were incubated at 23 °C for 2 days.

5.1.6 Conservation analysis

Clustal analysis (Goujon *et al.* 2010; Sievers *et al.* 2011) was performed using the genomic sequences of *S. bayanus*, *S. kudriavzevii*, *S. mikatae*, *S. cerevisiae* and *S. paradoxus* from Saccharomyces *sensu stricto* genus (Scannell *et al.* 2011), and imported into the Webpage of the Clustal Omega Multiple Sequence Alignment tool < http://www.ebi.ac.uk/Tools/msa/clustalo/>.

5.2 Light microscopy

5.2.1 Fluorescence microscopy

Cells were fixed with 3.7% formaldehyde at room temperature for 15 min, washed once with potassium phosphate/sorbitol buffer (100 mM potassium phosphate [pH 7.5], 1.2 M sorbitol), and then permeabilized with 1% Triton X-100 with 0.05 μg/ml DAPI in potassium phosphate/sorbitol buffer. For the Ndc80 localization experiments in Chapter 3, cells were resuspended in the VectaShield Antifade Mounting Medium with DAPI (Vector Labs,

Burlingame, CA, USA) instead of Triton. This method preserved the samples from photobleaching during imaging better. Cells were imaged using a DeltaVision microscope with a 100x/1.40 oil-immersion objective (DeltaVision, GE Healthcare, Sunnyvale, CA) and filters: DAPI (EX390/18, EM435/48), GFP/FITC (EX475/28, EM525/48), and mCherry (EX575/25, EM625/45). Images were acquired and deconvolved with a 3D iterative constrained deconvolution algorithm (enhanced ratio) for 15 iterations using the softWoRx software (softWoRx, GE Healthcare).

5.2.2 Indirect immunofluorescence

Tubulin indirect immunofluorescence was performed as described (Kilmartin & Adams 1984; Sawyer *et al.* 2019) using a rat anti-tubulin antibody (MCA78G, Bio-rad Antibodies, Kidlington, UK) at a dilution of 1:200 and a pre-absorbed anti-rat FITC antibody (712-095-153, Jackson ImmunoResearch Laboratories, Inc. West Grove, PA) at a dilution of 1:200. The meiotic stage of a cell was determined based on its spindle and DAPI morphologies. Metaphase I spindles were defined as a short bipolar spindle spanning a single DAPI mass; an anaphase I spindle was defined as a single elongated spindle spanning two DAPI masses; a pair of metaphase II spindles were defined as two short bipolar spindles each spanning a distinct DAPI mass within a single cell; and finally, a pair of anaphase II spindles was defined as two elongated spindles with 4 DAPI masses within a single cell. Spindle images were acquired as z-stacks (8–10 slices) with a step size of 0.5 μm using the DeltaVision microscope (GE Healthcare) described above. The spindle length was measured as follows. First, the images were projected using the maximum-intensity setting in FIJI (Schindelin *et al.* 2012). Next, the projected spindle length (defined as the spindle pole-to-pole distance) was measured using the "measure" plugin (Schindelin *et al.* 2012). The cells were staged to be in either meiosis I or meiosis II depending on the number of bipolar spindles. For cells undergoing meiosis II, both spindles were quantified, but only the longer of the two was reported. For each time point, the percentage of cells in each category was quantified: 1) meiosis I spindles that were less than 2 μm, 2) meiosis I spindles that were over 2 μm, 3) meiosis II spindles that were less than 2 μm, and 4) meiosis II spindles that were over 2 μm. Over 100 cells per time point were quantified.

5.3 RNA and Chromatin immunoprecipitation methods

5.3.1 Northern blotting

A previously described northern blot protocol was modified as below (Koster *et al.* 2014). RNA was extracted with acid phenol:chloroform:isoamyl alcohol (125:24:1; pH 4.7) and then isopropanol precipitated. Briefly, 1.85-3.7 OD_{600} of cells were harvested by centrifuging at 21 kcrf for 1 min, and frozen in liquid nitrogen. Pellets were thawed on ice, and vigorously shaked at 65 °C in 400 μl TES buffer (10 mM Tris [pH 7.5], 10 mM EDTA, 0.5% SDS), 200

μl of acid-washed glass beads (Sigma), and 400 μl acid phenol:chloroform:isoamyl alcohol (125:24:1; pH 4.7) for 30 min. The lysates were clarified by centrifuging at 21 krcf, 4 °C, for 10 min. The aqueous phase was transferred to 300 μl chloroform, vortexed, and centrifuged at 21 krcf, room temperature, for 5 min. To precipitate the RNA, the aqueous phase was added to 400 μl isopropanol supplemented with 0.33 M NaOAc, incubated at -20 °C for over two hours, and centrifuged at 21 krcf, 4 °C, for 20 min. The precipitated RNA pellets were washed with 80% ethanol, air dried, and resuspended in nuclease-free water. RNA samples (8–10 μg) were denatured in a glyoxal/DMSO mix (1 M deionized glyoxal, 50% v/v DMSO, 10 mM sodium phosphate buffer pH 6.5–6.8) at 70 °C for 10 min and then separated on a 1.1% agarose gel at 80 V for 3 hrs. RNAs were transferred onto nylon membranes by capillary transfer overnight. The membranes were blocked at 42 °C in ULTRAhyb Ultrasensitive Hybridization Buffer (Thermo Fisher, Waltham, MA) for at least 3 hrs before hybridization. Radioactive probes were synthesized using a Prime-It II Random Primer Labelling Kit (Agilent, Santa Clara, CA).

Quantification was performed with FIJI (Schindelin *et al.* 2012). For all the images, the LUT (lookup table) was inverted. Then, a rectangular box was drawn around a band of interest. The mean signal intensity (gray-scale) within the box area was calculated using the "measure" plugin. For background subtraction, the same box was moved directly above and below the band, the signal intensity of these two regions was measured, and the average background intensity (top and bottom) was calculated. After subtracting the average background intensity of a given lane from the signal intensity of the band in that lane, this corrected value for each time point was then normalized to the initial time point. The same-sized box was used for all the time points in one experiment.

5.3.2 Chromatin immunoprecipitation (IP)

The Ume6-3V5 chromatin IP experiments were performed as described previously with the following modifications (van Werven *et al.* 2012). Cells were fixed with formaldehyde (1% v/v) for 15 min. Frozen cell pellets were disrupted 4 times (5 min each) using a Beadbeater (Mini-Beadbeater-96, Biospec Products, Bartlesville, OK). Chromatin was sheared 5 rounds of 30 s ON/30 s OFF with a Bioruptor Pico (Diagenode, Denville, NJ) to a fragment size of 200 bp. Chromatin extracts were incubated with 20 μl of anti-V5 agarose beads (A7345, Sigma, St. Louis, MO) at 4 °C. The Ndt80-3V5 chromatin IP experiments were performed as described previously with the same modifications as used for Ume6-3V5 except for the sonication conditions (Strahl-Bolsinger *et al.* 1997). Chromatin was sheared 5 rounds of 10 s ON/30 s OFF with a Bioruptor Pico (Diagenode) to a fragment size of 500 bp. Reverse crosslinked input DNA and immunoprecipitated DNA fragments were amplified with Absolute SYBR green (AB4163/A, Thermo Fisher) and quantified with a 7500 Fast Real-Time PCR machine (Thermo Fisher) using the primer pairs directed against the upstream region and the coding region of *NDC80*, the *MAM1* promoter, and the *IME2* promoter. We also measured the signals from the *NUF2* promoter and *HMR*; both regions do not display sig-

nificant binding for either of the transcription factors. The oligonucleotide sequences used are listed in the next subsection.

5.3.3 RT-qPCR

RNA was isolated by acid phenol-chloroform extraction as described in the northern blotting section and reverse-transcribed into cDNA as follows. A total of 5 μg RNA was treated with DNase in a 50 μl reaction (TURBO DNA-free kit, Thermo Fisher). 2.5 μl of the DNase-treated RNA was incubated with 0.5 μl of 2 mg/ml random hexamers (primer "random", Sigma) in a 10 μl reaction at 65 °C for 5 min, and then cooled to 4 °C for 5 min. Per reaction, 4 μl of the 5X first strand buffer (Superscript II or III, Thermo Fisher), 2 μl 0.1 M DTT, and 1 μl 10 mM dNTPs (NEB) were then added, and the reaction was incubated at room temperature for 2 min. Next, 0.5 μl Superscript II or Superscript III enzyme was added (Superscript II or III, Thermo Fisher). The reaction was incubated at 25 °C for 10 min, then 42 °C for 50 min, and lastly 70 °C for 10 min. The single-stranded cDNA was quantified by real-time PCR using SYBR green mix (Thermo Fisher) as described above. The primers used for the RT-qPCR reactions are listed below.

Table 5.2: Primers used for northern blotting and RT-qPCR

Primer Name	**Oligonucleotides (5' to 3')**
NDC80_probe_F	GGAGAGGTAGAATCGTCCCTG
NDC80_probe_R	CTCCTCTTGAATAGCGCTTTGG
NUF2_probe_F	AACAGGGGATGGTCACTTACAGG
NUF2_probe_R	CCCACAAGTTCCGTTTCAGTTCG
SCR1_probe_F	GAAGTGTCCCGGCTATAATAAA
SCR1_probe_R	GACGCTGGATAAAACTCCCC
CIT1_probe_F	CCGTGTTAGACCCCGAAGAAG
CIT1_probe_R	GGGCAGAAACGTTACCACCTTC
NDC80_2_F	ACCCGGATATCTGTTCAGCC
NDC80_2_R	TGTGGCGAATTGTTGCTCTT
NDC80_6_F/*NDC80*^{LUTI}_F	GGTTGAGAGCCCCGTTAAGT
NDC80_6_R/*NDC80*^{LUTI}_R	TTGGCACTTTCAGTATGGGT
NDC80_7_F	CCCATACTGAAAGTGCCAAAAGA
NDC80_7_R	GGGACGATTCTACCTCTCCTGTG
pNUF2_F	GTCGCTGCGTATTCAGCGTA
pNUF2_R	GAACGCTGATATACTCGACTAAC
ACT1_F	GTACCACCATGTTCCCAGGTATT
ACT1_R	AGATGGACCACTTTCGTCGT
NDC80_9_F	TGCAAAGCTCAACAAGTACTGA
NDC80_9_R	TGCAGTTGGTATTTGGGACG
NDC80_ORF_F	ATCCGAGTGTGAACTGAAAGAAG

Table for primers: continued

NDC80_ORF_R	GAACTGCTCAGTTGAAATTCCC
IME2_URS1_F	CCAAATACGCTTTTTAAACTTGG
IME2_URS1_R	CTCAAATAGCCGCCGTAAC
MAM1_MSE_F	CACAATTGAAATCCGAGCTGT
MAM1_MSE_R	CATCTGAATTTTGAATGGCTTT
PFY1_F	ACGGTAGACATGATGCTGAGG
PFY1_R	ACGGTTGGTGGATAATGAGC

5.3.4 Single-molecule RNA FISH

Single-molecule RNA FISH was performed as described (Raj *et al.* 2008) with modifications. All the probes (Supplementary file 1E for probe sequences) were designed, synthesized, and labelled by Stellaris (Biosearch Technologies, Novato, CA). The unique region of $NDC80^{LUTI}$ was targeted by twenty 20-mer oligonucleotide probes coupled to CAL Fluor Red 590 (NDC80Long). Thirty 20-mer probes, coupled to Quasar 670 dye, were targeted to the coding region of *NDC80*(NDC80ORF). To measure our detection quality, 54 alternating probes (odd and even probes, 27 probes in each set) were designed to target the common region of $NDC80^{LUTI}$ and $NDC80^{ORF}$, and coupled with Quasar 670 dye (NDC80Even) and CAL Fluor Red 590 dye (NDC80Odd), respectively. The probe sequences are listed below.

Table 5.3: smFISH probes

Probe Name	**Oligonucleotides (5' to 3')**
NDC80ORF_1	tccatgtgatgtagcacatg
NDC80ORF_2	cagttggtatttgggacgta
NDC80ORF_3	ctgtttcttctcctcaattg
NDC80ORF_4	atgtcggttagaccttgatt
NDC80ORF_5	ttgtattcctggcaatactc
NDC80ORF_6	ttttatttatgcctcctgtg
NDC80ORF_7	aatgctgtaccatttgtacc
NDC80ORF_8	tgacgctgtttctactgttg
NDC80ORF_9	gctgccaagttgatttattg
NDC80ORF_10	agtttttgtctcttagtggc
NDC80ORF_11	aatctcctcttgaatagcgc
NDC80ORF_12	tagtaaagccgtaacctgga
NDC80ORF_13	acctacagccgaaatttgtg
NDC80ORF_14	atgccaagaaatttgtgcca
NDC80ORF_15	gctggctcagaattgttatt
NDC80ORF_16	ctgttcgtccaaagtcttta
NDC80ORF_17	ttcagttcttgcatcgaagg

Table smFISH probes: continued

NDC80ORF_18	tggttttgatcttttggctt
NDC80ORF_19	ctcagttgaaattccctttt
NDC80ORF_20	tttatcaagttccctagtca
NDC80ORF_21	ttccagctttctggatttaa
NDC80ORF_22	cgaatcgtattgcctcaacg
NDC80ORF_23	gactcgttaattccagatcc
NDC80ORF_24	gttgtctttctcaatggttt
NDC80ORF_25	ttcgttctcttgcttagaga
NDC80ORF_26	ctcaattctttgcgctacta
NDC80ORF_27	gaagttaccaattcctcagc
NDC80ORF_28	ttcttccaattttagttccg
NDC80ORF_29	cttgtatcgtttcctgttta
NDC80ORF_30	catgtatcacttgttggtgt
NDC80Long_1	ttttgctttcttactgatgt
NDC80Long_2	tcttgtggcgaattgttgct
NDC80Long_3	cctattgaccctacagagac
NDC80Long_4	tttccctgacaagagccctg
NDC80Long_5	tctttcctttgcattcacag
NDC80Long_6	aatgcttttcggacctccaa
NDC80Long_7	tctcttcaatcctaacatca
NDC80Long_8	ctggcacatagtacggtgaa
NDC80Long_9	ttcaatgttcagttataacc
NDC80Long_10	cagcccataatcacgatatt
NDC80Long_11	aatacttaacggggctctca
NDC80Long_12	atagactgcttacatcttta
NDC80Long_13	ggtattttaaccgctaatcg
NDC80Long_14	cagtatgggtaacccttgaa
NDC80Long_15	tctttttttctttggcact
NDC80Long_16	gactatatcattccatacgt
NDC80Long_17	ttttaggaaatattagtttt
NDC80Long_18	ccatttttggtgttgtttgt
NDC80Long_19	gtgaatgtattccaattatt
NDC80Long_20	cagggacgattctacctctc
NDC80Odd_1	atttttcttgttccgtttca
NDC80Odd_2	acgggtatctcttatggaat
NDC80Odd_3	tgtgatgtagcacatgttga
NDC80Odd_4	acgatgttgcagttggtatt
NDC80Odd_5	atgtcggttagaccttgatt
NDC80Odd_6	ttttatttatgcctcctgtg
NDC80Odd_7	tgacgctgtttctactgttg

Table smFISH probes: continued

NDC80Odd_8	ctattgctcagatgttgctg
NDC80Odd_9	aatctcctcttgaatagcgc
NDC80Odd_10	tagtaaagccgtaacctgga
NDC80Odd_11	atgccaagaaatttgtgcca
NDC80Odd_12	ttcaagcacatatccagttt
NDC80Odd_13	ctgttcgtccaaagtcttta
NDC80Odd_14	attaacagtttctccaccat
NDC80Odd_15	gattgtcattttgggtttgt
NDC80Odd_16	cttttcaaagccttccattt
NDC80Odd_17	ggatttcatctttccagtt
NDC80Odd_18	ctcagttgaaattccctttt
NDC80Odd_19	tttatcaagttccctagtca
NDC80Odd_20	agcttttgaatattccctcg
NDC80Odd_21	ccacgcgatctggttaaatt
NDC80Odd_22	gactcgttaattccagatcc
NDC80Odd_23	attcgcttcggataattcca
NDC80Odd_24	ctcaattctttgcgctacta
NDC80Odd_25	ttcttccaattttagttccg
NDC80Odd_26	catgtatcacttgttggtgt
NDC80Odd_27	actcttcaatgacgtttcct
NDC80Even_1	atagtacaccctaacgttta
NDC80Even_2	acttgttgagctttgcattt
NDC80Even_3	gacgtaaaccgatgagggtc
NDC80Even_4	ctgtttcttctcctcaattg
NDC80Even_5	ttgtattcctggcaatactc
NDC80Even_6	aatgctgtaccatttgtacc
NDC80Even_7	gctgccaagttgatttattg
NDC80Even_8	agtttttgtctcttagtggc
NDC80Even_9	aataaaccccttttgagtgg
NDC80Even_10	acctacagccgaaatttgtg
NDC80Even_11	tttgttcgtaccatccaatg
NDC80Even_12	gctggctcagaattgttatt
NDC80Even_13	gctcatatctttcttgtctt
NDC80Even_14	ttcagttcttgcatcgaagg
NDC80Even_15	tggttttgatcttttggctt
NDC80Even_16	ttcttgactcttttgcttca
NDC80Even_17	tcttcttctttcagttcaca
NDC80Even_18	tttctctttcttggttttgt
NDC80Even_19	ttccagctttctggatttaa
NDC80Even_20	cgaatcgtattgcctcaacg

Table smFISH probes: continued

NDC80Even_21	ctcgtaggagatagcttcat
NDC80Even_22	gttgtctttctcaatggttt
NDC80Even_23	ttcgttctcttgcttagaga
NDC80Even_24	gaagttaccaattcctcagc
NDC80Even_25	cttgtatcgtttcctgttta
NDC80Even_26	ttcgttttcagagttttcca
NDC80Even_27	atgttcagtttcaaactcca

For meiosis experiments, cells were sporulated as described above. To fix cells, 160 μl of 37% formaldehyde was added into 1840 μl of meiotic cultures and incubated at room temperature for 20 min with gentle agitation. The fixed samples were moved to 4 °C to continue fixing overnight. For vegetative samples, cells were grown in YPD to an OD_{600} of 0.4–0.6, fixed in formaldehyde at room temperature for 20 min, and then prepared for digestion as below.

Cells were washed three times in 1.5 ml cold Buffer B (0.1 M potassium phosphate [pH 7.5], 1.2 M sorbitol) and resuspended in 425 μl digestion buffer (425 μl Buffer B mixed with 40 μl 200 mM Vanadyl ribonucleoside complex (VRC) (NEB) with 50 μg of zymolyse (zymolase 100T, MP Biomedicals, Santa Ana, CA). Cells were digested at 30 °C until approximately 70% of cells were digested. This took about 15–20 min for early meiotic and vegetative samples and 30–35 min for pachytene and post meiotic prophase samples. Digested cells were gently washed with 1 ml of cold Buffer B and resuspended in 1 ml of 70% EtOH for 3.5–5 hr to allow permeabilization. To prepare for hybridization, cells were first incubated in 1 ml of 10% formamide wash buffer (10% formamide, 2X SSC) at room temperature for at least 15 min. For hybridization, each probe set (to a final concentration of 500 nM) and 20 mM VRC were added to hybridization buffer (1% Dextran sulfate (EMD Millipore, Billerica, MA), 1 mg/ml E. coli tRNA (Sigma), 2 mM VRC, 0.2 mg/ml BSA, 1X SSC, 10% formamide (Thermo Fisher) in nuclease-free water). Hybridization was performed overnight at 30 °C with gentle agitation. Samples were then incubated in the dark at 30 °C in 1 ml of 10% formamide wash buffer for 30 min. The buffer was then washed away, and the cells were stained with DAPI and resuspended in 50 μl of glucose-oxygen-scavenging buffer (GLOX buffer (10 mM Tris [pH 8.0], 2x SSC, 0.4% glucose)) solution without enzymes. Prior to imaging, 15 μl of GLOX solution with enzyme (1% v/v catalase, 1% v/v glucose oxidase (Sigma), 2 mM Trolox (Sigma)) was added to the sample. Images were acquired with the DeltaVision microscope (GE Healthcare) as described in the fluorescence microscopy section with two additional filters: TRITC (EX542/27, EM597/45) for CAL Fluor Red 590 and CY5 (EX632/22, EM679/34) for Quasar 670. Series of z-stacks (15–25 slices) were acquired with a step size of 0.2 μm.

To quantify FISH spots, the maximum-intensity projection of the z-stacks was first generated in FIJI (Schindelin *et al.* 2012). Next, the different channels were split, and these processed images were analysed with a custom software written in Matlab (Mathworks, Sun-

nyvale, CA). Cell boundaries were hand-drawn. The spot detection code first filtered the raw images using an eight pixel Gaussian kernel to remove background signal. Diffraction-limited spots corresponding to single mRNA were detected using an adaptation of the MTT spot-detection algorithm (Serge *et al.* 2008), using the following detection parameters: NA: 1.4; detection box: 5 pixels; error rate: 0.1; deflation loops: 0. With these detection settings, many low-intensity fluctuations in background fluorescence were detected as spots. To identify bona fide mRNA molecules, we plotted the signal (defined as the integrated value of the pixel intensities) against the signal-to-noise ratio (SNR; defined as the signal divided by the variance of the pixel values around the detected spot), identified a population of detections that were well separated from the background detections, and chose these signal and SNR values as thresholds. To confirm these threshold choices, we plotted the number of spots detected as a function of the threshold chosen, and found that these thresholds fell within a 'plateau', as others have described (Senecal *et al.* 2014; Raj *et al.* 2006), where an increase in the choice of threshold has little effect on the total number of mRNA detected. Inspection of detected mRNAs, post-threshold, was in good agreement with spots that were manually counted. Once chosen, the same "signal" and "SNR" thresholds were applied to all the images within a replicate. In general, we found that thresholds between replicates varied only slightly (For CF 590 probes, signal = 1100–1500 and SNR = 2.5–3; for Q670 probes, signal = 1000–2000 and SNR = 2–3).

After detection, spots between the CF 590 and Q 670 probe sets need to be paired to identify $NDC80^{LUTI}$ and $NDC80^{ORF}$ transcripts. Pairing was done using the knnsearch Matlab function to separately identify the closest CF 590 spot for each detected Q 670 spot, and vice versa. Two spots are only considered paired if they are mutual nearest neighbors. Using this as a criterion for pairing, greater than 95% of spot pairs occurred within 2 pixels of each other, which is well within the expected value given any chromatic and detection artifacts between the two color channels. By comparison, fewer than 10% of unpaired spots had nearest neighbor distance of less than four pixels, showing that the probability of misidentifying a spot pair is low. The number of cells with a given number of $NDC80^{LUTI}$ or $NDC80^{ORF}$ transcripts per cell was graphed as relative frequency histograms. The largest bin of each histogram was normalized to the same length across all the histograms.

For Chapter 3, to quantify smFISH spots, the maximum-intensity projection of the z-stacks was generated in FIJI (Schindelin *et al.* 2012), different channels were split, and the images were analysed by the StarSearch Program (Raj *et al.* 2008). Cell boundaries were hand-drawn. The thresholds were adjusted such that they fell within "plateaus," as described above. The same threshold was used for a given probe set in each experimental replicate. A $NDC80^{LUTI}$ transcript was identified as a colocalized spot where the two spots identified in either channel have pixels overlapped for over 50%. The number of $NDC80^{ORF}$ transcripts in each cell was calculated by subtracting the number of $NDC80^{LUTI}$ from the number of spots with Q 670 signal. To compare between different strains, the non-parametric Wilcoxon Rank Sum test was applied to the data pooled from two experimental repeats using Prism (GraphPad).

5.3.5 Statistical analysis of smFISH data

Per-cell statistics of the paired spots (i.e., *NDC80*^{LUTI} mRNA), Q 670-only spots (i.e., *NDC80*^{ORF}), and CF 590-only spots (false positives, early terminated transcripts, and degradation products) were collected and pooled between biological replicates. First, to determine whether sufficient data had been collected for a given data set, bootstrap analysis of the data was performed. For 500 iterations, the statistics from a single cell was randomly sampled from the data, and the mean and variance were calculated. This process was repeated for two cells randomly selected from the data, without replacement; then for three cells randomly selected, etc. until one half of the total data set size was reached. The mean and standard deviation of the paired and unpaired spots were plotted in Figure 2.5, Panel B. This figure shows that the mean is stable and that the change in the variance plateaus at a number far below the number of cells assayed, suggesting that our sample size is sufficiently large. For each sample, over 95 cells were counted and three independent experiments were performed. Thus, for each data set, we could ensure that enough cells were measured to accurately account for the biological variation intrinsic to the data set. To compare across different strains and conditions, the two-tailed non-parametric Wilcoxon Rank Sum test was applied to the pooled data obtained from three independent experimental repeats. The p-value was determined using the ranksum function in Matlab (Mathworks).

5.3.6 Software

All the code used for the smFISH analysis has been made available in the following code repository: https://gitlab.com/tjian-darzacq-lab/Chen_Tresenrider_et_al_2017 (copy archived at https://github.com/elifesciences-publications/Chen_Tresenrider_et_al_2017).

5.4 Protein methods

5.4.1 Denaturing IP and mass spectrometry (MS)

Denatured protein extracts were prepared as described in Sawyer *et al.* 2019, with a few modifications. After cells were harvested and dried completely, 150 μl zirconia beads and 150 μl lysis buffer (50 mM Tris [pH 7.5], 1 mM EDTA, 2.75 mM DTT, 1x PhosSTOP (Roche), 0.48 μg/ml Pefabloc SC (Sigma), 2 mM pepstatin A, and 2x cOmplete EDTA Free (Roche)) were added to each tube. Cells were lysed mechanically on a Mini-Beadbeater-96 (BioSpec Products) at room temperature for 5 min. SDS was added to a final concentration of 1%, the extracts were boiled at 95 °C for 5 min, and NP-40 lysis buffer (50 mM Tris [pH 7.5], 150 mM NaCl, 1% NP-40, and 5% glycerol, 1x PhosSTOP, 0.64 μg/ml Pefabloc SC (Sigma), 2.67 mM pepstatin A and 3x cOmplete EDTA Free) was added to a final volume of 1.5 ml (i.e., diluting SDS to 0.1%). Lysates were clarified by centrifuging at 15 krcf, 4 °C, for 15 min. The cleared lysates were pooled from 3 tubes (3,825 μl total) and added to 80 μl pre-equilibrated anti-V5 agarose beads (Sigma), and incubated in loBind tubes (Eppendorf,

Hamburg, Germany) at 4 °C for 2 hrs with rotation. Using loBind tubes and low-adhesion tubes (USA Scientific, Orlando, Florida) in the next step improves the amount of protein recovered from the IP. In each MS experiment, the cleared lysates pooled from 6 tubes were used, so two IP reactions were set up in parallel. The beads of the parallel IP reactions were washed once with the 3 ml High Salt Wash buffer (50 mM Tris, pH 7.5, 0.5 M NaCl, 1 mM EDTA, and 1% NP-40), combined into one low-adhesion tube (i.e., 160 μl beads final), and then washed once with 950 μl of High Salt Wash buffer. Next, the beads were washed twice with each of the following: (1) 950 μl Buffer 2 (50 mM Tris [pH 7.5], 150 mM NaCl, 10 mM $MgCl_2$, 0.05% NP-40, and 5% glycerol); and (2) 950 μl Buffer 3 (50 mM Tris [pH 7.5], 150 mM NaCl, 10 mM $MgCl_2$, and 5% glycerol). After the last wash, the wash buffer was aspirated completely, and the beads were resuspended in 80 μl trypsin buffer (2 M Urea, 50 mM Tris [pH 7.5], 5 μg/ml trypsin) to digest the bound proteins at 37 °C for 1 hr with agitation. The beads were centrifuged at 100 rcf for 30 s, and the digested peptides (the supernatant) were collected. The beads were then washed twice with 60 μl Urea buffer (2 M Urea, 50 mM Tris [pH 7.5]). The supernatant of both washes was collected and combined with the digested peptides (i.e. the final volume is 200 μl). After brief centrifugation, the combined digested peptides were cleared from residual beads and frozen in liquid nitrogen.

MS was performed by the Vincent J. Coates Proteomics/Mass Spectrometry Laboratory at University of California, Berkeley, as described in Sawyer *et al.* 2019. The mudPIT methods were used. A nano LC column (packed in a 100-μm inner-diameter glass capillary with an emitter tip) is composed of 10 cm of Polaris c18 5 μm packing material (Varian), followed by 4 cm of Partisphere 5 SCX (Whatman). The column was loaded with a pressure bomb, washed extensively with buffer A, and then directly coupled to an electrospray ionization source mounted on a LTQ XL linear ion trap mass spectrometer (Thermo Fisher). Chromatography was performed on an Agilent 1200 HPLC equipped with a split line to deliver a flow rate of 300 nl/min. Peptides were eluted using either a four-step or an eight-step mudPIT procedure (Washburn *et al.* 2001). Buffer A: 5% acetonitrile and 0.02% heptafluorobutyric acid (HFBA). Buffer B: 80% acetonitrile and 0.02% HFBA. Buffer C: 250 mM ammonium acetate, 5% acetonitrile, and 0.02% HFBA. Buffer D: the same as buffer C, but with 500 mM ammonium acetate. Proteins were identified by the Integrated Proteomics Pipeline (IP2; Integrated Proteomics Applications) using the parameters and cutoffs exactly as described by Sawyer *et al.* 2019.

5.4.2 Native IP, Co-IP, and TMT quantitative MS

For the TMT quantitative MS and co-IP experiments, cells were sporulated in 2% SPO (see the "*pGAL-NDT80 GAL4-ER* synchronization system" section for details). Four hours after the cells were transferred to 2% SPO, 200 mM PMSF (dissolved in ethanol) was added to cultures to a final concentration of 2 mM. For the MS and the co-IP experiments, 462 or 92 OD_{600} of cells, respectively, were harvested by centrifugating at 1700 rcf, 4 °C, for 2 min. The supernatant was discarded, and the cell pellets were transferred to 2-ml tubes,

centrifuged at 21 krcf, 4 °C, for 1 min. The supernatant was completely aspirated, and the pellets were snap frozen in liquid nitrogen.

To extract proteins, pellets were thawed on ice, and 500 μl of NP-40 Native IP Buffer was added (50 mM Tris [pH 7.5], 150 mM NaCl, 2 mM $MgCl_2$, 1% NP-40, supplemented with PhosSTOP tablet (1 tablet used in 10 ml buffer, Sigma), cOmplete ULTRA protease inhibitor cocktail (1 tablet used in 20 ml buffer, Sigma), 0.64 μg/ml Pefabloc SC (Sigma), and 2.7 μM Pepstatin A). Cells were lysed with 500 μl of zirconia beads (BioSpec) in a Fast-Prep-24 5G (MP Biomedicals LLC, Irvine, CA) using the "S. cerevisiae" setting at room temperature for 40 s. Next, the cell lysates were chilled in ice water bath for 2 min. The tubes were punctured with a G20.5 needle, and the lysates were collected in 15-ml tubes (precooled to -20 °C) by centrifuging at 3 krpm, 20-40 s. Lysates were clarified by centrifuging at 21 krcf, 4 °C, for 20 min and snap frozen in liquid nitrogen. The protein concentration of lysates was determined by Bradford Assay (Bio-rad, Hercules, CA).

Ndc80-3V5 IP was performed at a protein concentration of 10 mg/ml in NP-40 Native IP Buffer. For the TMT quantitative MS experiment, a total of 38-40 mg protein, pooled from 10 tubes of lysates, was added to 167 μl pre-equilibrated anti-V5 agarose beads (Sigma) in a total volume of 4 ml (i.e., beads constituted 1/24 of the total IP volume), incubated at 4 °C for 2.5 hrs with rotation, and then washed with each of the following: (1) once with 3.5 ml NP-40 Native IP Buffer, (2) once with 950 μl NP-40 Native IP Buffer, (3) twice with 950 μl Buffer 2, and (4) twice with 950 μl Buffer 3. After the last wash, the proteins on the beads were digested in trypsin buffer, washed with Urea buffer, and frozen in liquid nitrogen as described in the Denaturing IP section. The TMT quantitative MS was performed as described in Cheng *et al.* 2018.

The co-IP experiments were performed similarly, except the following: a total of 4 mg protein was incubated with 27 μl of anti-V5 agarose beads in a total volume of 400 μl, and washed twice with 950 μl NP-40 Native IP Buffer before washing with Buffer 2 and Buffer 3. After the last wash, the wash buffer was aspirated until 100 μl was left, and 50 μl 3x SDS sample buffer (187.5 mM Tris [pH 6.8], 6% β-mercaptoethanol, 30% glycerol, 9% SDS, 0.05% bromophenol blue) was added to the beads before boiling for 5 min. After brief centrifugation, the eluted proteins were separated by SDS-PAGE as described in the immunoblotting section.

5.4.3 Purification of the Ndc80 complex

Native Ndc80 complex was purified from asynchronously growing *S. cerevisiae* cells (UB16284 and UB19957) through anti-Flag immunoprecipitation of Spc24-6His-3Flag as described in Miller *et al.* 2016. Cells were grown in YPD. Protein lysates were prepared by lysing cells in a Freezer/Mill (SPEX SamplePrep) submerged in liquid nitrogen (Sarangapani *et al.* 2014). Lysed cells were resuspended in buffer H (BH) (25 mM HEPES [pH 8.0], 2 mM $MgCl_2$, 0.1 mM EDTA, 0.5 mM EGTA, 0.1% NP-40, 15% glycerol, and 750 mM KCl), supplemented with the protease inhibitors (20 μg/ml leupeptin, 20 μg/ml pepstatin A, 20 μg/ml chymostatin, 200 μM phenylmethylsulfonyl fluoride) and the phosphatase in-

hibitors (0.1 mM Na-orthovanadate, 0.2 μM microcystin, 2 mM β-glycerophosphate, 1 mM Na pyrophosphate, and 5 mM NaF). The resuspended cell lysates were ultracentrifuged at 98,500 g at 4 °C for 90 min. Dynabeads conjugated with α-Flag antibody (Sigma) were incubated with extract for 3 hrs with constant rotation, followed by three washes with BH containing the protease inhibitors, phosphatase inhibitors, 2 mM dithiothreitol (DTT), and 1 M KCl. The beads were further washed twice with BH containing 150 mM KCl and the protease inhibitors. Associated proteins were eluted from the beads by gently agitating the beads in elution buffer (0.5 mg/ml 3Flag peptide in BH with 150 mM KCl and the protease inhibitors) at room temperature for 30 min.

5.4.4 Kinase assay

The kinase assay was performed using a recombinant variant of Ipl1 (AurB*) that was created by fusing the C-terminal activation box of Sli15 to Ipl1 (a kind gift from S. Biggins's lab). The kinase-dead (KD) mutant of AurB* contains the K133R mutation. These two constructs were first reported in de Regt *et al.* 2018. To begin the reaction, in a volume of 6 μl, 6.63 ng of the purified WT-Ndc80 or (Δaa2-28)-Ndc80 was incubated with 1 μM AurB* or KD in BH0.15 (same ingredients as BH except with 150 mM KCl) for 4 min at room temperature. Next, 6 μl of hot ATP mix (1.1 μl of 100 mM ATP, 3 μl of 6,000 Ci/mmol 10 mCi/ml γ-32P ATP, and 275 μl of BH0.15) was added to the kinase/substrate mix. After 1-min or 5-min incubation at 25 °C (see Figure Legend for details), reactions were stopped by adding 6 μl of 3x SDS sample buffer, and boiling at 95 °C for 5-10 min. Proteins were separated by SDS-PAGE as described in the immunoblot section. The gel was fixed and silver stained based on the manufacturer's instructions (Thermo Scientific). After the staining was stopped by incubating the gel in 5% acetic acid for 10 min, the gel was dried by vacuum at 80 °C for 1 hr. The dried gel was exposed to a phosphor storage screen for over 24 hours. Screens were imaged with a Typhoon Scanner (GE Healthcare).

5.4.5 Immunoblot

Protein extracts were prepared using a trichloroacetic acid (TCA) extraction protocol. Briefly, about 4 OD_{600} units of cells were treated with 5% trichloroacetic acid at 4 °C for at least 15 min. Following an acetone wash, the cell pellet was subsequently dried. The cell pellet was lysed with 100 μl glass beads in 100 μl lysis buffer (50 mM Tris–HCl [pH 7.5], 1 mM EDTA, 2.75 mM DTT, protease inhibitor cocktail (cOmplete EDTA-free, Roche, Basel, Switzerland) using a Mini-Beadbeater-96 (Biospec Products). Next, 3x SDS sample buffer was added and the cell lysate was boiled for 5 min. Proteins were separated by PAGE using 4–12% Bis-Tris Bolt gels (Thermo Fisher) and transferred onto nitrocellulose membranes (0.45 μm, Bio-rad) using a semi-dry transfer apparatus (Trans-Blot Turbo Transfer System, Bio-rad). The membranes were blocked in PBS Odyssey Blocking Buffer (LI-COR Biosciences, Lincoln, NE) for at least 30 min before incubation overnight at 4 °C with a mouse anti-V5 antibody (R960-25, Thermo Fisher) at a 1:2000 dilution. We monitored Hxk1 or

Hxk2 levels using a rabbit anti-hexokinase antibody (H2035, US Biological, Salem, MA) at a 1:10,000-1:20,000 dilution, Pgk1 levels with a 1:10,000 diluted mouse anti-Pgk1 antibody (SC7167, Molecular Probes, Carlsbad, CA), and Kar2 levels with a 1:200,000 rabbit anti-Kar2 antibody (provided by Mark Rose). Membranes were washed in PBST (phosphate buffered saline with 0.01% tween-20) and incubated with an anti-mouse secondary antibody conjugated to IRDye 800CW at a 1:15,000 dilution (926–32212, LI-COR Biosciences) and an anti-rabbit antibody conjugated to IRDye 680RD at a 1:15,000 dilution (926–68071, LI-COR Biosciences) to detect the V5 epitope and Hxk1/Hxk2, respectively. Immunoblot images were generated and quantified using the Odyssey system (LI-COR Biosciences).

Bibliography

1. Abeliovich, H. & Klionsky, D. J. Autophagy in yeast: mechanistic insights and physiological function. *Microbiol Mol Biol Rev* **65,** 463–79, table of contents (2001).
2. Ahuja, J. S., Sandhu, R., Mainpal, R., Lawson, C., Henley, H., Hunt, P. A., Yanowitz, J. L. & Borner, G. V. Control of meiotic pairing and recombination by chromosomally tethered 26S proteasome. *Science* **355,** 408–411 (2017).
3. Aivazidis, S., Coughlan, C. M., Rauniyar, A. K., Jiang, H., Liggett, L. A., Maclean, K. N. & Roede, J. R. The burden of trisomy 21 disrupts the proteostasis network in Down syndrome. *PLoS One* **12,** e0176307 (2017).
4. Akiyoshi, B., Nelson, C. R., Duggan, N., Ceto, S., Ranish, J. A. & Biggins, S. The Mub1/Ubr2 ubiquitin ligase complex regulates the conserved Dsn1 kinetochore protein. *PLoS Genet* **9,** e1003216 (2013).
5. Akiyoshi, B., Nelson, C. R., Ranish, J. A. & Biggins, S. Analysis of Ipl1-mediated phosphorylation of the Ndc80 kinetochore protein in Saccharomyces cerevisiae. *Genetics* **183,** 1591–5 (2009).
6. Akiyoshi, B., Sarangapani, K. K., Powers, A. F., Nelson, C. R., Reichow, S. L., Arellano-Santoyo, H., Gonen, T., Ranish, J. A., Asbury, C. L. & Biggins, S. Tension directly stabilizes reconstituted kinetochore-microtubule attachments. *Nature* **468,** 576–9 (2010).
7. Alatorre-Cobos, F., Cruz-Ramirez, A., Hayden, C. A., Perez-Torres, C. A., Chauvin, A. L., Ibarra-Laclette, E., Alva-Cortes, E., Jorgensen, R. A. & Herrera-Estrella, L. Translational regulation of Arabidopsis XIPOTL1 is modulated by phosphocholine levels via the phylogenetically conserved upstream open reading frame 30. *J Exp Bot* **63,** 5203–21 (2012).
8. Albertson, D. G., Rose, A. M. & Villeneuve, A. M. in *C. elegans II* (eds nd, Riddle, D. L., Blumenthal, T., Meyer, B. J. & Priess, J. R.) (Cold Spring Harbor Laboratory Press, Cold Spring Harbor (NY), 1997). <`http://dx.doi.org/`>.
9. Alexandru, G., Uhlmann, F., Mechtler, K., Poupart, M. A. & Nasmyth, K. Phosphorylation of the cohesin subunit Scc1 by Polo/Cdc5 kinase regulates sister chromatid separation in yeast. *Cell* **105,** 459–72 (2001).
10. Ambros, V. microRNAs: tiny regulators with great potential. *Cell* **107,** 823–6 (2001).

11. Anand, R., Memisoglu, G. & Haber, J. Cas9-mediated gene editing in Saccharomyces cerevisiae. *Protocol Exchange.* doi:10.1083/protex.2017.021a (2017).
12. Anderson, S. F., Steber, C. M., Esposito, R. E. & Coleman, J. E. UME6, a negative regulator of meiosis in Saccharomyces cerevisiae, contains a C-terminal Zn2Cys6 binuclear cluster that binds the URS1 DNA sequence in a zinc-dependent manner. *Protein Sci* **4,** 1832–43 (1995).
13. Andrews, S. J. & Rothnagel, J. A. Emerging evidence for functional peptides encoded by short open reading frames. *Nat Rev Genet* **15,** 193–204 (2014).
14. Aravamudhan, P., Goldfarb, A. A. & Joglekar, A. P. The kinetochore encodes a mechanical switch to disrupt spindle assembly checkpoint signalling. *Nat Cell Biol* **17,** 868–79 (2015).
15. Arribere, J. A. & Gilbert, W. V. Roles for transcript leaders in translation and mRNA decay revealed by transcript leader sequencing. *Genome Res* **23,** 977–87 (2013).
16. Asakawa, H., Hayashi, A., Haraguchi, T. & Hiraoka, Y. Dissociation of the Nuf2-Ndc80 complex releases centromeres from the spindle-pole body during meiotic prophase in fission yeast. *Mol Biol Cell* **16,** 2325–38 (2005).
17. Au, W. C., Crisp, M. J., DeLuca, S. Z., Rando, O. J. & Basrai, M. A. Altered dosage and mislocalization of histone H3 and Cse4p lead to chromosome loss in Saccharomyces cerevisiae. *Genetics* **179,** 263–75 (2008).
18. Avena, J. S., Burns, S., Yu, Z., Ebmeier, C. C., Old, W. M., Jaspersen, S. L. & Winey, M. Licensing of yeast centrosome duplication requires phosphoregulation of sfi1. *PLoS Genet* **10,** e1004666 (2014).
19. Bansal, P. K., Abdulle, R. & Kitagawa, K. Sgt1 associates with Hsp90: an initial step of assembly of the core kinetochore complex. *Mol Cell Biol* **24,** 8069–79 (2004).
20. Batista, P. J. & Chang, H. Y. Long noncoding RNAs: cellular address codes in development and disease. *Cell* **152,** 1298–307 (2013).
21. Batut, P., Dobin, A., Plessy, C., Carninci, P. & Gingeras, T. R. High-fidelity promoter profiling reveals widespread alternative promoter usage and transposon-driven developmental gene expression. *Genome Res* **23,** 169–80 (2013).
22. Benjamin, K. R., Zhang, C., Shokat, K. M. & Herskowitz, I. Control of landmark events in meiosis by the CDK Cdc28 and the meiosis-specific kinase Ime2. *Genes Dev* **17,** 1524–39 (2003).
23. Berchowitz, L. E., Gajadhar, A. S., van Werven, F. J., De Rosa, A. A., Samoylova, M. L., Brar, G. A., Xu, Y., Xiao, C., Futcher, B., Weissman, J. S., White, F. M. & Amon, A. A developmentally regulated translational control pathway establishes the meiotic chromosome segregation pattern. *Genes Dev* **27,** 2147–63 (2013).
24. Biggins, S. The composition, functions, and regulation of the budding yeast kinetochore. *Genetics* **194,** 817–46 (2013).

25. Bird, A. J., Gordon, M., Eide, D. J. & Winge, D. R. Repression of ADH1 and ADH3 during zinc deficiency by Zap1-induced intergenic RNA transcripts. *Embo j* **25,** 5726–34 (2006).

26. Blitzblau, H. G., Chan, C. S., Hochwagen, A. & Bell, S. P. Separation of DNA replication from the assembly of break-competent meiotic chromosomes. *PLoS Genet* **8,** e1002643 (2012).

27. Bowdish, K. S., Yuan, H. E. & Mitchell, A. P. Positive control of yeast meiotic genes by the negative regulator UME6. *Mol Cell Biol* **15,** 2955–61 (1995).

28. Brar, G. A., Hochwagen, A., Ee, L. S. & Amon, A. The multiple roles of cohesin in meiotic chromosome morphogenesis and pairing. *Mol Biol Cell* **20,** 1030–47 (2009).

29. Brar, G. A., Kiburz, B. M., Zhang, Y., Kim, J. E., White, F. & Amon, A. Rec8 phosphorylation and recombination promote the step-wise loss of cohesins in meiosis. *Nature* **441,** 532–6 (2006).

30. Brar, G. A., Yassour, M., Friedman, N., Regev, A., Ingolia, N. T. & Weissman, J. S. High-resolution view of the yeast meiotic program revealed by ribosome profiling. *Science* **335,** 552–7 (2012).

31. Buckingham, L. E., Wang, H. T., Elder, R. T., McCarroll, R. M., Slater, M. R. & Esposito, R. E. Nucleotide sequence and promoter analysis of SPO13, a meiosis-specific gene of Saccharomyces cerevisiae. *Proc Natl Acad Sci U S A* **87,** 9406–10 (1990).

32. Calvo, S. E., Pagliarini, D. J. & Mootha, V. K. Upstream open reading frames cause widespread reduction of protein expression and are polymorphic among humans. *Proc Natl Acad Sci U S A* **106,** 7507–12 (2009).

33. Camahort, R., Li, B., Florens, L., Swanson, S. K., Washburn, M. P. & Gerton, J. L. Scm3 is essential to recruit the histone h3 variant cse4 to centromeres and to maintain a functional kinetochore. *Mol Cell* **26,** 853–65 (2007).

34. Cao, L., Alani, E. & Kleckner, N. A pathway for generation and processing of double-strand breaks during meiotic recombination in S. cerevisiae. *Cell* **61,** 1089–101 (1990).

35. Carfi, A., Antocicco, M., Brandi, V., Cipriani, C., Fiore, F., Mascia, D., Settanni, S., Vetrano, D. L., Bernabei, R. & Onder, G. Characteristics of adults with down syndrome: prevalence of age-related conditions. *Front Med (Lausanne)* **1,** 51 (2014).

36. Carlile, T. M. & Amon, A. Meiosis I is established through division-specific translational control of a cyclin. *Cell* **133,** 280–91 (2008).

37. Casson, S. A., Chilley, P. M., Topping, J. F., Evans, I. M., Souter, M. A. & Lindsey, K. The POLARIS gene of Arabidopsis encodes a predicted peptide required for correct root growth and leaf vascular patterning. *Plant Cell* **14,** 1705–21 (2002).

38. Catlett, M. G. & Kaplan, K. B. Sgt1p is a unique co-chaperone that acts as a client adaptor to link Hsp90 to Skp1p. *J Biol Chem* **281,** 33739–48 (2006).

39. Cech, T. R. & Steitz, J. A. The noncoding RNA revolution-trashing old rules to forge new ones. *Cell* **157,** 77–94 (2014).

40. Chao, W. C., Kulkarni, K., Zhang, Z., Kong, E. H. & Barford, D. Structure of the mitotic checkpoint complex. *Nature* **484,** 208–13 (2012).

41. Cheerambathur, D. K., Prevo, B., Chow, T. L., Hattersley, N., Wang, S., Zhao, Z., Kim, T., Gerson-Gurwitz, A., Oegema, K., Green, R. & Desai, A. The Kinetochore-Microtubule Coupling Machinery Is Repurposed in Sensory Nervous System Morphogenesis. *Dev Cell* **48,** 864–872.e7 (2019).

42. Cheeseman, I. M., Brew, C., Wolyniak, M., Desai, A., Anderson, S., Muster, N., Yates, J. R., Huffaker, T. C., Drubin, D. G. & Barnes, G. Implication of a novel multiprotein Dam1p complex in outer kinetochore function. *J Cell Biol* **155,** 1137–45 (2001).

43. Cheeseman, I. M., Chappie, J. S., Wilson-Kubalek, E. M. & Desai, A. The conserved KMN network constitutes the core microtubule-binding site of the kinetochore. *Cell* **127,** 983–97 (2006).

44. Cheeseman, I. M., Drubin, D. G. & Barnes, G. in *J Cell Biol* 199–203 (2002). doi:10.1083/jcb.200201052. <http://dx.doi.org/10.1083/jcb.200201052>.

45. Cheeseman, I. M., Enquist-Newman, M., Muller-Reichert, T., Drubin, D. G. & Barnes, G. Mitotic spindle integrity and kinetochore function linked by the Duo1p/Dam1p complex. *J Cell Biol* **152,** 197–212 (2001).

46. Chen, J., Tresenrider, A., Chia, M., McSwiggen, D. T., Spedale, G., Jorgensen, V., Liao, H., van Werven, F. J. & Unal, E. Kinetochore inactivation by expression of a repressive mRNA. *Elife* **6.** doi:10.7554/eLife.27417. <http://dx.doi.org/10.7554/eLife.27417> (2017).

47. Chen, X., Gaglione, R., Leong, T., Bednor, L., de Los Santos, T., Luk, E., Airola, M. & Hollingsworth, N. M. Mek1 coordinates meiotic progression with DNA break repair by directly phosphorylating and inhibiting the yeast pachytene exit regulator Ndt80. *PLoS Genet* **14,** e1007832 (2018).

48. Chen, Y., Riley, D. J., Chen, P. L. & Lee, W. H. HEC, a novel nuclear protein rich in leucine heptad repeats specifically involved in mitosis. *Mol Cell Biol* **17,** 6049–56 (1997).

49. Chen, Y., Zhao, J., Jiao, Z., Wang, W., Wang, D., Yu, X., Shi, Z., Ge, N., Pan, Q., Xia, J., Niu, W., Zhao, R., Zhang, X. & Du, W. SKA1 overexpression is associated with poor prognosis in hepatocellular carcinoma. *BMC Cancer* **18,** 1240 (2018).

50. Cheng, H., Bao, X., Gan, X., Luo, S. & Rao, H. Multiple E3s promote the degradation of histone H3 variant Cse4. *Sci Rep* **7,** 8565 (2017).

51. Cheng, H., Bao, X. & Rao, H. The F-box Protein Rcy1 Is Involved in the Degradation of Histone H3 Variant Cse4 and Genome Maintenance. *J Biol Chem* **291,** 10372–7 (2016).

52. Cheng, Z., Otto, G. M., Powers, E. N., Keskin, A., Mertins, P., Carr, S. A., Jovanovic, M. & Brar, G. A. Pervasive, Coordinated Protein-Level Changes Driven by Transcript Isoform Switching during Meiosis. *Cell* **172,** 910–923.e16 (2018).

53. Chew, G. L., Pauli, A. & Schier, A. F. Conservation of uORF repressiveness and sequence features in mouse, human and zebrafish. *Nat Commun* **7,** 11663 (2016).

54. Chia, M., Tresenrider, A., Chen, J., Spedale, G., Jorgensen, V., Unal, E. & van Werven, F. J. Transcription of a 5' extended mRNA isoform directs dynamic chromatin changes and interference of a downstream promoter. *Elife* **6.** doi:10.7554/eLife.27420. <http://dx.doi.org/10.7554/eLife.27420> (2017).

55. Cho, U. S. & Harrison, S. C. Ndc10 is a platform for inner kinetochore assembly in budding yeast. *Nat Struct Mol Biol* **19,** 48–55 (2012).

56. Cho, U. S. & Harrison, S. C. Recognition of the centromere-specific histone Cse4 by the chaperone Scm3. *Proc Natl Acad Sci U S A* **108,** 9367–71 (2011).

57. Chu, S., DeRisi, J., Eisen, M., Mulholland, J., Botstein, D., Brown, P. O. & Herskowitz, I. The transcriptional program of sporulation in budding yeast. *Science* **282,** 699–705 (1998).

58. Chu, S. & Herskowitz, I. Gametogenesis in yeast is regulated by a transcriptional cascade dependent on Ndt80. *Mol Cell* **1,** 685–96 (1998).

59. Clarke, L. & Carbon, J. Isolation of a yeast centromere and construction of functional small circular chromosomes. *Nature* **287,** 504–9 (1980).

60. Clyne, R. K., Katis, V. L., Jessop, L., Benjamin, K. R., Herskowitz, I., Lichten, M. & Nasmyth, K. Polo-like kinase Cdc5 promotes chiasmata formation and cosegregation of sister centromeres at meiosis I. *Nat Cell Biol* **5,** 480–5 (2003).

61. Cole, H. A., Howard, B. H. & Clark, D. J. The centromeric nucleosome of budding yeast is perfectly positioned and covers the entire centromere. *Proc Natl Acad Sci U S A* **108,** 12687–92 (2011).

62. Cooper, K. F., Mallory, M. J., Egeland, D. B., Jarnik, M. & Strich, R. Ama1p is a meiosis-specific regulator of the anaphase promoting complex/cyclosome in yeast. *Proc Natl Acad Sci U S A* **97,** 14548–53 (2000).

63. Corbett, K. D. Molecular Mechanisms of Spindle Assembly Checkpoint Activation and Silencing. *Prog Mol Subcell Biol* **56,** 429–455 (2017).

64. Corbett, K. D., Yip, C. K., Ee, L. S., Walz, T., Amon, A. & Harrison, S. C. The monopolin complex crosslinks kinetochore components to regulate chromosome-microtubule attachments. *Cell* **142,** 556–67 (2010).

65. Corbin, V. & Maniatis, T. Role of transcriptional interference in the Drosophila melanogaster Adh promoter switch. *Nature* **337,** 279–82 (1989).

66. Covitz, P. A., Herskowitz, I. & Mitchell, A. P. The yeast RME1 gene encodes a putative zinc finger protein that is directly repressed by a1-alpha 2. *Genes Dev* **5,** 1982–9 (1991).

67. Daum, J. R., Wren, J. D., Daniel, J. J., Sivakumar, S., McAvoy, J. N., Potapova, T. A. & Gorbsky, G. J. Ska3 is required for spindle checkpoint silencing and the maintenance of chromosome cohesion in mitosis. *Curr Biol* **19,** 1467–72 (2009).

68. Davis-Roca, A. C., Muscat, C. C. & Wignall, S. M. Caenorhabditis elegans oocytes detect meiotic errors in the absence of canonical end-on kinetochore attachments. *J Cell Biol* **216,** 1243–1253 (2017).

69. Davydenko, O., Schultz, R. M. & Lampson, M. A. Increased CDK1 activity determines the timing of kinetochore-microtubule attachments in meiosis I. *J Cell Biol* **202,** 221–9 (2013).

70. De Wulf, P., McAinsh, A. D. & Sorger, P. K. Hierarchical assembly of the budding yeast kinetochore from multiple subcomplexes. *Genes Dev* **17,** 2902–21 (2003).

71. De Lichtenberg, U., Jensen, L. J., Brunak, S. & Bork, P. Dynamic complex formation during the yeast cell cycle. *Science* **307,** 724–7 (2005).

72. De Regt, A., Asbury, C. L. & Biggins, S. Tension on kinetochore substrates is insufficient to prevent Aurora-triggered detachment. *bioRxiv.* doi:10.1101/415992 (2018).

73. Dephoure, N., Hwang, S., O'Sullivan, C., Dodgson, S. E., Gygi, S. P., Amon, A. & Torres, E. M. Quantitative proteomic analysis reveals posttranslational responses to aneuploidy in yeast. *Elife* **3,** e03023 (2014).

74. Dewar, H., Tanaka, K., Nasmyth, K. & Tanaka, T. U. Tension between two kinetochores suffices for their bi-orientation on the mitotic spindle. *Nature* **428,** 93–7 (2004).

75. Dhatchinamoorthy, K., Shivaraju, M., Lange, J. J., Rubinstein, B., Unruh, J. R., Slaughter, B. D. & Gerton, J. L. Structural plasticity of the living kinetochore. *J Cell Biol* **216,** 3551–3570 (2017).

76. Dhatchinamoorthy, K., Unruh, J. R., Lange, J. J., Levy, M., Slaughter, B. D. & Gerton, J. L. The stoichiometry of the outer kinetochore is modulated by microtubule-proximal regulatory factors. *J Cell Biol* **218,** 2124–2135 (2019).

77. Diamond, A. E., Park, J. S., Inoue, I., Tachikawa, H. & Neiman, A. M. The anaphase promoting complex targeting subunit Ama1 links meiotic exit to cytokinesis during sporulation in Saccharomyces cerevisiae. *Mol Biol Cell* **20,** 134–45 (2009).

78. Dimitrova, Y. N., Jenni, S., Valverde, R., Khin, Y. & Harrison, S. C. Structure of the MIND Complex Defines a Regulatory Focus for Yeast Kinetochore Assembly. *Cell* **167,** 1014–1027.e12 (2016).

79. Donnelly, N., Passerini, V., Durrbaum, M., Stingele, S. & Storchova, Z. HSF1 deficiency and impaired HSP90-dependent protein folding are hallmarks of aneuploid human cells. *Embo j* **33,** 2374–87 (2014).

80. Dumont, J., Oegema, K. & Desai, A. A kinetochore-independent mechanism drives anaphase chromosome separation during acentrosomal meiosis. *Nat Cell Biol* **12,** 894–901 (2010).

81. Eisenberg, A. R., Higdon, A., Keskin, A., Hodapp, S., Jovanovic, M. & Brar, G. A. Precise Post-translational Tuning Occurs for Most Protein Complex Components during Meiosis. *Cell Rep* **25,** 3603–3617.e2 (2018).

82. Eissenberg, J. C. & Shilatifard, A. Histone H3 lysine 4 (H3K4) methylation in development and differentiation. *Dev Biol* **339,** 240–9 (2010).

83. Elserafy, M., Saric, M., Neuner, A., Lin, T. C., Zhang, W., Seybold, C., Sivashanmugam, L. & Schiebel, E. Molecular mechanisms that restrict yeast centrosome duplication to one event per cell cycle. *Curr Biol* **24,** 1456–66 (2014).

84. Enquist-Newman, M., Cheeseman, I. M., Van Goor, D., Drubin, D. G., Meluh, P. B. & Barnes, G. Dad1p, third component of the Duo1p/Dam1p complex involved in kinetochore function and mitotic spindle integrity. *Mol Biol Cell* **12,** 2601–13 (2001).

85. Errington, J. Regulation of endospore formation in Bacillus subtilis. *Nat Rev Microbiol* **1,** 117–26 (2003).

86. Esposito, R. E., Frink, N., Bernstein, P. & Esposito, M. S. The genetic control of sporulation in Saccharomyces. II. Dominance and complementation of mutants of meiosis and spore formation. *Mol Gen Genet* **114,** 241–8 (1972).

87. Eytan, E., Wang, K., Miniowitz-Shemtov, S., Sitry-Shevah, D., Kaisari, S., Yen, T. J., Liu, S. T. & Hershko, A. Disassembly of mitotic checkpoint complexes by the joint action of the AAA-ATPase TRIP13 and p31(comet). *Proc Natl Acad Sci U S A* **111,** 12019–24 (2014).

88. Faesen, A. C., Thanasoula, M., Maffini, S., Breit, C., Muller, F., van Gerwen, S., Bange, T. & Musacchio, A. Basis of catalytic assembly of the mitotic checkpoint complex. *Nature* **542,** 498–502 (2017).

89. Ferretti, C., Totta, P., Fiore, M., Mattiuzzo, M., Schillaci, T., Ricordy, R., Di Leonardo, A. & Degrassi, F. Expression of the kinetochore protein Hec1 during the cell cycle in normal and cancer cells and its regulation by the pRb pathway. *Cell Cycle* **9,** 4174–82 (2010).

90. Finley, D., Ulrich, H. D., Sommer, T. & Kaiser, P. The ubiquitin-proteasome system of Saccharomyces cerevisiae. *Genetics* **192,** 319–60 (2012).

91. Fischbock-Halwachs, J., Singh, S., Potocnjak, M., Hagemann, G., Solis-Mezarino, V., Woike, S., Ghodgaonkar-Steger, M., Weissmann, F., Gallego, L. D., Rojas, J., Andreani, J., Kohler, A. & Herzog, F. The COMA complex interacts with Cse4 and positions Sli15/Ipl1 at the budding yeast inner kinetochore. *Elife* **8.** doi:10.7554/eLife.42879. <http://dx.doi.org/10.7554/eLife.42879> (2019).

92. Foe, I. T., Foster, S. A., Cheung, S. K., DeLuca, S. Z., Morgan, D. O. & Toczyski, D. P. Ubiquitination of Cdc20 by the APC occurs through an intramolecular mechanism. *Curr Biol* **21,** 1870–7 (2011).

93. Franck, A. D., Powers, A. F., Gestaut, D. R., Gonen, T., Davis, T. N. & Asbury, C. L. Tension applied through the Dam1 complex promotes microtubule elongation providing a direct mechanism for length control in mitosis. *Nat Cell Biol* **9,** 832–7 (2007).

94. Furuyama, S. & Biggins, S. Centromere identity is specified by a single centromeric nucleosome in budding yeast. *Proc Natl Acad Sci U S A* **104,** 14706–11 (2007).

95. Gaba, A., Jacobson, A. & Sachs, M. S. Ribosome occupancy of the yeast CPA1 upstream open reading frame termination codon modulates nonsense-mediated mRNA decay. *Mol Cell* **20,** 449–60 (2005).

96. Gaitanos, T. N., Santamaria, A., Jeyaprakash, A. A., Wang, B., Conti, E. & Nigg, E. A. Stable kinetochore-microtubule interactions depend on the Ska complex and its new component Ska3/C13Orf3. *Embo j* **28,** 1442–52 (2009).

97. Galindo, M. I., Pueyo, J. I., Fouix, S., Bishop, S. A. & Couso, J. P. Peptides encoded by short ORFs control development and define a new eukaryotic gene family. *PLoS Biol* **5,** e106 (2007).

98. Garelli, A., Gontijo, A. M., Miguela, V., Caparros, E. & Dominguez, M. Imaginal discs secrete insulin-like peptide 8 to mediate plasticity of growth and maturation. *Science* **336,** 579–82 (2012).

99. Gascoigne, K. E. & Cheeseman, I. M. CDK-dependent phosphorylation and nuclear exclusion coordinately control kinetochore assembly state. *J Cell Biol* **201,** 23–32 (2013).

100. Ge, S., Skaar, J. R. & Pagano, M. APC/C- and Mad2-mediated degradation of Cdc20 during spindle checkpoint activation. *Cell Cycle* **8,** 167–71 (2009).

101. Gibson, D. G., Young, L., Chuang, R. Y., Venter, J. C., Hutchison C. A., 3. & Smith, H. O. Enzymatic assembly of DNA molecules up to several hundred kilobases. *Nat Methods* **6,** 343–5. ISSN: 1548-7091 (2009).

102. Gillis, A. N., Thomas, S., Hansen, S. D. & Kaplan, K. B. A novel role for the CBF3 kinetochore-scaffold complex in regulating septin dynamics and cytokinesis. *J Cell Biol* **171,** 773–84 (2005).

103. Giroux, C. N., Dresser, M. E. & Tiano, H. F. Genetic control of chromosome synapsis in yeast meiosis. *Genome* **31,** 88–94 (1989).

104. Görner, W., Durchschlag, E., Martinez-Pastor, M. T., Estruch, F., Ammerer, G., Hamilton, B., Ruis, H. & Schüller, C. Nuclear localization of the C2H2 zinc finger protein Msn2p is regulated by stress and protein kinase Aactivity. *Genes Dev* **12,** 586–97 (1998).

105. Goujon, M., McWilliam, H., Li, W., Valentin, F., Squizzato, S., Paern, J. & Lopez, R. A new bioinformatics analysis tools framework at EMBL-EBI. *Nucleic Acids Res* **38,** W695–9. ISSN: 0305-1048 (2010).

106. Guttman, M., Amit, I., Garber, M., French, C., Lin, M. F., Feldser, D., Huarte, M., Zuk, O., Carey, B. W., Cassady, J. P., Cabili, M. N., Jaenisch, R., Mikkelsen, T. S., Jacks, T., Hacohen, N., Bernstein, B. E., Kellis, M., Regev, A., Rinn, J. L. & Lander, E. S. Chromatin signature reveals over a thousand highly conserved large non-coding RNAs in mammals. *Nature* **458,** 223–7 (2009).

107. Guttmann-Raviv, N., Martin, S. & Kassir, Y. Ime2, a meiosis-specific kinase in yeast, is required for destabilization of its transcriptional activator, Ime1. *Mol Cell Biol* **22,** 2047–56 (2002).

108. Haber, J. E. in *Genetics* 33–64 (2012). doi:10.1534/genetics.111.134577. <http://dx.doi.org/10.1534/genetics.111.134577>.

109. Hamant, O., Golubovskaya, I., Meeley, R., Fiume, E., Timofejeva, L., Schleiffer, A., Nasmyth, K. & Cande, W. Z. A REC8-dependent plant Shugoshin is required for maintenance of centromeric cohesion during meiosis and has no mitotic functions. *Curr Biol* **15,** 948–54 (2005).

110. Hanfrey, C., Elliott, K. A., Franceschetti, M., Mayer, M. J., Illingworth, C. & Michael, A. J. A dual upstream open reading frame-based autoregulatory circuit controlling polyamine-responsive translation. *J Biol Chem* **280,** 39229–37 (2005).

111. Hanisch, A., Sillje, H. H. & Nigg, E. A. Timely anaphase onset requires a novel spindle and kinetochore complex comprising Ska1 and Ska2. *Embo j* **25,** 5504–15 (2006).

112. Hardwick, K. G., Weiss, E., Luca, F. C., Winey, M. & Murray, A. W. Activation of the budding yeast spindle assembly checkpoint without mitotic spindle disruption. *Science* **273,** 953–6 (1996).

113. Hassold, T., Hall, H. & Hunt, P. The origin of human aneuploidy: where we have been, where we are going. *Hum Mol Genet* **16 Spec No. 2,** R203–8 (2007).

114. Hayama, S., Daigo, Y., Kato, T., Ishikawa, N., Yamabuki, T., Miyamoto, M., Ito, T., Tsuchiya, E., Kondo, S. & Nakamura, Y. Activation of CDCA1-KNTC2, members of centromere protein complex, involved in pulmonary carcinogenesis. *Cancer Res* **66,** 10339–48 (2006).

115. Hepworth, S. R., Friesen, H. & Segall, J. NDT80 and the meiotic recombination checkpoint regulate expression of middle sporulation-specific genes in Saccharomyces cerevisiae. *Mol Cell Biol* **18,** 5750–61 (1998).

116. Heun, P., Erhardt, S., Blower, M. D., Weiss, S., Skora, A. D. & Karpen, G. H. Mislocalization of the Drosophila centromere-specific histone CID promotes formation of functional ectopic kinetochores. *Dev Cell* **10,** 303–15 (2006).

117. Hewawasam, G., Shivaraju, M., Mattingly, M., Venkatesh, S., Martin-Brown, S., Florens, L., Workman, J. L. & Gerton, J. L. Psh1 is an E3 ubiquitin ligase that targets the centromeric histone variant Cse4. *Mol Cell* **40,** 444–54 (2010).

118. Hinshaw, S. M., Dates, A. N. & Harrison, S. C. The structure of the yeast Ctf3 complex. *Elife* **8.** doi:10.7554/eLife.48215. <http://dx.doi.org/10.7554/eLife.48215> (2019).

119. Hinshaw, S. M., Makrantoni, V., Harrison, S. C. & Marston, A. L. The Kinetochore Receptor for the Cohesin Loading Complex. *Cell* **171,** 72–84.e13 (2017).

120. Hiruma, Y., Sacristan, C., Pachis, S. T., Adamopoulos, A., Kuijt, T., Ubbink, M., von Castelmur, E., Perrakis, A. & Kops, G. J. CELL DIVISION CYCLE. Competition between MPS1 and microtubules at kinetochores regulates spindle checkpoint signaling. *Science* **348,** 1264–7 (2015).

121. Hochwagen, A., Tham, W. H., Brar, G. A. & Amon, A. The FK506 binding protein Fpr3 counteracts protein phosphatase 1 to maintain meiotic recombination checkpoint activity. *Cell* **122,** 861–73 (2005).

122. Hofmann, C., Cheeseman, I. M., Goode, B. L., McDonald, K. L., Barnes, G. & Drubin, D. G. Saccharomyces cerevisiae Duo1p and Dam1p, novel proteins involved in mitotic spindle function. *J Cell Biol* **143,** 1029–40 (1998).

123. Hollerer, I., Barker, J. C., Jorgensen, V., Tresenrider, A., Dugast-Darzacq, C., Chan, L. Y., Darzacq, X., Tjian, R., Unal, E. & Brar, G. A. Evidence for an Integrated Gene Repression Mechanism Based on mRNA Isoform Toggling in Human Cells. *G3 (Bethesda)* **9,** 1045–1053 (2019).

124. Hornung, P., Maier, M., Alushin, G. M., Lander, G. C., Nogales, E. & Westermann, S. Molecular architecture and connectivity of the budding yeast Mtw1 kinetochore complex. *J Mol Biol* **405,** 548–59 (2011).

125. Huang, J., Brito, I. L., Villen, J., Gygi, S. P., Amon, A. & Moazed, D. Inhibition of homologous recombination by a cohesin-associated clamp complex recruited to the rDNA recombination enhancer. *Genes Dev* **20,** 2887–901 (2006).

126. Hunter, N. Meiotic Recombination: The Essence of Heredity. *Cold Spring Harb Perspect Biol* **7.** doi:10.1101/cshperspect.a016618. <http://dx.doi.org/10.1101/cshperspect.a016618> (2015).

127. Hwang, L. H., Lau, L. F., Smith, D. L., Mistrot, C. A., Hardwick, K. G., Hwang, E. S., Amon, A. & Murray, A. W. Budding yeast Cdc20: a target of the spindle checkpoint. *Science* **279,** 1041–4 (1998).

128. Hwang, S., Gustafsson, H. T., O'Sullivan, C., Bisceglia, G., Huang, X., Klose, C., Schevchenko, A., Dickson, R. C., Cavaliere, P., Dephoure, N. & Torres, E. M. Serine-Dependent Sphingolipid Synthesis Is a Metabolic Liability of Aneuploid Cells. *Cell Rep* **21,** 3807–3818 (2017).

129. Ingolia, N. T., Ghaemmaghami, S., Newman, J. R. & Weissman, J. S. Genome-wide analysis in vivo of translation with nucleotide resolution using ribosome profiling. *Science* **324,** 218–23 (2009).

130. Janke, C., Ortiz, J., Tanaka, T. U., Lechner, J. & Schiebel, E. Four new subunits of the Dam1-Duo1 complex reveal novel functions in sister kinetochore biorientation. *Embo j* **21,** 181–93 (2002).

131. Jehn, B., Niedenthal, R. & Hegemann, J. H. In vivo analysis of the Saccharomyces cerevisiae centromere CDEIII sequence: requirements for mitotic chromosome segregation. *Mol Cell Biol* **11,** 5212–21 (1991).

132. Jenni, S. & Harrison, S. C. Structure of the DASH/Dam1 complex shows its role at the yeast kinetochore-microtubule interface. *Science* **360,** 552–558 (2018).

133. Ji, Z., Gao, H., Jia, L., Li, B. & Yu, H. A sequential multi-target Mps1 phosphorylation cascade promotes spindle checkpoint signaling. *Elife* **6.** doi:10.7554/eLife.22513. <http://dx.doi.org/10.7554/eLife.22513> (2017).

134. Ji, Z., Gao, H. & Yu, H. CELL DIVISION CYCLE. Kinetochore attachment sensed by competitive Mps1 and microtubule binding to Ndc80C. *Science* **348,** 1260–4 (2015).

135. Jin, H., Avey, M. & Yu, H. G. Is cohesin required for spindle-pole-body/centrosome cohesion? *Commun Integr Biol* **5,** 26–9 (2012).

136. Johnstone, T. G., Bazzini, A. A. & Giraldez, A. J. Upstream ORFs are prevalent translational repressors in vertebrates. *Embo j* **35,** 706–23 (2016).

137. Jones, M. H., Bachant, J. B., Castillo, A. R., Giddings T. H., J. & Winey, M. Yeast Dam1p is required to maintain spindle integrity during mitosis and interacts with the Mps1p kinase. *Mol Biol Cell* **10,** 2377–91 (1999).

138. Kadosh, D. & Struhl, K. Histone deacetylase activity of Rpd3 is important for transcriptional repression in vivo. *Genes Dev* **12,** 797–805 (1998).

139. Kadosh, D. & Struhl, K. Repression by Ume6 involves recruitment of a complex containing Sin3 corepressor and Rpd3 histone deacetylase to target promoters. *Cell* **89,** 365–71 (1997).

140. Kadosh, D. & Struhl, K. Targeted recruitment of the Sin3-Rpd3 histone deacetylase complex generates a highly localized domain of repressed chromatin in vivo. *Mol Cell Biol* **18,** 5121–7 (1998).

141. Kampinga, H. H. & Craig, E. A. The HSP70 chaperone machinery: J proteins as drivers of functional specificity. *Nat Rev Mol Cell Biol* **11,** 579–92 (2010).

142. Kaplan, K. B., Hyman, A. A. & Sorger, P. K. Regulating the yeast kinetochore by ubiquitin-dependent degradation and Skp1p-mediated phosphorylation. *Cell* **91,** 491–500 (1997).

143. Kassir, Y., Granot, D. & Simchen, G. IME1, a positive regulator gene of meiosis in S. cerevisiae. *Cell* **52,** 853–62 (1988).

144. Katis, V. L., Galova, M., Rabitsch, K. P., Gregan, J. & Nasmyth, K. Maintenance of cohesin at centromeres after meiosis I in budding yeast requires a kinetochore-associated protein related to MEI-S332. *Curr Biol* **14,** 560–72 (2004).

145. Katis, V. L., Lipp, J. J., Imre, R., Bogdanova, A., Okaz, E., Habermann, B., Mechtler, K., Nasmyth, K. & Zachariae, W. Rec8 phosphorylation by casein kinase 1 and Cdc7-Dbf4 kinase regulates cohesin cleavage by separase during meiosis. *Dev Cell* **18,** 397–409 (2010).

146. Keeney, S. Mechanism and control of meiotic recombination initiation. *Curr Top Dev Biol* **52,** 1–53 (2001).

147. Keeney, S. Spo11 and the Formation of DNA Double-Strand Breaks in Meiosis. *Genome Dyn Stab* **2,** 81–123 (2008).

148. Keeney, S., Giroux, C. N. & Kleckner, N. Meiosis-specific DNA double-strand breaks are catalyzed by Spo11, a member of a widely conserved protein family. *Cell* **88,** 375–84 (1997).

149. Kilmartin, J. V. & Adams, A. E. Structural rearrangements of tubulin and actin during the cell cycle of the yeast Saccharomyces. *J Cell Biol* **98,** 922–33. ISSN: 0021-9525 (Print)0021-9525 (1984).

150. Kim Guisbert, K. S., Zhang, Y., Flatow, J., Hurtado, S., Staley, J. P., Lin, S. & Sontheimer, E. J. Meiosis-induced alterations in transcript architecture and noncoding RNA expression in S. cerevisiae. *Rna* **18,** 1142–53 (2012).

151. Kim, J. H., Lee, B. B., Oh, Y. M., Zhu, C., Steinmetz, L. M., Lee, Y., Kim, W. K., Lee, S. B., Buratowski, S. & Kim, T. Modulation of mRNA and lncRNA expression dynamics by the Set2-Rpd3S pathway. *Nat Commun* **7,** 13534 (2016).

152. Kim, J. O., Zelter, A., Umbreit, N. T., Bollozos, A., Riffle, M., Johnson, R., MacCoss, M. J., Asbury, C. L. & Davis, T. N. The Ndc80 complex bridges two Dam1 complex rings. *Elife* **6.** doi:10.7554/eLife.21069. <http://dx.doi.org/10.7554/eLife.21069> (2017).

153. Kim, J., Ishiguro, K., Nambu, A., Akiyoshi, B., Yokobayashi, S., Kagami, A., Ishiguro, T., Pendas, A. M., Takeda, N., Sakakibara, Y., Kitajima, T. S., Tanno, Y., Sakuno, T. & Watanabe, Y. Meikin is a conserved regulator of meiosis-I-specific kinetochore function. *Nature* **517,** 466–71 (2015).

154. Kim, S., Meyer, R., Chuong, H. & Dawson, D. S. Dual mechanisms prevent premature chromosome segregation during meiosis. *Genes Dev* **27,** 2139–46 (2013).

155. Kimura, K., Wakamatsu, A., Suzuki, Y., Ota, T., Nishikawa, T., Yamashita, R., Yamamoto, J., Sekine, M., Tsuritani, K., Wakaguri, H., Ishii, S., Sugiyama, T., Saito, K., Isono, Y., Irie, R., Kushida, N., Yoneyama, T., Otsuka, R., Kanda, K., Yokoi, T., Kondo, H., Wagatsuma, M., Murakawa, K., Ishida, S., Ishibashi, T., Takahashi-Fujii, A., Tanase, T., Nagai, K., Kikuchi, H., Nakai, K., Isogai, T. & Sugano, S. Diversification of transcriptional modulation: large-scale identification and characterization of putative alternative promoters of human genes. *Genome Res* **16,** 55–65 (2006).

156. King, E. M., van der Sar, S. J. & Hardwick, K. G. Mad3 KEN boxes mediate both Cdc20 and Mad3 turnover, and are critical for the spindle checkpoint. *PLoS One* **2,** e342 (2007).

157. Kitagawa, K., Skowyra, D., Elledge, S. J., Harper, J. W. & Hieter, P. SGT1 encodes an essential component of the yeast kinetochore assembly pathway and a novel subunit of the SCF ubiquitin ligase complex. *Mol Cell* **4,** 21–33 (1999).

158. Kitajima, T. S., Sakuno, T., Ishiguro, K., Iemura, S., Natsume, T., Kawashima, S. A. & Watanabe, Y. Shugoshin collaborates with protein phosphatase 2A to protect cohesin. *Nature* **441,** 46–52 (2006).

159. Kitamura, E., Tanaka, K., Kitamura, Y. & Tanaka, T. U. Kinetochore microtubule interaction during S phase in Saccharomyces cerevisiae. *Genes Dev* **21,** 3319–30 (2007).

160. Kondo, T., Hashimoto, Y., Kato, K., Inagaki, S., Hayashi, S. & Kageyama, Y. Small peptide regulators of actin-based cell morphogenesis encoded by a polycistronic mRNA. *Nat Cell Biol* **9,** 660–5 (2007).

161. Kondo, T., Plaza, S., Zanet, J., Benrabah, E., Valenti, P., Hashimoto, Y., Kobayashi, S., Payre, F. & Kageyama, Y. Small peptides switch the transcriptional activity of Shavenbaby during Drosophila embryogenesis. *Science* **329,** 336–9 (2010).

162. Koster, M. J., Yildirim, A. D., Weil, P. A., Holstege, F. C. & Timmers, H. T. Suppression of intragenic transcription requires the MOT1 and NC2 regulators of TATA-binding protein. *Nucleic Acids Res* **42,** 4220–9. ISSN: 0305-1048 (2014).

163. Krassovsky, K., Henikoff, J. G. & Henikoff, S. Tripartite organization of centromeric chromatin in budding yeast. *Proc Natl Acad Sci U S A* **109,** 243–8 (2012).

164. Krenn, V. & Musacchio, A. The Aurora B Kinase in Chromosome Bi-Orientation and Spindle Checkpoint Signaling. *Front Oncol* **5,** 225 (2015).

165. Kriegenburg, F., Jakopec, V., Poulsen, E. G., Nielsen, S. V., Roguev, A., Krogan, N., Gordon, C., Fleig, U. & Hartmann-Petersen, R. A chaperone-assisted degradation pathway targets kinetochore proteins to ensure genome stability. *PLoS Genet* **10,** e1004140 (2014).

166. Laband, K., Le Borgne, R., Edwards, F., Stefanutti, M., Canman, J. C., Verbavatz, J. M. & Dumont, J. Chromosome segregation occurs by microtubule pushing in oocytes. *Nat Commun* **8,** 1499 (2017).

167. Lamm, N., Ben-David, U., Golan-Lev, T., Storchova, Z., Benvenisty, N. & Kerem, B. Genomic Instability in Human Pluripotent Stem Cells Arises from Replicative Stress and Chromosome Condensation Defects. *Cell Stem Cell* **18,** 253–61 (2016).

168. Lampert, F., Hornung, P. & Westermann, S. The Dam1 complex confers microtubule plus end-tracking activity to the Ndc80 kinetochore complex. *J Cell Biol* **189,** 641–9 (2010).

169. Lampert, F., Mieck, C., Alushin, G. M., Nogales, E. & Westermann, S. Molecular requirements for the formation of a kinetochore-microtubule interface by Dam1 and Ndc80 complexes. *J Cell Biol* **200,** 21–30 (2013).

170. Lampson, M. A. & Black, B. E. Cellular and Molecular Mechanisms of Centromere Drive. *Cold Spring Harb Symp Quant Biol* **82,** 249–257 (2017).

171. Lampson, M. A. & Cheeseman, I. M. Sensing centromere tension: Aurora B and the regulation of kinetochore function. *Trends Cell Biol* **21,** 133–40 (2011).

172. Lardenois, A., Liu, Y., Walther, T., Chalmel, F., Evrard, B., Granovskaia, M., Chu, A., Davis, R. W., Steinmetz, L. M. & Primig, M. Execution of the meiotic noncoding RNA expression program and the onset of gametogenesis in yeast require the conserved exosome subunit Rrp6. *Proc Natl Acad Sci U S A* **108,** 1058–63 (2011).

173. Law, G. L., Raney, A., Heusner, C. & Morris, D. R. Polyamine regulation of ribosome pausing at the upstream open reading frame of S-adenosylmethionine decarboxylase. *J Biol Chem* **276,** 38036–43 (2001).

174. Lechner, J. & Carbon, J. A 240 kd multisubunit protein complex, CBF3, is a major component of the budding yeast centromere. *Cell* **64,** 717–25 (1991).

175. Lee, B. H. & Amon, A. Role of Polo-like kinase CDC5 in programming meiosis I chromosome segregation. *Science* **300,** 482–6 (2003).

176. Lee, J., Kitajima, T. S., Tanno, Y., Yoshida, K., Morita, T., Miyano, T., Miyake, M. & Watanabe, Y. Unified mode of centromeric protection by shugoshin in mammalian oocytes and somatic cells. *Nat Cell Biol* **10,** 42–52 (2008).

177. Leu, J. Y. & Roeder, G. S. The pachytene checkpoint in S. cerevisiae depends on Swe1-mediated phosphorylation of the cyclin-dependent kinase Cdc28. *Mol Cell* **4,** 805–14 (1999).

178. Li, J. M., Li, Y. & Elledge, S. J. Genetic analysis of the kinetochore DASH complex reveals an antagonistic relationship with the ras/protein kinase A pathway and a novel subunit required for Ask1 association. *Mol Cell Biol* **25,** 767–78 (2005).

179. Li, J., Xuan, J. W., Khatamianfar, V., Valiyeva, F., Moussa, M., Sadek, A., Yang, B. B., Dong, B. J., Huang, Y. R. & Gao, W. Q. SKA1 over-expression promotes centriole over-duplication, centrosome amplification and prostate tumourigenesis. *J Pathol* **234,** 178–89 (2014).

180. Li, P., Jin, H., Koch, B. A., Abblett, R. L., Han, X., Yates J. R., 3. & Yu, H. G. Cleavage of the SUN-domain protein Mps3 at its N-terminus regulates centrosome disjunction in budding yeast meiosis. *PLoS Genet* **13,** e1006830 (2017).

181. Li, P., Shao, Y., Jin, H. & Yu, H. G. Ndj1, a telomere-associated protein, regulates centrosome separation in budding yeast meiosis. *J Cell Biol* **209,** 247–59 (2015).

182. Li, Y., Bachant, J., Alcasabas, A. A., Wang, Y., Qin, J. & Elledge, S. J. The mitotic spindle is required for loading of the DASH complex onto the kinetochore. *Genes Dev* **16,** 183–97 (2002).

183. Lingelbach, L. B. & Kaplan, K. B. The interaction between Sgt1p and Skp1p is regulated by HSP90 chaperones and is required for proper CBF3 assembly. *Mol Cell Biol* **24,** 8938–50 (2004).

184. Liu, D., Vleugel, M., Backer, C. B., Hori, T., Fukagawa, T., Cheeseman, I. M. & Lampson, M. A. Regulated targeting of protein phosphatase 1 to the outer kinetochore by KNL1 opposes Aurora B kinase. *J Cell Biol* **188,** 809–20 (2010).

185. Liu, Y., Stuparevic, I., Xie, B., Becker, E., Law, M. J. & Primig, M. The conserved histone deacetylase Rpd3 and the DNA binding regulator Ume6 repress BOI1's meiotic transcript isoform during vegetative growth in Saccharomyces cerevisiae. *Mol Microbiol* **96,** 861–74 (2015).

186. Loidl, J., Klein, F. & Scherthan, H. Homologous pairing is reduced but not abolished in asynaptic mutants of yeast. *J Cell Biol* **125,** 1191–200 (1994).

187. London, N. & Biggins, S. Mad1 kinetochore recruitment by Mps1-mediated phosphorylation of Bub1 signals the spindle checkpoint. *Genes Dev* **28,** 140–52 (2014).

188. London, N., Ceto, S., Ranish, J. A. & Biggins, S. Phosphoregulation of Spc105 by Mps1 and PP1 regulates Bub1 localization to kinetochores. *Curr Biol* **22,** 900–6 (2012).

189. Longtine, M. S., McKenzie A., 3., Demarini, D. J., Shah, N. G., Wach, A., Brachat, A., Philippsen, P. & Pringle, J. R. Additional modules for versatile and economical PCR-based gene deletion and modification in Saccharomyces cerevisiae. *Yeast* **14,** 953–61. ISSN: 0749-503X (Print)0749-503x (1998).

190. Ma, H. T. & Poon, R. Y. C. TRIP13 Regulates Both the Activation and Inactivation of the Spindle-Assembly Checkpoint. *Cell Rep* **14,** 1086–1099 (2016).

191. MacQueen, A. J., Phillips, C. M., Bhalla, N., Weiser, P., Villeneuve, A. M. & Dernburg, A. F. Chromosome sites play dual roles to establish homologous synapsis during meiosis in C. elegans. *Cell* **123,** 1037–50 (2005).

192. Magny, E. G., Pueyo, J. I., Pearl, F. M., Cespedes, M. A., Niven, J. E., Bishop, S. A. & Couso, J. P. Conserved regulation of cardiac calcium uptake by peptides encoded in small open reading frames. *Science* **341,** 1116–20 (2013).

193. Maier, T., Guell, M. & Serrano, L. Correlation of mRNA and protein in complex biological samples. *FEBS Lett* **583,** 3966–73 (2009).

194. Malathi, K., Xiao, Y. & Mitchell, A. P. Interaction of yeast repressor-activator protein Ume6p with glycogen synthase kinase 3 homolog Rim11p. *Mol Cell Biol* **17,** 7230–6 (1997).

195. Malik, H. S. & Henikoff, S. Major evolutionary transitions in centromere complexity. *Cell* **138,** 1067–82 (2009).

196. Malvezzi, F., Litos, G., Schleiffer, A., Heuck, A., Mechtler, K., Clausen, T. & Westermann, S. A structural basis for kinetochore recruitment of the Ndc80 complex via two distinct centromere receptors. *Embo j* **32,** 409–23 (2013).

197. Marston, A. L., Tham, W. H., Shah, H. & Amon, A. A genome-wide screen identifies genes required for centromeric cohesion. *Science* **303,** 1367–70 (2004).

198. Martens, J. A., Laprade, L. & Winston, F. Intergenic transcription is required to repress the Saccharomyces cerevisiae SER3 gene. *Nature* **429,** 571–4 (2004).

199. Martínez-Pastor, M. T., Marchler, G., Schüller, C., Marchler-Bauer, A., Ruis, H. & Estruch, F. The Saccharomyces cerevisiae zinc finger proteins Msn2p and Msn4p are required for transcriptional induction through the stress response element (STRE). *EMBO J* **15,** 2227–35 (1996).

200. Maskell, D. P., Hu, X. W. & Singleton, M. R. Molecular architecture and assembly of the yeast kinetochore MIND complex. *J Cell Biol* **190,** 823–34 (2010).

201. Matos, J., Lipp, J. J., Bogdanova, A., Guillot, S., Okaz, E., Junqueira, M., Shevchenko, A. & Zachariae, W. Dbf4-dependent CDC7 kinase links DNA replication to the segregation of homologous chromosomes in meiosis I. *Cell* **135,** 662–78 (2008).

202. Maure, J. F., Komoto, S., Oku, Y., Mino, A., Pasqualato, S., Natsume, K., Clayton, L., Musacchio, A. & Tanaka, T. U. The Ndc80 loop region facilitates formation of kinetochore attachment to the dynamic microtubule plus end. *Curr Biol* **21,** 207–13 (2011).

203. McDonald, C. M., Cooper, K. F. & Winter, E. The Ama1-directed anaphase-promoting complex regulates the Smk1 mitogen-activated protein kinase during meiosis in yeast. *Genetics* **171,** 901–11 (2005).

204. McDonald, K. L., O'Toole, E. T., Mastronarde, D. N. & McIntosh, J. R. Kinetochore microtubules in PTK cells. *J Cell Biol* **118,** 369–83 (1992).

205. Meadows, J. C., Shepperd, L. A., Vanoosthuyse, V., Lancaster, T. C., Sochaj, A. M., Buttrick, G. J., Hardwick, K. G. & Millar, J. B. Spindle checkpoint silencing requires association of PP1 to both Spc7 and kinesin-8 motors. *Dev Cell* **20,** 739–50 (2011).

206. Meena, J. K., Cerutti, A., Beichler, C., Morita, Y., Bruhn, C., Kumar, M., Kraus, J. M., Speicher, M. R., Wang, Z. Q., Kestler, H. A., d'Adda di Fagagna, F., Gunes, C. & Rudolph, K. L. Telomerase abrogates aneuploidy-induced telomere replication stress, senescence and cell depletion. *Embo j* **34,** 1371–84 (2015).

207. Meyer, R. E., Chuong, H. H., Hild, M., Hansen, C. L., Kinter, M. & Dawson, D. S. Ipl1/Aurora-B is necessary for kinetochore restructuring in meiosis I in Saccharomyces cerevisiae. *Mol Biol Cell* **26,** 2986–3000 (2015).

208. Meyer, R. E., Kim, S., Obeso, D., Straight, P. D., Winey, M. & Dawson, D. S. Mps1 and Ipl1/Aurora B act sequentially to correctly orient chromosomes on the meiotic spindle of budding yeast. *Science* **339,** 1071–4 (2013).

209. Michaelis, C., Ciosk, R. & Nasmyth, K. Cohesins: chromosomal proteins that prevent premature separation of sister chromatids. *Cell* **91,** 35–45. ISSN: 0092-8674 (Print)0092-8674 (1997).

210. Miller, M. P., Amon, A. & Unal, E. Meiosis I: when chromosomes undergo extreme makeover. *Curr Opin Cell Biol* **25,** 687–96. ISSN: 0955-0674 (2013).

211. Miller, M. P., Asbury, C. L. & Biggins, S. A TOG Protein Confers Tension Sensitivity to Kinetochore-Microtubule Attachments. *Cell* **165,** 1428–1439. ISSN: 0092-8674 (2016).

212. Miller, M. P., Unal, E., Brar, G. A. & Amon, A. Meiosis I chromosome segregation is established through regulation of microtubule-kinetochore interactions. *Elife* **1,** e00117 (2012).

213. Miniowitz-Shemtov, S., Eytan, E., Kaisari, S., Sitry-Shevah, D. & Hershko, A. Mode of interaction of TRIP13 AAA-ATPase with the Mad2-binding protein p31comet and with mitotic checkpoint complexes. *Proc Natl Acad Sci U S A* **112,** 11536–40 (2015).

214. Miranda, J. J., De Wulf, P., Sorger, P. K. & Harrison, S. C. The yeast DASH complex forms closed rings on microtubules. *Nat Struct Mol Biol* **12,** 138–43 (2005).

215. Mitchell, A. P. & Bowdish, K. S. Selection for early meiotic mutants in yeast. *Genetics* **131,** 65–72 (1992).

216. Mitchell, A. P. & Herskowitz, I. Activation of meiosis and sporulation by repression of the RME1 product in yeast. *Nature* **319,** 738–42 (1986).

217. Mizuguchi, G., Xiao, H., Wisniewski, J., Smith, M. M. & Wu, C. Nonhistone Scm3 and histones CenH3-H4 assemble the core of centromere-specific nucleosomes. *Cell* **129,** 1153–64 (2007).

218. Mizuno, T., Nakazawa, N., Remgsamrarn, P., Kunoh, T., Oshima, Y. & Harashima, S. The Tup1-Ssn6 general repressor is involved in repression of IME1 encoding a transcriptional activator of meiosis in Saccharomyces cerevisiae. *Curr Genet* **33,** 239–47 (1998).

219. Monje-Casas, F., Prabhu, V. R., Lee, B. H., Boselli, M. & Amon, A. Kinetochore orientation during meiosis is controlled by Aurora B and the monopolin complex. *Cell* **128,** 477–90 (2007).

220. Mueller, P. P. & Hinnebusch, A. G. Multiple upstream AUG codons mediate translational control of GCN4. *Cell* **45,** 201–7 (1986).

221. Musacchio, A. & Desai, A. in *Biology (Basel)* (2017). doi:10.3390/biology6010005. <http://dx.doi.org/10.3390/biology6010005>.

222. Muscat, C. C., Torre-Santiago, K. M., Tran, M. V., Powers, J. A. & Wignall, S. M. Kinetochore-independent chromosome segregation driven by lateral microtubule bundles. *Elife* **4,** e06462 (2015).

223. Narita, N. N., Moore, S., Horiguchi, G., Kubo, M., Demura, T., Fukuda, H., Goodrich, J. & Tsukaya, H. Overexpression of a novel small peptide ROTUNDIFOLIA4 decreases cell proliferation and alters leaf shape in Arabidopsis thaliana. *Plant J* **38,** 699–713 (2004).

224. Neiman, A. M. Ascospore formation in the yeast Saccharomyces cerevisiae. *Microbiol Mol Biol Rev* **69,** 565–84 (2005).

225. Nicklas, R. B. How cells get the right chromosomes. *Science* **275,** 632–7 (1997).

226. Nicklas, R. B. & Koch, C. A. Chromosome micromanipulation. 3. Spindle fiber tension and the reorientation of mal-oriented chromosomes. *J Cell Biol* **43,** 40–50 (1969).

227. Ohashi, A., Ohori, M., Iwai, K., Nakayama, Y., Nambu, T., Morishita, D., Kawamoto, T., Miyamoto, M., Hirayama, T., Okaniwa, M., Banno, H., Ishikawa, T., Kandori, H. & Iwata, K. Aneuploidy generates proteotoxic stress and DNA damage concurrently with p53-mediated post-mitotic apoptosis in SAC-impaired cells. *Nat Commun* **6,** 7668 (2015).

228. Ohkuni, K., Takahashi, Y., Fulp, A., Lawrimore, J., Au, W. C., Pasupala, N., Levy-Myers, R., Warren, J., Strunnikov, A., Baker, R. E., Kerscher, O., Bloom, K. & Basrai, M. A. SUMO-Targeted Ubiquitin Ligase (STUbL) Slx5 regulates proteolysis of centromeric histone H3 variant Cse4 and prevents its mislocalization to euchromatin. *Mol Biol Cell.* doi:10.1091/mbc.E15-12-0827. <http://dx.doi.org/10.1091/mbc.E15-12-0827> (2016).

229. Okaz, E., Arguello-Miranda, O., Bogdanova, A., Vinod, P. K., Lipp, J. J., Markova, Z., Zagoriy, I., Novak, B. & Zachariae, W. Meiotic prophase requires proteolysis of M phase regulators mediated by the meiosis-specific APC/CAma1. *Cell* **151,** 603–18 (2012).

230. Oromendia, A. B., Dodgson, S. E. & Amon, A. Aneuploidy causes proteotoxic stress in yeast. *Genes Dev* **26,** 2696–708 (2012).

231. Ottoz, D. S., Rudolf, F. & Stelling, J. Inducible, tightly regulated and growth condition-independent transcription factor in Saccharomyces cerevisiae. *Nucleic Acids Res* **42,** e130 (2014).

232. Ozsarac, N., Straffon, M. J., Dalton, H. E. & Dawes, I. W. Regulation of gene expression during meiosis in Saccharomyces cerevisiae: SPR3 is controlled by both ABFI and a new sporulation control element. *Mol Cell Biol* **17,** 1152–9 (1997).

233. Pan, J. & Chen, R. H. Spindle checkpoint regulates Cdc20p stability in Saccharomyces cerevisiae. *Genes Dev* **18,** 1439–51 (2004).

234. Park, H. D., Luche, R. M. & Cooper, T. G. The yeast UME6 gene product is required for transcriptional repression mediated by the CAR1 URS1 repressor binding site. *Nucleic Acids Res* **20,** 1909–15 (1992).

235. Passerini, V., Ozeri-Galai, E., de Pagter, M. S., Donnelly, N., Schmalbrock, S., Kloosterman, W. P., Kerem, B. & Storchova, Z. The presence of extra chromosomes leads to genomic instability. *Nat Commun* **7,** 10754 (2016).

236. Pavelka, N., Rancati, G., Zhu, J., Bradford, W. D., Saraf, A., Florens, L., Sanderson, B. W., Hattem, G. L. & Li, R. Aneuploidy confers quantitative proteome changes and phenotypic variation in budding yeast. *Nature* **468,** 321–5 (2010).

237. Pekgoz Altunkaya, G., Malvezzi, F., Demianova, Z., Zimniak, T., Litos, G., Weissmann, F., Mechtler, K., Herzog, F. & Westermann, S. CCAN Assembly Configures Composite Binding Interfaces to Promote Cross-Linking of Ndc80 Complexes at the Kinetochore. *Curr Biol* **26,** 2370–8 (2016).

238. Petronczki, M., Matos, J., Mori, S., Gregan, J., Bogdanova, A., Schwickart, M., Mechtler, K., Shirahige, K., Zachariae, W. & Nasmyth, K. Monopolar attachment of sister kinetochores at meiosis I requires casein kinase 1. *Cell* **126,** 1049–64 (2006).

239. Pierce, M., Benjamin, K. R., Montano, S. P., Georgiadis, M. M., Winter, E. & Vershon, A. K. Sum1 and Ndt80 proteins compete for binding to middle sporulation element sequences that control meiotic gene expression. *Mol Cell Biol* **23,** 4814–25 (2003).

240. Plowman, R., Singh, N., Tromer, E. C., Payan, A., Duro, E., Spanos, C., Rappsilber, J., Snel, B., Kops, G., Corbett, K. D. & Marston, A. L. The molecular basis of monopolin recruitment to the kinetochore. *Chromosoma.* doi:10.1007/s00412-019-00700-0. <http://dx.doi.org/10.1007/s00412-019-00700-0> (2019).

241. Qurashi, A., Sahin, H. B., Carrera, P., Gautreau, A., Schenck, A. & Giangrande, A. HSPC300 and its role in neuronal connectivity. *Neural Dev* **2,** 18 (2007).

242. Raaijmakers, J. A., Tanenbaum, M. E., Maia, A. F. & Medema, R. H. RAMA1 is a novel kinetochore protein involved in kinetochore-microtubule attachment. *J Cell Sci* **122,** 2436–45 (2009).

243. Rabitsch, K. P., Gregan, J., Schleiffer, A., Javerzat, J. P., Eisenhaber, F. & Nasmyth, K. Two fission yeast homologs of Drosophila Mei-S332 are required for chromosome segregation during meiosis I and II. *Curr Biol* **14,** 287–301 (2004).

244. Rahmani, F., Hummel, M., Schuurmans, J., Wiese-Klinkenberg, A., Smeekens, S. & Hanson, J. Sucrose control of translation mediated by an upstream open reading frame-encoded peptide. *Plant Physiol* **150,** 1356–67 (2009).

245. Raj, A., Peskin, C. S., Tranchina, D., Vargas, D. Y. & Tyagi, S. Stochastic mRNA synthesis in mammalian cells. *PLoS Biol* **4,** e309. ISSN: 1544-9173 (2006).

246. Raj, A., van den Bogaard, P., Rifkin, S. A., van Oudenaarden, A. & Tyagi, S. Imaging individual mRNA molecules using multiple singly labeled probes. *Nat Methods* **5,** 877–9 (2008).

247. Ramey, V. H., Wang, H. W., Nakajima, Y., Wong, A., Liu, J., Drubin, D., Barnes, G. & Nogales, E. The Dam1 ring binds to the E-hook of tubulin and diffuses along the microtubule. *Mol Biol Cell* **22,** 457–66 (2011).

248. Ramey, V. H., Wong, A., Fang, J., Howes, S., Barnes, G. & Nogales, E. Subunit organization in the Dam1 kinetochore complex and its ring around microtubules. *Mol Biol Cell* **22,** 4335–42 (2011).

249. Ranjitkar, P., Press, M. O., Yi, X., Baker, R., MacCoss, M. J. & Biggins, S. An E3 ubiquitin ligase prevents ectopic localization of the centromeric histone H3 variant via the centromere targeting domain. *Mol Cell* **40,** 455–64 (2010).

250. Rao, H. B., Qiao, H., Bhatt, S. K., Bailey, L. R., Tran, H. D., Bourne, S. L., Qiu, W., Deshpande, A., Sharma, A. N., Beebout, C. J., Pezza, R. J. & Hunter, N. A SUMO-ubiquitin relay recruits proteasomes to chromosome axes to regulate meiotic recombination. *Science* **355,** 403–407 (2017).

251. Reddy, S. K., Rape, M., Margansky, W. A. & Kirschner, M. W. Ubiquitination by the anaphase-promoting complex drives spindle checkpoint inactivation. *Nature* **446,** 921–5 (2007).

252. Riedel, C. G., Katis, V. L., Katou, Y., Mori, S., Itoh, T., Helmhart, W., Galova, M., Petronczki, M., Gregan, J., Cetin, B., Mudrak, I., Ogris, E., Mechtler, K., Pelletier, L., Buchholz, F., Shirahige, K. & Nasmyth, K. Protein phosphatase 2A protects centromeric sister chromatid cohesion during meiosis I. *Nature* **441,** 53–61 (2006).

253. Rinn, J. L. & Chang, H. Y. Genome regulation by long noncoding RNAs. *Annu Rev Biochem* **81,** 145–66 (2012).

254. Rog, O. & Dernburg, A. F. Chromosome pairing and synapsis during Caenorhabditis elegans meiosis. *Curr Opin Cell Biol* **25,** 349–56 (2013).

255. Rohrig, H., Schmidt, J., Miklashevichs, E., Schell, J. & John, M. Soybean ENOD40 encodes two peptides that bind to sucrose synthase. *Proc Natl Acad Sci U S A* **99,** 1915–20 (2002).

256. Rojas-Duran, M. F. & Gilbert, W. V. Alternative transcription start site selection leads to large differences in translation activity in yeast. *Rna* **18,** 2299–305 (2012).

257. Romano, A., Guse, A., Krascenicova, I., Schnabel, H., Schnabel, R. & Glotzer, M. CSC-1: a subunit of the Aurora B kinase complex that binds to the survivin-like protein BIR-1 and the incenp-like protein ICP-1. *J Cell Biol* **161,** 229–36 (2003).

258. Roper, R. J. & Reeves, R. H. Understanding the basis for Down syndrome phenotypes. *PLoS Genet* **2,** e50 (2006).

259. Rosenberg, J. S., Cross, F. R. & Funabiki, H. KNL1/Spc105 recruits PP1 to silence the spindle assembly checkpoint. *Curr Biol* **21,** 942–7 (2011).

260. Rubin-Bejerano, I., Mandel, S., Robzyk, K. & Kassir, Y. Induction of meiosis in Saccharomyces cerevisiae depends on conversion of the transcriptional represssor Ume6 to a positive regulator by its regulated association with the transcriptional activator Ime1. *Mol Cell Biol* **16,** 2518–26 (1996).

261. Rundlett, S. E., Carmen, A. A., Suka, N., Turner, B. M. & Grunstein, M. Transcriptional repression by UME6 involves deacetylation of lysine 5 of histone H4 by RPD3. *Nature* **392,** 831–5 (1998).

262. Sagee, S., Sherman, A., Shenhar, G., Robzyk, K., Ben-Doy, N., Simchen, G. & Kassir, Y. in *Mol Cell Biol* 1985–95 (1998). <http://dx.doi.org/>.

263. Salah, S. M. & Nasmyth, K. Destruction of the securin Pds1p occurs at the onset of anaphase during both meiotic divisions in yeast. *Chromosoma* **109,** 27–34 (2000).

264. Sarangapani, K. K., Akiyoshi, B., Duggan, N. M., Biggins, S. & Asbury, C. L. Phosphoregulation promotes release of kinetochores from dynamic microtubules via multiple mechanisms. *Proc Natl Acad Sci U S A* **110,** 7282–7 (2013).

265. Sarangapani, K. K., Duro, E., Deng, Y., Alves Fde, L., Ye, Q., Opoku, K. N., Ceto, S., Rappsilber, J., Corbett, K. D., Biggins, S., Marston, A. L. & Asbury, C. L. Sister kinetochores are mechanically fused during meiosis I in yeast. *Science* **346,** 248–51 (2014).

266. Sawyer, E. M., Joshi, P. R., Jorgensen, V., Yunus, J., Berchowitz, L. E. & Unal, E. Developmental regulation of an organelle tether coordinates mitochondrial remodeling in meiosis. *J Cell Biol* **218,** 559–579 (2019).

267. Scannell, D. R., Zill, O. A., Rokas, A., Payen, C., Dunham, M. J., Eisen, M. B., Rine, J., Johnston, M. & Hittinger, C. T. The Awesome Power of Yeast Evolutionary Genetics: New Genome Sequences and Strain Resources for the Saccharomyces sensu stricto Genus. *G3 (Bethesda)* **1,** 11–25. ISSN: 2160-1836 (2011).

268. Scarborough, E. A., Davis, T. N. & Asbury, C. L. Tight bending of the Ndc80 complex provides intrinsic regulation of its binding to microtubules. *Elife* **8.** doi:10.7554/eLife.44489. <http://dx.doi.org/10.7554/eLife.44489> (2019).

269. Schindelin, J., Arganda-Carreras, I., Frise, E., Kaynig, V., Longair, M., Pietzsch, T., Preibisch, S., Rueden, C., Saalfeld, S., Schmid, B., Tinevez, J. Y., White, D. J., Hartenstein, V., Eliceiri, K., Tomancak, P. & Cardona, A. Fiji: an open-source platform for biological-image analysis. *Nat Methods* **9,** 676–82. ISSN: 1548-7091 (2012).

270. Schumacher, J. M., Golden, A. & Donovan, P. J. AIR-2: An Aurora/Ipl1-related protein kinase associated with chromosomes and midbody microtubules is required for polar body extrusion and cytokinesis in Caenorhabditis elegans embryos. *J Cell Biol* **143,** 1635–46 (1998).

271. Sczaniecka, M., Feoktistova, A., May, K. M., Chen, J. S., Blyth, J., Gould, K. L. & Hardwick, K. G. The spindle checkpoint functions of Mad3 and Mad2 depend on a Mad3 KEN box-mediated interaction with Cdc20-anaphase-promoting complex (APC/C). *J Biol Chem* **283,** 23039–47 (2008).

272. Senecal, A., Munsky, B., Proux, F., Ly, N., Braye, F. E., Zimmer, C., Mueller, F. & Darzacq, X. Transcription factors modulate c-Fos transcriptional bursts. *Cell Rep* **8,** 75–83 (2014).

273. Serge, A., Bertaux, N., Rigneault, H. & Marguet, D. Dynamic multiple-target tracing to probe spatiotemporal cartography of cell membranes. *Nat Methods* **5,** 687–94. ISSN: 1548-7091 (2008).

274. Shankar, R. K. & Backeljauw, P. F. Current best practice in the management of Turner syndrome. *Ther Adv Endocrinol Metab* **9,** 33–40 (2018).

275. Shearwin, K. E., Callen, B. P. & Egan, J. B. Transcriptional interference–a crash course. *Trends Genet* **21,** 339–45 (2005).

276. Sheltzer, J. M., Blank, H. M., Pfau, S. J., Tange, Y., George, B. M., Humpton, T. J., Brito, I. L., Hiraoka, Y., Niwa, O. & Amon, A. Aneuploidy drives genomic instability in yeast. *Science* **333,** 1026–30 (2011).

277. Sheltzer, J. M., Torres, E. M., Dunham, M. J. & Amon, A. Transcriptional consequences of aneuploidy. *Proc Natl Acad Sci U S A* **109,** 12644–9 (2012).

278. Shen, L., Yang, M., Lin, Q., Zhang, Z., Miao, C. & Zhu, B. SKA1 regulates the metastasis and cisplatin resistance of non-small cell lung cancer. *Oncol Rep* **35,** 2561–8 (2016).

279. Shirk, K., Jin, H., Giddings T. H., J., Winey, M. & Yu, H. G. The Aurora kinase Ipl1 is necessary for spindle pole body cohesion during budding yeast meiosis. *J Cell Sci* **124,** 2891–6 (2011).

280. Shonn, M. A., McCarroll, R. & Murray, A. W. Requirement of the spindle checkpoint for proper chromosome segregation in budding yeast meiosis. *Science* **289,** 300–3 (2000).

281. Shonn, M. A., Murray, A. L. & Murray, A. W. Spindle checkpoint component Mad2 contributes to biorientation of homologous chromosomes. *Curr Biol* **13,** 1979–84 (2003).

282. Shrestha, R. L., Ahn, G. S., Staples, M. I., Sathyan, K. M., Karpova, T. S., Foltz, D. R. & Basrai, M. A. Mislocalization of centromeric histone H3 variant CENP-A contributes to chromosomal instability (CIN) in human cells. *Oncotarget* **8,** 46781–46800 (2017).

283. Sievers, F., Wilm, A., Dineen, D., Gibson, T. J., Karplus, K., Li, W., Lopez, R., McWilliam, H., Remmert, M., Soding, J., Thompson, J. D. & Higgins, D. G. Fast, scalable generation of high-quality protein multiple sequence alignments using Clustal Omega. *Mol Syst Biol* **7,** 539. ISSN: 1744-4292 (2011).

284. Smith, A., Ward, M. P. & Garrett, S. Yeast PKA represses Msn2p/Msn4p-dependent gene expression to regulate growth, stress response and glycogen accumulation. *EMBO J* **17,** 3556–64 (1998).

285. Smith, H. E. & Mitchell, A. P. A transcriptional cascade governs entry into meiosis in Saccharomyces cerevisiae. *Mol Cell Biol* **9,** 2142–52 (1989).

286. Smith, H. E., Su, S. S., Neigeborn, L., Driscoll, S. E. & Mitchell, A. P. Role of IME1 expression in regulation of meiosis in Saccharomyces cerevisiae. *Mol Cell Biol* **10,** 6103–13 (1990).

287. Sourirajan, A. & Lichten, M. Polo-like kinase Cdc5 drives exit from pachytene during budding yeast meiosis. *Genes Dev* **22,** 2627–32 (2008).

288. Speliotes, E. K., Uren, A., Vaux, D. & Horvitz, H. R. The survivin-like C. elegans BIR-1 protein acts with the Aurora-like kinase AIR-2 to affect chromosomes and the spindle midzone. *Mol Cell* **6,** 211–23 (2000).

289. Stemmann, O., Neidig, A., Kocher, T., Wilm, M. & Lechner, J. Hsp90 enables Ctf13p/Skp1p to nucleate the budding yeast kinetochore. *Proc Natl Acad Sci U S A* **99,** 8585–90 (2002).

290. Stingele, S., Stoehr, G., Peplowska, K., Cox, J., Mann, M. & Storchova, Z. Global analysis of genome, transcriptome and proteome reveals the response to aneuploidy in human cells. *Mol Syst Biol* **8,** 608 (2012).

291. Stoler, S., Rogers, K., Weitze, S., Morey, L., Fitzgerald-Hayes, M. & Baker, R. E. Scm3, an essential Saccharomyces cerevisiae centromere protein required for G2/M progression and Cse4 localization. *Proc Natl Acad Sci U S A* **104,** 10571–6 (2007).

292. Strahl-Bolsinger, S., Hecht, A., Luo, K. & Grunstein, M. SIR2 and SIR4 interactions differ in core and extended telomeric heterochromatin in yeast. *Genes Dev* **11,** 83–93. ISSN: 0890-9369 (Print)0890-9369 (1997).

293. Strich, R., Surosky, R. T., Steber, C., Dubois, E., Messenguy, F. & Esposito, R. E. UME6 is a key regulator of nitrogen repression and meiotic development. *Genes Dev* **8,** 796–810 (1994).

294. Sun, S. C., Zhang, D. X., Lee, S. E., Xu, Y. N. & Kim, N. H. Ndc80 regulates meiotic spindle organization, chromosome alignment, and cell cycle progression in mouse oocytes. *Microsc Microanal* **17,** 431–9 (2011).

295. Taggart, J., MacDiarmid, C. W., Haws, S. & Eide, D. J. Zap1-dependent transcription from an alternative upstream promoter controls translation of RTC4 mRNA in zinc-deficient Saccharomyces cerevisiae. *Mol Microbiol* **106,** 678–689 (2017).

296. Tanaka, K., Kitamura, E., Kitamura, Y. & Tanaka, T. U. Molecular mechanisms of microtubule-dependent kinetochore transport toward spindle poles. *J Cell Biol* **178,** 269–81 (2007).

297. Tanaka, T. U. Kinetochore-microtubule interactions: steps towards bi-orientation. *Embo j* **29,** 4070–82 (2010).

298. Tang, T. T., Bickel, S. E., Young, L. M. & Orr-Weaver, T. L. Maintenance of sister-chromatid cohesion at the centromere by the Drosophila MEI-S332 protein. *Genes Dev* **12,** 3843–56 (1998).

299. Teichner, A., Eytan, E., Sitry-Shevah, D., Miniowitz-Shemtov, S., Dumin, E., Gromis, J. & Hershko, A. p31comet Promotes disassembly of the mitotic checkpoint complex in an ATP-dependent process. *Proc Natl Acad Sci U S A* **108,** 3187–92 (2011).

300. Theis, M., Slabicki, M., Junqueira, M., Paszkowski-Rogacz, M., Sontheimer, J., Kittler, R., Heninger, A. K., Glatter, T., Kruusmaa, K., Poser, I., Hyman, A. A., Pisabarro, M. T., Gstaiger, M., Aebersold, R., Shevchenko, A. & Buchholz, F. Comparative profiling identifies C13orf3 as a component of the Ska complex required for mammalian cell division. *Embo j* **28,** 1453–65 (2009).

301. Thorburn, R. R., Gonzalez, C., Brar, G. A., Christen, S., Carlile, T. M., Ingolia, N. T., Sauer, U., Weissman, J. S. & Amon, A. Aneuploid yeast strains exhibit defects in cell growth and passage through START. *Mol Biol Cell* **24,** 1274–89 (2013).

302. Tien, J. F., Umbreit, N. T., Gestaut, D. R., Franck, A. D., Cooper, J., Wordeman, L., Gonen, T., Asbury, C. L. & Davis, T. N. Cooperation of the Dam1 and Ndc80 kinetochore complexes enhances microtubule coupling and is regulated by aurora B. *J Cell Biol* **189,** 713–23 (2010).

303. Tipton, A. R., Wang, K., Link, L., Bellizzi, J. J., Huang, H., Yen, T. & Liu, S. T. BUBR1 and closed MAD2 (C-MAD2) interact directly to assemble a functional mitotic checkpoint complex. *J Biol Chem* **286,** 21173–9 (2011).

304. Tipton, A. R., Wang, K., Oladimeji, P., Sufi, S., Gu, Z. & Liu, S. T. Identification of novel mitosis regulators through data mining with human centromere/kinetochore proteins as group queries. *BMC Cell Biol* **13,** 15 (2012).

305. Tooley, J. & Stukenberg, P. T. The Ndc80 complex: integrating the kinetochore's many movements. *Chromosome Res* **19,** 377–91 (2011).

306. Torres, E. M., Sokolsky, T., Tucker, C. M., Chan, L. Y., Boselli, M., Dunham, M. J. & Amon, A. Effects of aneuploidy on cellular physiology and cell division in haploid yeast. *Science* **317,** 916–24 (2007).

307. Tresenrider, A. & Unal, E. One-two punch mechanism of gene repression: a fresh perspective on gene regulation. *Curr Genet* **64,** 581–588 (2018).

308. Tsuchiya, D., Gonzalez, C. & Lacefield, S. The spindle checkpoint protein Mad2 regulates APC/C activity during prometaphase and metaphase of meiosis I in Saccharomyces cerevisiae. *Mol Biol Cell* **22,** 2848–61 (2011).

309. Tsukada, M. & Ohsumi, Y. Isolation and characterization of autophagy-defective mutants of Saccharomyces cerevisiae. *FEBS Lett* **333,** 169–74 (1993).

310. Tung, K. S., Hong, E. J. & Roeder, G. S. The pachytene checkpoint prevents accumulation and phosphorylation of the meiosis-specific transcription factor Ndt80. *Proc Natl Acad Sci U S A* **97,** 12187–92 (2000).

311. Umbreit, N. T., Miller, M. P., Tien, J. F., Ortola, J. C., Gui, L., Lee, K. K., Biggins, S., Asbury, C. L. & Davis, T. N. Kinetochores require oligomerization of Dam1 complex to maintain microtubule attachments against tension and promote biorientation. *Nat Commun* **5,** 4951 (2014).

312. Van Dalfsen, K. M., Hodapp, S., Keskin, A., Otto, G. M., Berdan, C. A., Higdon, A., Cheunkarndee, T., Nomura, D. K., Jovanovic, M. & Brar, G. A. Global Proteome Remodeling during ER Stress Involves Hac1-Driven Expression of Long Undecoded Transcript Isoforms. *Dev Cell* **46,** 219–235.e8 (2018).

313. Van der Horst, A. & Lens, S. M. Cell division: control of the chromosomal passenger complex in time and space. *Chromosoma* **123,** 25–42 (2014).

314. Van Werven, F. J. & Amon, A. Regulation of entry into gametogenesis. *Philos Trans R Soc Lond B Biol Sci* **366,** 3521–31 (2011).

315. Van Werven, F. J., Neuert, G., Hendrick, N., Lardenois, A., Buratowski, S., van Oudenaarden, A., Primig, M. & Amon, A. Transcription of two long noncoding RNAs mediates mating-type control of gametogenesis in budding yeast. *Cell* **150,** 1170–81 (2012).

316. Visintin, R., Prinz, S. & Amon, A. CDC20 and CDH1: a family of substrate-specific activators of APC-dependent proteolysis. *Science* **278,** 460–3 (1997).

317. Wagner, E. J. & Carpenter, P. B. Understanding the language of Lys36 methylation at histone H3. *Nat Rev Mol Cell Biol* **13,** 115–26 (2012).

318. Wang, H. W., Ramey, V. H., Westermann, S., Leschziner, A. E., Welburn, J. P., Nakajima, Y., Drubin, D. G., Barnes, G. & Nogales, E. Architecture of the Dam1 kinetochore ring complex and implications for microtubule-driven assembly and force-coupling mechanisms. *Nat Struct Mol Biol* **14,** 721–6 (2007).

319. Wang, K., Sturt-Gillespie, B., Hittle, J. C., Macdonald, D., Chan, G. K., Yen, T. J. & Liu, S. T. Thyroid hormone receptor interacting protein 13 (TRIP13) AAA-ATPase is a novel mitotic checkpoint-silencing protein. *J Biol Chem* **289,** 23928–37 (2014).

320. Wang, W., Cherry, J. M., Nochomovitz, Y., Jolly, E., Botstein, D. & Li, H. Inference of combinatorial regulation in yeast transcriptional networks: a case study of sporulation. *Proc Natl Acad Sci U S A* **102,** 1998–2003 (2005).

321. Wang, Y., Chang, C. Y., Wu, J. F. & Tung, K. S. Nuclear localization of the meiosis-specific transcription factor Ndt80 is regulated by the pachytene checkpoint. *Mol Biol Cell* **22,** 1878–86 (2011).

322. Waples, W. G., Chahwan, C., Ciechonska, M. & Lavoie, B. D. Putting the brake on FEAR: Tof2 promotes the biphasic release of Cdc14 phosphatase during mitotic exit. *Mol Biol Cell* **20,** 245–55 (2009).

323. Washburn, B. K. & Esposito, R. E. Identification of the Sin3-binding site in Ume6 defines a two-step process for conversion of Ume6 from a transcriptional repressor to an activator in yeast. *Mol Cell Biol* **21,** 2057–69 (2001).

324. Washburn, M. P., Wolters, D. & Yates J. R., 3. Large-scale analysis of the yeast proteome by multidimensional protein identification technology. *Nat Biotechnol* **19,** 242–7. ISSN: 1087-0156 (Print)1087-0156 (2001).

325. Wei, R. R., Sorger, P. K. & Harrison, S. C. Molecular organization of the Ndc80 complex, an essential kinetochore component. *Proc Natl Acad Sci U S A* **102,** 5363–7 (2005).

326. Welburn, J. P., Grishchuk, E. L., Backer, C. B., Wilson-Kubalek, E. M., Yates J. R., 3. & Cheeseman, I. M. The human kinetochore Ska1 complex facilitates microtubule depolymerization-coupled motility. *Dev Cell* **16,** 374–85 (2009).

327. Wen, F. P., Guo, Y. S., Hu, Y., Liu, W. X., Wang, Q., Wang, Y. T., Yu, H. Y., Tang, C. M., Yang, J., Zhou, T., Xie, Z. P., Sha, J. H., Guo, X. & Li, W. Distinct temporal requirements for autophagy and the proteasome in yeast meiosis. *Autophagy* **12,** 671–88 (2016).

328. Westermann, S., Avila-Sakar, A., Wang, H. W., Niederstrasser, H., Wong, J., Drubin, D. G., Nogales, E. & Barnes, G. Formation of a dynamic kinetochore- microtubule interface through assembly of the Dam1 ring complex. *Mol Cell* **17,** 277–90 (2005).

329. Westermann, S., Cheeseman, I. M., Anderson, S., Yates J. R., 3., Drubin, D. G. & Barnes, G. Architecture of the budding yeast kinetochore reveals a conserved molecular core. *J Cell Biol* **163,** 215–22 (2003).

330. Wigge, P. A., Jensen, O. N., Holmes, S., Soues, S., Mann, M. & Kilmartin, J. V. Analysis of the Saccharomyces spindle pole by matrix-assisted laser desorption/ionization (MALDI) mass spectrometry. *J Cell Biol* **141,** 967–77 (1998).

331. Wigge, P. A. & Kilmartin, J. V. The Ndc80p complex from Saccharomyces cerevisiae contains conserved centromere components and has a function in chromosome segregation. *J Cell Biol* **152,** 349–60 (2001).

332. Williams, B. R., Prabhu, V. R., Hunter, K. E., Glazier, C. M., Whittaker, C. A., Housman, D. E. & Amon, A. Aneuploidy affects proliferation and spontaneous immortalization in mammalian cells. *Science* **322,** 703–9 (2008).

333. Winey, M., Mamay, C. L., O'Toole, E. T., Mastronarde, D. N., Giddings T. H., J., McDonald, K. L. & McIntosh, J. R. Three-dimensional ultrastructural analysis of the Saccharomyces cerevisiae mitotic spindle. *J Cell Biol* **129,** 1601–15 (1995).

334. Winey, M., Morgan, G. P., Straight, P. D., Giddings, T. H. & Mastronarde, D. N. in *Mol Biol Cell* 1178–88 (2005). doi:10.1091/mbc.E04-09-0765. <http://dx.doi.org/10.1091/mbc.E04-09-0765>.

335. Winter, E. The Sum1/Ndt80 transcriptional switch and commitment to meiosis in Saccharomyces cerevisiae. *Microbiol Mol Biol Rev* **76,** 1–15 (2012).

336. Xiao, Y. & Mitchell, A. P. Shared roles of yeast glycogen synthase kinase 3 family members in nitrogen-responsive phosphorylation of meiotic regulator Ume6p. *Mol Cell Biol* **20,** 5447–53 (2000).

337. Xie, B., Horecka, J., Chu, A., Davis, R. W., Becker, E. & Primig, M. Ndt80 activates the meiotic ORC1 transcript isoform and SMA2 via a bi-directional middle sporulation element in Saccharomyces cerevisiae. *RNA Biol* **13,** 772–82 (2016).

338. Xu, L., Ajimura, M., Padmore, R., Klein, C. & Kleckner, N. NDT80, a meiosis-specific gene required for exit from pachytene in Saccharomyces cerevisiae. *Mol Cell Biol* **15,** 6572–81 (1995).

339. Yokobayashi, S. & Watanabe, Y. The kinetochore protein Moa1 enables cohesion-mediated monopolar attachment at meiosis I. *Cell* **123,** 803–17 (2005).

340. Yu, H. Cdc20: a WD40 activator for a cell cycle degradation machine. *Mol Cell* **27,** 3–16 (2007).

341. Zelter, A., Bonomi, M., Kim, J. O., Umbreit, N. T., Hoopmann, M. R., Johnson, R., Riffle, M., Jaschob, D., MacCoss, M. J., Moritz, R. L. & Davis, T. N. The molecular architecture of the Dam1 kinetochore complex is defined by cross-linking based structural modelling. *Nat Commun* **6,** 8673 (2015).

342. Zernicka-Goetz, M., Morris, S. A. & Bruce, A. W. Making a firm decision: multifaceted regulation of cell fate in the early mouse embryo. *Nat Rev Genet* **10,** 467–77 (2009).

343. Zhao, G., Oztan, A., Ye, Y. & Schwarz, T. L. Kinetochore Proteins Have a Post-Mitotic Function in Neurodevelopment. *Dev Cell* **48,** 873–882.e4 (2019).

344. Zhou, Z., Feng, H., Zhou, B. R., Ghirlando, R., Hu, K., Zwolak, A., Miller Jenkins, L. M., Xiao, H., Tjandra, N., Wu, C. & Bai, Y. Structural basis for recognition of centromere histone variant CenH3 by the chaperone Scm3. *Nature* **472,** 234–7 (2011).

345. Zhu, J., Pavelka, N., Bradford, W. D., Rancati, G. & Li, R. Karyotypic determinants of chromosome instability in aneuploid budding yeast. *PLoS Genet* **8,** e1002719 (2012).

346. Zhu, J., Tsai, H. J., Gordon, M. R. & Li, R. Cellular Stress Associated with Aneuploidy. *Dev Cell* **44,** 420–431 (2018).

347. Zickler, D. & Kleckner, N. Meiotic chromosomes: integrating structure and function. *Annu Rev Genet* **33,** 603–754 (1999).

348. Zickler, D. & Kleckner, N. Recombination, Pairing, and Synapsis of Homologs during Meiosis. *Cold Spring Harb Perspect Biol* **7.** doi:10.1101/cshperspect.a016626. <http://dx.doi.org/10.1101/cshperspect.a016626> (2015).